An investigation into novel molecules involved in the development of the nervous system of *Drosophila melanogaster*.

David Robinson.

A thesis submitted in partial fulfilment of the requirements of the University of Greenwich for the Degree of Doctor of Philosophy.

December 2015.

DECLARATION

I certify that this work has not been accepted in substance for any degree, and is not concurrently being submitted for any degree other than that of Doctor of Philosophy being studied at the University of Greenwich. I also declare that this work is the result of my own investigations except where otherwise identified by references and that I have not plagiarised the work of others.

ACKNOWLEDGEMENTS

I would like to thank Dr. Samantha Alsbury, Dr. Simon Richardson, and Professor Guy Tear for their support and guidance throughout the project.

ABSTRACT

A major facet of nervous system development entails the projection of axons from neuronal cell bodies towards synaptic partners, such as other neurons or muscles. This process, referred to as "axon guidance," relies upon receptors on axons detecting secreted or membrane-associated guidance cues within the developing organism, which attract or repel axons. While many cues and receptors have been identified over the last few decades, many within studies of the relatively simple fly embryonic nervous system, bioinformatic analyses of the *Drosophila* proteome suggest numerous uncharacterised proteins might be implicated in directing axonal growth. Such proteins are predicted to be expressed at the cell membrane, to harbour domains common to established axon guidance proteins, and to be expressed in the nervous system while axons are extending. The current study focuses on three genes predicted to encode proteins with the above characteristics: *CG7565, CG31814*, and *otk2.* An examination of a line with a *P*-element in the coding sequence of *CG7565* revealed aberrations throughout the embryonic motor neurons. Abnormalities in these nerves were also observed in a line with a deficiency spanning *CG7565*, as well as in embryos misexpressing *CG7565* in motor neurons or somatic muscle. Motor neuron projections were absent in embryos harbouring a *P*-element in the 5' UTR of *CG31814*, which were rescued by the precise excision of the transposon. In null *otk2* mutant embryos, various motor axons were absent or abnormal, and aberrations in the same branches were apparent when misexpressing *otk2* in motor neurons or somatic muscle. Moreover, analyses of transheterozygous embryos provide evidence that *otk2* genetically interacts with the established axon guidance genes, *otk*, *sema-1a*, and *fz2*, and that *otk* interacts with *fz2*. Analysis of a line with a deficiency that removes *otk* and *otk2* revealed more severe phenotypes than were observed in single mutants, providing further support for cooperation between the off-tracks. Thus, taken together these observations implicate three largely uncharacterised genes in axon guidance and reveal novel insights into the signalling pathways in which these and established axon guidance genes participate.

Contents

Chapter 1: Introduction

1.1. The *Drosophila* embryo as a model for axon guidance

In order for an organism to function correctly, its nervous system needs to be precisely organised. A major component of nervous system development involves the navigation of axons from groups of neurons to particular targets, including other neurons and muscles (i.e., axon guidance). Human neurons, which exceed 1 trillion in number, typically make connections with over a thousand target cells (Tessier-Lavigne & Goodman, 1996), thus understanding how neuronal networks are created represents a substantial challenge.

Perhaps the most obvious benefit of using *Drosophila* embryos in investigations of axon guidance is the relative simplicity of their nervous system. This is especially true of the VNC, which, during the final stages of embryonic development, has a clear ladder-like structure, whereby each of the 'side rails' is constituted of three longitudinal tracts (running through the anterior-posterior axis) that are intersected perpendicularly by commissural tracts. Accordingly, any aberrations to this pattern that occur as a consequence of genetic manipulations can be very conspicuous. For example, in the case of *roundabout* (*robo*), *commissureless* (*comm*), and *slit* loss-of-function embryos, respectively, (1) the lateral ends of the VNC's commissures are intersected by short longitudinal projections that are contained to single segments, (2) the VNC lacks commissures almost entirely, or (3) the VNC is characterised by the collapse of the longitudinal projections onto the midline (Kidd et al., 1998a; Seeger et al., 1993). *robo* encodes a receptor for the midline repellent, Slit. In *robo* and *slit* loss-of-function embryos, longitudinal axons prematurely grow towards midline attractants, such as the netrins (Brankatschk & Dickson, 2006; Harris et al., 1996). Comm is implicated in the timely internalisation of Robo, which allows commissures to form (Kidd et al., 1998b), hence the absence of commissures in *comm* mutants.

Similarly, although not adopting such a basic structure, the embryonic motor neurons, of which there are 36 per hemisegment (Nose, 2012), innervate the muscle field via only six peripheral nerve branches: the ISN, the ISNb, the ISNd, the SNa, the SNc, and the TN (Figure 1A). Therefore, the absence, misrouting, or stalling of motor neurons can often be seen quite clearly.

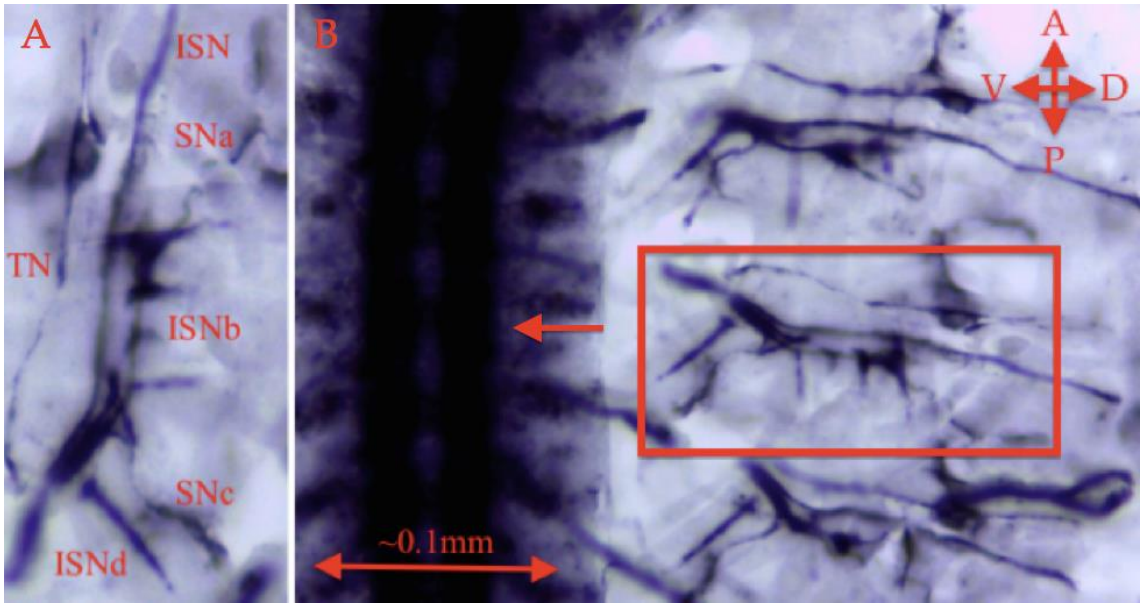

Figure 1. **The six embryonic motor neuron branches**. **A.** (right is posterior, up is dorsal) shows an individual hemisegment of a dissected wild type stage 17 embryo with the six peripheral motor neuron branches indicated: the TN, ISN, SNa, ISNb, SNc, and ISNd. **B**. The same hemisegment is shown (box), though is re-orientated (up is anterior, right is dorsal) and is flanked by two other hemisegments displaying stereotypical wild type motor neuron branch morphology. The ladder-like VNC is also indicated (arrow). Since undissected embryos are ~0.18 mm in width (Markow, Beall, & Matzkin, 2009), dissected embryos are probably ~0.57mm in width (0.18 X Pi). Thus, the right image, which shows approximately one half of a dissected embryo, represents ~0.29 mm from left to right. Embryos are ~0.51 mm in length (Markow, Beall, & Matzkin, 2009).

In addition to the simplicity of its nervous system, the *Drosophila* embryo has a number of other features that make it suitable for axon guidance research. For example, whilst axon guidance defects are likely to be lethal at later stages in development, the viability of embryos is generally unaffected. Consequently, *Drosophila* embryos allow for neurons to be studied *in situ*. This is facilitated by the availability of antibodies that allow for selective staining of specific neuronal populations (Fujita et al., 1982), such as those of the VNC (e.g., monoclonal antibody [mAb] BP102 [binding partner unknown]), sensory neurons (e.g., mAb 22C10, which binds to the microtubule-associated protein, Futsch; Hummel et al., 2000) or motor neurons (e.g., mAb 1D4, which binds to Fasciclin II [FasII]; Vactor et al., 1993]). There are also GAL4 driver lines that enable ectopic expression of genes of interest in tissues that are particularly relevant to embryonic axon guidance events. For instance, there are lines that express GAL4 pan-neuronally, in motor neurons, in the ventral midline, or in the muscle field by respectively placing the GAL4 gene under the control of the promoters of the endogenous genes, *embryonic lethal abnormal vision* (*elav*; Yao & White, 1994), *vesicular glutamate transporter* (*VGlut*; Mahr & Aberle, 2006), *single-minded* (*sim*;

Wharton et al., 1994), and *myocyte enhancer factor 2* (*Mef2*; Rangagnayakulu, Schulz & Olson, 1996).

1.2. Mechanisms of axon guidance

1.2.1. Chemoattraction and chemorepulsion

Extensive research, now spanning several decades, using common model organisms or neuronal cultures, has revealed much about the seemingly conserved mechanisms that underlie axon guidance. It is now clear that axons express receptors on their surfaces that are able to locate other neurons or organs by detecting diffused and membrane-bound signals expressed throughout the developing organism. In the case that signals are diffused, they become organised into concentration gradients, whereby signals are most abundant at their source. Growth cones, the hand-like structures adorning the tips of growing axons (described in greater depth below), are able to detect subtle differences in signal concentration, allowing them to grow away from or towards signals. Although their sensitivity to guidance cues appears to vary according to the specific 'window' of concentration to which they are exposed (i.e., higher or lower concentrations), growth cones can detect concentration differences of as little as 0.1% (Rosoff et al., 2004). In non-relative terms, Rosoff and colleagues (2004) calculate that a growth cone of 10 μm can discern between 1,000 molecules on a given side and 1,001 on the other. Even conservative estimates of growth cone sensitivity suggest that they are able to respond to 2% differences in concentration (Firtel & Chung, 2000). These results highlight the acute sensitivity of cells to concentrations of factors, an attribute that is required for migration and morphogenesis, as well as directed axonal growth.

Chemoattraction, originally suggested by Ramon y Cajal (1892, cited in Garcia-Lopez, Garcia-Marin, & Freire, 2010), describes the process of axonal growth towards secreted signals (Figure 2). Tessier-Lavigne and colleagues (1988) provided early evidence for chemoattraction through their work with the embryonic rat spinal cord. They demonstrated that the growth of commissural axons (those that cross the midline *in vivo*) from an explant in collagen gel depended upon the presence of a floor plate explant, and that the relative positioning of explants determined the direction of growth. Their observations suggested, therefore, that cells in the floor plate secrete a factor that is able to attract axons from a distance. Such signals are called "chemoattractants".

Serafini and colleagues (1994) later identified proteins that acted as chemoattractants for commissural axons in chick embryos, which they called Netrin-1 and Netrin-2. They also observed that these were homologous to a protein implicated in axon guidance in

C. elegans, UNC-6 (Ishii et al., 1992), suggesting a degree of phylogenetic conservation between vertebrates and invertebrates. Harris and colleagues (1996) subsequently identified the *Drosophila* homologues, Netrin-A (NetA) and Netrin-B (NetB). *Drosophila* embryos deficient in either protein have partially absent commissural tracts. Likewise, ectopic pan-neuronal expression of the netrins, whose secretion is normally limited to the midline, results in near-complete absence of commissures.

Whilst some research suggests an attractive role for the netrins, it is apparent that the effect a given ligand has upon axonal trajectories depends upon which receptors an axon expresses. For example, the vertebrate netrin receptor, Deleted in Colorectal Cancer (DCC), a transmembrane protein of the Ig superfamily (IgSF), is required for growth of commissural axons towards the netrin-expressing midline in rats (Keino-Masu et al., 1996). However, interactions between the receptor, Unc-5, and netrins result in chemorepulsion (axons grow away from secreted signals; Figure 2) in *Xenopus* (Hong et al., 1999). Repellent interactions between *unc-5*-expressing axons and netrins are also seen in *Drosophila* (Keleman & Dickson, 2001). Normally, axons in the VNC that express the NetA and NetB receptor, Frazzled, are attracted to the netrins in the midline; however, when *unc-5* is ectopically expressed in these axons, their capacity to enter the midline is inhibited. Complimenting this, driving expression of *netB* in the embryonic somatic musculature prevents formation of the SNa by axons that endogenously express *unc-5*. However, the phenotype is rescued in an *unc-5* loss-of-function background.

1.2.2. Contact attraction and contact repulsion

Signals are also expressed on the surface of cells and the extracellular matrix (ECM). Tissues can, therefore, act as substrates that are either permissive or prohibitive of axonal growth (Figure 2). As with long-range guidance mechanisms, the effect of a cell-surface ligand on axonal growth is related to which receptors the axon expresses; an axon with a particular set of receptors will respond to ligands in a manner that is distinct from that of an axon expressing an alternative set. Where one axon might stop upon encountering certain ligands, another might continue, allowing it to identify its appropriate stopping point. Given that the guidance molecules a cell expresses are determined by its position within the organism (just as cell type is), it is apparent that the formation of topographical maps can be explained in terms of these mechanisms.

The notion that neuronal differentiation ultimately determines connectivity was originally suggested by Sperry (1963), who made use of the regenerative capacity of amphibian axonal tracts to study the topographical relationship between retinal ganglion

cells (RGCs) and the optic tectum (the superior colliculus in mammals). By removing and rotating the eyes of frogs 180º, Sperry observed an alteration to their behaviour: they reacted to objects above them as if they were below and vice versa. This implied that, despite their reorientation, the retinal axons identified their usual targets. In turn, this lead to Sperry's postulation of the chemoaffinity hypothesis, which suggests that neurons and their targets display specific chemical tags that allow them to identify one another. Moreover, his work provided evidence against the then popular, though now inconceivable, opinion that functionality did not depend upon largely genetically predetermined neuronal networks (reviewed in Meyer, 1998).

Walter and colleagues (1987) provided additional support for the chemoaffinity hypothesis by investigating the substrate preferences of RGCs *in vitro*. Specifically, they presented retinal explants with adjacent strips of anterior and posterior chick optic tectum. In keeping with their *in vivo* behaviour, temporal retinal axons only grew on the anterior membrane, whereas nasal retinal axons showed no such preference. The results suggest that the 'tags' that axons and their targets possess are determined by their spatial location and that these are used for the establishment of appropriate connections.

It is now evident that the proteins known as the ephrins and their receptors, the ephs, are the ligands responsible for the convergent behaviour of nasal and temporal RGC axons (Drescher et al., 1995). More precisely, the 'A' family of Ephs and Ephrins is responsible for the development of this aspect of the topographical map (the anteroposterior axis). On the other hand, the 'B' family is responsible for the preferences of dorsal and ventral RGCs for lateral and medial tectum, respectively (Hindges et al., 2002). In *Drosophila*, Ephrin forms a repulsive border around the embryonic VNC that prevents *eph*-expressing interneurons from aberrantly entering the periphery (Bossing & Brand, 2002).

Unlike other guidance molecules, such as the netrins, ephrins appear to be exclusively membrane-bound (Chilton, 2006). Despite not being secreted, there is evidence that ephrins can be arranged into concentration gradients. For example, Monschau and colleagues (1997) analysed the distribution of two chick ephrin proteins with glycophosphatidylinositol (GPI) anchors, RAGS and ELF-1. Both are present in the tectum, to which retinal ganglion axons project. Using fluorescently labelled antibodies for RAGs and ELF-1, they were able to quantify the intensity of the fluorescent signals across the tectum, demonstrating that both proteins were expressed in gradients across the anteroposterior axis. As with long-range cues, axons can either grow towards (contact attraction) or away from (contact repulsion) higher concentrations of

membrane-bound ligands (Nakamoto et al., 1996; Hindges et al., 2002). The functional diversity of the ephrins, which are typically conceived of as ligands, is also evident in their capacity to initiate signalling cascades within the cells to which they are bound (Bruckner et al., 1997). Axons, therefore, are not necessarily mere navigators of their environment, but are capable of affecting it too.

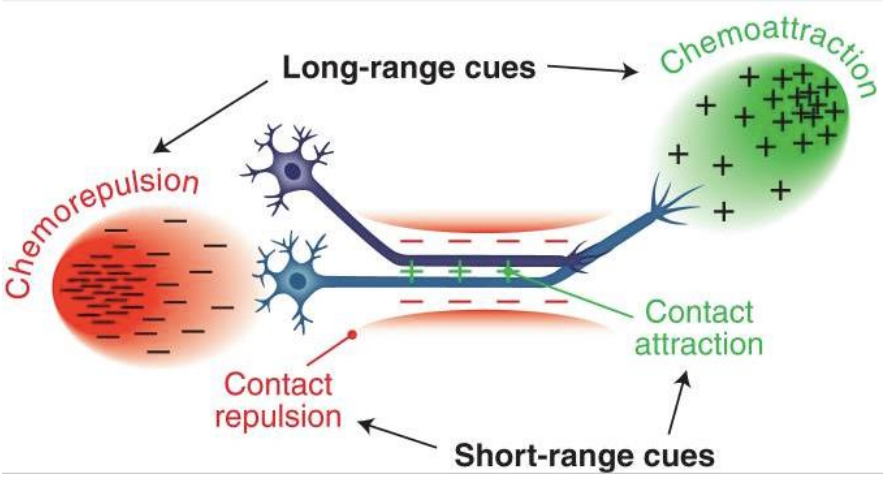

Figure 2. **Chemoattraction, chemorepulsion, contact attraction, and contact repulsion** (taken from Kolodkin & Tessier-Lavigne, 2011). Secreted signals (red) create a gradient that is implicated in the long-range repulsion of axons, whilst other secreted signals (green) create a gradient that is implicated in the long-range attraction of axons. In the centre there exists a channel (constituted of green "+" symbols) of membrane-bound molecules that are permissive of axon growth (contact attraction). Surrounding this channel are regions (constituted of red "-" symbols) containing membrane-bound molecules that are prohibitive of axon growth (contact repulsion).

1.2.3. Fasciculation

Selective fasciculation and defasciculation represent specific manifestations of contact attraction and repulsion, respectively. Within the context of axon guidance, fasciculation refers to the attachment of growing axons ("followers") to existing nerve tracts, which act as pathways towards targets. The axons responsible for the initial laying of tracts are known as "pioneers" (Harrison, 1910). Rather than requiring many cells whose signals create a gradient, the correct growth of an axon guided by existing fibres, then, might only require a small number of cells that express specific tags.

The *Drosophila* ISN (Figures 1A and 3) is a peripheral tract that is pioneered by aCC/RP2 neurons (Sánchez-Soriano & Prokop, 2005). Axons within the ISN express FasII, which is the *Drosophila* homologue of vertebrate neural cell adhesion molecules (N-CAMs; Grenningloh et al., 1991). N-CAMs mediate cell adhesion through homophilic and heterophilic interactions (Rønn et al., 1998). Whilst follower neurons of

the ISN normally coarrest with prematurely stalled aCC/RP2 neurons, the effect is significantly reduced if the pioneers do not express FasII (Sanchez-Soriano & Prokop, 2005), suggesting that followers normally fasciculate to pioneers and rely upon them for guidance.

However, followers usually need to be able to defasciculate at particular times. For instance, the 'b' branch of the *Drosophila* ISN, the ISNb (Figures 1A and 3), needs to detach from the ISN during embryonic development in order to innervate the internal ventrolateral muscles (VLMs; 6, 7, 12, & 13) and external VLMs (14, 28, & 30; Figure 3). Semaphorin 1a (Sema-1a), a transmembrane member of a large family of conserved glycoproteins, which is expressed within embryonic motor axon branches, is implicated in the appropriate defasciculation of the ISNb from the ISN. Individual axons, of the RP1, RP3, RP4, RP5 and V neurons, also fail to emerge from the ISNb in the absence of Sema-1a (Terman et al., 2002; Yu et al., 1998; Yu, Huang, & Kolodkin, 2000). The RP3 axon innervates the cleft between muscles 6 and 7; the RP1 and RP4 axons innervate muscle 13; and the RP5 and V axons innervate muscle 12 (Figure 3). Similar phenotypes are apparent in mutants that do not encode the Sema-1a receptor, PlexinA (PlexA; Winberg et al., 1998).

The incomplete penetrance of phenotypes in *sema-1a* mutants, however, alludes to there being other genes that influence defasciculation in *Drosophila* motor neurons. Indeed, a multitude of genes have been linked to the ISNb failing to defasciculate from the ISN (known as an ISNb bypass). The phenotype has been observed in loss-of-function experiments involving *kruppel* (*kr*) and *capricious* (*caps*) (Abrell & Jäckle, 2001), *notch* (Crowner et al., 2003), *beaten path* (*beat*), *fasciclin 2* (*fasII*) and *connectin* (*conn*) (Fambrough & Goodman, 1996), *leukocyte-antigen-related-like* (*lar*) (Shindelholz et al., 2001), *syndecan* (*sdc*) (Fox & Zinn, 2005), *protein tyrosine phosphatase 69D* (*ptp69D*), *protein tyrosine phosphatase 99A* (*ptp99A*), and *protein tyrosine phosphatase 10D* (*ptp10D*) (Sun et al., 2001), *rac* (Hu et al., 2001), *tolkin* (*tok*) (Meyer & Aberle, 2006), *multiplexin* (*mp*) (Meyer & Moussian, 2009), *endonuclease G inhibitor* (*endoGI*) (O'Keefe et al., 2010), *pod1* (Rothenburg et al., 2003), *sidestep* (*side*) (Sink et al., 2001), *molecule interacting with CasL* (*mical*) (Terman et al., 2002), and *caskin* (*ckn*) (Weng et al., 2011). The phenotype is also present when the expression of various genes is driven in neurons, including *plexin B* (*plexB*) (Hu et al., 2001), *mical* (Terman et al., 2002), *ckn* (Weng et al., 2011), *eve* (Labrador et al., 2005; Landgraf et al., 1999b), *abl tyrosine kinase* (*abl*) and *chromosome bows* (*chb*) (Lee et al., 2004), and *olig family* (*oli*) (Oyallon et al., 2012). The vast number of genes that have been linked to one

particular phenotype in a single embryonic branch highlights the complexity of the genetic networks that underlie the growth of axons.

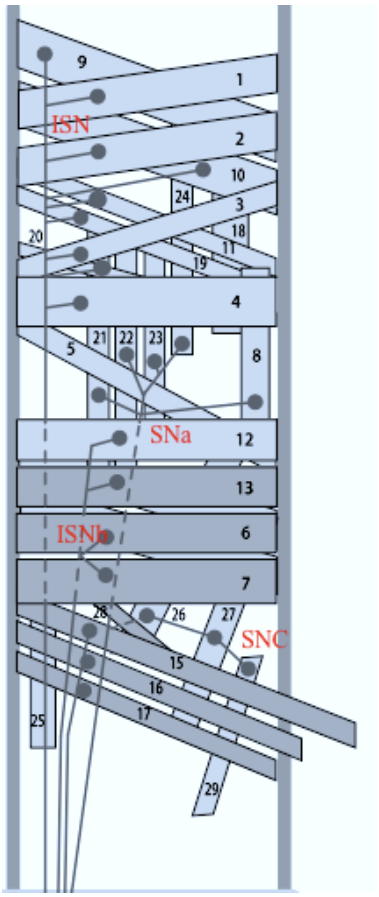

Figure 3. **Schematic of the somatic muscles and four of the motor nerves in a single hemisegment as seen from the interior of the *Drosophila* embryo** (modified from Nose, 2012; a few muscles [8, 14, 18, and 30] are not shown). In studies of axon guidance, *Drosophila* embryos, which are vaguely cylindrical, though with rounded ends, are typically dissected by cutting along the dorsal midline, removing the internal organs, and flattening the remaining tissue. Consequently, the top of the above image represents the dorsal side of the embryo, whilst the bottom is the ventral side. The posterior is towards the right. The numbers of the muscles are indicated in black and four of the six motor neuron branches of the periphery are indicated in red: the intersegmental nerve (ISN) the, intersegmental nerve "b" (ISNb), the segmental nerve "a" (SNa), and the segmental nerve "c" (SNc). See Figure 1A for the location of the remaining two peripheral motor neuron branches (the transverse nerve [TN] and the intersegmental nerve "d" [ISNd]).

1.3. Growth cone dynamics

While many guidance cues and receptors have been identified and linked to specific responses in axons, a major challenge for the field is elucidating how these interact with proteins that are implicated in orchestrating the cytoskeletal rearrangements that underlie axon guidance. As described above, the ends of growing axons are adorned

with hand-like structures referred to as growth cones, which, with their relatively large surface areas, are able to detect modest differences in cue concentrations (Firtel & Chung, 2000; Rosoff et al., 2004). The major structural components of growth cones are filamentous actin (F-actin) and microtubules, comprised, respectively, of monomeric actin (G-actin) and tubulin. In the peripheral region of the growth cone, F-actin bundles form finger-like protrusions known as filopodia, between which are sheet-like regions, known as lamellipodia, comprised of meshwork F-actin. Most microtubules terminate in a more interior region of the growth cone, known as the central domain; however, some "dynamic" microtubules pass through the hemicircumferential ring of actin, known as the F-actin arc, and into the transitional zone and peripheral domain, where they make contact with F-actin bundles (Figure 4). Many processes contribute to the dynamic reconfigurations of these structures in response to guidance cues (some of which are discussed below). However, these processes essentially all contribute to the polymerisation/stabilisation or depolymerisation/destabilisation of F-actin and microtubules, which, respectively, are associated with protrusion (e.g., towards an attractive signal) or retraction (e.g., away from a repulsive signal).

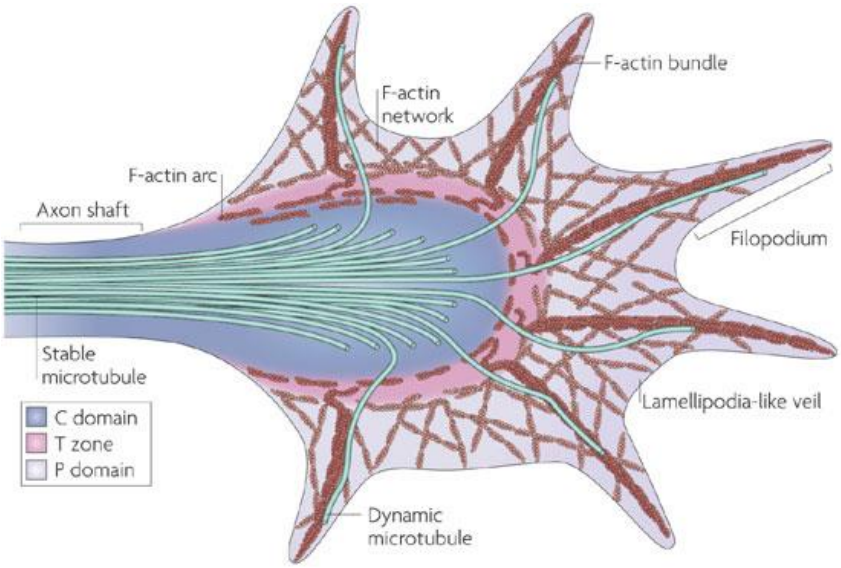

Figure 4. **The structure of the growth cone** (taken from Lowery & Van Vactor, 2009). The central domain (C domain) is comprised of stable microtubules. It is bordered by an F-actin arc, which represents the region of the transition zone (T zone). The outer region of the growth cone, the peripheral domain (P domain), is comprised primarily of F-actin bundles, which form the finger-like filopodia, and an F-actin network, which is the foundation for the lamellipodia (also known as "veils"). Dynamic microtubules also enter the peripheral domain where they make contact with F-actin bundles.

Nucleation is required for the development of filamentous actin, which refers to the forming of a stable multimer of actin monomers (Firat-Karalar & Welch, 2011). The *Drosophila* protein Dishevelled Associated Activator of Morphogenesis (DAAM) is implicated in actin nucleation (reviewed in Dent et al., 2011), which has been linked to axon guidance in the fly adult mushroom body (Gombos et al., 2015). Its activation by Dishevelled (Dsh; Liu et al., 2008), a noncanonical Wnt signalling molecule, suggests that DAAM is likely involved in axonal responses to Wnt guidance cues. Subsequent to nucleation, nascent actin filaments need to be able to accept additional monomers on their barbed ends. *Drosophila* Enabled (Ena) has been put forward as a barbed-end binding protein that is implicated in transferring actin monomers to polymerising filaments (reviewed in Dent et al., 2011). This role, however, appears to be at odds with certain experimental evidence. For example, Ena physically interacts with Robo and is required for Robo/Slit-mediated repulsive guidance (Bashaw et al., 2000), which is curious given Ena's putative role in protrusion. Similarly, overexpression of clasps, vertebrate orthologues of *Drosophila chb*, in COS cells increases stabilisation of microtubules (Akhmanova et al., 2001), which is seemingly incongruent with their mediating repellent activity. However, Lee and colleagues (2004) demonstrate *chb* is required to prevent ectopic crossing of the embryonic midline by longitudinal fascicles that are normally repelled by Slit. Genetic interactions between *chb*, *slit*, and *abl* (encoding an effector of Slit/Robo signalling) and *chb*'s expression in the growth cone suggest that Chb is implicated in affecting growth cone dynamics in response to Robo activation. Examining *Xenopus* growth cones, Lee and colleagues (2004) observed that Clasp is localised to the ends of microtubules that have entered the peripheral domain of the growth cone. However, *clasp* overexpression prevents microtubule advance and growth cone translocation. They propose, therefore, that microtubule stabilisation might inhibit dynamic microtubules, and thus might contribute to repellent responses.

The processes described above – actin nucleation and polymerisation, and microtubule stabilisation – are generally thought to occur in regions of the growth cone responding to attractive cues. Thus, in response to repellent signals these processes are likely minimised in the appropriate region of the growth cone. At the same time, however, reactions to repellent cues are also mediated in an active fashion. For example, the *Drosophila* protein Molecule interacting with CasL (Mical) has been shown to bind and disassemble F-actin and F-actin bundles (Hung et al., 2010). Congruent with this, Mical binds to PlexA and is implicated Sema-1a/PlexA-mediated repulsive guidance in embryonic motor axons (Terman et al., 2002).

1.4. Axon guidance and nervous system disorders

A number of developmental disorders have been linked to axon guidance genes. For example, as discussed above, Robo is a *Drosophila* immunoglobulin (Ig) protein required for the correct development of nerve tracts in the CNS (Kidd et al., 1988a; Kidd et al., 1998b; Seeger et al., 1993). Anitha and colleagues (2008) found that certain single nucleotide polymorphisms (SNPs) within human *robo3* and *robo4* were more prevalent in a sample of individuals with autism (characterised by communicative and social impairment) than in controls. They also reported that levels of *robo1* and *robo2* mRNA were reduced in the autistic group. Although members of the robo family have been linked to a number of developmental processes, including differentiation of serotonergic neurons (Couch et al., 2004), there is evidence that connections between brain areas implicated in social behaviour are disrupted in autism (reviewed in Grady & Keightley, 2002), suggesting that *robo*'s association with autism may be linked to its role in axon guidance.

Abnormal growth of axons might also underlie other developmental disorders, such as dyslexia, the symptoms of which are associated with SNPs in *robo1* (Mascheretti et al., 2014). Also, recent research indicates that whether *robo*-expressing axons in *Drosophila* grow towards or away from Slit depends upon interactions with Down Syndrome Cell Adhesion Molecule 1 (Dscam1; Alavi et al., 2015), an axon guidance molecule that, in its 38,016 possible isoforms, can confer upon developing neurons unique identities, thus promoting self-avoidance and maximising synaptic field coverage (Hattori et al., 2008; Neves et al., 2004; Schmucker et al., 2000). As the name implies, human *Dscam*, which can partially rescue lethality and dendritic aberrations in *Drosophila* larvae (Huang et al., 2011), is located in the Down syndrome critical region on the 21st chromosome and is thought to contribute to the condition (Yamakawa et al., 1998). Human *Dscam* has also been linked to bipolar disorder, a condition characterised by periods of depression and mania; Kenji and colleagues' (2008) analyses of bipolar and control postmortem brains revealed an association between bipolar and certain polymorphisms in *Dscam*, which, in turn, were linked to altered levels of *Dscam* mRNA. Interestingly, specific polymorphisms within the netrins have also been associated with bipolar disorder, contributing to the notion that aberrant miswiring might contribute to the condition (Eastwood et al., 2008). A greater understanding of how such molecules are implicated in *Drosophila* axon guidance will likely facilitate insights into various mental disorders, especially those of a neurodevelopmental origin.

Although the wiring of an organism's nervous system occurs during development, some researchers have proposed that axon pathfinding defects might predispose individuals to develop neurodegenerative diseases, which are typically associated with old age. Lesnick and colleagues (2007), for example, suggest that Parkinson's disease (PD) might be related to aberrant axonal growth during development. PD is characterised by pathology in the basal ganglia; specifically, there is a dopamine deficiency in the striatum and dopaminergic neurons in the substantia nigra die. Symptoms include tremor, rigidity, and bradykinesia (slowness of movement; reviewed in Davie, 2008). Lesnick and colleagues (2007) identified 1,460 SNPs associated with 117 axon guidance genes that are expressed in human brain and determined that a number of these could be used to produce models that could predict PD susceptibility, age of onset, and survival. They also observed that expression of a proportion of the genes in these models was altered in brain areas that are affected in PD. SLIT2, for instance, was down regulated in the substantia nigra. In *Drosophila*, Slit acts as the ligand for Robo, repelling axons that would otherwise aberrantly cross the midline (Brose et al., 1999; Kidd et al., 1999a; Seeger et al., 1993). In mice, Slit2 appears to have a similar function; axons in ascending dopamine pathways erroneously cross the midline, resulting in a reduction of dopaminergic neurons innervating the striatum in *slit2* mutants (Kawano et al., 2003). Taken together, these studies provide support for the "miswiring hypothesis" of PD.

As alluded to above, there is also evidence that axon guidance defects might underlie certain psychotic conditions, such as schizophrenia and bipolar disorder. Both disorders have been linked to variations in neuregulin 1 (NRG1) (Williams et al., 2003; Heron et al., 2005), which, in mice, is implicated in neuronal migration and axon guidance (Cautinat et al., 2006). Magnetic Resonance Imaging (MRI) of populations with schizophrenia and bipolar suggest that they present with reduced white matter (largely constituted of axons) in the anterior limb of the internal capsule (ALIC; McIntosh et al., 2005). McIntosh and colleagues (2008) observed that, in a population unaffected by either disorder, white matter density and integrity (i.e., integrity of the myelin that insulates axons), as assessed by MRI and Diffusion Tensor MRI (DTI), respectively, varied according to genotypes at a locus of a SNP within NRG1. The SNP is in the promoter region of NRG1 and a particular allele that is more prevalent in schizophrenia is associated with increased levels of mRNA of an individual NRG1 isoform in postmortem hippocampus (Law et al., 2006). These findings imply that alterations to NRG1 expression influence susceptibility to schizophrenia and bipolar and that this relationship might depend upon NRG1's role in axon guidance.

It is evident, therefore, that our current understanding of various neurological disorders has been enhanced by having identified axon guidance genes. However, Hill and colleagues (2012) argue that it is also likely that the development of stem cell-based treatments for neurological deficits will require a comprehensive understanding of the phenotypes of induced neurons, including (but not limited to) their expression of and response to axon guidance cues. Knowing which factors specific induced neurons express will allow for predictions to be made about how axons might integrate with endogenous cells if placed in an organism at a particular place and time. Characterising stem cell-derived neurons depends on a more fundamental understanding of which genes are implicated in axon guidance, as well as of the mechanisms that they utilise.

1.5. Development of the embryonic motor axons

It has been established above that secreted and membrane/ECM-bound cues attract or repel axons depending on the receptors that axons express, and that axons themselves can express factors on their surfaces that mediate de/fasciculation. Ultimately, these secreted and membrane-associated proteins alter growth cones dynamics. Of course, these processes are evident in developing *Drosophila* embryonic motor neurons, which first appear in the periphery at stage 14, when the two pioneer axons of the ISN, aCC and RP2, grow out of the CNS (Sink & Whittington, 1991). These cells use a range of pre-established structures to navigate towards the dorsal muscle field, including the trachea, sensory neurons, and muscle precursors, known as persistent twist (PT) cells (Bate et al., 1991; Vactor et al., 1993). A number of other cells subsequently grow along the ISN and also innervate dorsal muscles (1, 2, 3, 4, 9, 10, 11, 18, 19, 20; Vactor et al., 1993). Two of the most prominent structures of the ISN are its first (FB) and second (SB) lateral branches. Approximately, 10 genes have been linked aberrations in the formation of the FB and SB (Appendix A).

At around stage 15, the SNa exits the CNS, establishing a tract that is distinct from the ISN, and projects dorsolaterally to innervate the lateral muscles (5, 8, 21, 22, 23, 24; Sink & Whittington, 1991; Vactor et al., 1993). With the ISN and SNa in place, the ISNb, ISNd, and SNc have tracts to follow to their approximate final destinations. The ISNb initially grows in close contact to the ISN, but disassociates from it in order to innervate the internal (6, 7, 12, 13) and external (14, 28, 30) VLMs (Vactor et al., 1993). Innervation of the internal VLMs does not occur until late stage 16, when the RP3 axon innervates the cleft between muscles 6 and 7, RP1 and RP4 axons (MN13s) innervate muscle 13, and RP5 and V axons (MN12s) innervate muscle 12 (Inaki et al., 2007; Kurusu et al., 2008). There are many reports of the ISNb failing to disassociate

from the ISN and/or failing to develop the finer projections that innervate the internal VLMS (see ISNb, RP3, MN12s, and MN13s in Appendix A); ~70 genes have been linked to aberrant ISNb development. From the ISNb, the ISNd projects ventrolaterally to innervate a subset of the ventral muscles (15,16, 17). Likewise, the SNc projects ventrolaterally from the SNa to innervate the remaining ventral muscles (26, 27, 29; Vactor et al., 1993). Relative to the ISNb, defects in the ISNd and SNc are less frequently reported (Appendix A). In the abdominal segment boundaries, two axons of the TN (TMN25, TMNp) project from the CNS to form a tract with a peripheral neuron, the lateral bipolar neuron. Collectively, these cells innervate muscle 25, as well as the alary muscles attached to the heart and aorta (Gorczyca et al., 1994; Thor & Thomas, 1997).

1.6. Identifying novel axon guidance candidates

Bioinformatic analyses of the fly proteome have revealed numerous uncharacterised proteins that are potentially involved in axon guidance. Vogel and colleagues (2003), for example, identified *Drosophila* proteins of the IgSF that are predicted to be secreted or localised to the cell membrane. These conclusions were based on algorithms that identify signal sequences (SignalP; Nielsen et al., 1999; indicative that proteins will be processed within the secretory pathway), transmembrane helices (TMHMM; Krogh et al., 2001), and GPI anchors (Predictor programme; Eisenhaber et al., 1999). It is noteworthy that proteins with Ig domains are known to have a prominent role in cell-cell communication, including the aforementioned netrins, plexins, and semaphorins.

The expression profiles of a number of these uncharacterised, secreted/membrane-associated proteins have since been investigated in *Drosophila* embryos using *in situ* hybridization (Alsbury et al., in preparation). Three proteins that are expressed in the nervous system towards the end of embryonic development, Otk2, CG7565, and CG31814, are the focus of the current study, which used immunohistochemistry (IHC) to determine whether embryonic motor axonal development was aberrant in loss- and gain-of-function populations.

Out of the candidate genes, *otk2* was selected for further investigation on the basis of its paralogy to an established axon guidance gene, *off-track* (*otk*; Alsbury et al., in preparation; Linnemannstöns et al., 2014; Vogel et al., 2003), which, through its involvement in the semaphorin signalling pathway, is implicated in the guidance of embryonic motor axons (Winberg et al., 2001).

otk is related to vertebrate Protein Tyrosine Kinase 7 (PTK7). PTK7 has been associated with various types of cancer. For example, Chen and colleagues' (2014) metaanalysis of 13 microarray datasets based on over 2,000 lung samples indicated that *ptk7* expression is higher in adenocarcinomas relative to normal lung tissue. Application of short hairpin RNA (shRNA) to adenocarcinoma cell lines decreased viability and increased apoptosis. Similarly, injecting cells with reduced *ptk7* expression into mice implanted with adenocarcinoma tissue resulted in reductions in tumour size. Analogous results have been reported for cancer of the bile duct (intrahepatic cholangiocarcinoma [ICC]; Jin et al., 2014). *ptk7* has also been linked to a range of developmental processes (reviewed in Peradziryi et al., 2012), including planar cell polarity (PCP). Mice mutant for *ptk7* exhibit defects in neural tube closure and polarity of inner ear hair cells (Lu et al., 2004). *ptk7* also plays a role in migration. The migration of chick heart cells in the conotuncal segment is promoted through interactions between PTK7 and Plex-A1, which together comprise a receptor complex for Sema6D (Toyofuku et al., 2004). Conversely, interactions between Plex-A1 and Endothelial Growth Factor Receptor Type 2 are associated with inhibited migration in the ventricle, suggesting that the presence of alternative coreceptors for Plex-A1 can initiate contrasting outcomes. The notion that PTK7/Otk can act as a molecular switch has also been proposed within the context of Wnt signalling; respectively, binding of Low Density Lipoprotein Receptor-related Protein 6 (LRP6) or PTK7 to Frizzled receptors is associated with activation of canonical (β-catenin/Armadillo-dependent) and non-canonical (β-catenin/Armadillo-independent) Wnt signalling pathways (reviewed in Peradziryi et al., 2012). Although limited, there is also evidence that *ptk7* is implicated in axon growth. Yamada and colleagues (2007) observed reduced neurite extension in human neuroblastoma cell cultures (SH-SY5Y) in which *ptk7* expression was inhibited with small interfering RNA (siRNA).

Otk2 co-immunoprecipitates with Otk, as well as other proteins known to affect embryonic motor neuron development (Linnemannstöns et al., 2014); namely, Frizzled 2 (Fz2; Inaki et al., 2007) and Wnt2 (Liebl, McKeown, & Hing, 2010). Although *otk2* has been linked to genital development (Linnemannstöns et al., 2014), its role in axon guidance has not been investigated.

While there are no fly homologues of CG7565, it is related to two human and two mouse proteins, referred to in both organisms as KIAA0319 and KIAA0319-like (KIAA0319L). There is evidence that implies that mouse and human KIAA0319 are implicated in nervous system development (Masuda et al., 2009; Paracchini et al.,

2006). Additionally, polymorphisms within human KIAA0319 and KIAA0319L are associated with developmental dyslexia (DD; Couto et al., 2008; Mascheretti et al., 2014). Congruent with this, variations in KIAA0319 affect white matter volume in language-associated brain areas (Darki et al., 2012).

CG31814 was deemed to be of particular interest because of its belonging to a novel four-member family of uncharacterised proteins (Alsbury et al., in preparation). Moreover, CG31814 is a putative Defective in Proboscis Extension Response (Dpr) interacting protein (DIP; Ozkan et al., 2013), members of which have been linked to larval motor axon guidance (Kurusu et al., 2008).

1.7. Aims

Various factors suggest, therefore, that Otk2, CG7565, and CG31814 are likely implicated in embryonic nervous system development; these include their expression within the nervous system, their predicted secreted/membrane-associated localisation, and evidence of the roles of their homologues. The current study aimed to investigate, using immunohistochemistry, whether altering the activity of the genes encoding these three proteins influenced the formation of the embryonic motor axons. Moreover, given that Otk2 is paralogous to Otk (Alsbury et al., in preparation; Linnemannstöns et al., 2014; Vogel et al., 2003), which is implicated in Sema-1a signalling (Winberg et al., 2001), and that Otk and Otk2 bind Fz2 (Linnemannstöns et al., 2014), the study aimed to investigate, by analysing the motor axons of transheterozygous embryos, whether there are genetic interactions between the genes encoding Otk, Otk2, Sema-1a, and Fz2.

Chapter 2: Methodology

2.1. Culture conditions

Flies were kept at 25°C on standard agar-cornmeal-glucose-yeast food.

2.2. DNA extraction, PCR and gel electrophoresis

DNA was taken from individual adult flies, which were ground within 1.5 ml tubes with pipette tips in 24 µl of a buffer containing 10 mM Tris-Cl (pH 8.2), 1 mM ethylenediaminetetraacetic acid (EDTA), and 25 mM NaCl. A further 25 µl of buffer was subsequently added, along with 1 µl (20 µg) of proteinase K (*Sigma-Aldrich*, USA), and samples were incubated for 0.5 h at 56 °C, followed by 2 minutes (min) at 95 °C. Samples were next centrifuged for 15 min at 13,000 RPM, following which 45 µl of the supernatant was transferred to a new 1.5 ml tube and stored at -20 °C.

PCRs to be used exclusively for gel electrophoresis were run with 10 µl DreamTaq DNA polymerase (*Thermo Scientific*, USA), 0.8 µl forward primer (0.8 pM), 0.8 µl reverse primer (0.8 pM), 1 µl DNA template, and 7.4 µl sterile distilled water (SDW) (20 µl total volume). PCRs were initially heated to 94 °C for 180 seconds (s), followed by 35 cycles of 94 °C for 30 s (denaturation), 55 °C for 30 s (annealing), and 72 °C for 120 s (elongation), followed by a single stage of 72 °C for 300 s. 10 µl of the PCR products and 10 µl GeneRuler 100 bp or 1 kb GeneRuler DNA ladder (*Thermo Scientific*, USA) were run in 1 % agarose gels (1 g agarose [*Fisher Scientific*], 100 ml sodium borate buffer [0.5 mM, *Fisher Scientific*, USA]) containing 4 µl (1:25.000) Gel Red Nucleic Acid Stain (*Biotium*) for 0.75 h using a *Consort* (Belgium) EV245 power source (500 mA, 250 V, 50 W) and a *Galileo Bioscience* (USA) tray (model: 80-1214). Gels were photographed with a *Synoptics* (UK) 3.0 MP camera within a *Syngene* (UK) InGenius3 gel dock in conjunction with version 1.2.5.0 *GeneSys* (USA) software.

2.3. DNA preparation for sequencing

PCRs to be used for sequencing were run as described above, though 50 µl, rather than 20 µl, PCRs were run, thus 25 µl DreamTaq DNA polymerase, 2 µl forward primer (2 pM), 2 µl reverse primer (2 pM), 2.5 µl template, and 18.5 µl SDW were used. Larger PCRs were used to ensure that sufficient DNA would be obtained for sequencing. 10 µl of PCR products were run in 1% agarose gels as described above to check that the reaction had worked. The remaining 40 µl was cleaned using *Pan-Biotech*'s (Germany) PAN DNA clean solution. The 40 µl PCR product was incubated in a 1.5 ml tube at room temperature for 10 min with 80 µl PAN DNA clean solution, and then centrifuged

at 13,000 RPM for 10 min. The supernatant was then replaced with 80 µl 70 % molecular biology grade ethanol (*Fisher Scientific*, USA) and centrifuged at 13,000 RPM for 10 min. The ethanol was removed and the DNA resuspended in 10 µl SDW. DNA concentration was determined using a BioDrop-uLITE (*Imgen Technologies*, USA), and samples were diluted with SDW to adhere to the concentrations specified by *Eurofins* (Luxembourg) before being sent for sequencing.

2.4. Egg collection and immunohistochemistry

Flies were placed for 21 h at 25 °C in a "large" embryo collection cage (*Genesee Scientific*, USA) containing a 100 mm x 20 mm dish (*BD Biosciences*, USA) approximately half full of set Grape Juice (*Genesee Scientific*, USA). Embryos were transferred to a mesh fixed between a 50 ml plastic tube, which had been cut in half, and its lid. Embryos were transferred by covering the Grape Juice with distilled water and pipetting them onto the mesh, allowing the embryos to be separated from the water. Embryos were dechorionated (removal of the outer chorion layer, as well as the impermeable and opaque vitelline membrane) by soaking them in 50 % general purpose grade sodium hypochlorite solution (*Fisher Scientific*, USA) for 5 min, and then washed with distilled water. Using a small paintbrush, embryos were transferred from the mesh to a 1.5 ml tube containing a fixing solution consisting of 450 µl phosphate-buffered saline (PBS; 0.01M; *Fisher Scientific*, USA), 500 µl heptane (*Fisher Scientific*, USA), and 50 µl formaldehyde (*Fisher Scientific*, USA). Embryos were incubated for 0.5 h (all incubations were completed at room temperature with rotation). The bottom half of the solution, containing PBS and formaldehyde, was removed and replaced with 500 µl methanol (*Fisher Scientific*, USA). The tube was shaken vigourously by hand for 1 min to remove the embryos from their vitelline membranes. The membranes localise to the interface between the methanol and heptane, whilst the embryos fall to the bottom of the tube. The membranes and solution were removed and the embryos were washed with 300 µl of methanol three times (washes entail pipetting a solution into the tube, which causes the embryos to become suspended before returning to the bottom of the tube). Methanol was replaced by 300 µl PBT (99.5% 0.01M PBS, 0.5% Triton X-100 [*Fisher Scientific*, USA]) and the embryos were incubated twice for 5 min and once for 0.5 h. Embryos were then incubated for 0.5 h in 285 µl PBT and 15 µl normal goat serum (NGS; *Sigma-Aldrich*, USA) for 0.5 h. Embryos were then incubated for 2 h in 285 µl and 15 µl of new PBT and NGS, respectively, as well as 60 µl (1:5) mAb 1D4 (*Developmental Studies Hybridoma Bank*, USA), which stains motor neurons and interneurons (Vactor et al., 1993), and 1.5 µl anti β-gal (*Promega*, USA), which binds

β-gal in embryos with *CyOwg* chromosomes, allowing for the identification of heterozygotes. (Some experiments utilised Otk and Otk2 antibodies [Linnemannstöns et al., 2014] instead of 1D4, which, respectively, were used at 1:500 [0.6 µl] and 1:100 ratio [3 µl]). Embryos were then washed with 300 µl PBT three times, incubated with 300 µl PBT four times for 15 min, incubated with 300 µl PBT for 0.5 h, and incubated with 285 µl PBT and 15 µl NGS for 0.5 h. Embryos were then incubated for 2 h in 285 µl and 15 µl of new PBT and NGS, respectively, as well as 1 µl (1:300) alkaline phosphatase (AP)-conjugated goat anti-mouse IgG (*Sigma-Aldrich*, USA) (in experiments with the Otk and Otk2 antibodies, 1 µl (1:300) of AP-conjugated goat anti-guinea pig IgG [*Sigma-Aldrich*, USA] and 1 µl of AP-conjugated goat anti-rabbit IgG [*Sigma-Aldrich*, USA], respectively, were used). Embryos were then washed three times with 300 µl PBT, then incubated with 300 µl PBT four times for 15 min, then washed twice in AP buffer (0.1 M NaCl, 0.05 M MgCl2, 0.1 M tris[hydroxymethyl]aminomethane [pH 9.5], 0.2 % Triton-X 100), and incubated in AP buffer for 10 min. To initiate the colour reaction, the AP buffer was replaced with 400 µl 5-bromo-4-chloro-3-indoyl-phosphate/nitro blue tetrazolium (BCIP®/NBT) Liquid Substrate System (*Sigma-Aldrich*, USA), and the embryos and solution were transferred to a well of a 24-well plate (*Thermo Scientific*, USA) and were observed through a 4 x light microscope (*Medline Scientific Limited*, UK) for ~15 min or until the staining allowed for the neurons to be seen clearly. Embryos were then transferred back to the 1.5 ml tube and were washed three times with 300 µl PBT, incubated with PBT three times for 10 min, and washed once with PBS. Embryos were kept in a solution of 70% glycerol (*Fisher Scientific*, UK) and 30% PBS, and were stored at 4 °C.

2.5. Dissections and microscopy

Using tungsten needles, embryos were filleted from the dorsal side to create flat-mount preparations under a *Nikon* (Japan) SMZ800 microscope in 70 % glycerol on a *Sail Brand* (China) glass slide (25.4mm x 76.2 mm, 1–1.2mm thick). This involved rolling embryos onto their ventral side (the location of the VNC), cutting along the anteroposterior axis of the dorsal midline, removing organs, and flattening the remaining tissue, thereby revealing the VNC and peripheral nerves. Dissected embryos were mounted under *Menzel-Gläser* (Germany) coverslips (22 mm x 22 mm, 0.13–0.17 mm thick). Images of embryos were taken with a *Leica* (Germany) DM500 microscope at 40 x in conjunction with *Leica* (Germany) LAS EZ software.

2.6. Statistical analyses

Hemisegments from abdominal segments A2–A7 were assessed for phenotypes in both wild type and non-wild type embryos. These hemisegments are generally used in axon guidance studies because the basic pattern of their axons is consistent between hemisegments. Conversely, A1 and A9, and the thoracic hemisegments, each exhibit distinct axon morphologies. For a given phenotype, each hemisegment was classified as being phenotypically normal or exhibiting one or more abnormal phenotypes. Therefore, classifications resulted in categorical frequency data. Differences in the frequencies of phenotypes between wild type and non-wild type genotypes were, therefore, investigated with chi-squared tests of independence. However, in instances where expected counts were lower than five, Fisher's exact test was instead employed (Fisher, 1922).

Version 20 of *IBM*'s (USA) Statistical Package for the Social Sciences (SPSS) was used to complete statistical analyses. Most analyses of motor axon phenotypes were conducted on data derived from late stage 16 and stage 17 embryos, which, in wild types, have fully developed motor axons. The following analyses were based exclusively on late stage 16 and stage 17 embryos: RP3 axon absent, MN13s absent, MN13s anterior, MN13s anterior and posterior, MN12s absent, MN12s anterior, SNa aberrant bifurcation. The RP3 axon, the MN13s, the MN12s, and SNa are depicted in, for example, Figure 11. While these projections do not form until late stage 16, other branches are fully formed by the start of stage 16. Therefore, in order to increase statistical power, some analyses included early/mid stage 16 embryos, as well as late stage 16 and stage 17 embryos. The following analyses were based on this wider range of ages: ISNb absent, ISNd absent, SNc absent, FB absent, SB absent, and SB anterior. The ISNb, ISNd, SNc, FB, and SB are depicted in, for example, Figure 11.

Chapter 3: *EY03841*17*

3.1. Introduction

Vogel and colleagues (2003) identified all members of the *Drosophila* immunoglobulin superfamily (IgSF). Ig proteins have important roles during development, and many have been linked to axon guidance in *Drosophila*, including Down syndrome cell adhesion molecule 1 (Dscam1) (Hummel et al., 2003; Sawaya et al., 2008; Schmucker et al., 2000; Shi et al., 2007; Wang et al., 2002; Wojtowicz et al., 2004), Sidestep (Side) (Meyer et al., 2006; Siebert et al., 2009; Sink et al., 2001), Fasciclin 3 (Fas III) (Suzuki et al., 2000), Neuromusculin (Nrm) (Kurusu et al., 2008), Off-track (Otk) (Cafferty et al., 2004; Winberg et al., 2001), Protein tyrosine phosphatase 69D (Ptp69D) (Desai et al., 1996; Jeon et al., 2008; Sun et al., 2001), Beaten path Ia (Beat-Ia) (Fambrough & Goodman, 1996; Zarin et al., 2014), and Beat-IIIc (Inaki et al., 2007). Using programmes that recognise glycophosphatidylinositol (GPI) anchors (Predictor), transmembrane helices (Transmembrane Hidden Markov Model [TMHMM]), or signal sequences (SignalP), they were able to determine whether the 142 Ig proteins they identified were secreted or expressed at the cell surface. Further analyses identified the presence of non-Ig domains. Consequently, they were able to categorise proteins according to whether or not they exclusively harboured Ig domains and according to whether they were predicted to be secreted or expressed at the cell surface. Categorisations also took into account experimental evidence of the functions of characterised Ig proteins. Otk2, then known as CG8964, was identified as belonging to a class of cell-surface receptors harbouring cytoplasmic domains with kinase or phosphatase activity and extracellular domains comprised exclusively of Ig or Fibronectin type III (FnIII) domains. The two other members of this class, Otk and Ptp69, have been linked to axon guidance in the fly peripheral and central nervous systems (Cafferty et al., 2004; Desai et al., 1996; Jeon et al., 2008; Sun et al., 2001; Winberg et al., 2001). Over a region of 433 amino acids, Otk2 exhibits 53% identity to Otk (Vogel et al., 2003).

More recently, Linnemannstöns and colleagues (2014) proposed that Otk and Otk2 are paralogues that arose from a gene duplication event that occurred in *Drosophila* species, though not other arthropods. This assertion is based on the sequence similarity between the Off-tracks (similar to Vogel et al., 2003, they report 53% identity over 427 amino acids) and the fact that *otk* and *otk2* are located next to each other on the 2nd chromosome. While their Basic Local Alignment Search Tool (BLAST) analyses

indicate that Otk2 is the most closely related *Drosophila* protein to Otk, the second and third hits, respectively, were Ror and Heartless. While there is no experimental evidence pertaining to the molecular function or biological processes in which Ror participates, it is expressed in the embryonic nervous system (Wilson et al., 1993). There is direct evidence, however, that Heartless is implicated in the development of the ventral nerve cord (VNC; Olofsson & Page, 2005; Shishido et al., 1997). Linnemannstöns and colleagues (2014) propose that Otk is a 114 kD protein with a cytoplasmic kinase homology domain and five extracellular Ig domains and that Otk2 is a 48 kD protein with a short cytoplasmic domain of 69 amino acids and three extracellular Ig domains. Their co-immunoprecipitation (Co-IP) experiments suggest that Otk and Otk2 can form homodimers, as well as form heterodimers with each other (via interactions between their transmembrane domains) and with Frizzled (Fz), Frizzled 2 (Fz2), and Wnt2. They report that both *otk* and *otk2* are expressed within the embryonic and larval central nervous systems, including within neuronal processes in the VNC and within photoreceptor neurons.

This description of *otk* expression is consistent with previous reports of Otk distribution (Pulido et al., 1992) and with evidence of its role in axon guidance within the embryonic VNC (Winberg et al., 2001) and larval photoreceptor cells (Cafferty et al., 2004). Winberg and colleagues also provide evidence that Otk is implicated in embryonic motor axon guidance and suggest that it forms part of a receptor complex with Plexin-A (Plex-A), which is the receptor for the neuronally-expressed repellent, Semaphorin-1a (Sema-1a; Terman et al., 2002; Winberg et al., 2001; Winberg et al., 1998; Yu et al., 1998; Yu, Huang, & Kolodkin, 2000). Linnemannstöns and colleagues' (2014) Co-IP results suggest, however, that Otk and Otk2 might also participate in Wnt signalling pathways, which have been linked to axon guidance and synaptic development in the fly (Inaki et al., 2007; Liebl et al., 2010; Sato et al., 2006; Yoshikawa et al., 2003). While genetic interactions between the off-tracks, frizzleds, and semaphorins are explored in the subsequent chapter, where more detailed descriptions of the reports immediately above are provided, the current study initially sought to determine whether embryos lacking *otk2* activity would exhibit defects within the motor neurons. This was approached by attempting to imprecisely excise a transposon located within the intergenic region next to the 5' UTR of *otk2*. The full details of the crossing scheme and the screening process are described in the results section below. A list of the flies referred to in the thesis is provided in Appendix D.

3.2. Results

Investigating whether *otk2* is implicated in embryonic motor axon guidance was initially approached by attempting to delete all or part of its sequence by imprecisely excising a transposon in the intergenic region (IGR) adjacent to *otk2*'s 5' UTR in a line referred to *EY03841* (*y^1 w^{67c23}*; *P{EPgy2}EY03841/CyO*). It was first necessary to establish the reported position of the transposon in this line.

3.2.1. Confirming the position of the *EY03841* insertion

To confirm the reported location of the transposon in the *EY03841* line, a primer was acquired that had been designed to bind within EY transposons, 111 bp from the 3' end, referred to as "EY.3.F" (Hoskins et al., 2011). This was used in conjunction with the forward primer of a pair referred to as "8964 insertion," which were initially designed for an alternative purpose (discussed below). The 8964 insertion forward primer binds to the 5' UTR of *otk2*, 116 bp from its 5' end and 144 bp from the reported position of the transposon in the IGR (Figure 5 depicts the relative positions all of genomic regions and primers referred to in this results section). Thus, the 8964 insertion forward and EY.3.F primers should produce a 297 bp (111 bp + 144 bp + 42 bp [combined length of primers]) product with *EY03841* DNA. A sequenced PCR product corresponded to this length. The electropherogram (not shown) was inspected for sample quality; only a region of 176 bp, in which each nucleotide had a *Eurofins* quality score of >=30 (indicating at least 99.9% accuracy of base call), was used for comparisons. The derived sequence was entered into BLAST to search for matching sequences within the *Drosophila* genome. Ninety-six bp of the *EY03841* DNA aligned to the wild type 5' UTR of *otk2* and the adjacent IGR until the reported position of the transposon (Figure 6A). Next, the 176 bp sequence was entered into BLAST as a query and the 111 bp between the 3' end of the transposon and the start of the EY.3.F primer was entered as a subject. The previously unaccounted for 80 bp (176 bp – 96 bp) aligned to the 3' end of the transposon (Figure 6B). These results therefore support the reported position of the insertion.

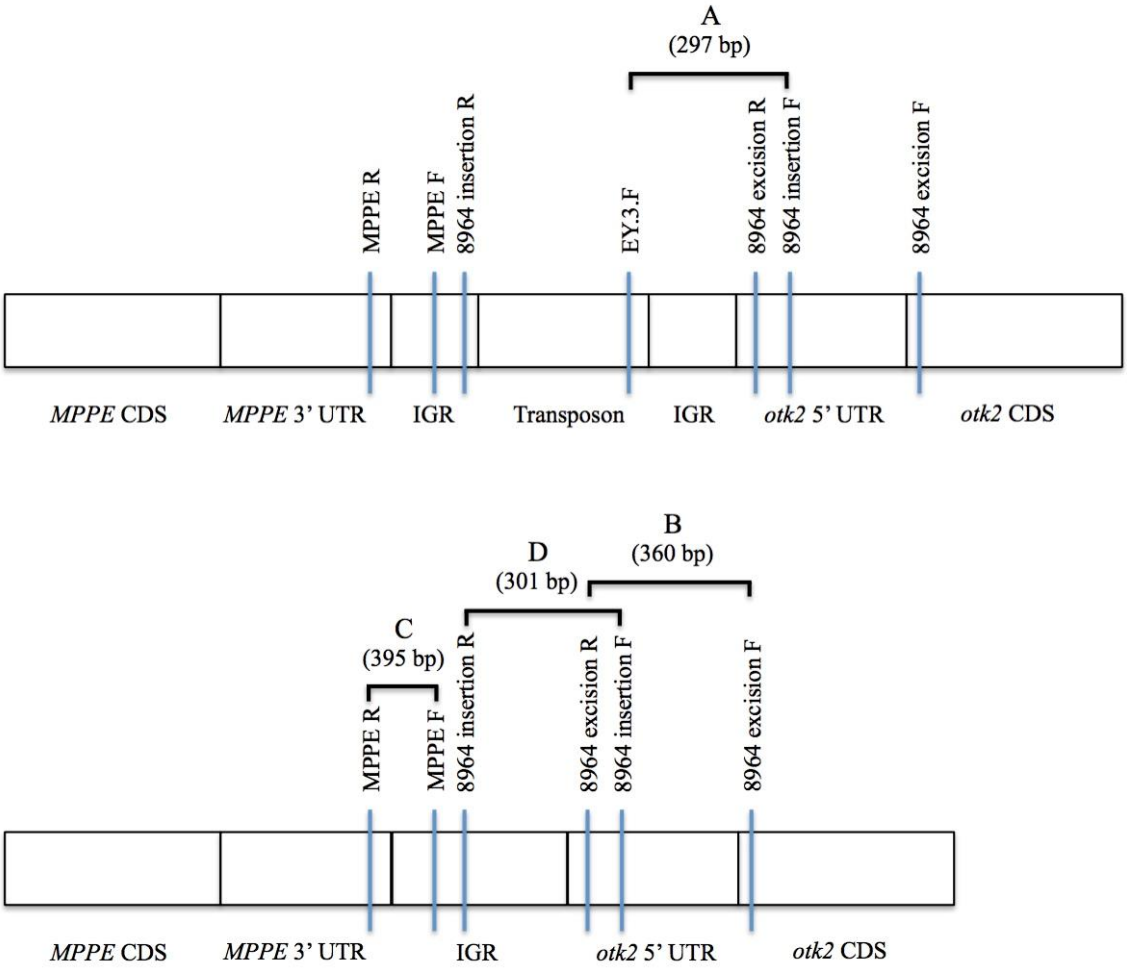

Figure 5. **The relative positions of genomic regions and primers**. The images depict the relative positions of genomic regions (not to scale) referred to in the results section of this chapter in *EY03841* (top) and *EY03841*17* DNA (bottom). The relative positions of the primers are represented by blue vertical lines. MPPE F and 8964 insertion R are depicted as binding to discrete regions of DNA, though in reality there is overlap between the regions they bind to. EY.3.F and 8964 insertion F (A) were used to confirm the reported position of the transposon in *EY03841* DNA (see "Confirming the position of the *EY03841* insertion"). 8964 excision F and 8964 excision R (B) were used to screen lines in which the transposon had been removed, with the hope of identifying imprecise excision-mediated deletions (see "Screening for imprecise excisions"). MPPE F and MPPE R (C) were used to provide evidence that *MPPE* had not been affected by the removal of the transposon in *EY03841*17* flies (see "Screening for imprecise excisions"). 8964 insertion F and 8964 insertion R (D) were used to create PCR products for sequencing the prior region of the transposon in order to molecularly characterise the effect of its removal in *EY03841*17* flies (see "Precise characterisation of the putative imprecise excision *EY03841*17*).

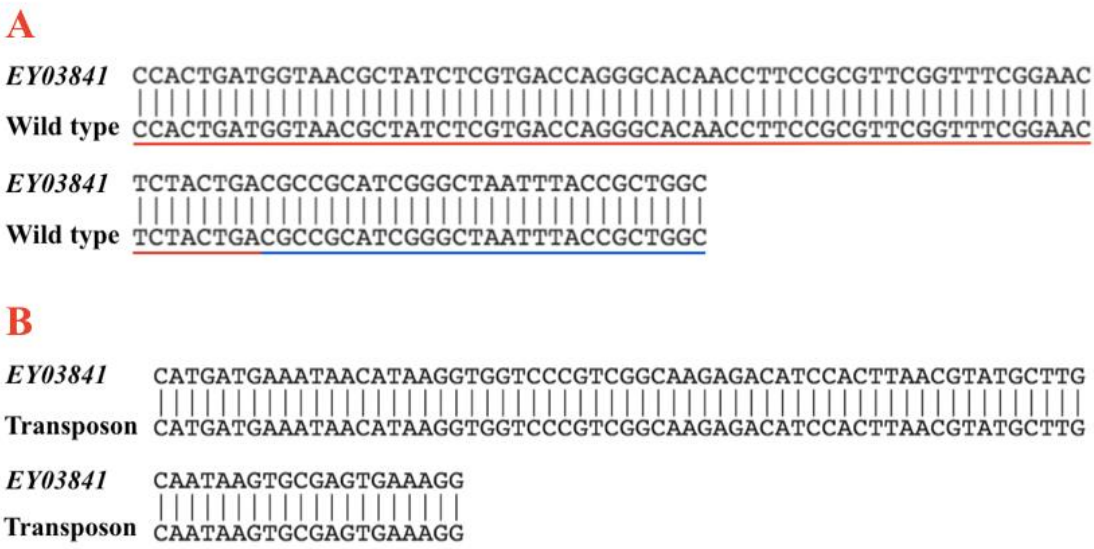

Figure 6. **The transposon in the *EY03841* line is in its reported position**. A PCR was run with homozygous *EY03841* DNA with 8964 insertion forward and EY.3.F primers, which, respectively, bind the 5' UTR of *otk2* and the 3' end of EY transposons. The transposon is reported to be in the IGR adjacent to the 5' UTR of *otk2*. The PCR product was sequenced and the 176 bp sequence was aligned to the *Drosophila* genome (**A**) and the EY transposon (**B**). Ninety-six bp of the sequence aligns to the 5' UTR of *otk2* (underlined in red) and the adjacent IGR (underlined in blue) as far as the reported position of the transposon. The remaining 80 bp of the sequence aligns to the transposon.

3.2.2. Removal of the transposon and screening for imprecise excisions

Having established the position of the transposon, *EY03841* flies were crossed to flies possessing transposase activity (*w*; *Sp/CyO*; *Sb*, *Δ 2-3/TM6b*, *Δ 2-3*) in order to remove the transposon, with the hope of doing so imprecisely, thereby removing *otk2* coding sequence. The following crossing scheme was used:

♂♂ y^1w^{67c23}; *P{EPgy2}EY03841/CyO; +/+* X ♀♀ *w; Sp/CyO; Sb, Δ 2-3/TM6b, Δ 2-3*

↓

♂ y^1w^1; *P{EPgy2}EY03841/CyO; Sb, Δ 2-3/+* X ♀♀ *w; Sco/CyOwg; +/+*

↓

♂ y^1w^1; *P{EPgy2}EY03841/CyOwg; +/+* X ♀♀ *w; Sco/CyOwg; +/+*

↓

♂♂ y^1w^1; *P{EPgy2}EY03841/CyOwg; +/+* X ♀♀ y^1w^1; *P{EPgy2}EY03841/CyOwg; +/+*

To assess whether the excision had resulted in any offspring with deletions affecting *otk2*, primers (referred to as "CG8964 excision") were designed to amplify a 360 bp product in the region of the 5' end of *otk2*. Specifically, the forward primer binds within the first exon of *otk2*, and the reverse primer binds within the 5' UTR of *otk2*, 80 bp from the insertion site in the IGR (Figure 5; Appendix B). These were applied to DNA from lines in which the transposon had been removed. It was assumed that, had an excision removed genetic material within the region of the primers, PCR would not work or products would be reduced in length, which could be assessed by gel electrophoresis. The primers were only applied to DNA from flies that were homozygous for the *EY03831* chromosome (as indicated by the absence of the curly wing phenotype seen in heterozygotes with the *CyOwg* balancer). Of the 80 screened populations, DNA from one line, referred to as *EY03841*17*, repeatedly did not produce a band with the 8964 excision primers, suggesting that an imprecise excision had been achieved. Bands were consistently seen when using DNA from wild types or other populations in which the transposon had been excised (Figure 7). Moreover, it was observed that there were few straight-winged flies (homozygotes) in the *EY03841*17* population, indicating that they possibly harboured a semi-lethal mutation.

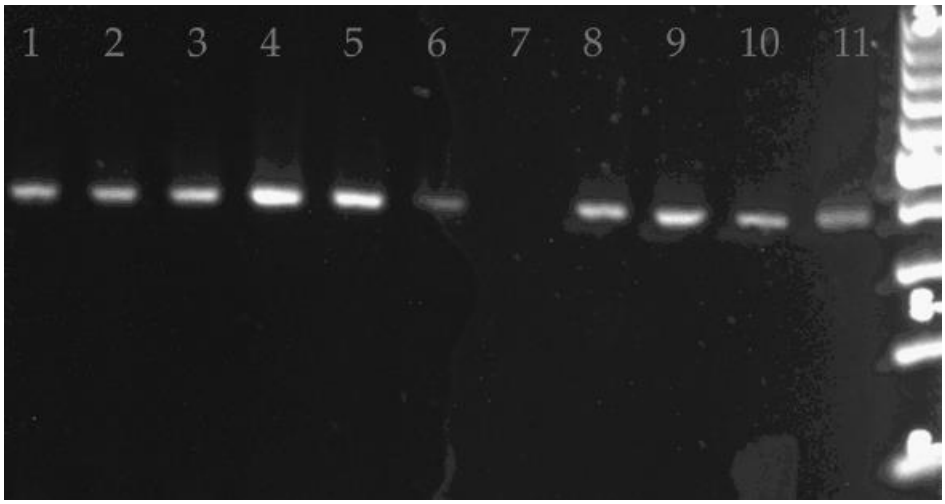

Figure 7. **Gel electrophoresis image of *EY03841* excision line and wild type DNA amplified with CG8964 excision primers**. Lanes 1-6 and 8-10 show bands derived from *EY03841* excision lines other than *EY03841*17*. Lane 11 shows a band derived from wild type DNA. These bands, which correspond to the expected product size of 360 bp (the 4th band from the bottom of the 100 bp ladder [right] corresponds to DNA of 400 bp), suggest that the excision of the *EY03841* transposon was precise. The absence of a band in lane 7, into which a PCR product from *EY03841*17* DNA was loaded, suggests that one or both of the primers was/were unable to bind to its/their target DNA, implying that the sequence in this region had been affected by an imprecise excision of the transposon.

Having obtained evidence that suggested that the excision of the transposon in the *EY03841*17* line had disrupted *otk2*, it was necessary to determine whether the gene on

the other side of the IGR, *MPPE*, had been affected. Primers referred to as "MPPE" were designed to assess this (Figure 5; Appendix B). The forward primer was designed to bind DNA within the IGR, 117 bp from the insertion site and 176 bp from the 3' end of *MPPE*; the reverse primer was designed to DNA within the 3' UTR of *MPPE*, 178 bp from its 3' end. These primers produced bands of the expected size (395 bp), suggesting that *MPPE* had not been influenced by the excision of the transposon (Figure 8).

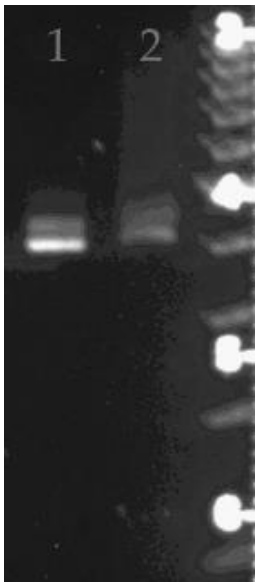

Figure 8. **Gel image of *EY03841*17* and wild type DNA amplified with MPPE primers**. Lane 1 shows a band derived from *EY03841*17* DNA and lane 2 shows a band derived from wild type DNA. Both are adjacent to the 4th band from the bottom (representing DNA of 400 bp) of the 100 bp ladder (right), which is consistent with the expected product size of 395 bp. The presence of a band in lane 1 suggests that *MPPE* was not affected by the excision of the transposon in the *EY03841*17* line.

3.2.3. Precise characterisation of the putative imprecise excision in *EY03841*17*

To characterise the putative imprecise excision in the *EY03841*17* line on a molecular level, primers ("8964 insertion") were designed to bind either side of where the transposon had been, so that the region could be sequenced. The forward primer was designed to bind within the 5' UTR of *otk2*, 116 bp from the IGR; the reverse primer was designed to bind within the IGR, 115 bp from the insertion site (Figure 5; Appendix B). The expected product size was 301 bp. A sequenced PCR product corresponded to this length. The electropherogram (not shown) was inspected for sample quality; only a region of 232 bp, in which each nucleotide had a *Eurofins* quality score of >=30 (indicating at least 99.9% accuracy of base call), was used for comparisons. The derived sequence was entered into BLAST to search for matching sequences within the *Drosophila* genome. The *EY03841*17* DNA aligned to the wild type 5' UTR of *otk2*

and the adjacent IGR. Unexpectedly, there was no evidence of a deletion in the prior position of the transposon, though three non-adjacent nucleotides in the IGR and two non-adjacent nucleotides in the 5' UTR of *otk2* differed from the wild type sequence (Figure 9). Since no differences were observed between the parent line (*EY03841*) and wild type sequences (Figure 6A), these alternative nucleotides are thought to be a consequence of the excision, though the precise mechanisms are not clear.

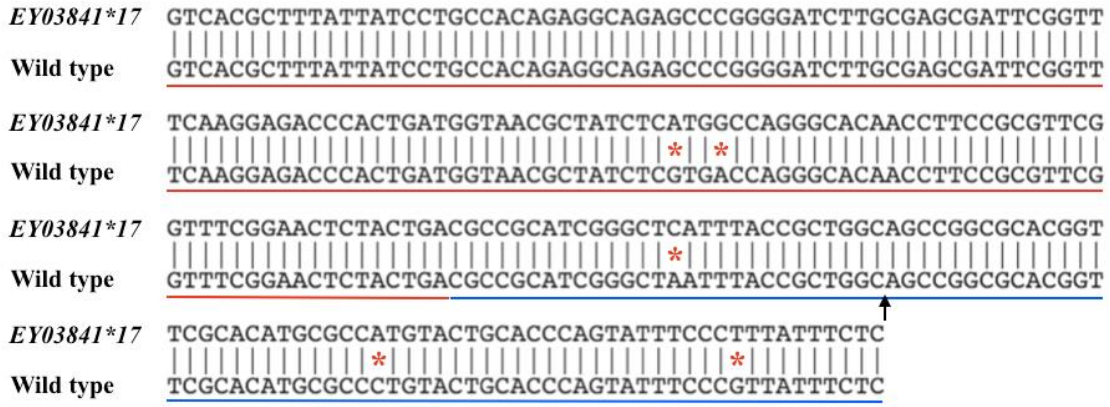

Figure 9. **A comparison of *EY03841*17* and wild type DNA between the 8964 insertion primers**. No deletion was evident in the prior position of the transposon (black arrow), though three nucleotides in the IGR (underlined in blue) and two nucleotides in the 5' UTR of *otk2* (underlined in red) differed between genotypes (asterisks).

3.2.4. *otk2* is expressed *EY03841*17* embryos

While the sequencing data suggested that the excision of the transposon in the *EY03841*17* line had not created a genomic deletion, it remained possible that the altered nucleotides within *otk2*'s 5' UTR had affected its expression. While this was not tested quantitatively (e.g., with real-time PCR [RT-PCR]), thus keeping open the possibility that *otk2* expression is dysregulated in *EY03841*17* flies, immunohistochemistry with an Otk2 antibody (Linnemannstöns et al., 2014) indicated that *otk2* was expressed in *EY03841*17* embryos (Figure 10C; a more detailed description of *otk2* expression is provided in Figure 19, Chapter 4).

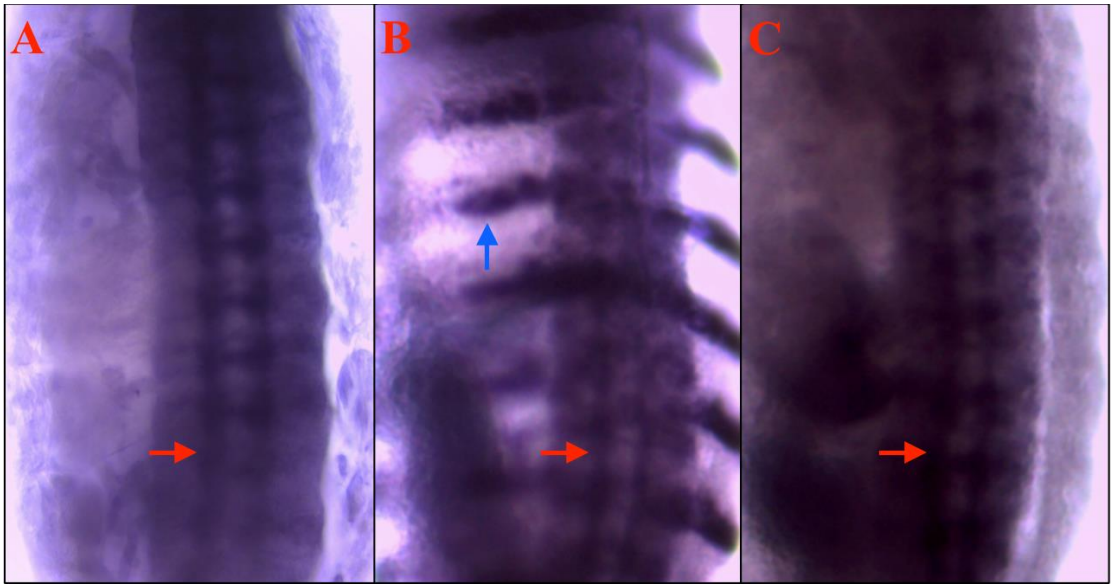

Figure 10. ***otk2* expression in wild type and heterozygous and homozygous *EY03841*17* embryos**. **A.** Wild type. Staining is evident in the ventral nerve cord (red arrow). **B.** *EY03841*17* heterozygote. Staining is evident in the ventral nerve cord (red arrow). In addition to the Otk antibody, an anti β-gal antibody was utilised to identify embryos with the CyOwg chromosome (i.e., heterozygotes), in which the *wingless* enhancer drives expression of β-gal in abdominal stripes (blue arrow). **C.** Abdominal stripes are not apparent, indicating that the embryo is homozygous for the *EY03841*17* chromosome. However, there is staining in the ventral nerve cord (red arrow), suggesting that *otk2* is expressed in *EY03841*17* homozygotes.

3.2.5. Phenotypic analysis: *EY03841*17*

Despite a lack of evidence for the disruption of *otk2*, several severe and highly penetrant abnormalities were identified in the motor axons of *EY03841*17* embryos. In certain cases, entire branches appeared to be absent; namely, the ISNb (Figure 12), ISNd (Figure 13), and SNc (Figure 15). In other cases, specific projections that extend from main branches were absent; namely, the lateral or dorsal branches of the SNa (Figure 14), and the first (FB; Figure 16) and second (SB; Figure 17) branches of the ISN. The full length of a wild type hemisegment, with the branches that are abnormal in *EY03841*17* embryos indicated, is shown in Figure 11 for reference.

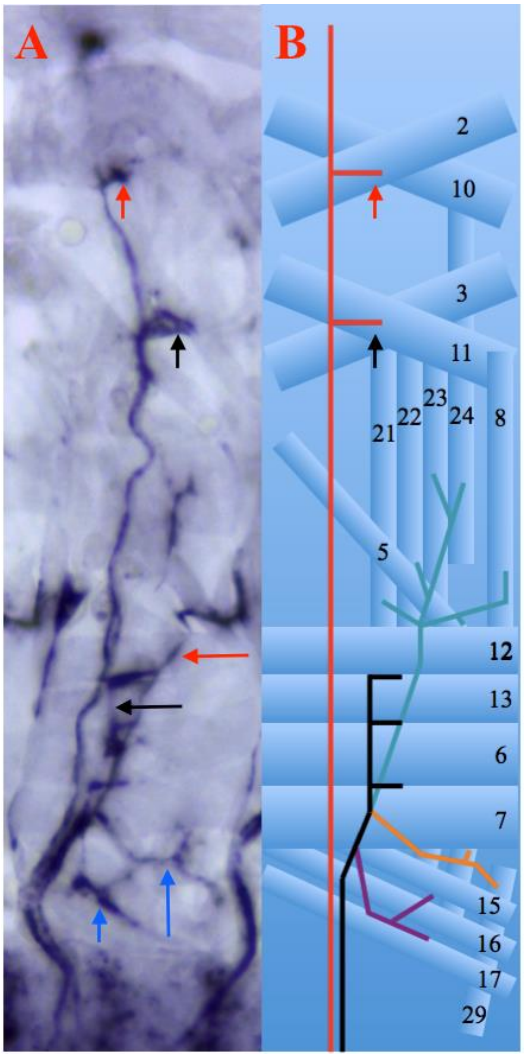

Figure 11. **A wild type hemisegment with the branches that are abnormal in *EY03841*17* embryos indicated**. **A.** A photomicrograph of a wild type hemisegment with the branches that are abnormal in *EY03841*17* embryos indicated (right is posterior, up is dorsal): SB (short red arrow), FB (short black arrow), SNa (long red arrow), ISNb (long black arrow), SNc (long blue arrow), ISNd (short blue arrow). **B.** A schematic of a wild type hemisegment with the same branches indicated (right is posterior, up is dorsal): ISN (red) with FB (short red arrow) and SB (short black arrow), SNa (turquoise), ISNb (black), SNc (orange), and ISNd (purple). The muscles innervated by these branches are indicated by numbers. Two of the muscles innervated by the SNc, 26 and 27, are shown but not labelled. Muscles not innervated by the affected branches are not shown.

ISNb absent

The ISNb was absent more often in *EY03841*17* hemisegments (73.2%) than in wild types (2%), (Figure 12).

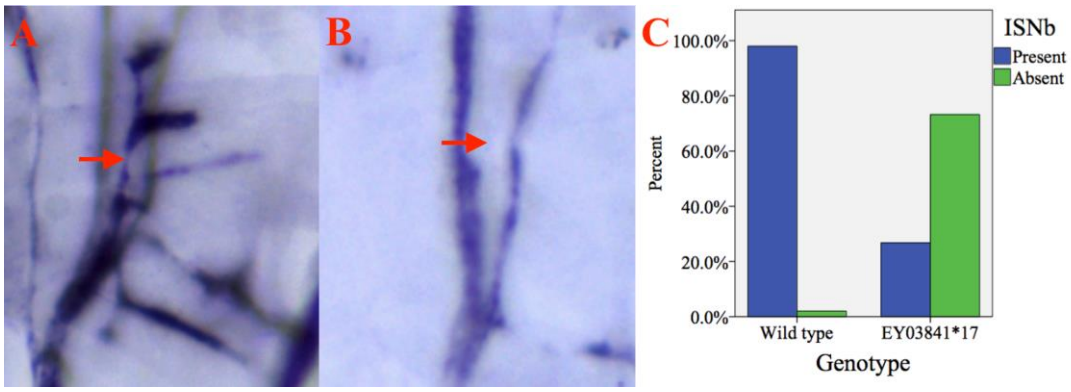

D	ISNb present	ISNb absent
Wild type	98% (240)	2% (5)
*EY03841*17*	27% (30)	73% (82)

Figure 12. Image A (right is posterior, up is dorsal) shows the ventral section of a wild type hemisegment with the ISNb (red arrow). Image B (right is posterior, up is dorsal) shows the ventral section of an *EY03841*17* hemisegment without the ISNb (red arrow). The graph (C) shows the percentage of hemisegments with and without the ISNb in 30 wild type and 20 *EY03841*17* embryos. The table (D) shows the percentage and number (in parentheses) of hemisegments with and without the ISNb.

A chi-square test for independence revealed that the ISNb was absent significantly more often in *EY03841*17* hemisegments than in wild types, χ^2 (1, n = 357) = 211.25, p < .001.

ISNd absent

The ISNd was absent more often in *EY03841*17* hemisegments (94.3%) than in wild types (17.7%), $p < .001$ (Figure 13).

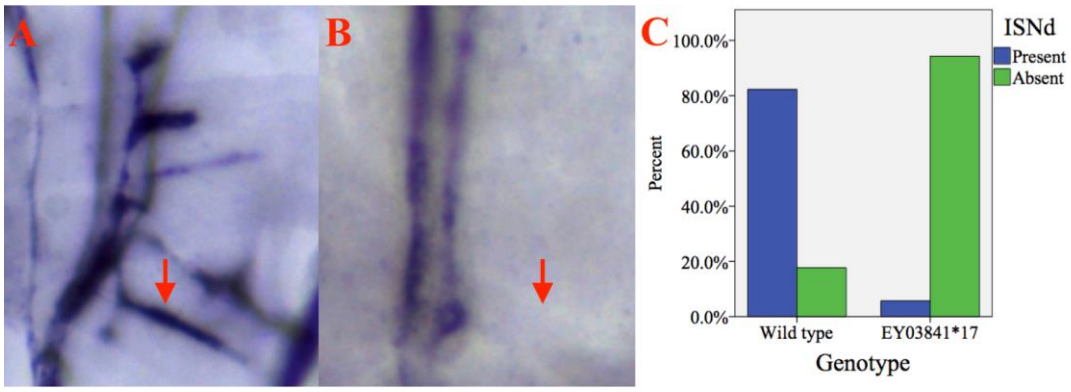

D	ISNd present	ISNd absent
Wild type	82.3% (144)	17.7% (31)
*EY03841*17*	5.7% (7)	94.3% (116)

Figure 13. Image A (right is posterior, up is dorsal) shows the ventral section of a wild type hemisegment with the ISNd (red arrow). Image B (right is posterior, up is dorsal) shows the ventral section of an *EY03841*17* hemisegment without the ISNd (red arrow). The graph (C) shows the percentage of hemisegments with and without the ISNd in 30 wild type and 20 *EY03841*17* embryos. The table (D) shows the percentage and number (in parentheses) of hemisegments with and without the ISNd.

A chi-square test for independence revealed that the ISNd was absent significantly more often in *EY03841*17* hemisegments than in wild types, χ^2 (1, n = 298) = 169.54, $p <$ .001.

SNa aberrant bifurcation

In wild types, the SNa bifurcates, producing dorsal and lateral branches. In *EY03831*17* embryos, the dorsal and/or lateral branches were occasionally absent (Figure 14). Bifurcation is normal (both branches are present) in 96.3% and 72% of wild type and *EY03831*17* hemisegments, respectively. The dorsal branch is absent in 0.9% of wild type hemisegments and 11.4% of *EY03831*17* hemisegments. The lateral branch is absent in 2.8% of wild type hemisegments and 16.7% of *EY03831*17* hemisegments.

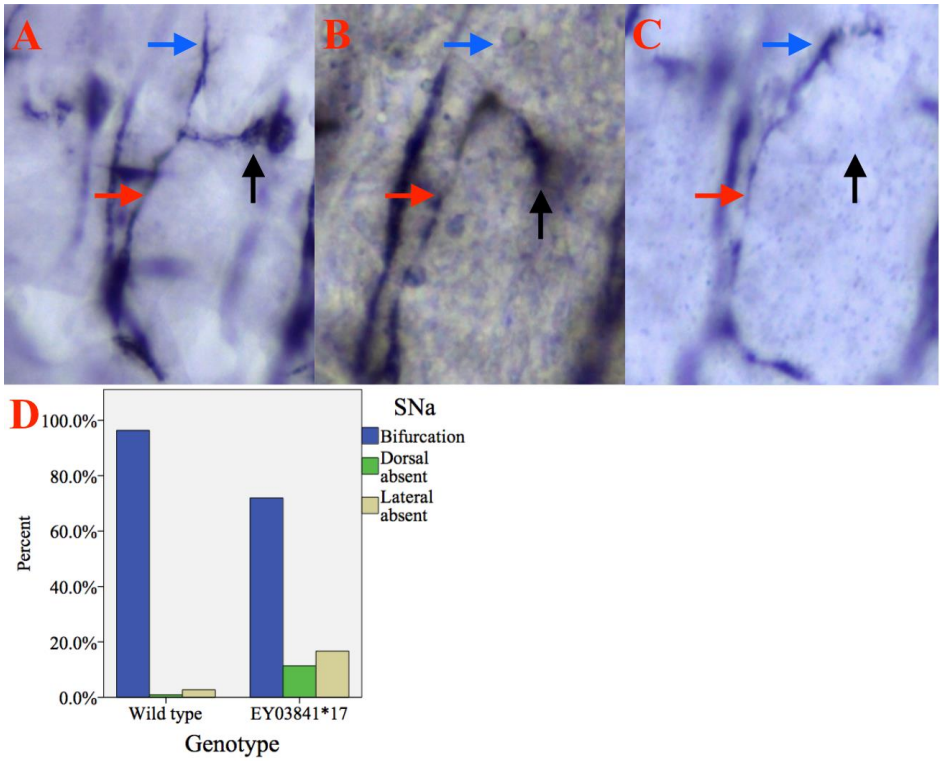

E	Bifurcated	Dorsal branch absent	Lateral branch absent
Wild type	96.3% (105)	0.9% (1)	2.8% (3)
*EY03841*17*	71.9% (95)	11.4% (15)	16.7% (22)

Figure 14. Image A (right is posterior, up is dorsal) shows the ventral section of a wild type hemisegment with a bifurcated SNa (red arrow), with the dorsal (blue arrow) and lateral (black arrow) branches indicated. Image B (right is posterior, up is dorsal) shows the ventral section of an *EY03841*17* hemisegment with a SNa (red arrow) with the lateral branch (black arrow), though without the dorsal branch (blue arrow). Image C (right is posterior, up is dorsal) shows the ventral section of an *EY03841*17* hemisegment with a SNa (red arrow) with the dorsal branch (blue arrow), though without the lateral branch (black arrow). The graph (D) shows the percentage of hemisegments in which the SNa bifurcates or lacks the dorsal or lateral branches in 30 wild type and 20 *EY03841*17* embryos. The table (E) shows the percentage and number (in parentheses) of hemisegments in which the SNa bifurcates or lacks the dorsal or lateral branches.

A chi-square test for independence revealed a significant effect of genotype with regard to bifurcation of the SNa, χ^2 (2, n = 241) = 25.23, p < .001.

SNc absent

The SNc was absent more often in *EY03841*17* hemisegments (53.1%) than in wild types (7.5%) (Figure 15).

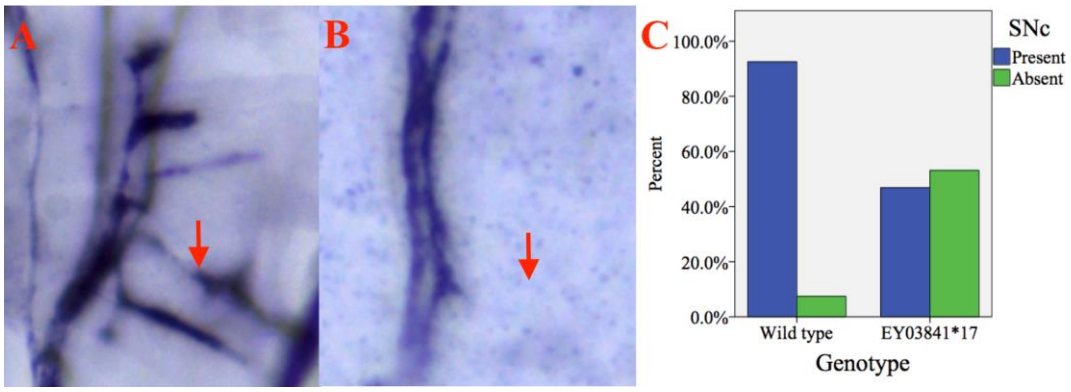

D	SNc present	SNc absent
Wild type	92.5% (161)	7.5% (13)
*EY03841*17*	46.9% (60)	53.1% (68)

Figure 15. Image A (right is posterior, up is dorsal) shows the ventral section of a wild type hemisegment with the SNc (red arrow). Image B (right is posterior, up is dorsal) shows the ventral section of an *EY03841*17* hemisegment without the SNc (red arrow). The graph (C) shows the percentage of hemisegments with and without the SNc in 30 wild type and 20 *EY03841*17* embryos. The table (D) shows the percentage and number (in parentheses) of hemisegments with and without the SNc.

A chi-square test for independence revealed that the SNc was absent significantly more often in *EY03841*17* hemisegments than in wild types, χ^2 (1, n = 302) = 78.31, p < .001.

FB absent

The FB was absent more often in *EY03841*17* hemisegments (62.4%) than in wild types (7.6%) (Figure 16).

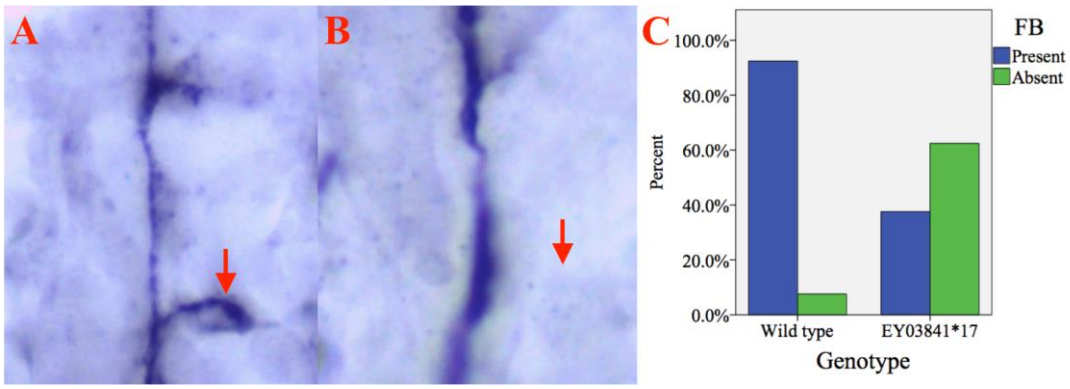

D	FB present	FB absent
Wild type	92.4% (195)	7.6% (16)
*EY03841*17*	37.6% (56)	62.4% (93)

Figure 16. Image A (right is posterior, up is dorsal) shows the dorsal section of a wild type hemisegment with the FB (red arrow). Image B (right is posterior, up is dorsal) shows the dorsal section of an *EY03841*17* hemisegment without the FB (red arrow). The graph (C) shows the percentage of hemisegments with and without the FB in 30 wild type and 20 *EY03841*17* embryos. The table (D) shows the percentage and number (in parentheses) of hemisegments with and without the FB.

A chi-square test for independence test revealed that the FB was absent significantly more often in *EY03841*17* hemisegments than in wild types, χ^2 (1, n = 360) = 124.38, p < .001.

SB absent

The SB was absent more often in *EY03841*17* hemisegments (70.9%) than in wild types (30.7%) (Figure 17).

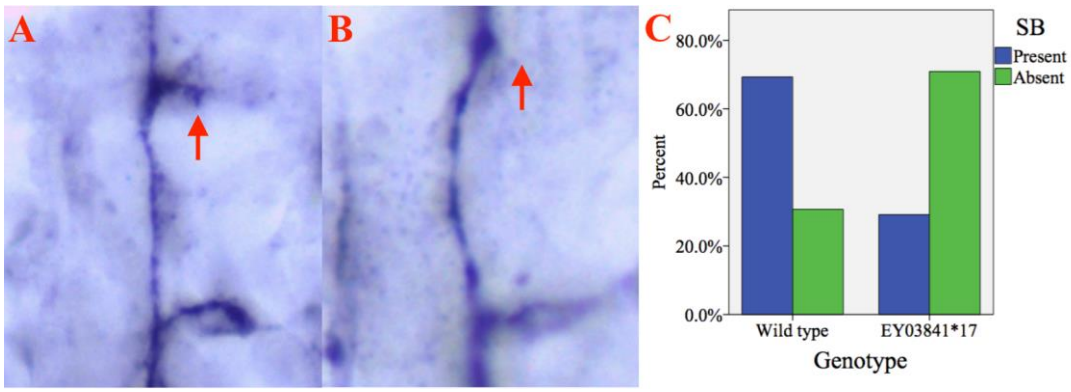

D	SB present	SB absent
Wild type	69.3% (70)	30.7% (31)
*EY03841*17*	29.1% (30)	70.9% (73)

Figure 17. Image A (right is posterior, up is dorsal) shows the dorsal section of a wild type hemisegment with the SB (red arrow). Image B (right is posterior, up is dorsal) shows the dorsal section of an *EY03841*17* hemisegment without the SB (red arrow). The graph (C) shows the percentage of hemisegments with and without the SB in 30 wild type and 20 *EY03841*17* embryos. The table (D) shows the percentage and number (in parentheses) of hemisegments with and without the SB.

A chi-square test for independence revealed that the SB was absent significantly more often in *EY03841*17* hemisegments than in wild types, χ^2 (1, n = 204) = 32.95, p < .001.

3.3. Discussion

Vogel and colleagues (2003) identified Otk2 as a transmembrane Ig protein whose structure resembles the established axon guidance protein, Otk (Cafferty et al., 2004; Winberg et al., 2001). They suggested that the Off-tracks belong to a class of proteins that also includes PTP69D, which has also been linked to axon guidance (Berger et al., 2008; Desai et al., 1996; Grueber et al., 2007; Jeon et al., 2008; Sun et al., 2001). Linnemannstöns and colleagues (2014) provided evidence that, in addition to forming homodimers, the Off-tracks physically interact with each other, as well as with other proteins (Fz, Fz2, Wnt2) that have been shown to underlie axon guidance and synaptic development in the fly embryonic motor neurons and visual system (Inaki et al., 2007;

Liebl et al., 2010; Sato et al., 2006). Given the associations between these proteins and Otk2, the current study sought to determine whether Otk2 is implicated in the development of the embryonic motor axons.

This was approached by attempting to imprecisely excise a transposon reported to be located within the intergenic region by the 5' UTR of *otk2*. The position of the transposon was first confirmed through PCR and sequencing (Figure 6). Offspring in which the transposon had been excised were screened for imprecise excisions with PCR. DNA from the line referred to as *EY03841*17* was consistently associated with an absence of bands when using primers ("8964 excision") designed to amplify a product based on the sequence between the first exon of *otk2* and its 5'UTR (Figure 7). While the absence of bands suggested that the excision had been imprecise, sequenced PCR products of ~300 bp, derived from the application of the "8964 insertion" primers, which bound either side of the prior insertion site, indicated that no genetic material had been deleted. Several nucleotides in the *EY03841*17* DNA did, however, differ from the *EY03841* and wild type DNA, including two in the 5' UTR (Figure 9). This raised the possibility that expression of *otk2* might have been altered in *EY03841*17* embryos. Although this remains a possibility, the utilisation of an Otk2 antibody indicated that *otk2* is expressed in *EY03841*17* embryos (Figure 10). Quantitative techniques, such as real-time PCR (RT-PCR), would be required to determine whether the extent of *otk2* expression differs in *EY03841*17* flies relative to wild types.

Thus, the attempt to create an imprecise excision that abolished *otk2* activity was not successful. Despite a lack of evidence for the disruption of *otk2*, several severe and highly penetrant abnormalities were identified in the motor axons of *EY03841*17* embryos. A number of branches were frequently absent: the ISNb (Figure 12), ISNd (Figure 13), SNc (Figure 15), the first (FB; Figure 16) and second (SB; Figure 17) branches of the ISN, and the dorsal or lateral branches of the SNa (Figure 14).

The gene (or genes) responsible for these abnormalities remains to be determined. It can be assumed, however, that the aberration is present on the 2nd chromosome, which was balanced in the *EY03841*17* population; had the aberration, which appears to entail semi-lethality, been on an alternative chromosome, it likely would have been lost over time due to recombination. One approach to investigating which gene is responsible for the phenotypes is to acquire lines with deficiencies that collectively cover the 2nd chromosome; pairing these deficiencies with the *EY03841*17* chromosome would allow one to determine the genomic region of the aberration by assessing which combination of chromosomes is associated with the phenotypes.

While this screening process could be approached by testing deficiencies in an arbitrary order, it might be more efficient to first test deficiencies for regions containing genes that have been linked to phenotypes resembling those of *EY03831*17*; Appendix A lists the genes that are associated with a combination of FB, SB, ISNb, ISNd, SNa dorsal branch/SNa lateral branch, or SNc absent phenotypes. Three or more of these phenotypes have been reported for the 2nd chromosome genes *beaten-path* (*beat*; Fambrough & Goodman, 1996; Landgraf et al., 1999), *even skipped* (*eve*; Labrador et al., 2005; Landgraf et al. (1999), *leukocyte-antigen-related-like* (*lar*; Desai et al., 1997; Fox & Zinn, 2005; Shindelholz et al., 2001; Sun et al., 2001), and *semaphorin-1a* (*sema-1a*; Ayoob et al., 2004; Cho et al., 2012; Terman et al., 2002; Winberg et al., 1998; Yu et al., 1998; Yu, Huang, & Kolodkin, 2000). However, *lar* is unlikely responsible for the *EY03841*17* phenotypes since its ISNb absent and SNa aberrant bifurcation phenotypes are respectively seen in loss- and gain-of-function experiments (it seems improbable that the *EY03841*17* aberration would up- and down-regulate a gene's activity). Similarly, the penetrance of certain phenotypes in *sema-1a* mutants is incongruent with their penetrance in *EY03841*17* embryos (e.g., the ISNb is absent in 7% and 73.2% of hemisegments, respectively). The ISNb is absent in ~95% of hemisegments in which *eve* expression is driven in neurons under the control of *Elav-GAL4*, which more closely resembles the penetrance in *EY03841*17* embryos. *eve* is endogenously expressed in the embryonic nervous system, thus it is not inconceivable that an aberration in an *eve*-associated regulatory region would elicit *EY03841*17*-like phenotypes. Likewise, *beat* mutants exhibit ISNb and SNc absent phenotypes at frequencies somewhat resembling those in *EY03841*17* (~40% and ~80% respectively in *beat* mutants, compared to 73.2% and 53.1%). Therefore, while it might ultimately be revealed that an uncharacterised gene is responsible for the *EY03841*17* phenotypes, a reasonable starting point in this process would be to pair the *EY03841*17* chromosome with deficiencies that remove *eve* or *beat*.

In conclusion, although the gene responsible for the *EY03841*17* phenotypes remains to be determined, the above suggestions should allow this to be rectified. With regard to investigating *otk2*'s role in embryonic motor axon guidance, a null mutant, $otk2^{C26}$, was acquired from Linnemannstöns and colleagues (2014) subsequent to the excision experiment. Experiments involving the $otk2^{C26}$ line are described in Chapter 4.

Chapter 4: *otk2*

4.1. Introduction

As discussed in greater detail at the start of the previous chapter, Vogel and colleagues (2003) identified Off-track2 (Otk2) as a cell surface or secreted member of the immunoglobulin superfamily (IgSF). They reported that, over the full length of Otk2 (433 amino acids), it exhibits 53% identity to the established axon guidance molecule, Off-track (Otk; Cafferty et al., 2004; Winberg et al., 2001). Likewise, Linnemannstöns and colleagues (2014) proposed that Otk and Otk2, which are located next to each other on the second chromosome, are paralogues that arose from a gene duplication event. Otk harbours five extracellular Ig domains and an intracellular kinase homology domain; Otk2 harbours three extracellular Ig domains and a short cytoplasmic domain of 69 amino acids (Linnemannstöns et al., 2014). Their IHC results indicate that *otk2* is expressed in the ventral nerve cord towards the end of embryonic development, which is consistent with the *in situ* hybridisation data of other researchers (Alsbury et al., in preparation; Figure 18).

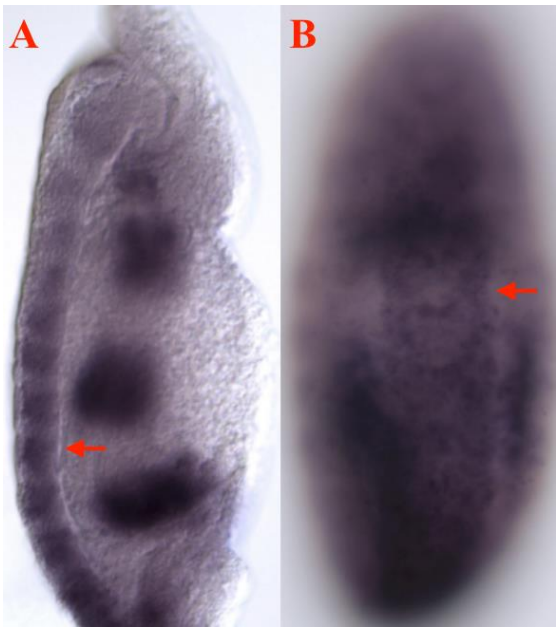

Figure 18. **Expression of *otk2* revealed by *in situ* hybridisation** (modified from Alsbury et al., in preparation). **A.** A lateral view of a stage 14 embryo (up is anterior, left is ventral) with expression evident in the VNC (red arrow). **B.** A ventral view of a stage 15 embryo (up is anterior) with expression evident in the VNC (red arrow).

Otk2's paralogue, Otk, binds to PlexinA (PlexA), which is the receptor for the transmembrane semaphorin, Semaphorin-1a (Sema-1a; Winberg et al., 2001). The semaphorins are a conserved family of proteins, which have been associated with various roles, including apoptosis (Bagnard et al., 2001; Shirvan et al., 1999), migration

(Marin et al., 2001), organogenesis (review in Hinck, 2004), and dendritic growth (Polleux, Morrow, & Ghosh, 2000). However, the semaphorins are perhaps best known for their involvement in axon guidance, particularly as repellents (Ayoob et al., 2004; Cho et al., 2012; Huang & Kolodkin, 2000; Terman et al., 2002; Winberg et al., 1998; Yu et al., 1998; Yu, Huang, & Kolodkin, 2000). As outlined in Chapter 1, *sema-1a* is implicated in the development of the "b" branch of the intersegmental nerve (ISNb), a peripheral branch constituted of motor neurons. In *sema-1a* loss-of-function embryos, the ISNb fails to defasciculate from the ISN (~7% of hemisegments), fails to innervate the cleft between muscles 6 and 7 (~18% of hemisegments), generates ectopic projections where it would normally innervate muscles 6 and 7 (~35% of hemisegments) or muscle 12 (~15% of hemisegments), or stalls prematurely (~49% of hemisegments). The ISNb also fails to defasciculate from the ISN when *sema-1a* is ectopically expressed throughout the somatic musculature with a *24B-GAL4* driver, which drives expression from stage 11 to the end of embryonic development (Luo et al., 1994). Respectively, this occurs in ~24% and ~58% of hemisegments in flies with wild type and *sema-1a* loss-of-function backgrounds. Muscles 6 and 7 are normally innervated by the RP3 neuron. However, the RP3 axon fails to innervate muscles 6 and 7 when *sema-1a* expression is driven by *24B-GAL4* in 41% and 87% of hemisegments in flies with wild type and *sema-1a* loss-of-function backgrounds. Abnormalities associated with *sema-1a* are, however, seen in a number of other motor neuron branches. For example, driving *sema-1a* expression in muscle with a *24B-GAL4* driver in a null background also results in the absence of the first (FB; ~29% of hemisegments) and second (SB; ~32% of hemisegments) lateral branches of the ISN. There are also segmental nerve "a" (SNa) phenotypes in these embryos, including a fusion bypass phenotype (the SNa fasciculates to the ISN, and thus does not enter the muscle field; ~12% of hemisegments), absence of the dorsal branch (~19% of hemisegments), or failure of the dorsal branch to bifurcate (~62% of hemisegments). In loss-of-function embryos, the transverse nerve (TN) can stall and the dorsal branch of the SNa fails to bifurcate (in ~88% of hemisegments). Loss-of-function embryos also exhibit defects in the CNS. For instance, the third (outermost) longitudinal connective may be discontinuous or may collapse onto the middle (MP1) longitudinal tract. There are also defects in the intersegmental nerve "d" (ISNd; ~36% of hemisegments) and segmental nerve "c" (SNc; ~11% of hemisegments), which are often absent or truncated in *sema-1a* loss-of-function lines.

Similar phenotypes have been reported for *plexA*, which encodes a Sema-1a receptor. *plexA* loss-of-function embryos exhibit the same ISNb, SNa and third longitudinal

connective phenotypes as those seen in *sema-1a* loss-of-function flies. The ISNb phenotypes are, however, on average about twice as penetrant compared to the *sema-1a* loss-of-function embryos. Also, the TN, rather than stalling, projects abnormally onto muscles 6 and 7 in over a third of hemisegments. The contrasting behaviour of the TN between *plexA* and *sema-1a* loss-of-function lines suggests that PlexA might interact with ligands other than Sema-1a (Winberg et al., 1998). Driving expression of *plexA* in neurons results in discontinuity in all three of the longitudinal connectives, the outermost of which (the third) sends projections towards the periphery. Phenotypes in the FB, SB, ISNd or SNc are not reported for *plexA* lines (Winberg et al., 1998).

Regarding Otk's role in *Drosophila* axon guidance, Winberg and colleagues (2001) argue that it acts as a coreceptor for PlexA. Congruent with this, *otk* loss-of-function embryos exhibit the same ISNb, SNa, and third longitudinal connective phenotypes as those seen in *sema-1a* and *plexA* loss-of-function flies. ISNb phenotypes in *otk* loss-of-function embryos are, on average, approximately 50% more frequent than in *sema-1a* loss-of-function embryos, though about 50% less frequent than in *plexA* loss-of-function embryos. The inner longitudinal connectives also appear to unravel. Phenotypes relating to the TN, FB, SB, ISNd, or SNc, however, are not reported for *otk* lines, nor are the consequences (if any) of driving Otk expression in muscle. The above ISNb phenotypes are also evident in *plex-A*/*sema-1a*, *plex-A*/*otk*, and *sema-1a*/*otk* transheterozygotes, indicative of their involvement in a single signalling pathway. The dorsal branch of the SNa does not bifurcate in the former two transheterozygotes. It is not stated whether there are phenotypes in the TN or CNS in these transheterozygous lines (Winberg et al., 1998; Winberg et al., 2001; Yu et al., 1998).

In addition to motor neurons, *otk* is required for wiring of the *Drosophila* visual system (Cafferty et al., 2004). Photoreceptor (R cell) axons innervate two layers of the optic ganglia, with R1–R6 cells connecting with the lamina layer, and R7–R8 cells connecting with the medulla layer. In third instar larvae, *otk* is normally expressed in cells R1–R6, which aberrantly project to the medulla layer in flies harbouring the otk^{3} null allele (also employed by Winberg et al., 2001). In contrast to Winberg and colleagues, who propose that Otk's primary function in axon guidance is to mediate defasciculation, Cafferty and colleagues suggest that Otk is required to recognise target signals that indicate to axons that they have reached their destination. Moreover, they observed that the phenotypes of *sema-1a* mutants in the visual system, unlike in motor neurons, are dissimilar to those in *otk* mutants, implying that Otk might participate in alternative signalling pathways in the two systems.

Despite these reports of *otk*'s role in axon guidance, Linnemannstöns and colleagues (2014), who were primarily interested in the gene's role in PCP, did not observe axon guidance defects in their newly created null allele, otk^{A1}. Moreover, in contrast to the otk^{3} allele generated by Winberg and colleagues (2001), the otk^{A1} flies were viable. These observations, coupled with the fact that a wild type *otk* transgene had never been used to rescue lethality in the otk^{3} line, lead Linnemannstöns and colleagues to suggest that the previously observed axonal defects and lethality might have been attributable to a second-site mutation, thus casting doubt on *otk's* putative role in axon guidance (Cafferty et al, 2004; Winberg et al., 2001).

Linnemannstöns and colleagues' (2014) report raised a number of other interesting questions regarding the functioning of *otk*. In particular, their Co-Immunoprecipitation (Co-IP) tests indicated that Otk, in addition to binding itself homodimerically, could form a heterodimer with Otk2. These observations raised the possibility that Otk2 might form part of Winberg and colleagues' (2001) putative PlexA-Otk receptor complex and that it might contribute to axons' responses to Sema-1a. Their results also indicated that Otk and Otk2 could form complexes with Frizzled 2 (Fz2). Fz2 is a member of the conserved Frizzled family of seven pass transmembrane proteins, which, via extracellular cysteine rich domains (CRDs), act as receptors for the Wnts. The Wnts, of which there are seven in *Drosophila*, are secreted glycoproteins that are implicated in a multitude of developmental processes, including pattern formation (Chen & Struhl, 1999), PCP (Strutt et al., 2012), synaptic development (Mosca & Schwarz, 2010) and axon guidance (Inaki et al., 2007; Sato et al., 2006; Yoshikawa et al., 2003), and have been linked to various diseases, most notably cancer (reviewed in Moon et al., 2004). Fz2, expressed in embryonic motor neurons, is a receptor for Wnt4 (Peradziryi et al., 2011; Wu & Nusse, 2002), which is present in muscles 12 and 13, where it appears to act as a repellant (Inaki et al., 2007). In *wnt4* mutant embryos or embryos expressing a dominant negative form of *fz2* in neurons, muscle 13 synapses are enlarged and muscle 12 synapses are reduced, suggesting that Wnt4 and Fz2 prevent muscle 13 innervation by axons that normally innervate muscle 12 (MN12s). Fz2 and Wnt4 have also been studied within the context of *Drosophila* retinotopic mapping (Sato et al., 2006), whereby the spatial distribution of retinal neurons is mirrored in the precise laminal location to which their axons project. In contrast to Inaki and colleagues (2007), however, the work of Sato and colleagues suggests that Wnt4 attracts, rather than repels, Fz2-expressing axons. Specifically, Wnt4, whose expression is limited to the ventral section of the lamina in late third instar larvae, is proposed to attract Fz2-expressing ventral axons. Ventral axons in flies mutant for either *fz2* or *wnt4* or that

ectopically express wnt4 in the dorsal lamina exhibit dorsal misrouting. Therefore, while *otk* and *fz2* have, independently, been implicated in axon guidance, Linnemannstöns and colleagues' work suggests that the influence of each gene on axonal navigation might depend upon the activity of the other.

Given Otk2's paralogy to Otk, the current study investigated, using a null allele generated by Linnemannstöns and colleagues (2014), $otk2^{C26}$, whether *otk2* loss-of-function results in abnormalities in the embryonic motor neurons. In light of conflicting reports regarding the consequences of *otk* loss-of-function (Linnemannstöns et al., 2014; Cafferty et al., 2004; Winberg et al., 2001), the study also sought to clarify, using the otk^{A1} allele, whether *otk* is indeed required for the correct formation of the embryonic motor neurons. Moreover, since Cafferty and colleagues propose that Otk is implicated in target selection, while Winberg and colleagues emphasise a role in defasciculation, further analysis of the phenotypes associated with *otk* might help to define its influence over axons. A line with a deficiency spanning *otk* and *otk2* (sequence location: 2R:7779605;8059989), referred to as *BSC199*, was used to investigate whether loss of both genes' activity would enhance phenotypes associated with single mutants. Considering Linnemannstöns and colleagues' (2014) Co-IP results, the study also investigated whether there were axonal abnormalities in various transheterozygous lines, (1) *otk/+, otk2/+*, (2) *otk/+; fz2/+*, and (3) *otk2/+; fz2/+*, which would indicate whether there were genetic interactions between these genes. The full array of motor axons within homozygous *fz2* loss-of-function embryos was also examined, as Inaki and colleagues' (2007) analysis focused exclusively on the MN12s and axons innervating muscle 13 (MN13s). Additionally, further analysis of phenotypes associated with *fz2* might help clarify whether its role in axon guidance is primarily repellant (Inaki et al., 2007) or attractive (Sato et al., 2006). Similarly, homozygous *sema-1a* loss-of-function embryos were examined to confirm prior reports of its associated axonal abnormalities (Winberg et al., 1998; Yu et al., 1998) and *otk2/+*, *sema-1a/+* transheterozygous embryos were examined to probe whether Otk2 participates in Sema-1a-based navigation. Finally, gain-of-function experiments using a line with an upstream activator sequence (UAS) in the 5' region of *otk2* (*EY03841*), in conjunction with GAL4 lines that drive expression in embryonic motor neurons (*OK371-GAL4*) or throughout the embryonic somatic musculature (*Mef2-GAL4*) were completed to gain insights into the precise function of Otk2 in axon guidance. *OK371-GAL4* drives expression from stage 15 until the end of embryonic development and *Mef2-GAL4* drives expression from stage 7 until the end of embryonic development (Mahr & Aberle, 2006; Rangagnayakulu, Schulz & Olson, 1996), thus both promote

target gene expression while the motor neurons are navigating and making connections with the muscle field. A list of the full genotypes of the flies referred to in this thesis is presented in Appendix D.

4.2. Results

4.2.1. *otk* and *otk2* expression

To confirm that otk and otk2 were not expressed in the otk^{A1} and $otk2^{C26}$ lines, respectively, an otk antibody was applied to otk^{A1} embryos and an otk2 antibody was applied to $otk2^{C26}$ embryos. Staining was not evident in either experiment (not shown). Both antibodies were also applied to wild type embryos to investigate the proteins' patterns of distribution in stage 16 embryos. Both proteins are clearly present in the VNC, particularly in the region of the longitudinal fascicles and anterior commissures, and, to as lesser extent, the posterior commissures. However, while Otk appears to be present in the motor neurons, there is little convincing evidence that this is also true for Otk2, which seems to be expressed in exit glia in the region in which motor neurons enter the periphery (Figure 19).

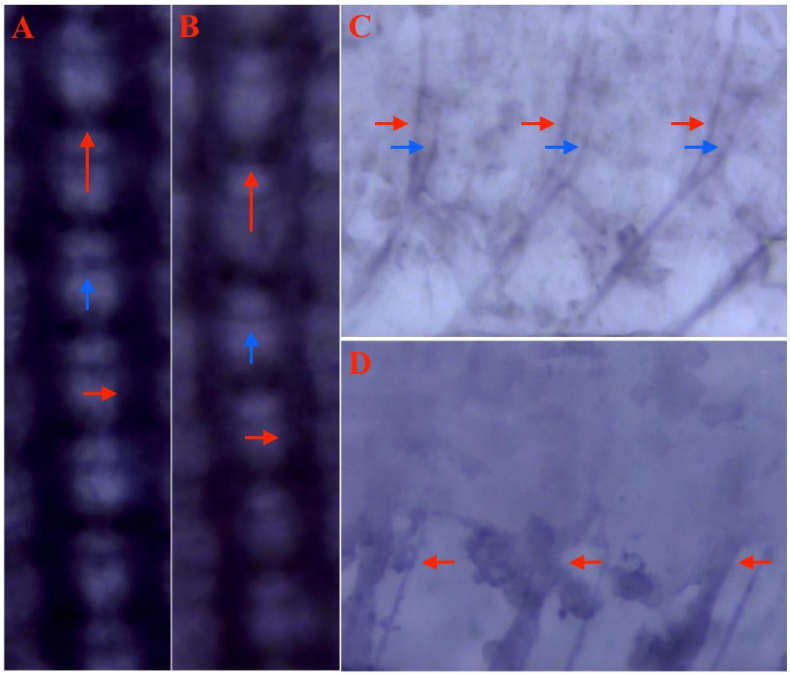

Figure 19. **Expression of *otk* and *otk2* in stage 16 wild type VNC and periphery**. **A.** An Otk antibody boldly stains the regions of the longitudinal fascicles (short red arrow) and anterior commissures (long red arrow) of the VNC, and posterior commissures (blue arrow) more faintly. **B.** A very similar staining pattern is observed with an Otk2 antibody, whereby the regions of the longitudinal fascicles (short red arrow) and anterior commissures (long red arrow) are clearly seen, and, to a lesser extent, the posterior commissures (blue arrow). **C.** The ventral half of the periphery is shown in three hemisegments. Otk is seen in the motor neurons, including the ISN (red arrow) and ISNb (blue arrows). **D.** The ventral half of the periphery is shown in three hemisegments. There is no clear evidence that Otk2 is expressed in motor neurons. Instead it is seen in exit glia in the region in which the motor neurons enter the periphery (red arrows).

4.2.2. Confirming expression in GAL4 drivers

To confirm that the GAL4 lines (*Mef2-GAL4* and *OK371-GAL4*) would drive expression in the target tissues, they were crossed with a line containing a UAS-lacZ element, and embryos were stained using an anti β-gal antibody (Figure 20).

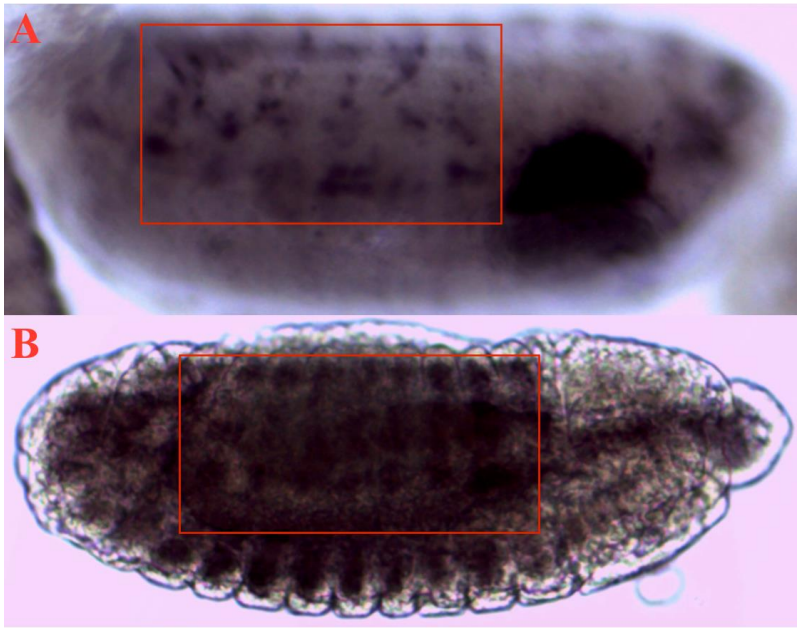

Figure 20. **β-gal expression in *OK371* X *UAS-lacZ* and *Mef2* X *UAS-lacZ* embryos. A**. A stage 15 *OK371* X *UAS-lacZ* whole embryo stained against β-gal (left is posterior, up is dorsal). Fine markings are evident in the region of the motor neurons (red box) indicative of β-gal expression within them. **B**. A stage 13 *Mef2* X *UAS-lacZ* whole embryo stained for β-gal (left is posterior, up is dorsal). Broad bands are evident in the region of the somatic muscles (red box) indicative of β-gal expression within them.

4.2.3. Phenotypic analysis: *otk2^{C26}*

An inspection of the motor neurons of *otk2^{C26}* embryos suggested that various branches were frequently absent or abnormal. Often, the MN13s were absent (Figure 22) or projected anteriorly (Figure 23) or both anteriorly and posteriorly (Figure 24), the MN12s projected anteriorly (Figure 25) and the RP3 axon was absent (Figure 26). The full length of a wild type hemisegment, with the branches that are abnormal in *otk2* experiments indicated, is shown in Figure 21 for reference. Figure 76 (p.112) shows the penetrance of phenotypes in *otk2^{C26}*, as well as their frequency in all other genotypes analysed in this chapter.

Throughout the thesis, MN12 projections are described as being normal, mild, or severe. In wild types, the MN12s typically extend dorsally from the muscle 13 innervation point, and then attach to muscle 12 via posterior projections or posterior and anterior projections of equal length (“normal”). In mild cases, MN12s extend dorsally, and then attach to muscle 12 via anterior projections or posterior and anterior

projections, the latter being greater in length. In severe cases, MN12s extend anteriorly from the muscle 13 innervation point. In such cases, projections were deemed to have grown anteriorly if they extended at an angle equal or greater to 30° from the region of the ISNb between the muscle 6/7 and muscle 13 innervation points.

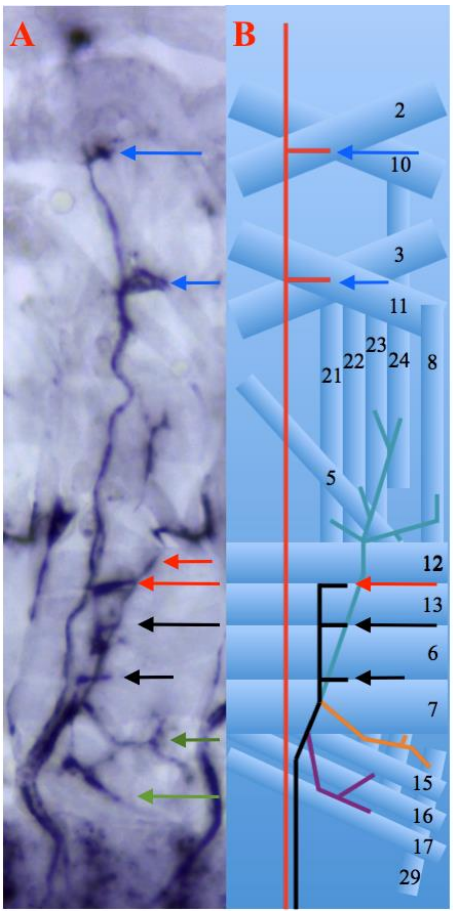

Figure 21. **A wild type hemisegment with the SNa, ISNd, SNc, ISNb (comprised of MN12s, MN13s, and the RP3 axon), and FB and SB indicated. A.** A photomicrograph of a wild type hemisegment (right is posterior, up is dorsal) with the following branches indicated: SB (long blue arrow), FB (short blue arrow), SNa (short red arrow), MN12s (long red arrow), MN13s (long black arrow), RP3 axon (short black arrow), SNc (short green arrow), and ISNd (long green arrow). **B.** A schematic of a wild type hemisegment with the same branches indicated (right is posterior up is dorsal): ISN (red) with SB (long blue arrow) and FB (short blue arrow), SNa (turquoise), ISNb (black) with MN12s (long red arrow), MN13s (long black arrow), and RP3 axon (short black arrow), SNc (orange), and ISNd (purple). The muscles innervated by these branches are indicated by numbers. Two of the muscles innervated by the SNc, 26 and 27, are shown but not labelled. Muscles not innervated by the affected branches are not shown.

MN13s absent

The MN13s were absent more often in *otk2*^{C26} hemisegments (30.8%) than in wild types (11.9%) (Figure 22).

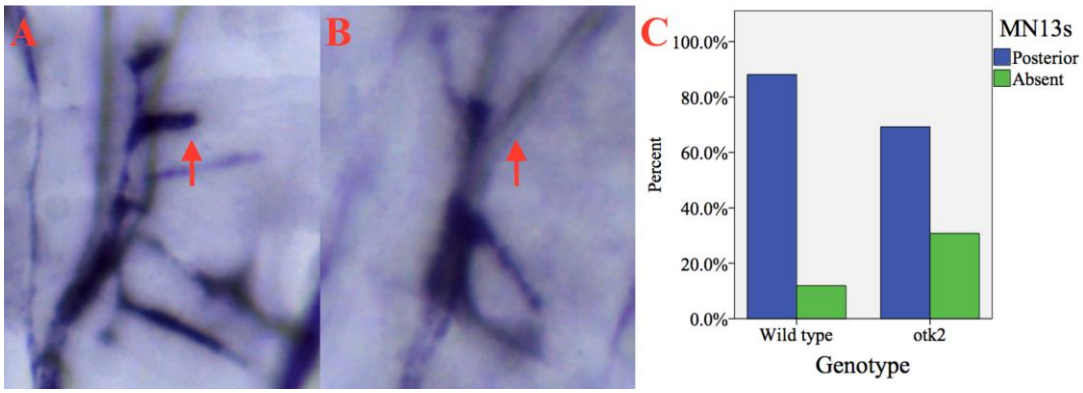

D	MN13s posterior	MN13s absent
Wild type	88.1% (133)	11.9% (18)
otk2^{C26}	69.2% (63)	30.8% (28)

Figure 22. Image A (right is posterior, up is dorsal) shows the ventral section of a wild type hemisegment with the MN13s indicated (red arrow). Image B (right is posterior, up is dorsal) shows the ventral section of an *otk2*^{C26} hemisegment without the MN13s (red arrow). The graph (C) shows the percentage of hemisegments in which the MN13s are present or absent in 27 wild type and 19 *otk2*^{C26} embryos. The table (D) shows the percentage and number of hemisegments in which the MN13s are present or absent in the same embryos.

A chi-square test for independence revealed that the MN13s were absent significantly more often in *otk2*^{C26} hemisegments than in wild types, χ^2 (1, n = 242) = 13.1, p < .001.

MN13s project anteriorly

The MN13s projected anteriorly more often in *otk2*^{C26} hemisegments (12.5%) than in wild types (2.9%) (Figure 23).

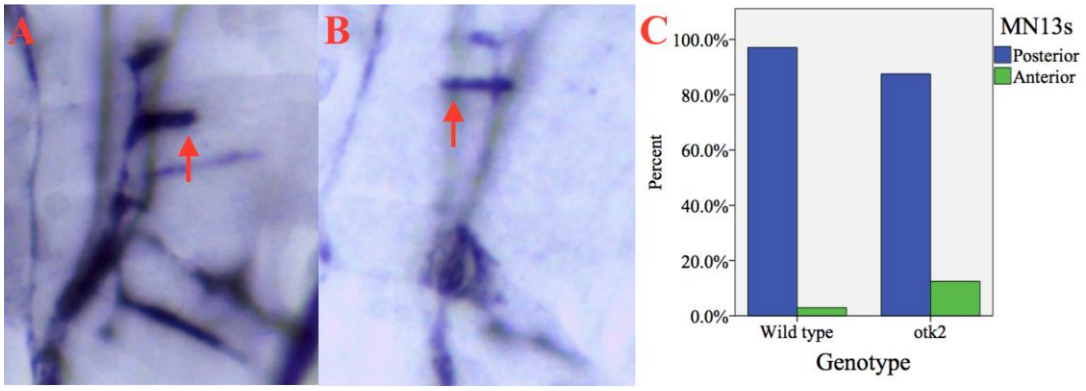

D	MN13s posterior	MN13s anterior
Wild type	97.1% (133)	2.9% (4)
otk2^{C26}	87.5% (63)	12.5% (9)

Figure 23. Image A (right is posterior, up is dorsal) shows the ventral section of a wild type hemisegment in which the MN13s project posteriorly (red arrow). Image B (right is posterior, up is dorsal) shows the ventral section of an *otk2*^{C26} hemisegment in which the MN13s project anteriorly (red arrow). The graph (C) shows the percentage of hemisegments in which the MN13s project posteriorly or anteriorly in 27 wild type and 19 *otk2*^{C26} embryos. The table (D) shows the percentage and number of hemisegments in which the MN13s project posteriorly or anteriorly in the same embryos.

Fisher's exact test revealed that the MN13s projected anteriorly significantly more often in *otk2*^{C26} hemisegments than in wild types, $p < .05$.

MN13s project anteriorly and posteriorly

The MN13s projected anteriorly and posteriorly more often in *otk2*^{C26} hemisegments (22.2%) than in wild types (7%) (Figure 24).

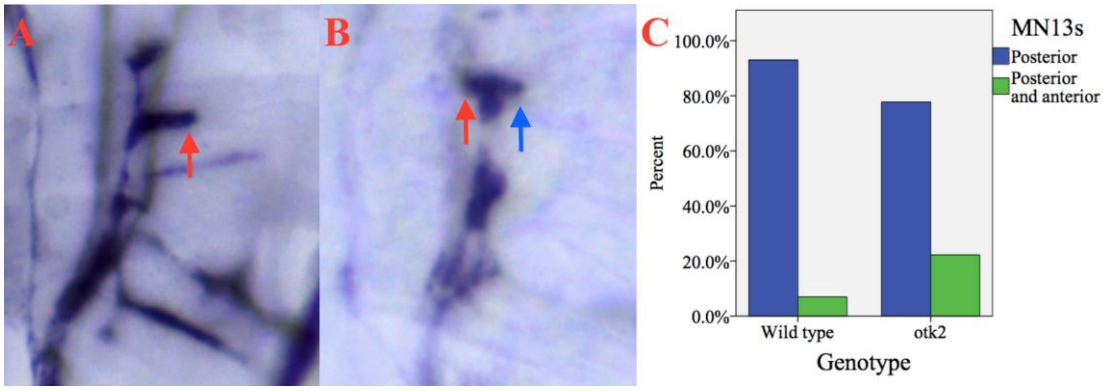

D	MN13s posterior	MN13s posterior and anterior
Wild type	93% (133)	7% (10)
otk2^{C26}	77.8% (63)	22.2% (18)

Figure 24. Image A (right is posterior, up is dorsal) shows the ventral section of a wild type hemisegment in which the MN13s project posteriorly (red arrow). Image B (right is posterior, up is dorsal) shows the ventral section of an *otk2*^{C26} hemisegment in which the MN13s project anteriorly (red arrow) and posteriorly (blue arrow). The graph (C) shows the percentage of hemisegments in which the MN13s project posteriorly or anteriorly and posteriorly in 27 wild type and 19 *otk2*^{C26} embryos. The table (D) shows the percentage and number of hemisegments in which the MN13s project posteriorly or anteriorly and posteriorly in the same embryos.

A chi-square test for independence revealed that the MN13s projected anteriorly and posteriorly significantly more often in *otk2*^{C26} hemisegments than in wild types, χ^2 (1, n = 224) = 10.97, p < .01.

MN12s project anteriorly

The MN12s of *otk*^{C26} embryos projected anteriorly. 42.6% of *otk2*^{C26} hemisegments exhibited the mild phenotype (Figure 25B), compared to 20% of wild type hemisegments. 15.8% of *otk2*^{C26} hemisegments exhibited the severe phenotype (Figure 25C), compared to 8.8% of wild type hemisegments.

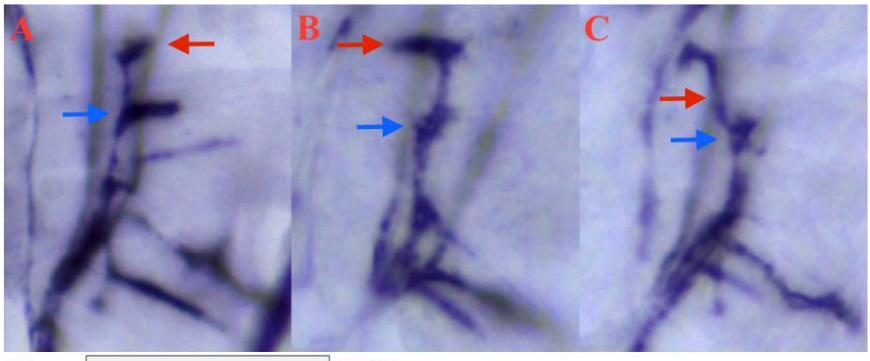

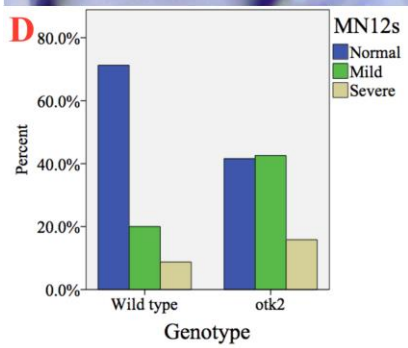

E	MN12s normal	MN12s mild	MN12s severe
Wild type	71.2% (57)	20% (16)	8.8% (7)
otk2^{C26}	41.6% (42)	42.6% (43)	15.8% (16)

Figure 25. Image A (right is posterior, up is dorsal) shows the ventral section of a wild type hemisegment in which the MN12s project dorsally at the muscle 13 innervation point (blue arrow) before projecting posteriorly (red arrow). Image B (right is posterior, up is dorsal) shows the ventral section of an *otk2*^{C26} hemisegment in which the MN12s project dorsally at the muscle 13 innervation point (blue arrow) before projecting anteriorly (red arrow). Image C (right is posterior, up is dorsal) shows the ventral section of an *otk2*^{C26} hemisegment in which the MN12s (red arrow) project anteriorly at the muscle 13 innervation point (blue arrow). The graph (D) shows the percentage of hemisegments that exhibit the normal, mild, and severe phenotypes in 27 wild type and 19 *otk2*^{C26} embryos. The table (E) shows the percentage and number of hemisegments exhibiting normal, mild, and severe phenotypes in the same embryos.

A chi-square test for independence test revealed a significant effect of genotype with regard to the trajectory of the MN12s, χ^2 (2, n = 181) = 15.93, p < .001.

RP3 axon absent

The RP3 axon was absent more often in *otk2*^{C26} hemisegments (55.6%) than in wild types (20.1%) (Figure 26).

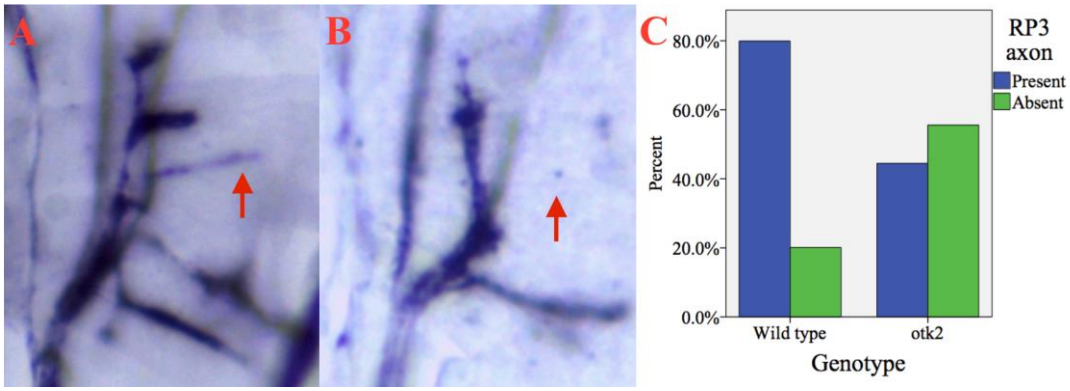

D	RP3 axon posterior	RP3 axon absent
Wild type	79.9% (147)	20.1% (37)
otk2^{C26}	44.4% (48)	55.6% (60)

Figure 26. Image A (right is posterior, up is dorsal) shows the ventral section of a wild type hemisegment with the RP3 axon indicated (red arrow). Image B (right is posterior, up is dorsal) shows the ventral section of an *otk2*^{C26} hemisegment without the RP3 axon (red arrow). The graph (C) shows the percentage of hemisegments in which the RP3 axon is present or absent in 27 wild type and 19 *otk2*^{C26} embryos. The table (D) shows the percentage and number of hemisegments in which the RP3 axon is present or absent in the same embryos.

A chi-square test for independence revealed that the RP3 axon was absent significantly more often in *otk2*^{C26} hemisegments than in wild types, χ^2 (1, n = 292) = 38.55, p < .001.

4.2.4. Phenotypic analysis: *otk*^{A1}

In light of conflicting reports regarding *otk*'s contribution to embryonic motor axon pathfinding (Linnemannstöns et al., 2014; Winberg et al., 2001), *otk*^{A1} embryos were examined for abnormal phenotypes. *otk*^{A1} embryos exhibited the same phenotypes as those seen in *otk2*^{C26} embryos; namely, the MN13s were absent (Figure 30) or projected anteriorly (Figure 31) or both anteriorly and posteriorly (Figure 32), the MN12s projected anteriorly (Figure 33) and the RP3 axon was absent (Figure 34). However, the ISNb (Figure 29) and the SB (Figure 27) were also absent. When present, the SB often projected anteriorly (Figure 28).

SB absent

The SB was absent more often in *otk*^{A1} hemisegments (56.7%) than in wild types (30.7%) (Figure 27).

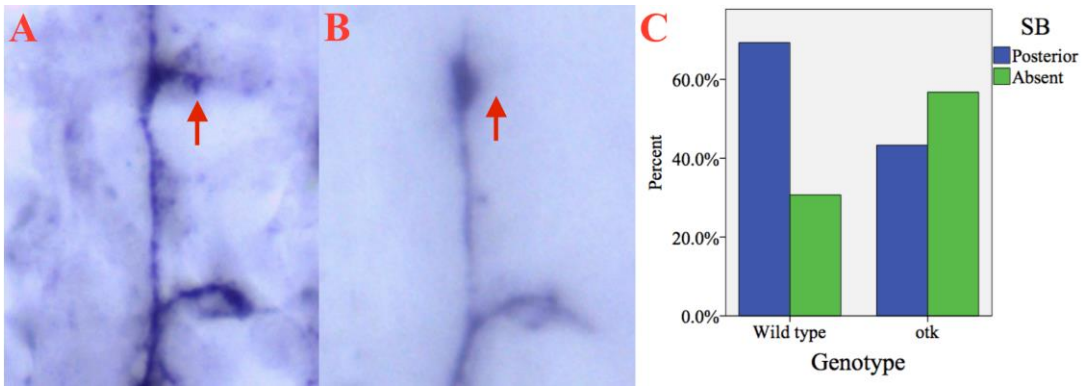

D	SB posterior	SB absent
Wild type	69.3% (70)	30.7% (31)
otk^{A1}	43.3% (58)	56.7% (76)

Figure 27. Image A (right is posterior, up is dorsal) shows the dorsal section of a wild type hemisegment with the SB indicated (red arrow). Image B (right is posterior, up is dorsal) shows the dorsal section of an *otk*^{A1} hemisegment without the SB (red arrow). The graph (C) shows the percentage of hemisegments in which the SB is present or absent in 30 wild type and 32 *otk*^{A1} embryos. The table (D) shows the percentage and number of hemisegments in which the SB is present or absent in the same embryos.

A chi-square test for independence revealed that the SB was absent significantly more often in *otk*^{A1} hemisegments than in wild types, χ^2 (1, n = 235) = 15.73, p < .001.

SB anterior

The SB projected anteriorly more often in *otk*^{A1} hemisegments (24.7%) than in wild types (9.1%) (Figure 28).

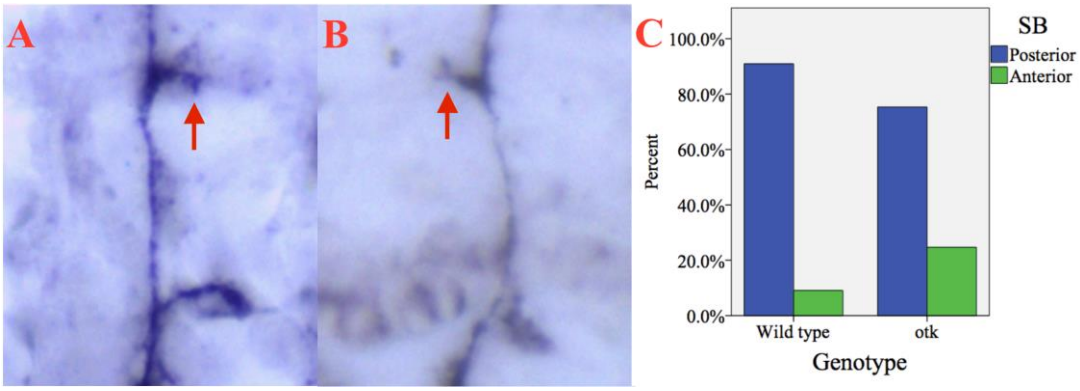

D	SB posterior	SB anterior
Wild type	90.9% (70)	9.1% (7)
otk^{A1}	75.3% (58)	24.7% (19)

Figure 28. Image A (right is posterior, up is dorsal) shows the dorsal section of a wild type hemisegment with the SB projecting posteriorly (red arrow). Image B (right is posterior, up is dorsal) shows the dorsal section of an *otk*^{A1} hemisegment with the SB projecting anteriorly (red arrow). The graph (C) shows the percentage of hemisegments in which the SB projects posteriorly or anteriorly in 30 wild type and 32 *otk*^{A1} embryos. The table (D) shows the percentage and number of hemisegments in which the SB projects posteriorly or anteriorly in the same embryos.

A chi-squared for independence revealed that the SB projected anteriorly significantly more often in *otk*^{A1} hemisegments than in wild types, χ^2 (1, n = 154) = 6.66, p < .05.

ISNb absent

The ISNb was absent more often in *otk*^{A1} hemisegments (7.1%) than in wild types (2%) (Figure 29).

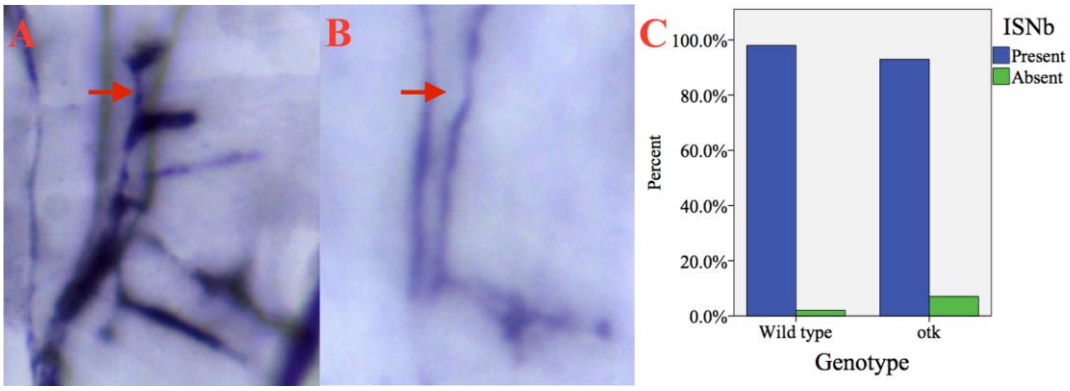

D	ISNb present	ISNb absent
Wild type	98% (240)	2% (5)
otk^{A1}	92.9% (290)	7.1% (22)

Figure 29. Image A (right is posterior, up is dorsal) shows the ventral section of a wild type hemisegment with the ISNb indicated (red arrow). Image B (right is posterior, up is dorsal) shows the ventral section of an *otk*^{A1}hemisegment with the absence of the ISNb indicated (red arrow). The graph (C) shows the percentage of hemisegments in which the ISNb is present or absent in 30 wild type and 32 *otk*^{A1} embryos. The table (D) shows the percentage and number of hemisegments in which the SB is present or absent in the same embryos.

A chi-square test for independence revealed that the ISNb was absent significantly more often in *otk*^{A1} hemisegments than in wild types, χ^2 (1, n = 557) = 7.47, p < .01.

MN13s absent

The MN13s were absent more often in *otk*^{A1} hemisegments (23%) than in wild types (11.9%) (Figure 30).

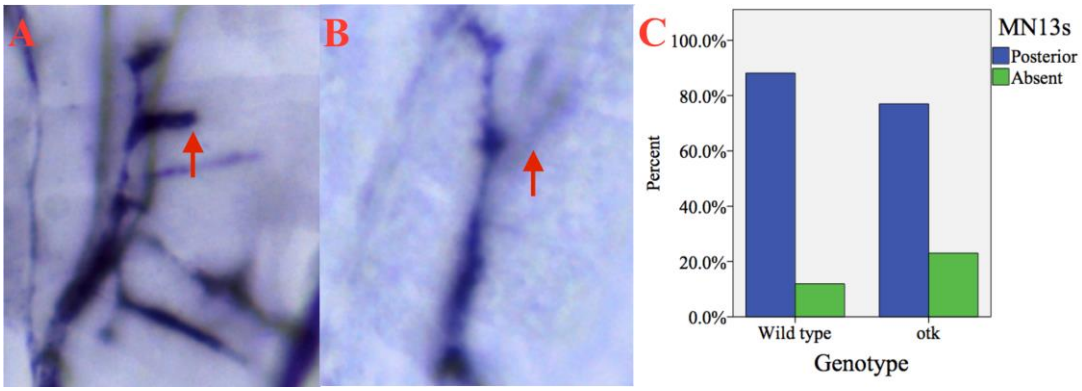

D	MN13s posterior	MN13s absent
Wild type	88.1% (133)	11.9% (18)
otk^{A1}	77% (87)	23% (26)

Figure 30. Image A (right is posterior, up is dorsal) shows the ventral section of a wild type hemisegment with the MN13s indicated (red arrow). Image B (right is posterior, up is dorsal) shows the ventral section of an *otk*^{A1} hemisegment without the MN13s (red arrow). The graph (C) shows the percentage of hemisegments in which the MN13s are present or absent in 27 wild type and 26 *otk*^{A1} embryos. The table (D) shows the percentage and number of hemisegments in which the MN13s are present or absent in the same embryos.

A chi-square test for independence revealed that the MN13s were absent significantly more often in *otk*^{A1} hemisegments than in wild types, χ^2 (1, n = 264) = 5.72, p < .05.

MN13s project anteriorly

The MN13s projected anteriorly more often in *otk*^{A1} hemisegments (20.9%) than in wild types (2.9%) (Figure 31).

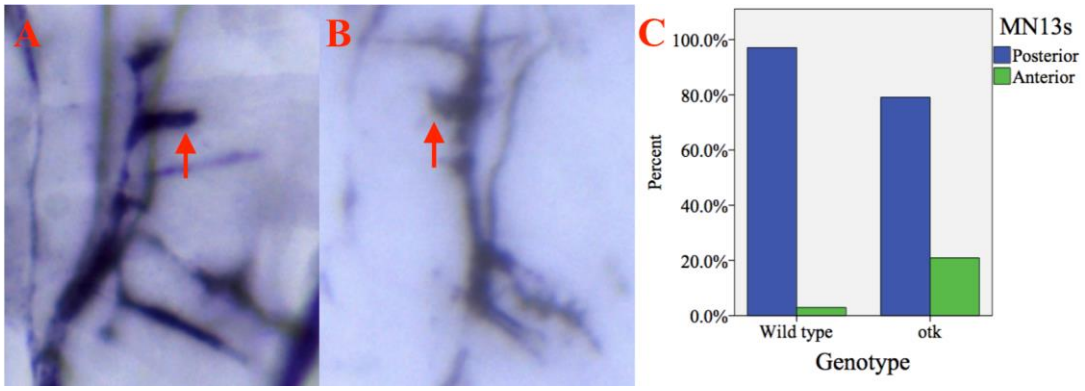

D	MN13s posterior	MN13s anterior
Wild type	97.1% (133)	2.9% (4)
otk^{A1}	79.1% (87)	20.9% (23)

Figure 31. Image A (right is posterior, up is dorsal) shows the ventral section of a wild type hemisegment in which the MN13s project posteriorly (red arrow). Image B (right is posterior, up is dorsal) shows the ventral section of an *otk*^{A1} hemisegment in which the MN13s project anteriorly (red arrow). The graph (C) shows the percentage of hemisegments in which the MN13s project posteriorly or anteriorly in 27 wild type and 26 *otk*^{A1} embryos. The table (D) shows the percentage and number of hemisegments in which the MN13s project posteriorly or anteriorly in the same embryos.

A chi-square test for independence revealed that the MN13s projected anteriorly significantly more often in *otk*^{A1} hemisegments than in wild types, χ^2 (1, n = 247) = 20.28, p < .001.

MN13s project anteriorly and posteriorly

The MN13s projected anteriorly and posteriorly more often in *otk*^{A1} hemisegments (20%) than in wild types (7%) (Figure 32).

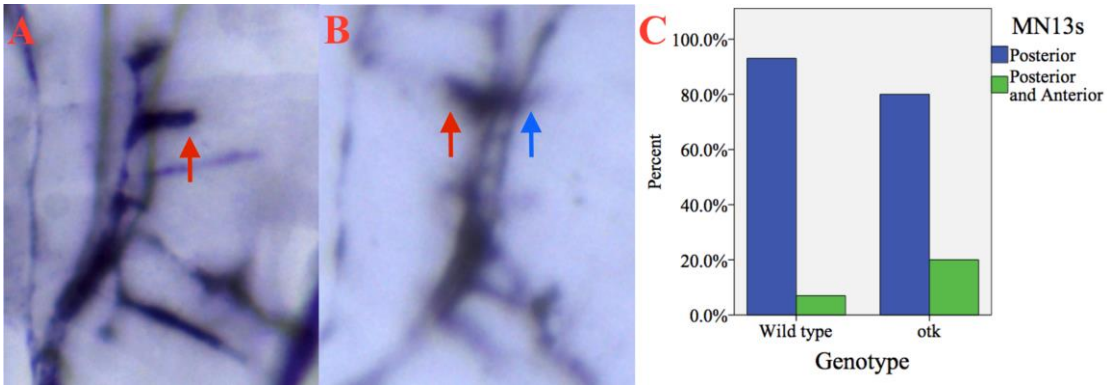

D	MN13s posterior	MN13s posterior and anterior
Wild type	93% (133)	7% (10)
otk^{A1}	80% (88)	20% (22)

Figure 32. Image A (right is posterior, up is dorsal) shows the ventral section of a wild type hemisegment in which the MN13s project posteriorly (red arrow). Image B (right is posterior, up is dorsal) shows the ventral section of an *otk*^{A1} hemisegment in which the MN13s project anteriorly (red arrow) and posteriorly (blue arrow). The graph (C) shows the percentage of hemisegments in which the MN13s project posteriorly or anteriorly and posteriorly in 27 wild type and 26 *otk*^{A1} embryos. The table (D) shows the percentage and number of hemisegments in which the MN13s project posteriorly or anteriorly and posteriorly in the same embryos.

A chi-square test for independence revealed that the MN13s projected anteriorly and posteriorly significantly more often in *otk*^{A1} hemisegments than in wild types, χ^2 (1, n = 253) = 9.52, p < .01.

MN12s project anteriorly

The MN12s of *otk*^{A1} embryos projected anteriorly. 26.5% of *otk*^{A1} hemisegments exhibited the mild phenotype, compared to 20% of wild type hemisegments (Figure 33B). 32.4% of *otk*^{A1} hemisegments exhibited the severe phenotype, compared to 8.8% of wild type hemisegments (Figure 33C).

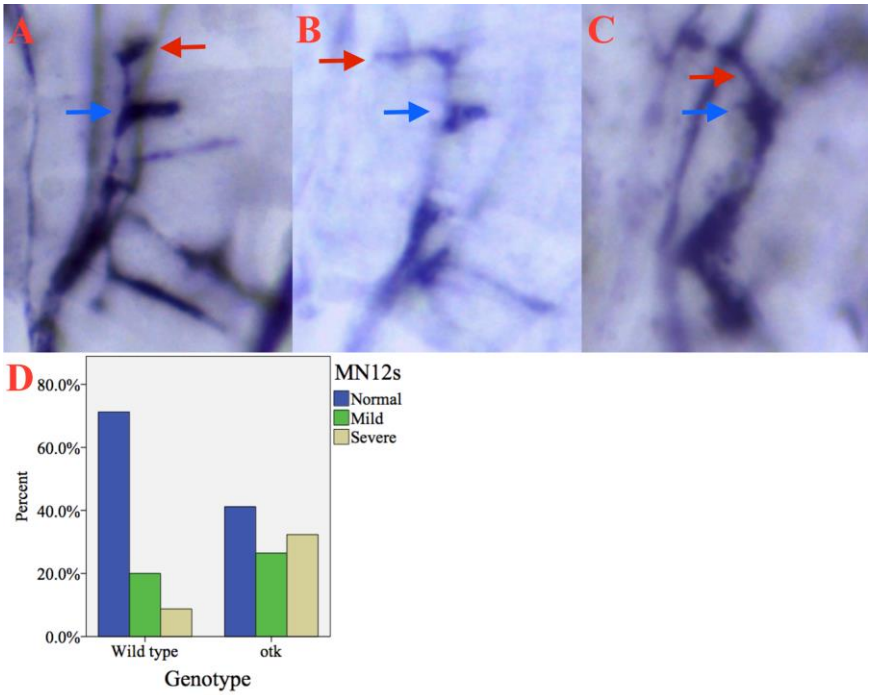

E	MN12s normal	MN12s mild	MN12s severe
Wild type	71.2% (57)	20% (16)	8.8% (7)
otk^{A1}	41.2% (42)	26.5% (27)	32.4% (33)

Figure 33. Image A (right is posterior, up is dorsal) shows the ventral section of a wild type hemisegment in which the MN12s project dorsally at the muscle 13 innervation point (blue arrow) before projecting posteriorly (red arrow). Image B (right is posterior, up is dorsal) shows the ventral section of an *otk*^{A1} hemisegment in which the MN12s project dorsally at the muscle 13 innervation point (blue arrow) before projecting anteriorly (red arrow). Image C (right is posterior, up is dorsal) shows the ventral section of an *otk*^{A1} hemisegment in which the MN12s (red arrow) project anteriorly at the muscle 13 innervation point (blue arrow). The graph (D) shows the percentage of hemisegments that exhibit the normal, mild, and severe phenotypes in 27 wild type and 26 *otk*^{A1} embryos. The table (E) shows the percentage and number of hemisegments exhibiting normal, mild, and severe phenotypes in the same embryos.

A chi-square test for independence test revealed a significant effect of genotype with regard to the trajectory of the MN12s, χ^2 (2, n = 182) = 19.61, p < .001.

RP3 axon absent

The RP3 axon was absent more often in *otk*^{A1} hemisegments (38.6%) than in wild types (20.1%) (Figure 34).

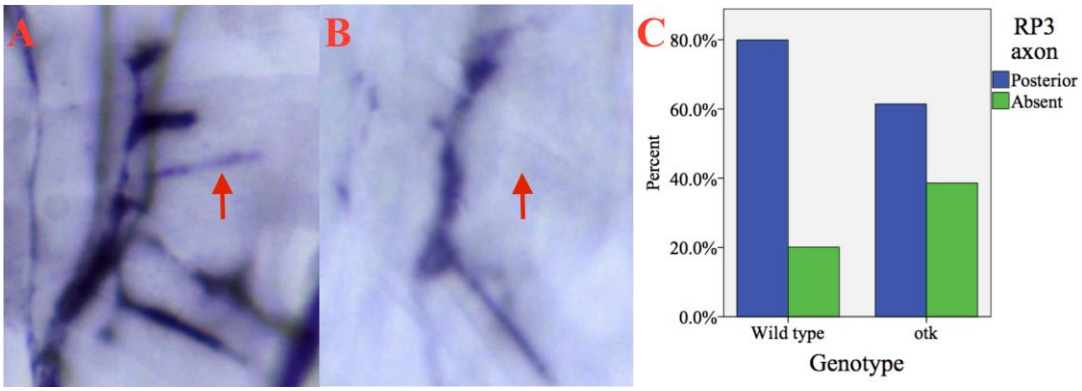

D	RP3 axon posterior	RP3 axon absent
Wild type	79.9% (147)	20.1% (37)
otk^{A1}	61.4% (105)	38.6% (66)

Figure 34. Image A (right is posterior, up is dorsal) shows the ventral section of a wild type hemisegment with the RP3 axon indicated (red arrow). Image B (right is posterior, up is dorsal) shows the ventral section of an *otk*^{A1} hemisegment without the RP3 axon (red arrow). The graph (C) shows the percentage of hemisegments in which the RP3 axon is present or absent in 27 wild type and 26 *otk*^{A1} embryos. The table (D) shows the percentage and number of hemisegments in which the RP3 axon is present or absent in the same embryos.

A chi-square test for independence revealed that the RP3 axon was absent significantly more often in *otk*^{A1} hemisegments than in wild types, χ^2 (1, n = 355) = 14.71, p < .001.

4.2.5. Phenotypic analysis: *BSC199*

While *otk*^{A1} and *otk2*^{C26} embryos exhibit abnormal motor axon phenotypes with statistically significant frequencies, the penetrance of most of the phenotypes is relatively low (e.g., the ISNb is absent in only 7.1% of *otk*^{A1} hemisegments), which implies a level of redundancy. The *BSC199* deficiency line, which removes both *otk* and *otk2*, was used to investigate whether loss of both off-tracks would enhance phenotypic penetrance or severity. *BSC199* flies exhibit more severe phenotypes than the *otk*^{A1} and *otk2*^{C26} mutants. For example, although specific projections derived from the ISNb are absent in *otk*^{A1} and *otk2*^{C26} embryos (i.e., RP3 axon, MN12s, MN13s), the ISNb itself is

rarely absent. However, the ISNb is infrequently seen in *BSC199* embryos (Figure 35). Consequently, presence/absence of the RP3 axon, MN12s, and MN13s was not investigated. In addition to the ISNb, the ISNd (Figure 36), SNc (Figure 38), FB (Figure 39), and SB (Figure 40) are absent. Similarly, the dorsal or lateral branches of the SNa are missing (Figure 37).

ISNb absent

The ISNb was absent more often in *BSC199* hemisegments (82.8%) than in wild types (2%) (Figure 35).

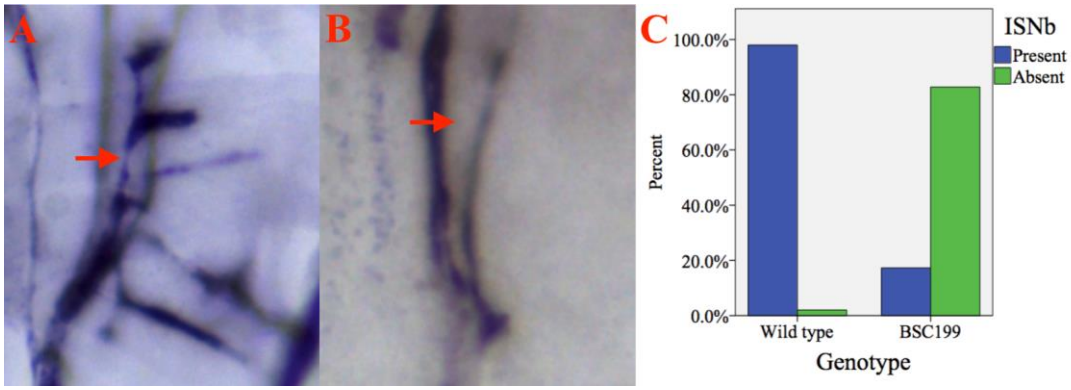

D	ISNb present	ISNb absent
Wild type	98% (240)	2% (5)
BSC199	17.2% (5)	82.8% (24)

Figure 35. Image A (right is posterior, up is dorsal) shows the ventral section of a wild type hemisegment with the ISNb (red arrow). Image B (right is posterior, up is dorsal) shows the ventral section of a *BSC199* hemisegment without the ISNb (red arrow). The graph (C) shows the percentage of hemisegments with and without the ISNb in 30 wild type embryos and 3 *BSC199* embryos. The table (D) shows the percentage and number of hemisegments with and without the ISNb.

Fisher's exact test revealed that the ISNb was absent significantly more often in *BSC199* hemisegments than in wild types, $p < .001$.

ISNd absent

The ISNd was absent more often in *BSC199* hemisegments (91.2%) than in wild types (17.7%) (Figure 36).

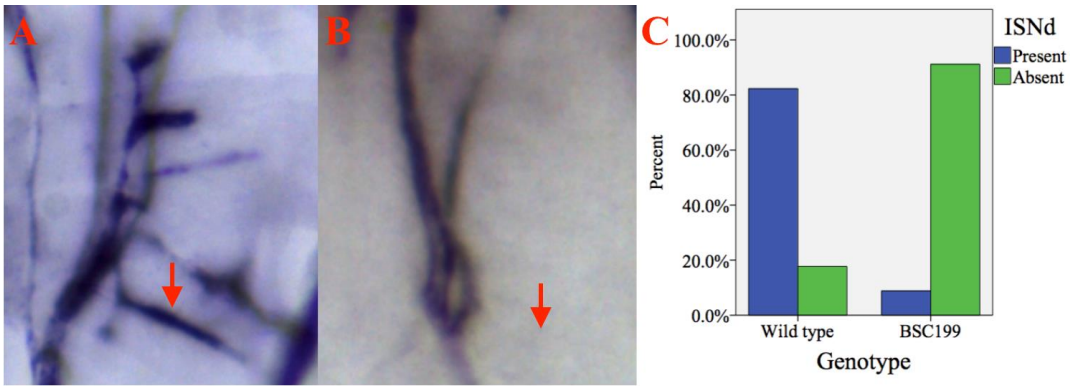

D	ISNd present	ISNd absent
Wild type	82.3% (144)	17.7% (31)
BSC199	8.8% (3)	91.2% (31)

Figure 36. Image A (right is posterior, up is dorsal) shows the ventral section of a wild type hemisegment with the ISNd (red arrow). Image B (right is posterior, up is dorsal) shows the ventral section of a *BSC199* hemisegment without the ISNd (red arrow). The graph (C) shows the percentage of hemisegments with and without the ISNd in 30 wild type and 3 *BSC199* embryos. The table (D) shows the percentage and number of hemisegments with and without the ISNd.

A chi-square test for independence revealed that the ISNd was absent significantly more often in *BSC199* hemisegments than in wild types, χ^2 (1, n = 209) = 73.64, p < .001.

SNa aberrant bifurcation

SNa bifurcation is aberrant in *BSC199* embryos (Figure 37). Bifurcation is normal (both branches are present) in 96.3% and 45.2% of wild type and *BSC199* hemisegments, respectively. The dorsal branch is absent in 0.9% of wild type hemisegments and 19.4% of *BSC199* hemisegments. The lateral branch is absent in 2.8% of wild type hemisegments and 35.5% of *BSC199* hemisegments.

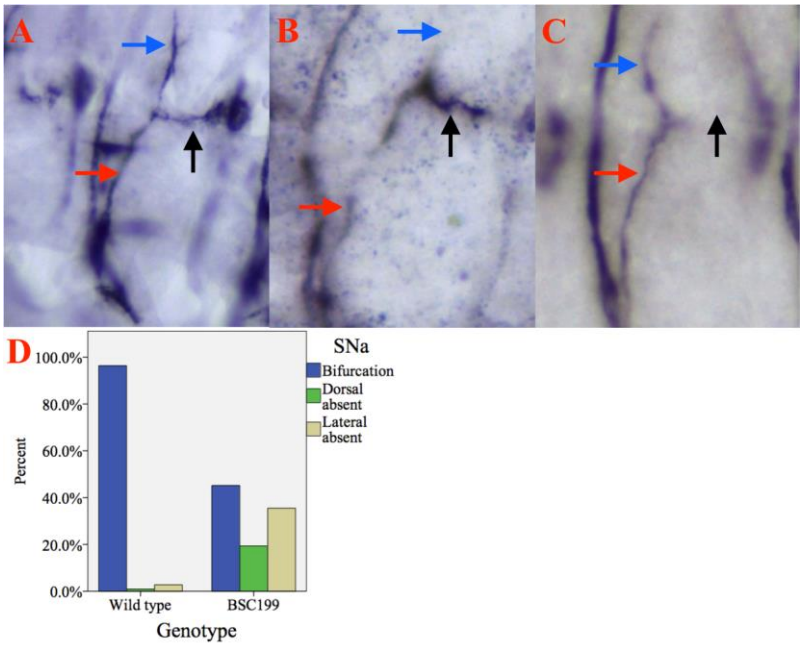

	Bifurcated	Dorsal branch absent	Lateral branch absent
Wild type	96.3% (105)	0.9% (1)	2.8% (3)
BSC199	45.2% (14)	19.4% (6)	35.4% (11)

Figure 37. Image A (right is posterior, up is dorsal) shows the ventral section a wild type hemisegment with a bifurcated SNa (red arrow), with the dorsal (blue arrow) and lateral (black arrow) branches indicated. Image B (right is posterior, up is dorsal) shows the ventral section of a *BSC199* hemisegment with the SNa (red arrow) with the lateral branch (black arrow), though without the dorsal branch (blue arrow). Image C (right is posterior, up is dorsal) shows the ventral section of a *BSC199* hemisegment with the SNa (red arrow) with the dorsal branch (blue arrow), though without the lateral branch (black arrow). The graph (D) shows the percentage of hemisegments in which the SNa bifurcates or lacks the dorsal or lateral branches in 30 wild type and 3 *BSC199* embryos. The table (E) shows the percentage and number of hemisegments in which the SNa bifurcates or lacks the dorsal or lateral branches.

Fisher's exact test revealed a significant effect of genotype with regard to bifurcation of the SNa, $p < .001$.

SNc absent

The SNc was absent more often in *BSC199* hemisegments (66.7%) than in wild types (7.5%) (Figure 38).

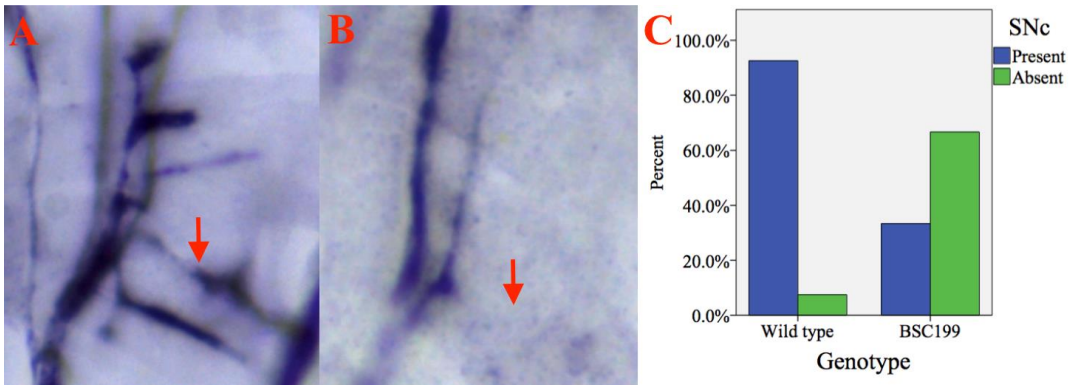

D	SNc present	SNc absent
Wild type	92.5% (161)	7.5% (13)
BSC199	33.3% (12)	66.7% (24)

Figure 38. Image A (right is posterior, up is dorsal) shows the ventral section of a wild type hemisegment with the SNc (red arrow). Image B (right is posterior, up is dorsal) shows the ventral section of a *BSC199* hemisegment without the SNc (red arrow). The graph (C) shows the percentage of hemisegments with and without the SNc in 30 wild type embryos and 3 *BSC199* embryos. The table (D) shows the percentage and number of hemisegments with and without the SNc.

A chi-square test for independence revealed that the SNc was absent significantly more often in *BSC199* hemisegments than in wild types, χ^2 (1, n = 210) = 72.01, p < .001.

FB absent

The FB was absent more often in *BSC199* hemisegments (60.6%) than in wild types (7.6%) (Figure 39).

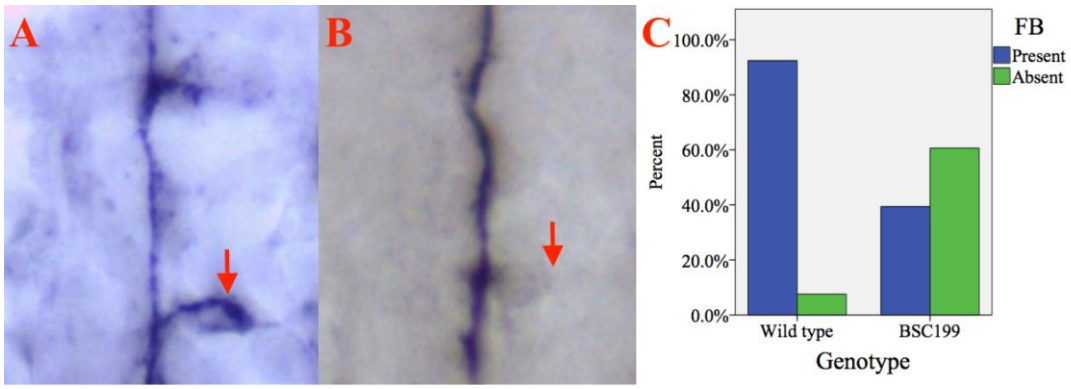

D	FB present	FB absent
Wild type	92.4% (195)	7.6% (16)
BSC199	39.4% (13)	60.6% (20)

Figure 39. Image A (right is posterior, up is dorsal) shows the dorsal section of a wild type hemisegment with the FB (red arrow). Image B (right is posterior, up is dorsal) shows the dorsal section of a *BSC199* hemisegment without the FB (red arrow). The graph (C) shows the percentage of hemisegments with and without the FB in 30 wild type and 3 *BSC199* embryos. The table (D) shows the percentage and number of hemisegments with and without the FB.

Fisher's exact test revealed that the FB was absent significantly more often in *BSC199* hemisegments than in wild types, $p < .001$.

SB absent

The SB was absent more often in *BSC199* hemisegments (76%) than in wild types (30.7%) (Figure 40).

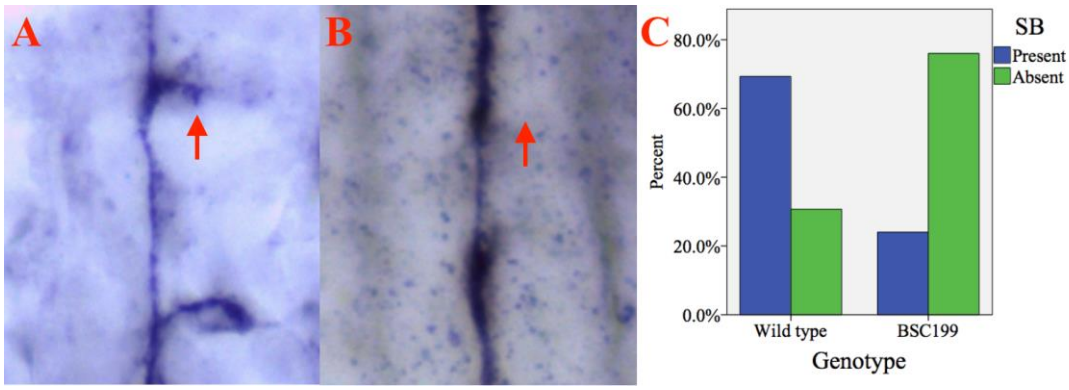

D	SB present	SB absent
Wild type	69.3% (70)	30.7% (31)
BSC199	24% (6)	76% (19)

Figure 40. Image A (right is posterior, up is dorsal) shows the dorsal section of a wild type hemisegment with the SB (red arrow). Image B (right is posterior, up is dorsal) shows the dorsal section of a *BSC199* hemisegment without the SB (red arrow). The graph (C) shows the percentage of hemisegments with and without the SB in 30 wild type and 3 *BSC199* embryos. The table (D) shows the percentage and number of hemisegments with and without the SB.

Fisher's exact test revealed that the SB was absent significantly more often in *BSC199* hemisegments than in wild types, $p < .001$.

4.2.6. Phenotypic analysis: *sema-1a*

Otk and Otk2 physically interact (Linnemannstöns et al., 2014) and Otk forms part of a receptor complex with PlexA (Winberg et al., 2001), which is implicated in Sema-1a-based signalling (Winberg et al., 1998). Therefore, it is conceivable that Otk2 also participates in this pathway. This idea was investigated by analysing embryos that were transheterozygous for functional copies of *otk2* and *sema-1a* after it was established that *sema-1a* homozygous embryos exhibit motor axon phenotypes resembling those in previous reports (Terman et al., 2002; Winberg et al., 2001; Winberg et al., 1998; Yu et al., 1998; Yu, Huang, & Kolodkin, 2000). In *sema-1a* embryos, the MN13s were absent (Figure 44), projected anteriorly (Figure 45), or projected anteriorly and posteriorly (Figure 46). The FB (Figure 41), SB (Figure 42), ISNb (Figure 43), MN12s (Figure 47), and RP3 axon (Figure 48) were also absent.

FB absent

The FB was absent more often in *sema-1a* hemisegments (23.9%) than in wild types (7.6%) (Figure 41).

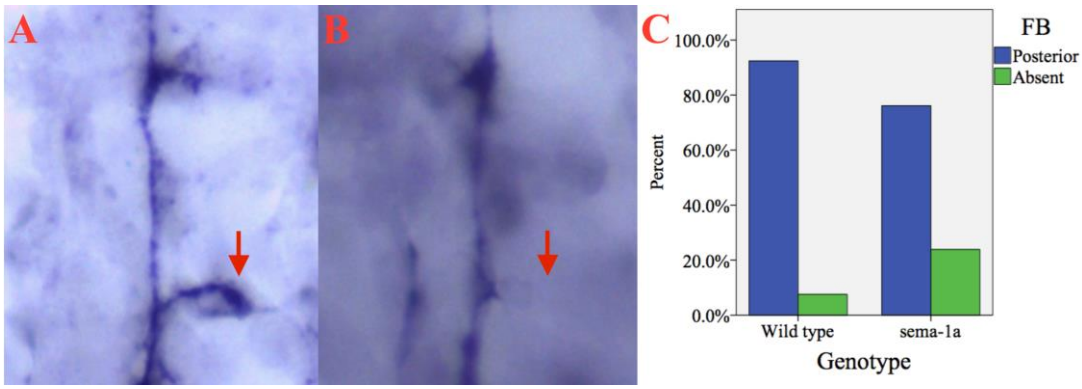

D	FB posterior	FB absent
Wild type	92.4% (195)	7.6% (16)
sema-1a	76.1% (51)	23.9% (16)

Figure 41. Image A (right is posterior, up is dorsal) shows the dorsal section of a wild type hemisegment with the FB indicated (red arrow). Image B (right is posterior, up is dorsal) shows the dorsal section of a *sema-1a* hemisegment without the FB (red arrow). The graph (C) shows the percentage of hemisegments in which the FB is present or absent in 30 wild type and 16 *sema-1a* embryos. The table (D) shows the percentage and number of hemisegments in which the FB is present or absent in the same embryos.

A chi-square test for independence revealed that the FB was absent significantly more often in *sema-1a* hemisegments than in wild types, χ^2 (1, n = 278) = 13.26, p < .001.

SB absent

The SB was absent more often in *sema-1a* hemisegments (66.7%) than in wild types (30.7%) (Figure 42).

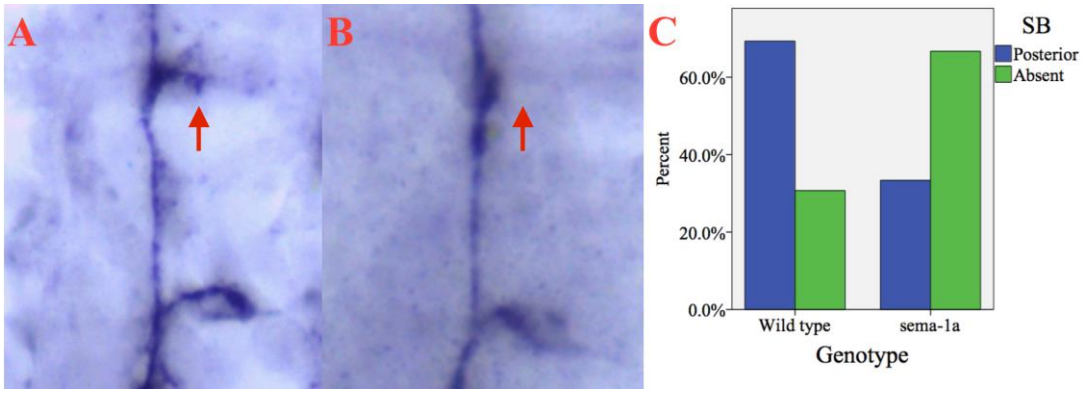

D	SB posterior	SB absent
Wild type	69.3% (70)	30.7% (31)
sema-1a	33.3% (7)	66.7% (14)

Figure 42. Image A (right is posterior, up is dorsal) shows the dorsal section of a wild type hemisegment with the SB indicated (red arrow). Image B (right is posterior, up is dorsal) shows the dorsal section of a sema-*1a* hemisegment without the SB (red arrow). The graph (C) shows the percentage of hemisegments in which the SB is present or absent in 30 wild type and 16 *sema-1a* embryos. The table (D) shows the percentage and number of hemisegments in which the SB is present or absent in the same embryos.

A chi-square test for independence revealed that the SB was absent significantly more often in *sema-1a* hemisegments than in wild types, χ^2 (1, n = 122) = 9.66, p < .01.

ISNb absent

The ISNb was absent more often in *sema-1a* hemisegments (19.6%) than in wild types (2%) (Figure 43).

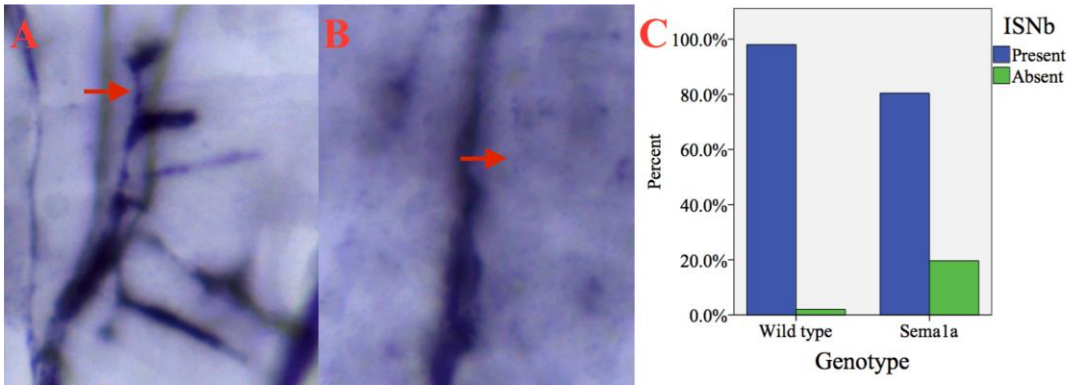

D	ISNb present	ISNb absent
Wild type	98% (240)	2% (5)
sema-1a	80.4% (86)	19.6% (21)

Figure 43. Image A (right is posterior, up is dorsal) shows the ventral section of a wild type hemisegment with the ISNb indicated (red arrow). Image B (right is posterior, up is dorsal) shows the ventral section of a *sema-1a* hemisegment without the ISNb (red arrow). The graph (C) shows the percentage of hemisegments in which the ISNb is present or absent in 30 wild type and 16 *sema-1a* embryos. The table (D) shows the percentage and number of hemisegments in which the ISNb is present or absent in the same embryos.

A chi-square test for independence revealed that ISNb was absent significantly more often in *sema-1a* hemisegments than in wild types, χ^2 (1, n = 352) = 33.67, p < .001.

MN13s absent

The MN13s were absent more often in *sema-1a* hemisegments (40.6%) than in wild types (11.9%) (Figure 44).

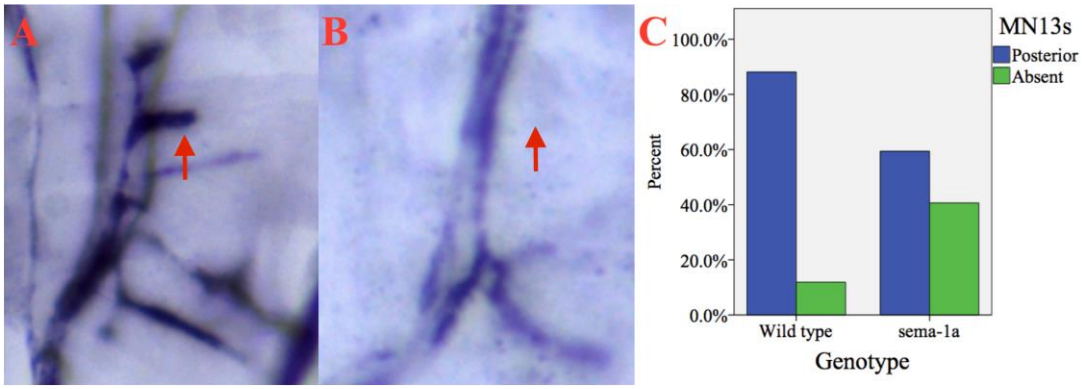

D	MN13s posterior	MN13s absent
Wild type	88.1% (133)	11.9% (18)
sema-1a	59.4% (19)	40.6% (13)

Figure 44. Image A (right is posterior, up is dorsal) shows the ventral section of a wild type hemisegment with the MN13s indicated (red arrow). Image B (right is posterior, up is dorsal) shows the ventral section of a *sema-1a* hemisegment without the MN13s (red arrow). The graph (C) shows the percentage of hemisegments in which the MN13s are present or absent in 27 wild type and 11 *sema-1a* embryos. The table (D) shows the percentage and number of hemisegments in which the MN13s are present or absent in the same embryos.

A chi-square test for independence revealed that the MN13s were absent significantly more often in *sema-1a* hemisegments than in wild types, χ^2 (1, n = 183) = 15.46, p < .001.

MN13s project anteriorly

The MN13s projected anteriorly more often in *sema-1a* hemisegments (24%) than in wild types (2.9%) (Figure 45).

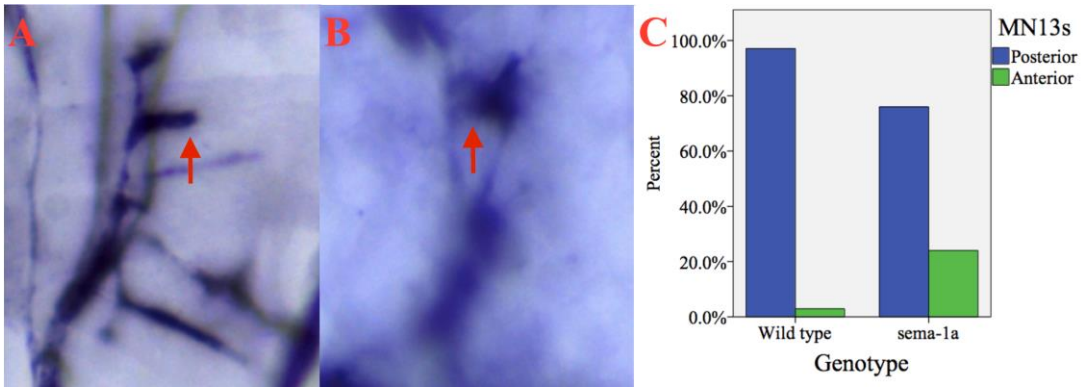

D	MN13s posterior	MN13s anterior
Wild type	97.1% (133)	2.9% (4)
sema-1a	76% (19)	24% (6)

Figure 45. Image A (right is posterior, up is dorsal) shows the ventral section of a wild type hemisegment in which the MN13s project posteriorly (red arrow). Image B (right is posterior, up is dorsal) shows the ventral section of a *sema-1a* hemisegment in which the MN13s project anteriorly (red arrow). The graph (C) shows the percentage of hemisegments in which the MN13s project posteriorly or anteriorly in 27 wild type and 11 *sema-1a* embryos. The table (D) shows the percentage and number of hemisegments in which the MN13s project posteriorly or anteriorly in the same embryos.

Fisher's exact test revealed that the MN13s projected anteriorly significantly more often in *sema-1a* hemisegments than in wild types, $p < .001$.

MN13s project anteriorly and posteriorly

The MN13s projected anteriorly and posteriorly more often in *sema-1a* hemisegments (26.9%) than in wild types (7%) (Figure 46).

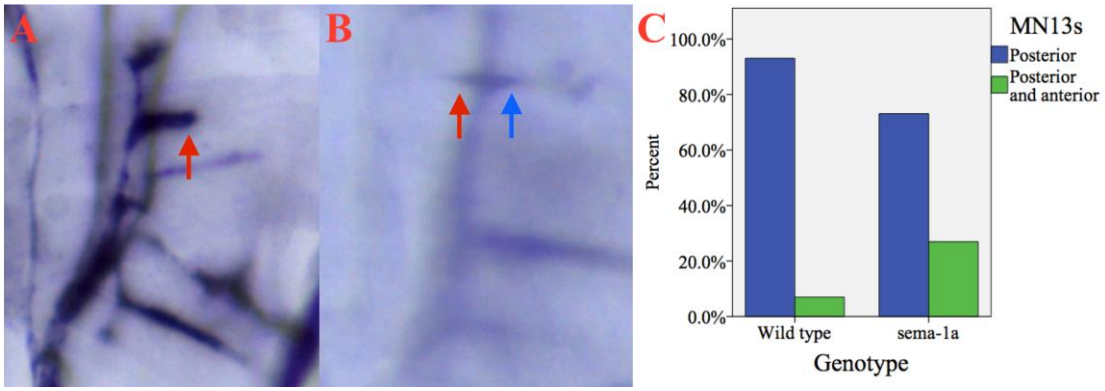

D	MN13s posterior	MN13s posterior and anterior
Wild type	93% (133)	7% (10)
sema-1a	73.1% (19)	26.9% (7)

Figure 46. Image A (right is posterior, up is dorsal) shows the ventral section of a wild type hemisegment in which the MN13s project posteriorly (red arrow). Image B (right is posterior, up is dorsal) shows the ventral section of a *sema-1a* hemisegment in which the MN13s project anteriorly (red arrow) and posteriorly (blue arrow). The graph (C) shows the percentage of hemisegments in which the MN13s project posteriorly or anteriorly and posteriorly in 27 wild type and 11 *sema-1a* embryos. The table (D) shows the percentage and number of hemisegments in which the MN13s project posteriorly or anteriorly and posteriorly in the same embryos.

Fisher's exact test revealed that the MN13s projected anteriorly and posteriorly significantly more often in *sema-1a* hemisegments than in wild types, $p < .01$.

MN12s absent

The MN12s were absent more often in *sema-1a* hemisegments (60%) than in wild types (22.6%) (Figure 47).

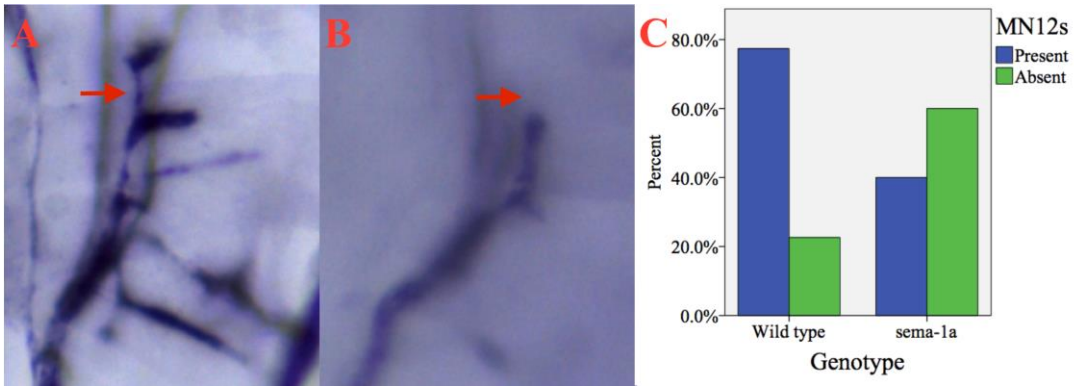

D	MN12s present	MN12s absent
Wild type	77.4% (130)	22.6% (38)
sema-1a	40% (14)	60% (21)

Figure 47. Image A (right is posterior, up is dorsal) shows the ventral section of a wild type hemisegment with the MN12s indicated (red arrow). Image B (right is posterior, up is dorsal) shows the ventral section of a *sema-1a* hemisegment without the MN12s (red arrow). The graph (C) shows the percentage of hemisegments in which the MN12s are present or absent in 27 wild type and 11 *sema-1a* embryos. The table (D) shows the percentage and number of hemisegments in which the MN12s are present or absent in the same embryos.

A chi-square test for independence revealed that the MN12s were absent significantly more often in *sema-1a* hemisegments than in wild types, χ^2 (1, n = 203) = 19.63, p < .001.

RP3 axon absent

The RP3 axon was absent more often in *sema-1a* hemisegments (62.2%) than in wild types (20.1%) (Figure 48).

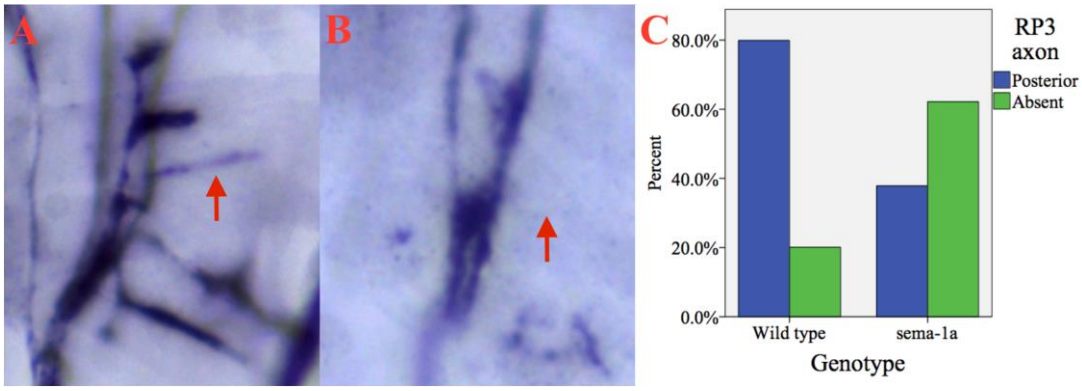

D	RP3 axon posterior	RP3 axon absent
Wild type	79.9% (147)	20.1% (37)
sema-1a	37.8% (14)	62.2% (23)

Figure 48. Image A (right is posterior, up is dorsal) shows the ventral section of a wild type hemisegment with the RP3 axon indicated (red arrow). Image B (right is posterior, up is dorsal) shows the ventral section of a *sema-1a* hemisegment without the RP3 axon (red arrow). The graph (C) shows the percentage of hemisegments in which the RP3 axon is present or absent in 27 wild type and 11 *sema-1a* embryos. The table (D) shows the percentage and number of hemisegments in which the RP3 axon is present or absent in the same embryos.

A chi-square test for independence revealed that the RP3 axon was absent significantly more often in *sema-1a* hemisegments than in wild types, χ^2 (1, n = 221) = 27.55, p < .001.

4.2.7. Phenotypic analysis: *fz2*

Prior analyses of motor axons in embryos with altered *fz2* activity focused exclusively on the MN12s and MN13s (Inaki et al., 2007). The current study, therefore, assessed the entire length of the motor axons for abnormalities. Defects were not observed in the MN13s, the FB, or SB in *fz2* embryos. However, they did exhibit MN12 anterior projections (Figure 49), and the RP3 axon was frequently absent (Figure 50).

MN12s project anteriorly

The MN12s of *fz2* embryos projected anteriorly. 59% of *fz2* hemisegments exhibited the mild phenotype (Figure 49B), compared to 20% of wild type hemisegments. 27.9% of *fz2* hemisegments exhibited the severe phenotype (Figure 49C), compared to 8.8% of wild type hemisegments.

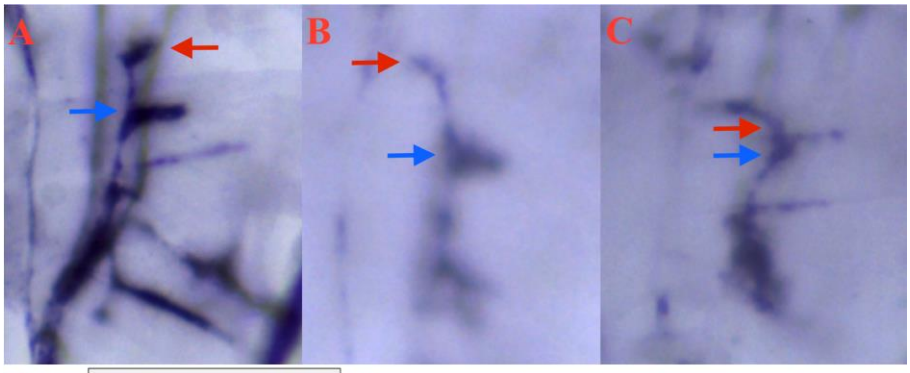

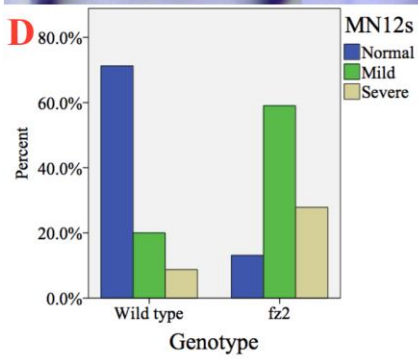

E	MN12s normal	MN12s mild	MN12s severe
Wild type	71.2% (57)	20% (16)	8.8% (7)
fz2	13.1% (8)	59% (36)	27.9% (17)

Figure 49. Image A (right is posterior, up is dorsal) shows the ventral section of a wild type hemisegment in which the MN12s project dorsally at the muscle 13 innervation point (blue arrow) before projecting posteriorly (red arrow). Image B (right is posterior, up is dorsal) shows the ventral section of an *fz2* hemisegment in which the MN12s project dorsally at the muscle 13 innervation point (blue arrow) before projecting anteriorly (red arrow). Image C (right is posterior, up is dorsal) shows the ventral section of an *fz2* hemisegment in which the MN12s (red arrow) project anteriorly at the muscle 13 innervation point (blue arrow). The graph (D) shows the percentage of hemisegments that exhibit the normal, mild, and severe phenotypes in 27 wild type and 18 *fz2* embryos. The table (E) shows the percentage and number of hemisegments exhibiting normal, mild, and severe phenotypes in the same embryos.

A chi-square test for independence test revealed a significant effect of genotype with regard to the trajectory of the MN12s, χ^2 (2, n = 141) = 47.09, p < .001.

RP3 axon absent

The RP3 axon was absent more often in *fz2* hemisegments (54.7%) than in wild types (20.1%) (Figure 50).

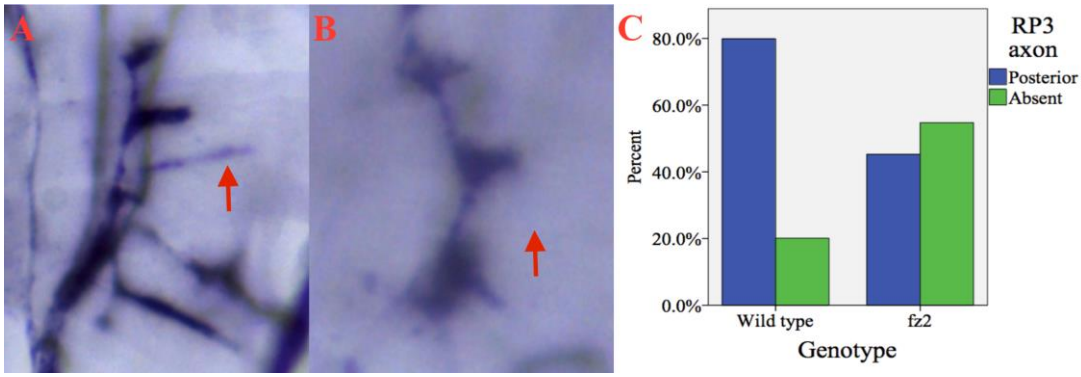

D	RP3 axon posterior	RP3 axon absent
Wild type	79.9% (147)	20.1% (37)
fz2	45.3% (43)	54.7% (52)

Figure 50. Image A (right is posterior, up is dorsal) shows the ventral section of a wild type hemisegment with the RP3 axon indicated (red arrow). Image B (right is posterior, up is dorsal) shows the ventral section of an *fz2* hemisegment without the RP3 axon (red arrow). The graph (C) shows the percentage of hemisegments in which the RP3 axon is present or absent in 27 wild type and 18 *fz2* embryos. The table (D) shows the percentage and number of hemisegments in which the RP3 axon is present or absent in the same embryos.

A chi-square test for independence revealed that the RP3 axon was absent significantly more often in *fz2* hemisegments than in wild types, χ^2 (1, n = 279) = 34.58, p < .001.

4.2.8. Phenotypic analysis: *otk/+, otk2/+*

Given that Otk and Otk2 physically interact (Linnemannstöns et al., 2014) and that *BSC199* embryos, which lack *otk* and *otk2* activity, have more severe phenotypes than single mutants, it is conceivable that the off-tracks participate in a shared signalling pathway. To test this, the motor axons of embryos transheterozygous for functional copies of the off-tracks were examined. In *otk/+, otk2/+* transheterozygous embryos, the SB (Figure 51) and RP3 axon (Figure 54) were frequently absent, and the MN13s (Figure 52) and MN12s (Figure 53) often projected anteriorly.

SB absent

The SB was absent more often in *otk/+, otk2/+* hemisegments (65.2%) than in wild types (30.7%) (Figure 51).

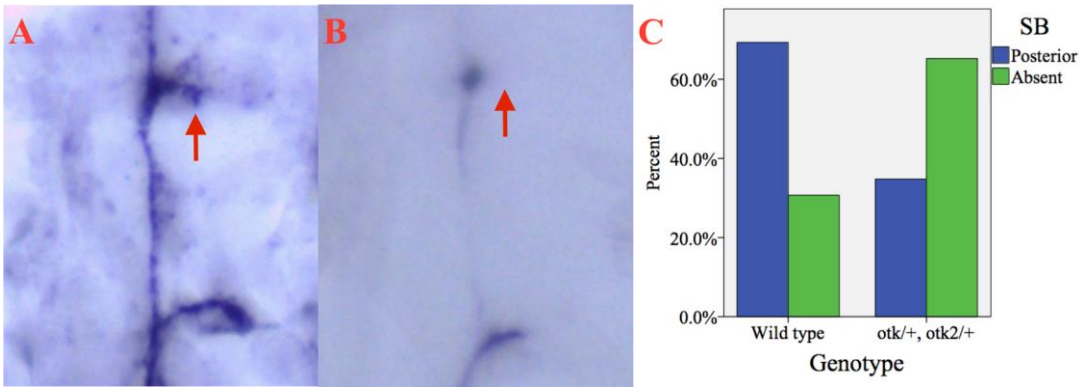

D	SB posterior	SB absent
Wild type	69.3% (70)	30.7% (31)
otk/+, otk2/+	34.8% (16)	65.2% (30)

Figure 51. Image A (right is posterior, up is dorsal) shows the dorsal section of a wild type hemisegment with the SB indicated (red arrow). Image B (right is posterior, up is dorsal) shows the dorsal section of an *otk/+, otk2/+* hemisegment without the SB (red arrow). The graph (C) shows the percentage of hemisegments in which the SB is present or absent in 30 wild type and 20 *otk/+, otk2/+* embryos. The table (D) shows the percentage and number of hemisegments in which the SB is present or absent in the same embryos.

A chi-square test for independence revealed that the SB was absent significantly more often in *otk/+, otk2/+* hemisegments than in wild types, χ^2 (1, n = 147) = 15.52, p < .001.

MN13s project anteriorly

The MN13s projected anteriorly more often in *otk/+, otk2/+* hemisegments (15.2%) than in wild types (2.9%) (Figure 52).

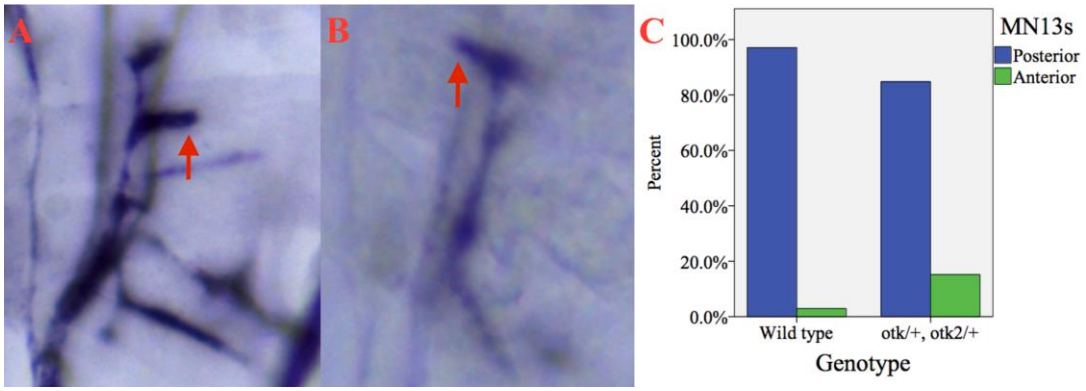

D	MN13s posterior	MN13s anterior
Wild type	97.1% (133)	2.9% (4)
otk/+, otk2/+	84.8% (67)	15.2% (12)

Figure 52. Image A (right is posterior, up is dorsal) shows the ventral section of a wild type hemisegment in which the MN13s project posteriorly (red arrow). Image B (right is posterior, up is dorsal) shows the ventral section of an *otk/+, otk2/+* hemisegment in which the MN13s project anteriorly (red arrow). The graph (C) shows the percentage of hemisegments in which the MN13s project posteriorly or anteriorly in 27 wild type and 16 *otk/+, otk2/+* embryos. The table (D) shows the percentage and number of hemisegments in which the MN13s project posteriorly or anteriorly in the same embryos.

A chi-square test for independence revealed that the MN13s projected anteriorly significantly more often in *otk/+, otk2/+* hemisegments than in wild types, χ^2 (1, n = 216) = 11, $p < .01$.

MN12s project anteriorly

The MN12s of *otk/+, otk2/+* embryos projected anteriorly. 49% of *otk/+, otk2/+* hemisegments exhibited the mild phenotype (Figure 53B), compared to 20% of wild type hemisegments. 28.6% of *otk/+, otk2/+* hemisegments exhibited the severe phenotype (Figure 53C), compared to 8.8% of wild type hemisegments.

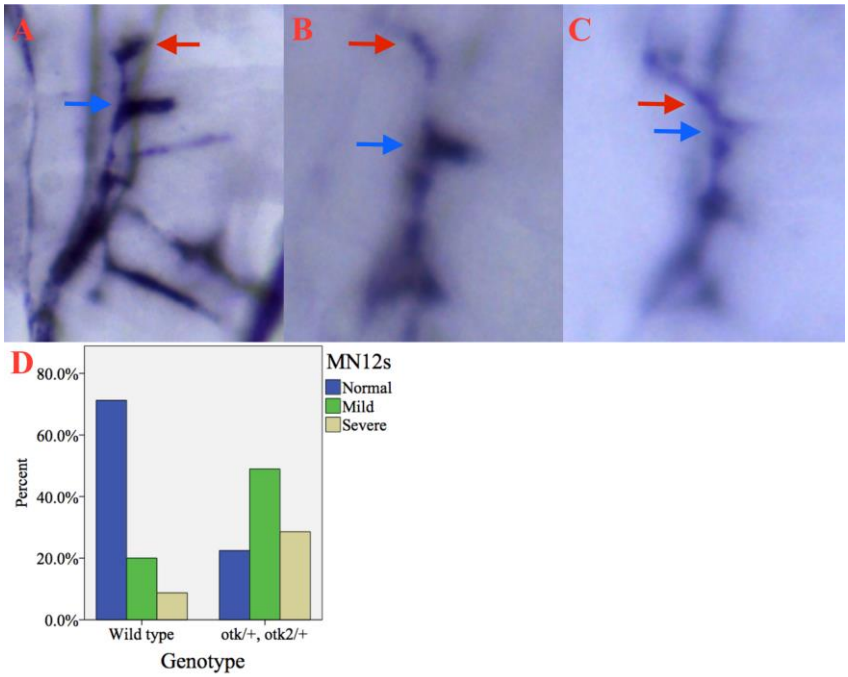

E	MN12s normal	MN12s mild	MN12s severe
Wild type	71.2% (57)	20% (16)	8.8% (7)
otk/+, otk2/+	22.4% (11)	49% (24)	28.6% (14)

Figure 53. Image A (right is posterior, up is dorsal) shows the ventral section of a wild type hemisegment in which the MN12s project dorsally at the muscle 13 innervation point (blue arrow) before projecting posteriorly (red arrow). Image B (right is posterior, up is dorsal) shows the ventral section of an *otk/+, otk2/+* hemisegment in which the MN12s project dorsally at the muscle 13 innervation point (blue arrow) before projecting anteriorly (red arrow). Image C (right is posterior, up is dorsal) shows the ventral section of an *otk/+, otk2/+* hemisegment in which the MN12s (red arrow) project anteriorly at the muscle 13 innervation point (blue arrow). The graph (D) shows the percentage of hemisegments that exhibit the normal, mild, and severe phenotypes in 27 wild type and 16 *otk/+, otk2/+* embryos. The table (E) shows the percentage and number of hemisegments exhibiting normal, mild, and severe phenotypes in the same embryos.

A chi-square test for independence test revealed a significant effect of genotype with regard to the trajectory of the MN12s, χ^2 (2, n = 129) = 29.29, p < .001.

RP3 axon absent

The RP3 axon was absent more often in *otk/+, otk2/+* hemisegments (53.5%) than in wild types (20.1%) (Figure 54).

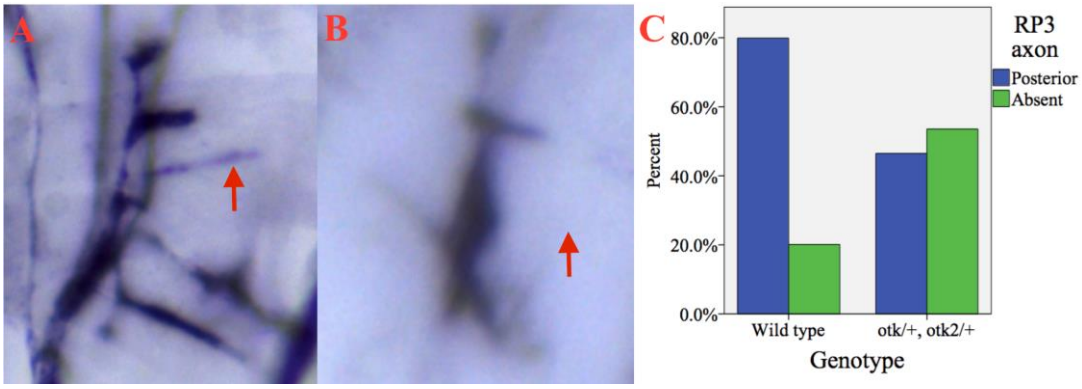

D	RP3 axon posterior	RP3 axon absent
Wild type	79.9% (147)	20.1% (37)
otk/+, otk2/+	46.5% (46)	53.5% (53)

Figure 54. Image A (right is posterior, up is dorsal) shows the ventral section of a wild type hemisegment with the RP3 axon indicated (red arrow). Image B (right is posterior, up is dorsal) shows the ventral section of an *otk/+, otk2/+* hemisegment without the RP3 axon (red arrow). The graph (C) shows the percentage of hemisegments in which the RP3 axon is present or absent in 27 wild type and 16 *otk/+, otk2/+* embryos. The table (D) shows the percentage and number of hemisegments in which the RP3 axon is present or absent in the same embryos.

A chi-square test for independence revealed that the RP3 axon was absent significantly more often in *otk/+, otk2/+* hemisegments than in wild types, χ^2 (1, n = 283) = 33.16, p < .001.

4.2.9. Phenotypic analysis: *otk2/+, sema1a/+*

Otk and Otk2 physically interact (Linnemannstöns et al., 2014) and Otk forms part of a receptor complex with PlexA (Winberg et al., 2001), which is implicated in Sema-1a-based signalling (Winberg et al., 1998). Therefore, it is conceivable that Otk2 also participates in this pathway. This idea was investigated by analysing embryos that were transheterozygous for functional copies of *otk2* and *sema-1a*. *otk2/+, sema1a/+* transheterozygous embryos exhibited the SB anterior phenotype (Figure 55), MN13s

absent (Figure 56) and anterior phenotypes (Figure 57), MN12s absent (Figure 58) and anterior phenotypes (Figure 59), and the RP3 axon absent phenotype (Figure 60).

SB anterior

The SB projected anteriorly more often in *otk2/+, sema1a/+* hemisegments (26.9%) than in wild types (9.1%) (Figure 55).

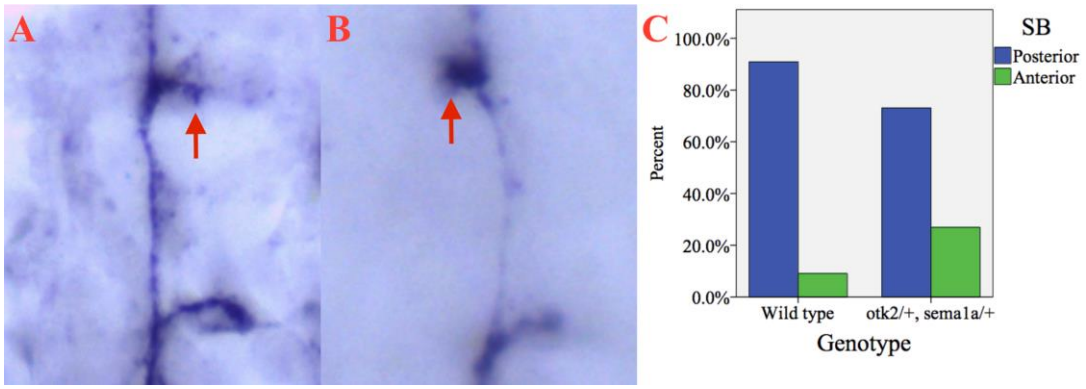

D	SB posterior	SB anterior
Wild type	90.9% (70)	9.1% (7)
otk2/+, sema1a/+	73.1% (38)	26.9% (14)

Figure 55. Image A (right is posterior, up is dorsal) shows the dorsal section of a wild type hemisegment with the SB projecting posteriorly (red arrow). Image B (right is posterior, up is dorsal) shows the dorsal section of an *otk2/+, sema1a/+* hemisegment with the SB projecting anteriorly (red arrow). The graph (C) shows the percentage of hemisegments in which the SB projects posteriorly or anteriorly in 30 wild type and 17 *otk2/+, sema1a/+* embryos. The table (D) shows the percentage and number of hemisegments in which the SB projects posteriorly or anteriorly in the same embryos.

A chi-squared for independence revealed that the SB projected anteriorly significantly more often in *otk2/+, sema1a/+* hemisegments than in wild types, χ^2 (1, n = 129) = 7.24, $p < .01$.

MN13s absent

The MN13s were absent more often in *otk2/+, sema1a/+* hemisegments (25.4%) than in wild types (11.9%) (Figure 56).

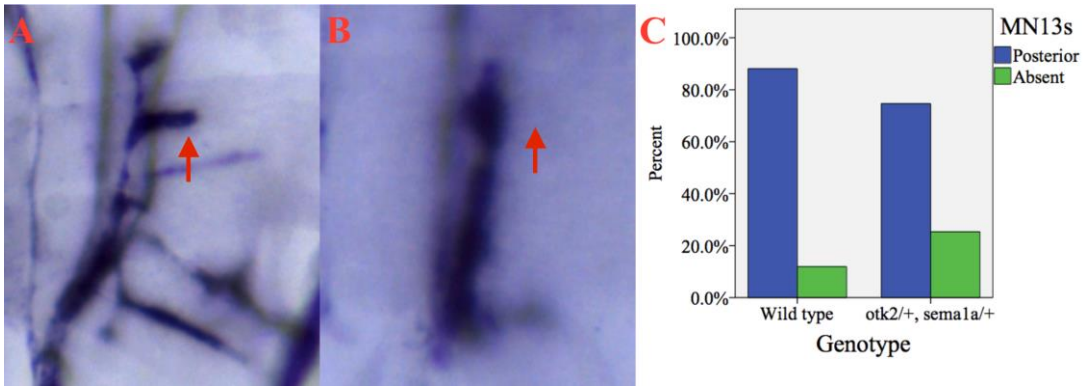

D	MN13s posterior	MN13s absent
Wild type	88.1% (133)	11.9% (18)
otk2/+, sema1a/+	74.6% (53)	25.4% (18)

Figure 56. Image A (right is posterior, up is dorsal) shows the ventral section of a wild type hemisegment with the MN13s indicated (red arrow). Image B (right is posterior, up is dorsal) shows the ventral section of an *otk2/+, sema1a/+* hemisegment without the MN13s (red arrow). The graph (C) shows the percentage of hemisegments in which the MN13s are present or absent in 27 wild type and 13 *otk2/+, sema1a/+* embryos. The table (D) shows the percentage and number of hemisegments in which the MN13s are present or absent in the same embryos.

A chi-square test for independence revealed that the MN13s were absent significantly more often in *otk2/+, sema1a/+* hemisegments than in wild types, χ^2 (1, n = 222) = 6.41, $p < .05$.

MN13s project anteriorly

The MN13s projected anteriorly more often in *otk2/+, sema1a/+* hemisegments (13.1%) than in wild types (2.9%) (Figure 57).

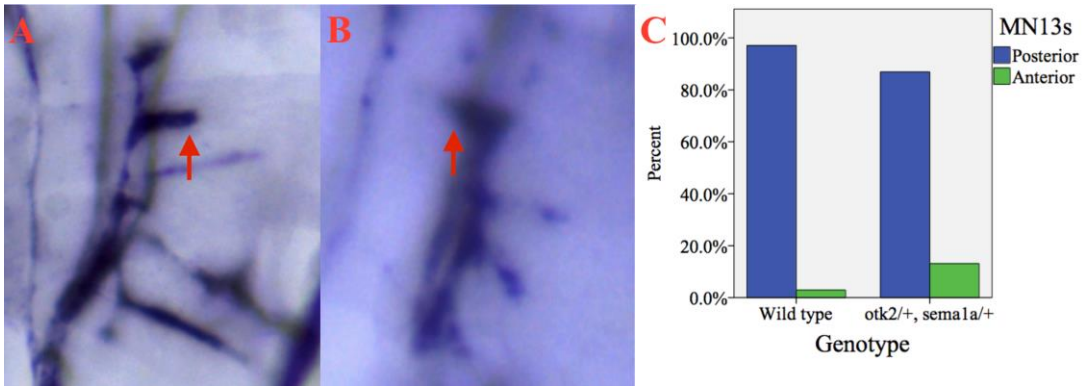

D	MN13s posterior	MN13s anterior
Wild type	97.1% (133)	2.9% (4)
otk2/+, sema1a/+	86.9% (53)	13.1% (8)

Figure 57. Image A (right is posterior, up is dorsal) shows the ventral section of a wild type hemisegment in which the MN13s project posteriorly (red arrow). Image B (right is posterior, up is dorsal) shows the ventral section of an *otk2/+, sema1a/+* hemisegment in which the MN13s project anteriorly (red arrow). The graph (C) shows the percentage of hemisegments in which the MN13s project posteriorly or anteriorly in 27 wild type and 13 *otk2/+, sema1a/+* embryos. The table (D) shows the percentage and number of hemisegments in which the MN13s project posteriorly or anteriorly in the same embryos.

A chi-square test for independence revealed that the MN13s projected anteriorly significantly more often in *otk2/+, sema1a/+* hemisegments than in wild types, χ^2 (1, n = 198) = 7.71, $p < .01$.

MN12s absent

The MN12s were absent more often in *otk2/+, sema-1a/+* hemisegments (34.6%) than in wild types (22.6%) (Figure 58).

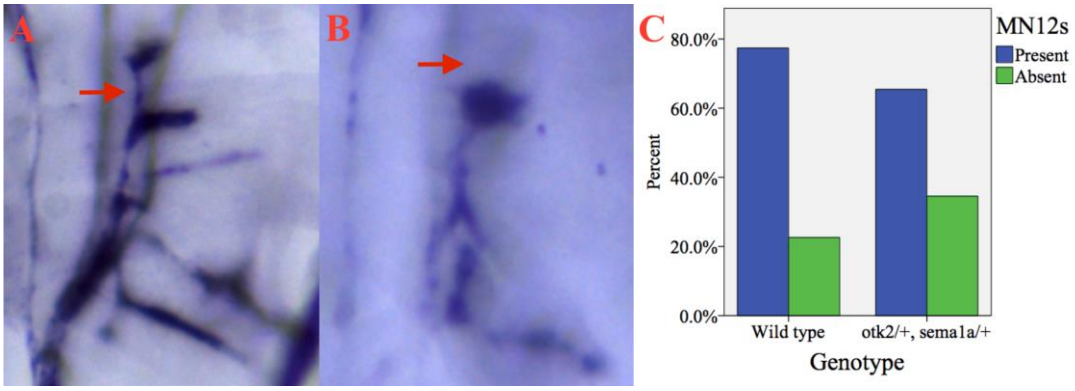

D	MN12s present	MN12s absent
Wild type	77.4% (130)	22.6% (38)
otk2/+, sema1a/+	65.4% (53)	34.6% (28)

Figure 58. Image A (right is posterior, up is dorsal) shows the ventral section of a wild type hemisegment with the MN12s indicated (red arrow). Image B (right is posterior, up is dorsal) shows the ventral section of an otk*2/+, sema-1a/+* hemisegment without the MN12s (red arrow). The graph (C) shows the percentage of hemisegments in which the MN12s are present or absent in 27 wild type and 13 *otk2/+, sema-1a/+* embryos. The table (D) shows the percentage and number of hemisegments in which the MN12s are present or absent in the same embryos.

A chi-square test for independence revealed that the MN12s were absent significantly more often in *otk2/+, sema-1a/+* hemisegments than in wild types, χ^2 (1, n = 249) = 4.01, $p < .05$.

MN12s project anteriorly

The MN12s of *otk2/+, sema-1a/+* embryos projected anteriorly. 47.4% of *otk2/+, sema-1a/+* hemisegments exhibited the mild phenotype (Figure 59B), compared to 20% of wild type hemisegments. 36.8% of *otk2/+, sema-1a/+* hemisegments exhibited the severe phenotype (Figure 59C), compared to 8.8% of wild type hemisegments.

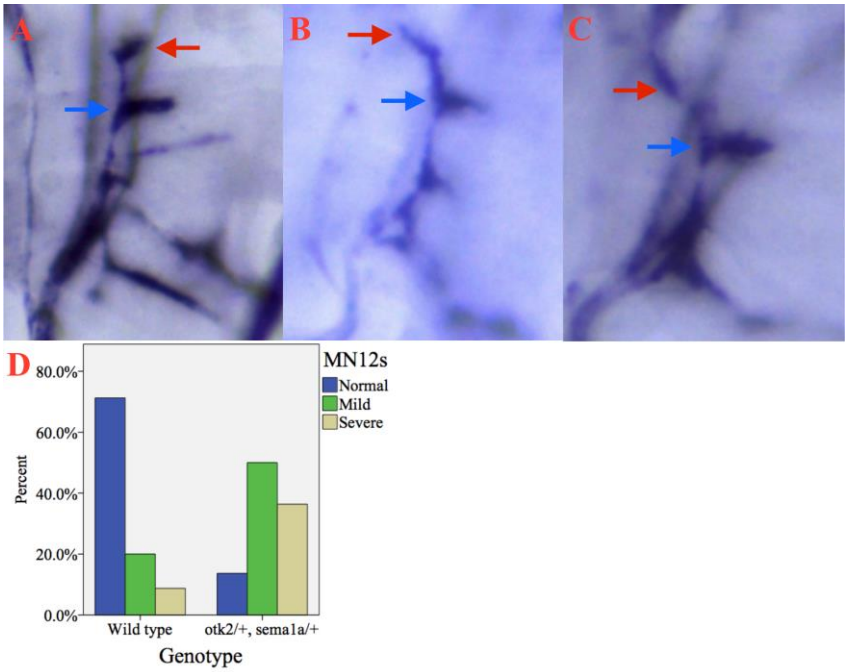

E	MN12s normal	MN12s mild	MN12s severe
Wild type	71.2% (57)	20% (16)	8.8% (7)
otk2/+, sema1a/+	15.8% (3)	47.4% (9)	36.8% (7)

Figure 59. Image A (right is posterior, up is dorsal) shows the ventral section of a wild type hemisegment in which the MN12s project dorsally at the muscle 13 innervation point (blue arrow) before projecting posteriorly (red arrow). Image B (right is posterior, up is dorsal) shows the ventral section of an *otk2/+, sema-1a/+* hemisegment in which the MN12s project dorsally at the muscle 13 innervation point (blue arrow) before projecting anteriorly (red arrow). Image C (right is posterior, up is dorsal) shows the ventral section of an *otk2/+, sema-1a/+* hemisegment in which the MN12s (red arrow) project anteriorly at the muscle 13 innervation point (blue arrow). The graph (D) shows the percentage of hemisegments that exhibit the normal, mild, and severe phenotypes in 27 wild type and 13 *otk2/+, sema-1a/+* embryos. The table (E) shows the percentage and number of hemisegments exhibiting normal, mild, and severe phenotypes in the same embryos.

A chi-square test for independence test revealed a significant effect of genotype with regard to the trajectory of the MN12s, χ^2 (2, n = 99) = 20.91, p < .001.

RP3 axon absent

The RP3 axon was absent more often in *otk2/+, sema-1a/+* hemisegments (66.3%) than in wild types (20.1%) (Figure 60).

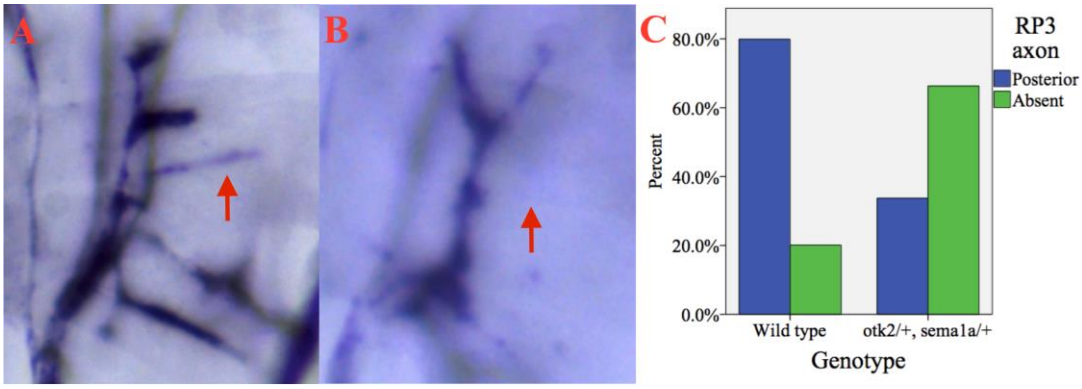

D	RP3 axon posterior	RP3 axon absent
Wild type	79.9% (147)	20.1% (37)
otk2/+, sema1a/+	33.7% (31)	66.3% (61)

Figure 60. Image A (right is posterior, up is dorsal) shows the ventral section of a wild type hemisegment with the RP3 axon indicated (red arrow). Image B (right is posterior, up is dorsal) shows the ventral section of an *otk2/+, sema-1a/+* hemisegment without the RP3 axon (red arrow). The graph (C) shows the percentage of hemisegments in which the RP3 axon is present or absent in 27 wild type and 13 *otk2/+, sema-1a/+* embryos. The table (D) shows the percentage and number of hemisegments in which the RP3 axon is present or absent in the same embryos.

A chi-square test for independence revealed that the RP3 axon was absent significantly more often in *otk2/+, sema-1a/+* hemisegments than in wild types, χ^2 (1, n = 276) = 57.16, $p < .001$.

4.2.10. Phenotypic analysis: *otk2/+; fz2/+*

Since Otk2 and Fz2 physically interact (Linnemannstöns et al., 2014) and embryos with altered *otk2* or *fz2* activity exhibit motor axon defects (Inaki et al., 2007; this current study), it is conceivable that they participate in a shared signalling pathway. To test this, the motor axons of embryos transheterozygous for functional copies of *otk2* and *fz2* were examined. *otk2/+; fz2/+* transheterozygous embryos exhibited the SB absent (Figure 61), MN13s absent (Figure 62), RP3 axon absent (Figure 64), and MN12s anterior (Figure 63) phenotypes.

SB absent

The SB was absent more often in *otk2/+; fz2/+* hemisegments (47.1%) than in wild types (30.7%) (Figure 61).

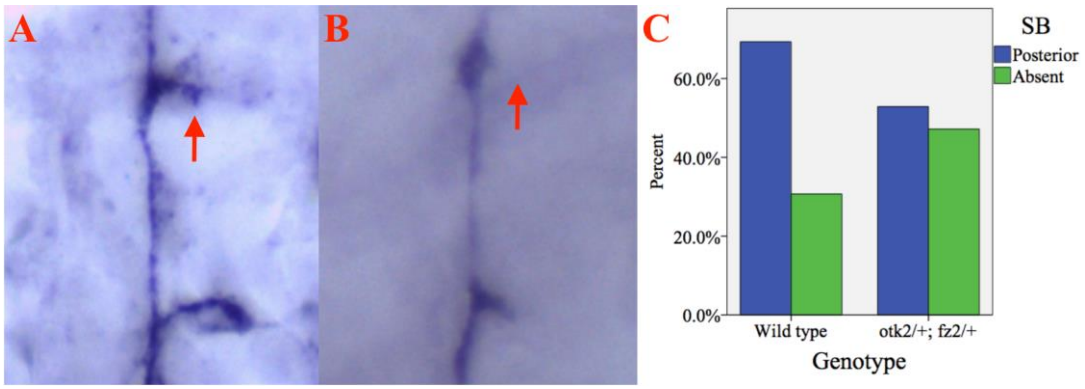

D	SB posterior	SB absent
Wild type	69.3% (70)	30.7% (31)
otk2/+; fz2/+	52.9% (37)	47.1% (33)

Figure 61. Image A (right is posterior, up is dorsal) shows the dorsal section of a wild type hemisegment with the SB indicated (red arrow). Image B (right is posterior, up is dorsal) shows the dorsal section of an *otk2/+; fz2/+*hemisegment without the SB (red arrow). The graph (C) shows the percentage of hemisegments in which the SB is present or absent in 30 wild type and 17 *otk2/+; fz2/+* embryos. The table (D) shows the percentage and number of hemisegments in which the SB is present or absent in the same embryos.

A chi-square test for independence revealed that the SB was absent significantly more often in *otk2/+; fz2/+* hemisegments than in wild types, χ^2 (1, n = 171) = 4.78, p < .05.

MN13s absent

The MN13s were absent more often in *otk2/+; fz2/+* hemisegments (23.6%) than in wild types (11.9%) (Figure 62).

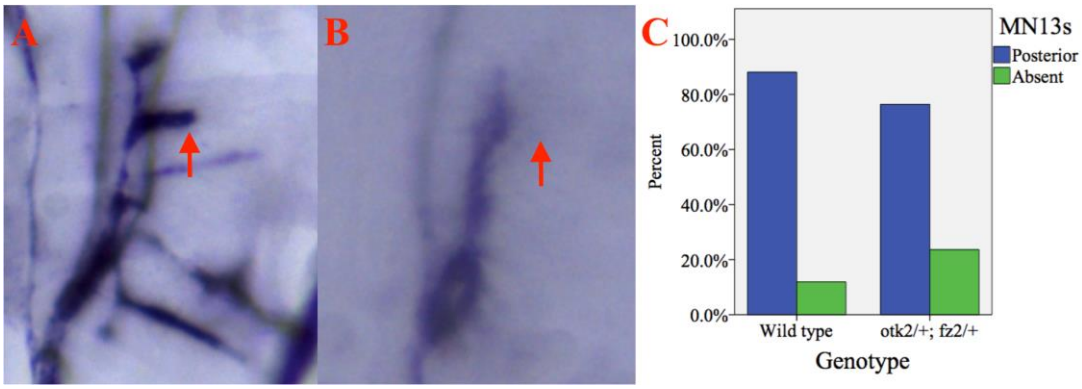

D	MN13s posterior	MN13s absent
Wild type	88.1% (133)	11.9% (18)
otk2/+; fz2/+	76.4% (55)	23.6% (17)

Figure 62. Image A (right is posterior, up is dorsal) shows the ventral section of a wild type hemisegment with the MN13s indicated (red arrow). Image B (right is posterior, up is dorsal) shows the ventral section of an *otk2/+; fz2/+* hemisegment without the MN13s (red arrow). The graph (C) shows the percentage of hemisegments in which the MN13s are present or absent in 27 wild type and 12 *otk2/+; fz2/+* embryos. The table (D) shows the percentage and number of hemisegments in which the MN13s are present or absent in the same embryos.

A chi-square test for independence revealed that the MN13s were absent significantly more often in *otk2/+; fz2/+* hemisegments than in wild types, χ^2 (1, n = 223) = 5.04, p < .05.

MN12s project anteriorly

The MN12s of *otk2/+; fz2/+* embryos projected anteriorly. 41.3% of *otk2/+; fz2/+* hemisegments exhibited the mild phenotype (Figure 63B), compared to 20% of wild type hemisegments. 21.7% of *otk2/+; fz2/+* hemisegments exhibited the severe phenotype (Figure 63C), compared to 8.8% of wild type hemisegments.

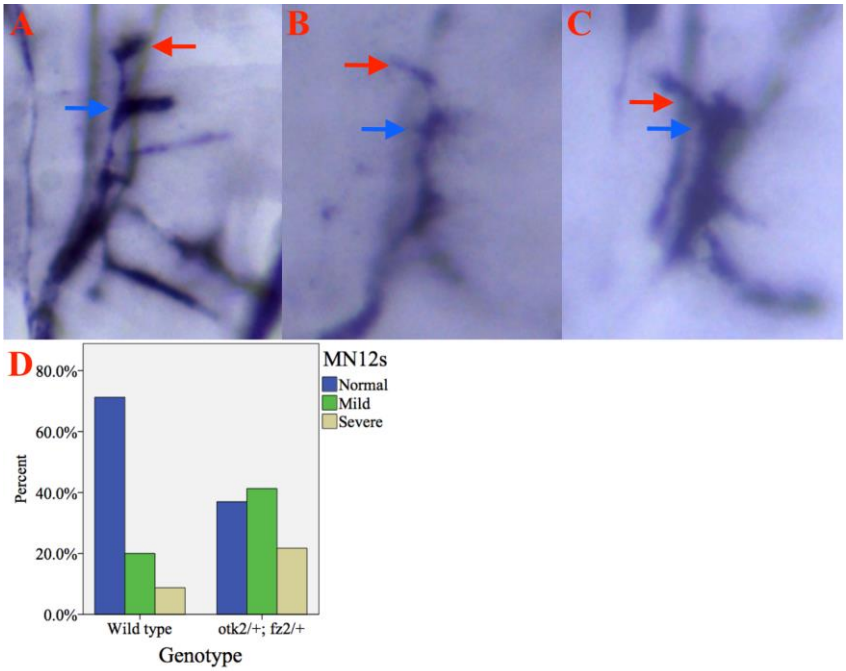

E	MN12s normal	MN12s mild	MN12s severe
Wild type	71.2% (57)	20% (16)	8.8% (7)
otk2/+; fz2/+	37% (17)	41.3% (19)	21.7% (10)

Figure 63. Image A (right is posterior, up is dorsal) shows the ventral section of a wild type hemisegment in which the MN12s project dorsally at the muscle 13 innervation point (blue arrow) before projecting posteriorly (red arrow). Image B (right is posterior, up is dorsal) shows the ventral section of an *otk2/+; fz2/+* hemisegment in which the MN12s project dorsally at the muscle 13 innervation point (blue arrow) before projecting anteriorly (red arrow). Image C (right is posterior, up is dorsal) shows the ventral section of an *otk2/+; fz2/+* hemisegment in which the MN12s (red arrow) project anteriorly at the muscle 13 innervation point (blue arrow). The graph (D) shows the percentage of hemisegments that exhibit the normal, mild, and severe phenotypes in 27 wild type and 12 *otk2/+; fz2/+* embryos. The table (E) shows the percentage and number of hemisegments exhibiting normal, mild, and severe phenotypes in the same embryos.

A chi-square test for independence test revealed a significant effect of genotype with regard to the trajectory of the MN12s, χ^2 (2, n = 126) = 14.27, p < .01.

RP3 axon absent

The RP3 axon was absent more often in *otk2/+; fz2/+* hemisegments (51.3%) than in wild types (20.1%) (Figure 64).

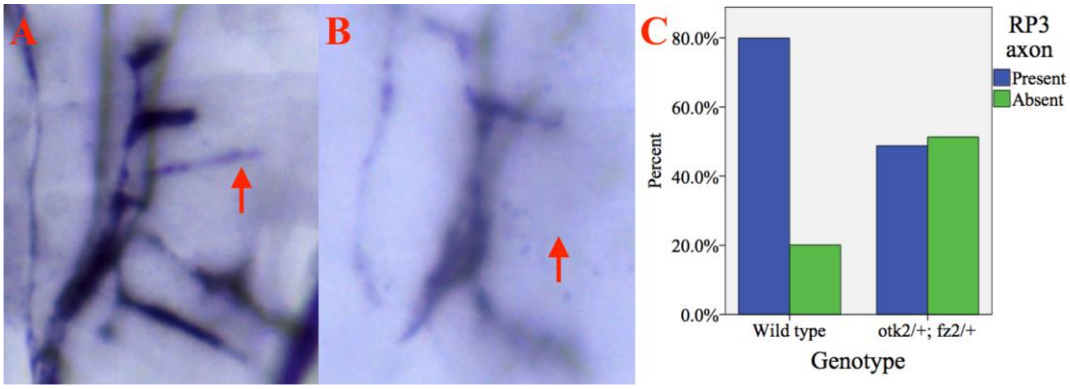

D	RP3 axon posterior	RP3 axon absent
Wild type	79.9% (147)	20.1% (37)
otk2/+; fz2/+	48.7% (38)	51.3% (40)

Figure 64. Image A (right is posterior, up is dorsal) shows the ventral section of a wild type hemisegment with the RP3 axon indicated (red arrow). Image B (right is posterior, up is dorsal) shows the ventral section of an *otk2/+; fz2/+* hemisegment without the RP3 axon (red arrow). The graph (C) shows the percentage of hemisegments in which the RP3 axon is present or absent in 27 wild type and 12 *otk2/+; fz2/+* embryos. The table (D) shows the percentage and number of hemisegments in which the RP3 axon is present or absent in the same embryos.

A chi-square test for independence revealed that the RP3 axon was absent significantly more often in *otk2/+; fz2/+* hemisegments than in wild types, χ^2 (1, n = 262) = 25.65, p < .001.

4.2.11. Phenotypic analysis: *otk/+; fz2/+*

Since Otk and Fz2 physically interact (Linnemannstöns et al., 2014) and embryos with altered *otk* or *fz2* activity have motor axon defects (Inaki et al., 2007; Winberg et al., 2001), it is conceivable that they participate in a shared signalling pathway. To test this, the motor axons of embryos transheterozygous for functional copies of *otk* and *fz2* were examined. The MN12s (Figure 66) and MN13s (Figure 65) of *otk/+; fz2/+* embryos projected anteriorly.

MN13s project anteriorly

The MN13s projected anteriorly more often in *otk/+; fz2/+* hemisegments (20.4%) than in wild types (2.9%) (Figure 65).

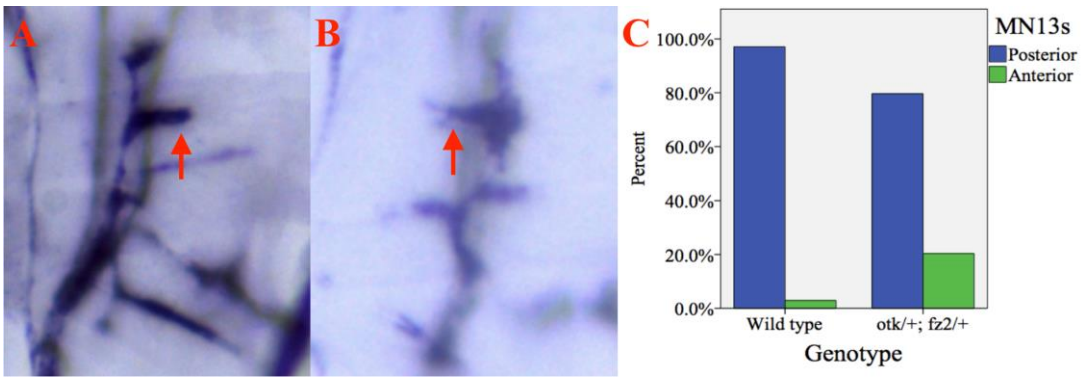

D	MN13s posterior	MN13s anterior
Wild type	97.1% (133)	2.9% (4)
otk/+; fz2/+	79.6% (43)	20.4% (11)

Figure 65. Image A (right is posterior, up is dorsal) shows the ventral section of a wild type hemisegment in which the MN13s project posteriorly (red arrow). Image B (right is posterior, up is dorsal) shows the ventral section of an *otk/+; fz2/+* hemisegment in which the MN13s project anteriorly (red arrow). The graph (C) shows the percentage of hemisegments in which the MN13s project posteriorly or anteriorly in 27 wild type and 10 *otk/+; fz2/+* embryos. The table (D) shows the percentage and number of hemisegments in which the MN13s project posteriorly or anteriorly in the same embryos.

Fisher's exact test revealed that the MN13s projected anteriorly significantly more often in *otk/+; fz2/+* hemisegments than in wild types, $p < .001$.

MN12s project anteriorly

The MN12s of *otk/+; fz2/+* embryos projected anteriorly. 38.2% of *otk/+; fz2/+* hemisegments exhibited the mild phenotype (Figure 66B), compared to 20% of wild type hemisegments. 30.9% of *otk/+; fz2/+* hemisegments exhibited the severe phenotype (Figure 66C), compared to 8.8% of wild type hemisegments.

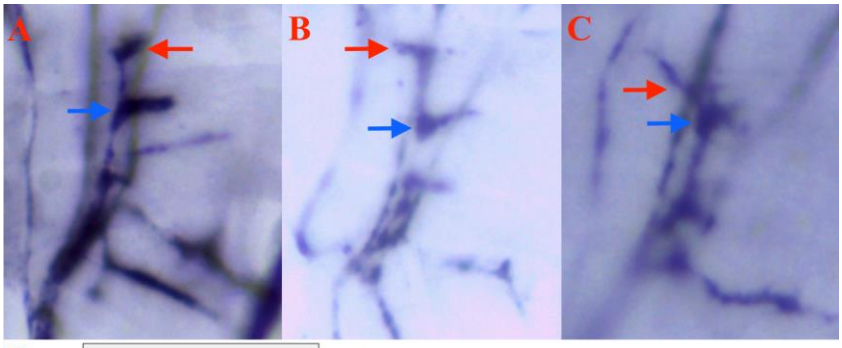

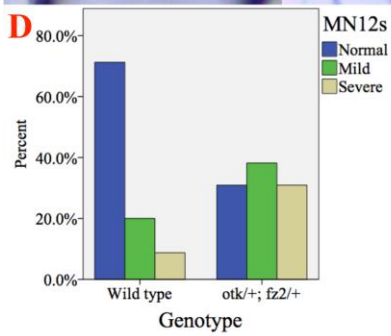

E	MN12s normal	MN12s mild	MN12s severe
Wild type	71.2% (57)	20% (16)	8.8% (7)
otk/+; fz2/+	30.9% (17)	38.2% (21)	30.9% (17)

Figure 66. Image A (right is posterior, up is dorsal) shows the ventral section of a wild type hemisegment in which the MN12s project dorsally at the muscle 13 innervation point (blue arrow) before projecting posteriorly (red arrow). Image B (right is posterior, up is dorsal) shows the ventral section of an *otk/+; fz2/+* hemisegment in which the MN12s project dorsally at the muscle 13 innervation point (blue arrow) before projecting anteriorly (red arrow). Image C (right is posterior, up is dorsal) shows the ventral section of an *otk/+; fz2/+* hemisegment in which the MN12s (red arrow) project anteriorly at the muscle 13 innervation point (blue arrow). The graph (D) shows the percentage of hemisegments that exhibit the normal, mild, and severe phenotypes in 27 wild type and 10 *otk/+; fz2/+* embryos. The table (E) shows the percentage and number of hemisegments exhibiting normal, mild, and severe phenotypes in the same embryos.

A chi-square test for independence test revealed a significant effect of genotype with regard to the trajectory of the MN12s, χ^2 (2, n = 135) = 22.61, p < .001.

4.2.12. Phenotypic analysis: *OK371 X EY03841*

Having established that motor axons are aberrant in *otk2* loss-of-function embryos, *otk2* expression was driven in motor neurons using an *OK371-GAL4* driver in order to gain insights into *otk2*'s precise function. *OK371-GAL4* flies were crossed with *EY03841* flies, which harbour a UAS in the 5' region of *otk2*. In contrast to a number of the loss-of-function genotypes referred to immediately above, the FB (Figure 67) and SB (Figure 68) of the ISN were present more often in *OK371 X EY03841* embryos than in wild types. Similarly, the MN12s grew posteriorly and the RP3 axon was present at frequencies closely resembling wild types. The MN13s, however, were often absent (Figure 69) or projected anteriorly (Figure 70).

Reduced FB absence

The FB was present more often in *OK371 X EY03841* hemisegments (99.3%) than in wild types (92.4%) (Figure 67).

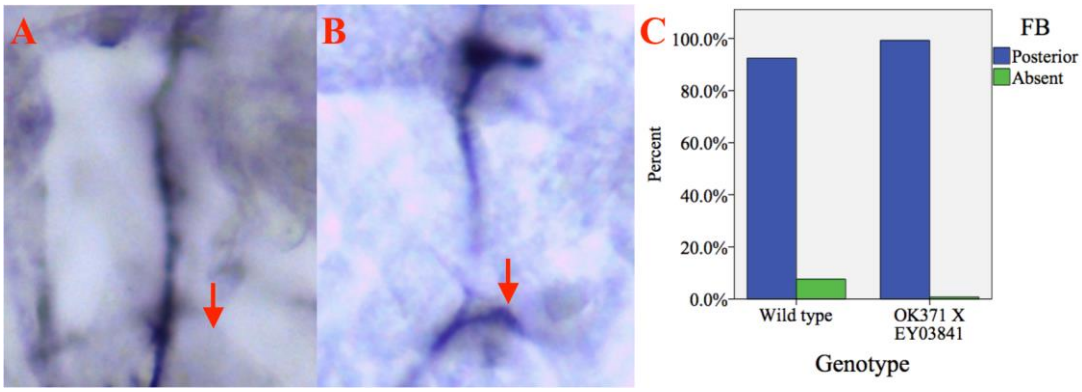

D	FB posterior	FB absent
Wild type	92.4% (195)	7.6% (16)
OK371 X EY03841	99.3% (134)	0.7% (1)

Figure 67. Image A (right is posterior, up is dorsal) shows the dorsal section of a wild type hemisegment without the FB (red arrow). Image B (right is posterior, up is dorsal) shows the dorsal section of an *OK371 X EY03841* hemisegment with the FB (red arrow). The graph (C) shows the percentage of hemisegments in which the FB is present or absent in 30 wild type and 19 *OK371 X EY03841* embryos. The table (D) shows the percentage and number of hemisegments in which the FB is present or absent in the same embryos.

A chi-square test for independence revealed that the FB was present significantly more often in *OK371 X EY03841* hemisegments than in wild types, χ^2 (1, n = 346) = 8.25, p < .01.

Reduced SB absence

The SB was present more often in *OK371 X EY03841* hemisegments (82.7%) than in wild types (69.3%) (Figure 68).

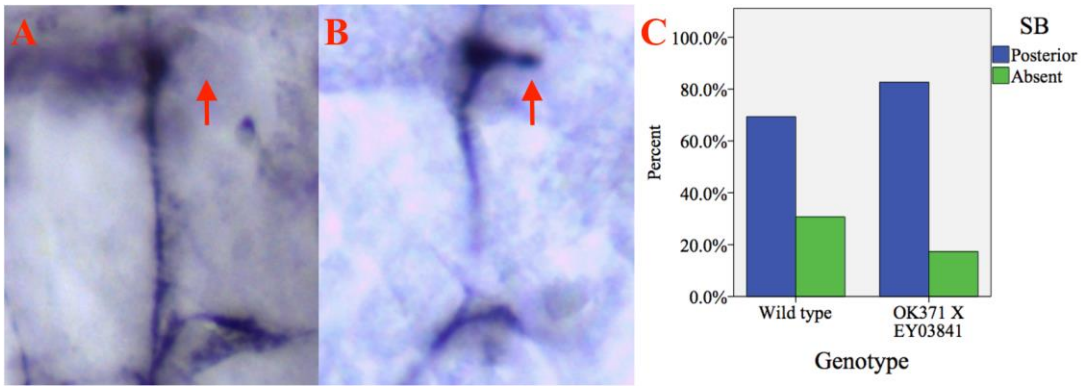

D	SB posterior	SB absent
Wild type	69.3% (70)	30.7% (31)
OK371 X EY03841	82.7% (62)	17.3% (13)

Figure 68. Image A (right is posterior, up is dorsal) shows the dorsal section of a wild type hemisegment without the SB (red arrow). Image B (right is posterior, up is dorsal) shows the dorsal section of an *OK371 X EY03841* hemisegment with the SB (red arrow). The graph (C) shows the percentage of hemisegments in which the SB is present or absent in 30 wild type and 19 *OK371 X EY03841* embryos. The table (D) shows the percentage and number of hemisegments in which the SB is present or absent in the same embryos.

A chi-square test for independence revealed that the SB was present significantly more often in *OK371 X EY03841* hemisegments than in wild types, χ^2 (1, n = 176) = 4.1, p < .05.

MN13s absent

The MN13s were absent more often in *OK371 X EY03841* hemisegments (29.8%) than in wild types (11.9%) (Figure 69).

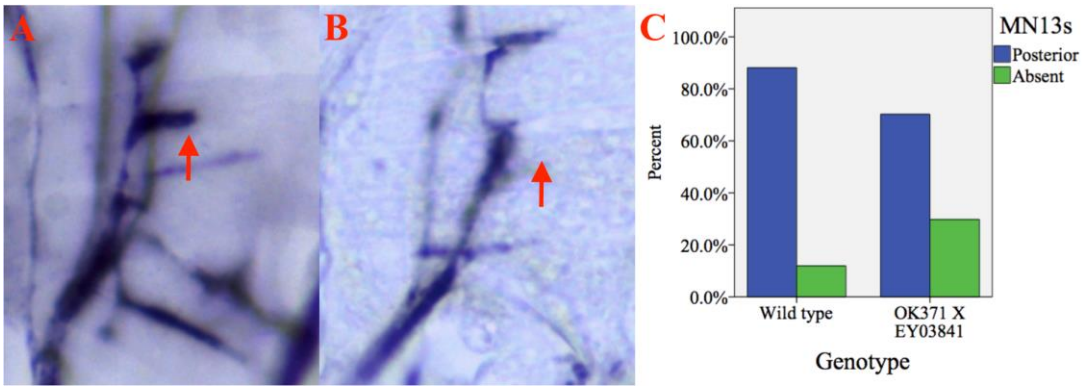

D	MN13s posterior	MN13s absent
Wild type	88.1% (133)	11.9% (18)
OK371 X EY03841	70.2% (59)	29.8% (25)

Figure 69. Image A (right is posterior, up is dorsal) shows the ventral section of a wild type hemisegment with the MN13s indicated (red arrow). Image B (right is posterior, up is dorsal) shows the ventral section of an *OK371 X EY03841* hemisegment without the MN13s (red arrow). The graph (C) shows the percentage of hemisegments in which the MN13s are present or absent in 27 wild type and 17 *OK371 X EY03841* embryos. The table (D) shows the percentage and number of hemisegments in which the MN13s are present or absent in the same embryos.

A chi-square test for independence revealed that the MN13s were absent significantly more often in *OK371 X EY03841* hemisegments than in wild types, χ^2 (1, n = 235) = 11.49, $p < .01$.

MN13s project anteriorly

The MN13s projected anteriorly more often in *OK371 X EY03841* hemisegments (10.6%) than in wild types (2.9%) (Figure 70).

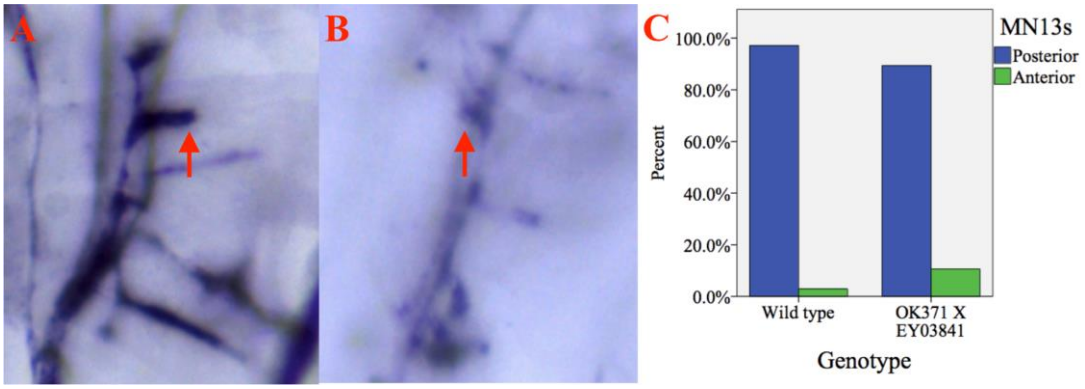

D	MN13s posterior	MN13s anterior
Wild type	97.1% (133)	2.9% (4)
OK371 X EY03841	89.4% (59)	10.6% (7)

Figure 70. Image A (right is posterior, up is dorsal) shows the ventral section of a wild type hemisegment in which the MN13s project posteriorly (red arrow). Image B (right is posterior, up is dorsal) shows the ventral section of an *OK371 X EY03841* hemisegment in which the MN13s project anteriorly (red arrow). The graph (C) shows the percentage of hemisegments in which the MN13s project posteriorly or anteriorly in 27 wild type and 17 *OK371 X EY03841* embryos. The table (D) shows the percentage and number of hemisegments in which the MN13s project posteriorly or anteriorly in the same embryos.

Fisher's exact test revealed that the MN13s projected anteriorly significantly more often in *OK371 X EY03841* hemisegments than in wild types, $p < .05$.

4.2.13. Phenotypic analysis: *Mef2 X EY03841*

In addition to the *OK371-GAL4* driver a *Mef2-GAL4* driver was used to drive expression of *otk2* in the somatic musculature to gain further insights into its precise role. *Mef2* flies were also crossed with *EY03841* flies. *Mef2 X EY03841* embryos exhibited FB (Figure 71), RP3 (Figure 75), and MN12 absent (Figure 73) phenotypes. Additionally, MN12s projected anteriorly (Figure 74) and MN13s were occasionally elongated towards the posterior (Figure 72). MN13s were deemed to be elongated if their length was greater than the distance between the dorsal edge of their anterior end and the cleft between muscles 6 and 7.

FB absent

The FB was absent more often in *Mef2 X EY03841* hemisegments (21.4%) than in wild types (7.6%) (Figure 71).

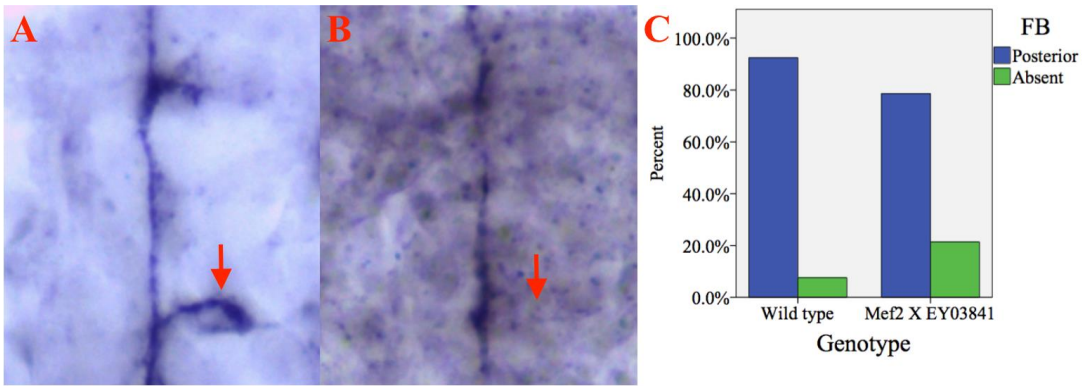

D	FB posterior	FB absent
Wild type	92.4% (195)	7.6% (16)
Mef2 X EY03841	78.6% (158)	21.4% (43)

Figure 71. Image A (right is posterior, up is dorsal) shows the dorsal section of a wild type hemisegment with the FB indicated (red arrow). Image B (right is posterior, up is dorsal) shows the dorsal section of a *Mef2 X EY03841* hemisegment without the FB (red arrow). The graph (C) shows the percentage of hemisegments in which the FB is present or absent in 30 wild type and 28 *Mef2 X EY03841* embryos. The table (D) shows the percentage and number of hemisegments in which the FB is present or absent in the same embryos.

A chi-square test for independence revealed that the FB was absent significantly more often in *Mef2 X EY03841* hemisegments than in wild types, χ^2 (1, n = 412) = 16, p < .001.

MN13s elongated posteriorly

The MN13s were elongated posteriorly significantly more often in *Mef2 X EY03841* hemisegments (10.8%) than in wild types (2.2%) (Figure 72).

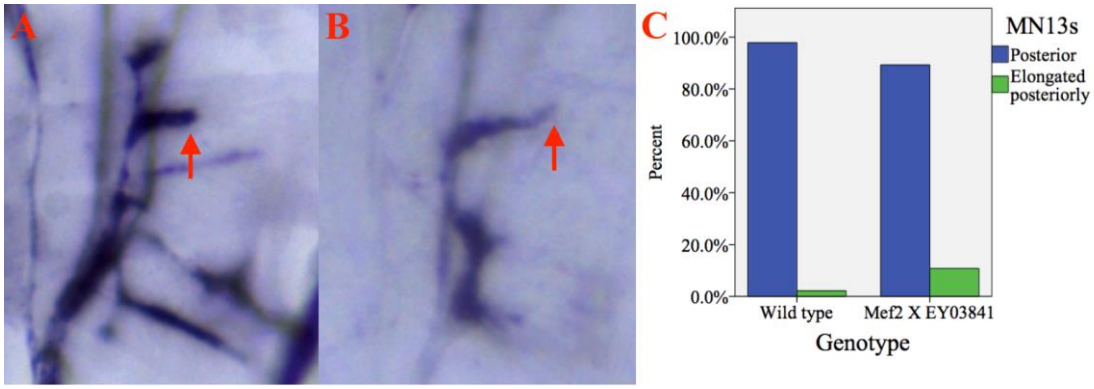

D	MN13s posterior	MN13s elongated posteriorly
Wild type	97.8% (133)	2.2% (3)
Mef2 X EY03841	89.2% (83)	10.8% (10)

Figure 72. Image A (right is posterior, up is dorsal) shows the ventral section of a wild type hemisegment with the MN13s indicated (red arrow). Image B (right is posterior, up is dorsal) shows the ventral section of a *Mef2 X EY03841* hemisegment with MN13s elongated posteriorly (red arrow). The graph (C) shows the percentage of hemisegments in which the MN13s are of normal length or are elongated in 27 wild type and 15 *Mef2 X EY03841* embryos. The table (D) shows the percentage and number of hemisegments in which the MN13s are of normal length or are elongated in the same embryos.

A chi-square test for independence revealed that the MN13s were elongated posteriorly significantly more often in *Mef2 X EY03841* hemisegments than in wild types, χ^2 (1, n = 229) = 7.54, $p < .01$.

MN12s absent

The MN12s were absent more often in *Mef2 X EY03841* hemisegments (50%) than in wild types (22.6%) (Figure 73).

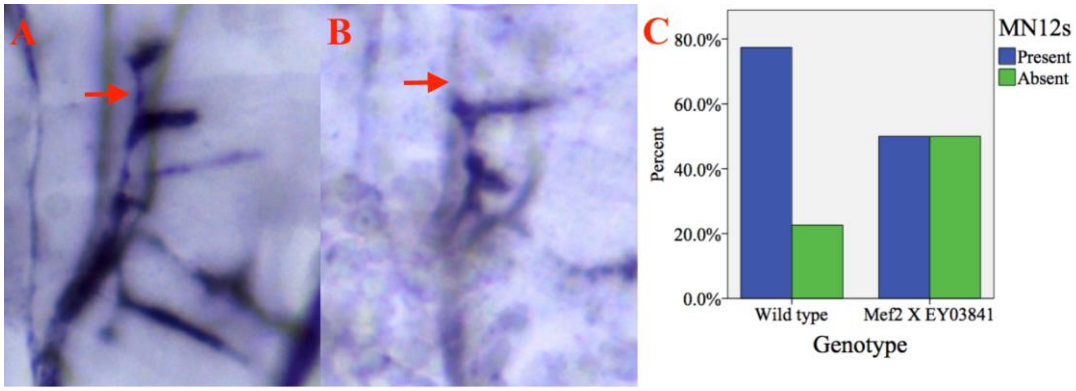

D	MN12s present	MN12s absent
Wild type	90.9% (70)	9.1% (7)
Mef2 X EY03841	50% (57)	50% (57)

Figure 73. Image A (right is posterior, up is dorsal) shows the ventral section of a wild type hemisegment with the MN12s indicated (red arrow). Image B (right is posterior, up is dorsal) shows the ventral section of a *Mef2 X EY03841* hemisegment without the MN12s (red arrow). The graph (C) shows the percentage of hemisegments in which the MN12s are present or absent in 27 wild type and 15 *Mef2 X EY03841* embryos. The table (D) shows the percentage and number of hemisegments in which the MN12s are present or absent in the same embryos.

A chi-square test for independence revealed that the MN12s were absent significantly more often in *Mef2 X EY03841* hemisegments than in wild types, χ^2 (1, n = 282) = 22.79, p < .001.

MN12s project anteriorly

The MN12s of *Mef2 X EY03841* embryos projected anteriorly. 33.3% of *Mef2 X EY03841* hemisegments exhibited the mild phenotype (Figure 74B), compared to 20% of wild type hemisegments. 21.2% of *Mef2 X EY03841* hemisegments exhibited the severe phenotype (Figure 74C), compared to 8.8% of wild type hemisegments.

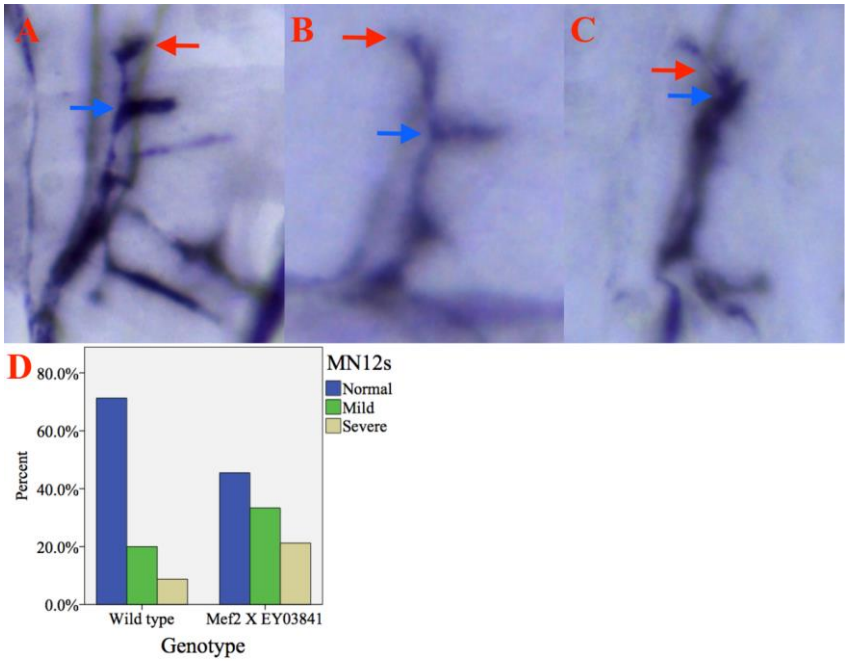

E	MN12s normal	MN12s mild	MN12s severe
Wild type	71.2% (57)	20% (16)	8.8% (7)
Mef2 X EY03841	45.5% (15)	33.3% (11)	21.2% (7)

Figure 74. Image A (right is posterior, up is dorsal) shows the ventral section of a wild type hemisegment in which the MN12s project dorsally at the muscle 13 innervation point (blue arrow) before projecting posteriorly (red arrow). Image B (right is posterior, up is dorsal) shows the ventral section of a *Mef2 X EY03841* hemisegment in which the MN12s project dorsally at the muscle 13 innervation point (blue arrow) before projecting anteriorly (red arrow). Image C (right is posterior, up is dorsal) shows the ventral section of a *Mef2 X EY03841* hemisegment in which the MN12s (red arrow) project anteriorly at the muscle 13 innervation point (blue arrow). The graph (D) shows the percentage of hemisegments that exhibit the normal, mild, and severe phenotypes in 27 wild type and 15 *Mef2 X EY03841* embryos. The table (E) shows the percentage and number of hemisegments exhibiting normal, mild, and severe phenotypes in the same embryos.

Fisher's exact test revealed a significant effect of genotype with regard to the trajectory of the MN12s, $p < .05$.

RP3 axon absent

The RP3 axon was absent more often in *Mef2 X EY03841* hemisegments (63.6%) than in wild types (20.1%) (Figure 75).

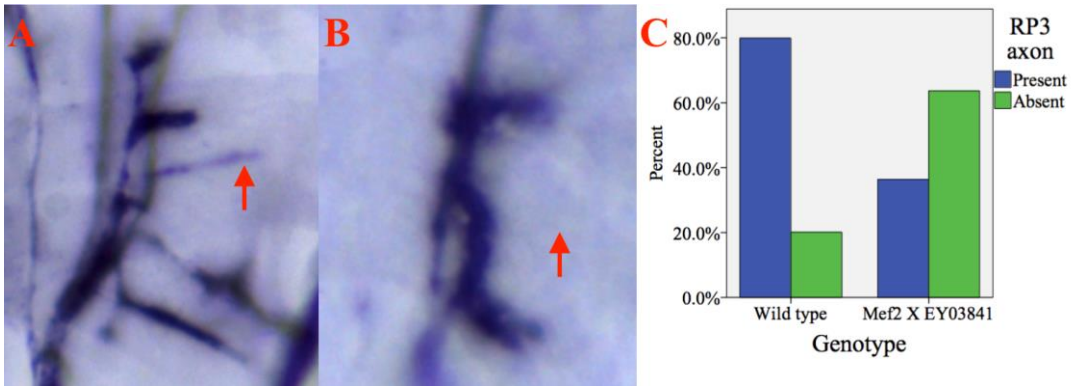

D	RP3 axon posterior	RP3 axon absent
Wild type	79.9% (147)	20.1% (37)
Mef2 X EY03841	36.4% (24)	63.6% (42)

Figure 75. Image A (right is posterior, up is dorsal) shows the ventral section of a wild type hemisegment with the RP3 axon indicated (red arrow). Image B (right is posterior, up is dorsal) shows the ventral section of a *Mef2 X EY03841* hemisegment without the RP3 axon (red arrow). The graph (C) shows the percentage of hemisegments in which the RP3 axon is present or absent in 27 wild type and 15 *Mef2 X EY03841* embryos. The table (D) shows the percentage and number of hemisegments in which the RP3 axon is present or absent in the same embryos.

A chi-square test for independence revealed that the RP3 axon was absent significantly more often in *Mef2 X EY03841* hemisegments than in wild types, χ^2 (1, n = 250) = 42.58, p < .001.

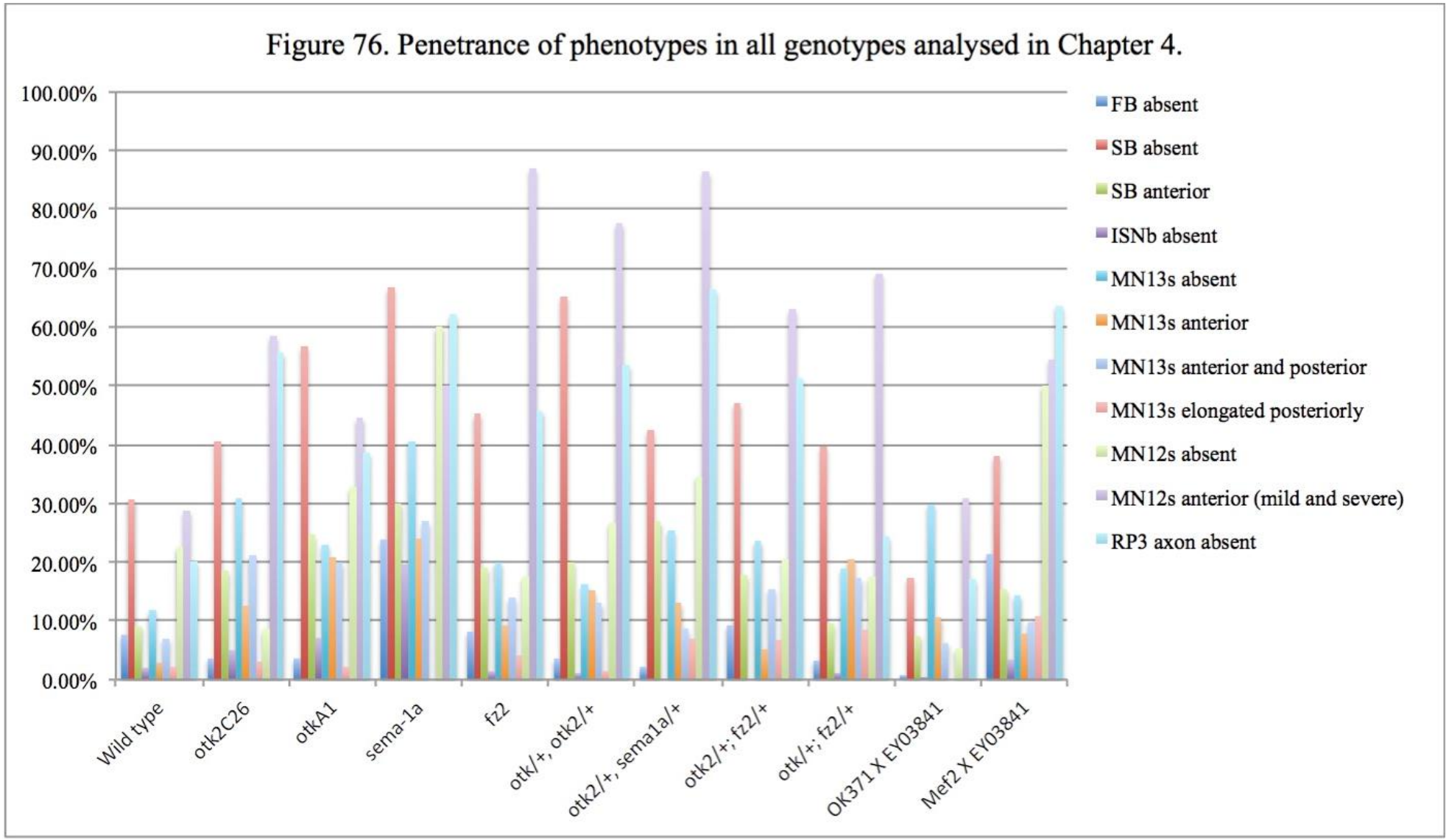
Figure 76. Penetrance of phenotypes in all genotypes analysed in Chapter 4.
100.00%
90.00%
80.00%
70.00%
60.00%
50.00%
40.00%
30.00%
20.00%
10.00%
0.00%
Wild type
otk2C26
otkA1
sema-1a
fz2
otk/+; otk2/+
otk2/+; sema1a/+
otk2/+; fz2/+
otk/+; fz2/+
OK371 X EY03841
Mef2 X EY03841
FB absent
SB absent
SB anterior
ISNb absent
MN13s absent
MN13s anterior
MN13s anterior and posterior
MN13s elongated posteriorly
MN12s absent
MN12s anterior (mild and severe)
RP3 axon absent

4.3. Discussion

otk2 is a paralogue of *otk* (Linnemannstöns et al., 2014; Vogel et al., 2003), a gene that has been linked to defasciculation between embryonic motor neurons (Winberg et al., 2001) and to target recognition by larval photoreceptor cells (Cafferty et al., 2004). However, the authors of a recent study that focused on PCP did not observe axonal abnormalities in *otk* null mutants (Linnemannstöns et al., 2014; the axons were not, however, examined in detail). It has been proposed that Otk forms a complex with PlexA (Winberg et al., 2001), which is the receptor for the neuronally-expressed repellent Sema-1a (Winberg et al., 1998; Yu et al., 1998). Co-IP results indicate that Otk and Otk2 can form heterodimers (Linnemannstöns et al., 2014), which raises the possibility that Otk2 participates in Sema-1a/PlexA signalling. However, Linnemannstöns and colleagues also observed interactions between the off-tracks and Fz2. This finding, coupled with reports of axon guidance defects in embryonic motor neurons and photoreceptor cells in experiments involving *fz2* (Inaki et al., 2007; Sato et al., 2006), hints at a role for the off-tracks in wnt-mediated guidance. Therefore, the primary aims of the current study were to determine whether *otk2* is implicated in embryonic motor axon guidance and to investigate whether it genetically interacts with *otk*, *sema-1a*, and *fz2*. Gain-of-function experiments involving *otk2* were also completed to probe the precise role of *otk2* in axon guidance.

In order to understand how Otk2 might function in embryonic motor axon guidance, it is necessary to establish its distribution in the embryo. Pulido and colleagues (1992) reported that *otk* is expressed in the VNC and in motor neurons towards the end of embryonic development, and Linnemannstöns and colleagues (2014) report that *otk* and *otk2* exhibit identical expression patterns. Using Otk and Otk2 antibodies provided by Linnemannstöns and colleagues, it was established that both genes are indeed expressed in the VNC. Specifically, they produce staining within the regions of the longitudinal fascicles and the anterior and posterior commissures. The signal is substantially stronger in the region of the anterior commissures relative to the region of the posterior commissures (Figure 19A/B), suggesting that the Otks might have a role in commissure selection. Yoshikawa and colleagues (2003), for example, report that axons that cross the midline via the anterior commissure express *derailed* (*drl*), which encodes a receptor for the repellent, Wnt5. *drl* and *wnt5* are expressed in anterior and posterior commissures, respectively. While both off-tracks were expressed in the CNS, only Otk was clearly visible in motor neurons (Figure 19C). On the other hand, Otk2 seems to be expressed in glia within the region in which motor axons exit the VNC (i.e., in “exit

glia," Figure 19D). Thus, these results refute the suggestion that the expression patterns of *otk* and *otk2* are identical (Linnemannstöns et al., 2014). Although no clear *otk2* expression was detected in the motor neurons, it is acknowledged that this might merely reflect a failure to detect expression rather than genuine absence. Indeed, *plexA*, for example, is clearly expressed in the embryonic CNS, though is virtually undetectable in the PNS. Nonetheless, *plexA* mutants have conspicuous abnormal motor axon phenotypes, which are thought to reflect local *plexA* activity (Yu et al., 1998). In light of this, subsequent discussions regarding Otk2's role in axon guidance assume that there might be expression within the motor neurons, as well as in surrounding structures (e.g., the somatic muscles).

The $otk2^{C26}$ null allele (Linnemannstöns et al., 2014) was used to investigate whether *otk2* is required for embryonic motor axon guidance. $otk2^{C26}$ embryos exhibited various abnormalities: the MN13s were absent (30.8%, Figure 22), projected anteriorly (12.5%, Figure 23), or projected anteriorly and posteriorly (22.2%, Figure 24); the MN12s projected anteriorly (42.6% mild, 15.8% severe, Figure 25); and the RP3 axon was absent (55.6%, Figure 26). *otk2* gain-of-function experiments were also completed to provide insights into the precise role of the gene/protein. Driving expression of *otk2* in motor neurons with *OK371-GAL4* also had an effect on the MN13s, which were absent (29.8%, Figure 69) or projected anteriorly (10.6%, Figure 70). The MN12s and RP3 axon, however, were normal, while the FB (99.3%, Figure 67) and SB (82.7%, Figure 68) were present more often than in wild types, perhaps representing an up-regulation of defasciculation-based mechanisms between axons of the ISN. Conversely, driving expression of *otk2* within somatic musculature with *Mef2-GAL4* increased absence of the FB (21.4%, Figure 71), though there was no effect on the SB (not shown). The MN12s were also absent (50%, Figure 73) or projected anteriorly (33.3% mild, 21.2% severe, Figure 74). The MN13s were elongated posteriorly (10.8%, Figure 72). The loss of MN12s and elongation of MN13s resembled Inaki and colleagues' (2007) observation that the size of MN12 synapses was inversely related to the size of MN13 synapses in *fz2* and *wnt4* experiments. However, there was not a significant relationship between the presence/absence of the MN12s and whether or not MN13s were elongated posteriorly (not shown).

Employing both loss- and gain-of-function experiments allowed for a more in-depth analysis of the potential roles of Otk2 than either would enable alone. Out of the phenotypes, it is perhaps most straightforward to provide an interpretation of the behaviour of the FB in the three experiments above. For example, the lack of a FB

phenotype in the *otk2*^{C26} embryos might reflect genetic redundancy, while the increased presence of the branch when expression was driven in motor neurons might be indicative of an up-regulation of defasciculation-based mechanisms between axons. Since defasciculation can be interpreted as a type of repulsion, increased absence of the FB when expression was driven in somatic muscles might represent axons failing to enter a region with increased repellent activity. This interpretation, however, rests on the assumption that Otk2 can promote repulsion within and outside of axons. Bi-directional signalling, whereby guidance molecules (e.g., Sema-1a) act as both ligands and receptors, occurs in embryonic motor axon guidance (Jeong, Juhaszova, & Kolodkin, 2013). It is therefore conceivable that Otk2 influences axons' trajectories internally and externally. The lack of a SB phenotype in *otk2*^{C26} embryos and the increased presence of the SB when driving expression in motor neurons might also be explained, respectively, in terms of redundancy and increased defasciculation. The lack of a SB phenotype when driving expression in somatic muscles might be related to the high frequency with which the SB is absent in wild types (i.e., any effect of ectopic *otk2* expression results in a small relative change in the SB absent phenotype frequency). Thus the FB and SB absent phenotypes in *otk2*^{C26}, *OK371-GAL4 X EY03841*, and *Mef2-GAL4 X EY03841* embryos point toward a role for Otk2 in repellent activity.

However, the behaviour of the MN12s and MN13s does not appear to be congruent with Otk2 promoting repulsion. For instance, the elongation of MN13s when *otk2* expression is driven in muscles seems more compatible with a system in which Otk2 promotes growth. While the absence of MN13s in *otk2*^{C26} embryos could be explained by a lack of attractive activity in muscles or a lack of repellent activity in axons, the former is more congruent with other MN13 phenotypes. For example, a lack of repellent activity in muscles would not explain MN13 anterior projections. Conversely, in the absence of an attractive cue within muscle 13, it is possible that MN13s simply grow in any direction, including anteriorly. Similarity between *otk2*^{C26} and *OK371-GAL4 X EY03841* embryos with regard to MN13 phenotypes might reflect a disruption in the latter of the ratio of proteins implicated in guidance decisions, thus resulting in loss-of-function. As per the explanation of the behaviour of the FB, this interpretation assumes that Otk2 might participate in bi-directional signalling. As with MN13 anterior projections, the MN12 anterior projections in *otk2*^{C26} embryos might also be explained by the loss of an attractive cue within muscle 12. The MN12s were absent in half of *Mef2-GAL4 X EY03841* embryos, which is seemingly at odds with the supposition that Otk2 promotes attractive activity. However, it is conceivable that disrupting the normal relative distribution of the protein in neighbouring muscles inhibits stereotypical innervation.

Indeed, Inaki and colleagues (2007) observed enlarged MN13 synapses when driving expression of the repellent Wnt4, which they attribute to a reversal of the relative levels of Wnt4 in muscles 12 and 13. Thus, collectively, the phenotypes in *otk2*^{C26}, *OK371-GAL4 X EY03841*, and *Mef2-GAL4 X EY03841* embryos allude to roles for Otk2 in repulsive activity in the region of the FB and SB and attractive activity in the region of the ISNb. Contrasting roles within the context of axon guidance are certainly possible given that, for example, the effect a ligand has on an axon depends on the receptors it expresses (Ackerman et al., 1997; Keino-Masu et al., 1996). Moreover, the abundance of second messengers, such as cAMP and cGMP, can influence whether a particular guidance cue attracts or repels axons (Ming et al., 1997; Song et al., 1998).

While researchers using a particular *otk* allele (*otk*^{3}) have reported that loss of *otk* entails lethality and axon guidance defects in embryonic motor neurons and larval photoreceptors (Cafferty et al., 2004; Winberg et al., 2001), Linnemannstöns and colleagues (2014) reported that flies with their new allele (*otk*^{A1}) were viable and had no obvious abnormalities in embryonic motor axons. In the current study, however, motor axon guidance defects were detected in *otk*^{A1} embryos. Specifically, MN13s were absent (23%, Figure 30), grew anteriorly (20.9%, Figure 31) or grew anteriorly and posteriorly (20%, Figure 32). MN12s also grew anteriorly (26.5% mild, 32.4% severe, Figure 33). The ISNb was occasionally absent (7.1%, Figure 29), though when present the RP3 axon was often missing (38.6%, Figure 34). The SB was often absent (56.7%, Figure 27) or projected anteriorly (24.7%, Figure 28). Winberg and colleagues (2001) describe ISNb defects in terms of stalling at three choice points. At choice point 1 the ISNb defasciculates from the ISN and grows dorsoposteriorly. Errors at this stage therefore reflect the ISNb absent phenotype described here, which is assumed to represent the ISNb's failure to detach from the ISN. This occurs in 19% of *otk*^{3} hemisegments (Winberg et al., 2001), thus ~2.7 times more often than in *otk*^{A1} hemisegments. At choice point 2 the RP3 axon projects posteriorly from the ISNb to innervate the cleft between muscles 6 and 7. Errors at this stage therefore reflect the RP3 axon absent phenotype described here. This occurs in 37.9% of *otk*^{3} hemisegments (Winberg et al., 2001), which very closely resembles the penetrance observed here in *otk*^{A1} hemisegments. At choice point 3 MN13s project posteriorly and MN12s project dorsally. Winberg and colleagues (2001) report that either the MN13s or MN12s stall in 17.2% of *otk*^{3} hemisegments. The current study analysed MN13 and MN12 stalls individually, which are referred to as MN13s and MN12s "absent" phenotypes. However, of the 98 *otk*^{A1} hemisegments in which it was possible to determine the presence/absence of both the MN12s and MN13s, 48 (48.9%) hemisegments lacked one

projection or the other, thus choice point 3 errors were more frequent in *otk*^{A1} embryos compared to *otk*^{3} embryos. Overall, *otk*^{A1} embryos resemble *otk*^{3} embryos with regard to the ISNb absent, RP3 axon absent, and MN12s/MN13s absent phenotypes.

Winberg and colleagues (2001) interpreted their analysis of the ISNb in *otk*^{3} embryos as evidence of reduced defasciculation. The MN12s and MN13s of *otk*^{A1} embryos, however, in addition to stalling, have a tendency to grow anteriorly, which is difficult to explain in terms of decreased defasciculation. Cafferty and colleagues (2004) argue that Otk is required for photoreceptor target recognition. It may be that Otk has a similar role in embryonic motor axon guidance. For example, MN12 and MN13 axons in *otk*^{A1} embryos might not be able to detect muscle-derived cues and so exhibit undirected (anterior) growth. The SB is absent in *otk*^{A1} embryos, though when present often projects anteriorly. As with the MN12 and MN13 anterior trajectories, these phenotypes have not previously been reported for *otk* mutants. As above, while the absence of the SB might be interpreted as reduced defasciculation, it is less clear how the lack of such a mechanism would account for the SB's anterior projections.

Various observations pertaining to the *otk2*^{C26} and *otk*^{A1} embryos suggest that, individually, they are somewhat redundant. For instance, while the ISNb was absent significantly more often in *otk*^{A1} embryos relative to wild types, it was, nonetheless, present in ~93% of hemisegments. Also, although the FB was present at a frequency resembling wild types in *otk2*^{C26} embryos, it was present more often when *otk2* expression was driven in motor neurons and less often when *otk2* was driven in somatic muscles, which implies that Otk2 can affect the FB, but that it is not required for its development. Thus, it might be that one of the off-tracks can more or less compensate for the other. Therefore, a deficiency line (*BSC199*) was employed to investigate the consequences of removing both of the off-tracks. These exhibited severe and highly penetrant abnormalities, including in branches that were not aberrant in the single mutants. Namely, the ISNd (91.2%, Figure 36), SNc (66.7%, Figure 38), and dorsal (19.4%) and lateral (35.4%) branches of the SNa (Figure 37) were absent. As per *otk*^{A1} embryos, the ISNb was also absent, though much more frequently (82.4%, Figure 35). Consequently, it was not possible to analyse the ISNb for the more subtle phenotypes observed in the single mutants (e.g., the absence of the RP3 axon, MN13s, or MN12s). While the SB was absent in *otk*^{A1} embryos, this was ~1.3 times more penetrant in *BSC199* embryos (76%, Figure 40), and the FB was absent (60.6%, Figure 39). These results suggest that the loss of both off-tracks affects embryonic motor axon guidance much more than the loss of just one. However, the *BSC199* deficiency removes 44 other

genes. While no existing evidence implicates these genes in axon guidance, several have been linked to other aspects of nervous system development: *microcephalin* (*mcph1*; Rickmyre et al., 2007), *ribonucleoside diphosphate reductase small subunit* (*rnrs*; Neumüller et al., 2011), *DNA fragmentation factor-related protein 3* (*drep3*; Neumüller et al., 2011), *jelly belly* (*jeb*; Bazigou et al., 2007), and *pre-mRNA processing factor 8* (*prp8*; Neumüller et al., 2011). Therefore, it is possible that the phenotypes reported for *BSC199* embryos might be attributable to a gene or genes other than the off-tracks. Linnemannstöns and colleagues (2014) created a mutation that only removes *otk* and *otk2*, as well as part of *MPPE*. Utilisation of such a line would be required to assert with greater confidence whether or not the loss of both off-tracks results in the phenotypes reported here for *BSC199*.

There is abundant evidence for *sema-1a* having a role in axon guidance (Ayoob et al., 2004; Cho et al., 2012; Huang & Kolodkin, 2000; Terman et al., 2002; Winberg et al., 1998; Yu et al., 1998; Yu, Huang, & Kolodkin, 2000). However, to subsequently test whether *sema-1a* genetically interacts with *otk2* it was first necessary to confirm that the *sema-1a* line harboured motor axon guidance defects. Indeed, the MN13s were absent (40.6%, Figure 44), projected anteriorly (24%, Figure 45), or projected anteriorly and posteriorly (26.9%, Figure 46). Also, the RP3 axon (62.2%, Figure 45), ISNb (19.6%, Figure 43), FB (23.9%, Figure 41), SB (66.7%, Figure 42), and MN12s (60%, Figure 47) were absent. While Yu and colleagues (1998) also reported that the ISNb and RP3 axon were absent in *sema-1a* mutants (albeit at lower frequencies: 7% and 18% of hemisegments, respectively), further exact comparisons to their work are difficult because of their use of an alternative phenotype classification system and due to lack of information regarding penetrance. For example, as per the current investigation, they report that the FB and SB are absent, though do not specify how frequently. Also, they indicate that the ISNb stalls between muscles 6 and 13 in 39% of hemisegments, which resembles the MN12s absent analysis here. Thus, the *sema-1a* phenotypes reported here are generally in line with those described by Yu and colleagues (1998).

As with *sema-1a*, embryonic motor axon guidance phenotypes for *fz2* have already been reported (Inaki et al., 2002). However, prior analyses only examined the MN12s and MN13s. Therefore, the current investigation assessed the full length of the motor axons in *fz2* loss-of-function embryos. These exhibited MN12 anterior projections (59% mild, 27.9% severe, Figure 49) and the RP3 axon was absent (54.7%, Figure 50). Inaki and colleagues (2007) reported that, in embryos expressing a dominant negative form of *fz2* in neurons, MN12 synapses were reduced and MN13 synapses were enlarged. Their

interpretation of these results was that *fz2* is required by MN12s to bypass muscle 13; muscle 13 expresses *wnt4*, which, Inaki and colleagues (2007) argue, repels *fz2*-expressing axons. Precise measurements of the MN12 and MN13 synapses were not completed in the current study. However, MN13s were not elongated posteriorly in *fz2* embryos (not shown). A possible reason for the dissimilar MN13 behaviour is that Inaki and colleagues (2007) selectively inhibited *fz2* activity in neurons, while *fz2* activity was removed throughout the embryo in the present report. It is conceivable that *fz2* influences motor axons from within and outside of neurons. In line with this, Mosca and Schwarz (2010) demonstrate that *fz2* is expressed in the embryonic somatic musculature and is required for postsynaptic development. It is not clear how the anterior growth of MN12s could be accounted for by the model proposed by Inaki and colleagues (2007). One explanation is that *fz2* is required by MN12s to recognise cues on muscle 12, thus without *fz2* they grow in any direction, including anteriorly. This model is in line with Sato and colleagues' (2006) observation that Wnt4 attracts *fz2*-expresing ventral retinal axons to the ventral lamina. Given that the RP3 axon does not cross muscle 13, its absence in the present study cannot be explained in terms of recruitment to muscle 13. However, as with the MN12 anterior projections, the RP3 axon's absence might reflect a failure to recognise its target. Therefore, the current and prior findings (Mosca & Schwarz, 2010) suggest that Inaki and colleagues' (2007) model of Wn4/Fz2 in embryonic axon guidance is overly simplistic. Further experiments, such as selectively inhibiting *fz2* activity in the somatic musculature, are required to develop a more comprehensive picture.

Having established that embryos lacking either *otk*, *otk2*, *sema-1a*, or *fz2* activity exhibited motor axon guidance defects, evidence of genetic interactions between these genes was sought by analysing transheterozygous embryos. Embryos that only possess one copy of a functional gene rarely display axon guidance defects; conversely, abnormal phenotypes are often observed in embryos that only possess single functional copies of two genes that encode proteins implicated in a shared pathway. Linnemannstöns and colleagues (2014) reported that Otk and Otk2 physically interact, suggesting that they might contribute to a shared cascade. The presence of motor axon guidance defects in otk^{A1}/+, $otk2^{C26}$/+ embryos supports this hypothesis. The SB (65.2%, Figure 51) and RP3 axon (53.5%, Figure 54) were absent in these embryos. While the SB was absent significantly more often in otk^{A1} embryos than in wild types, this was not the case for $otk2^{C26}$ embryos. However, the RP3 axon was absent in both otk^{A1} and $otk2^{C26}$ embryos. Additionally the MN13s (15.2%, Figure 52) and MN12s (49% mild, 28.6% severe, Figure 53) projected anteriorly in embryos transheterozygous

for functional copies of the off-tracks. However, SB anterior projections, which are seen in *otk*^{A1} embryos, were not observed. Likewise, neither the MN13s absent phenotype or MN13s anterior and posterior phenotype were seen the *otk*^{A1}/+, *otk2*^{C26}/+ transheterozygotes, which were both observed in *otk*^{A1} and *otk2*^{C26} embryos. All three genotypes exhibited the MN13s anterior phenotype. Therefore, although there is incomplete overlap between the phenotypes, these data suggest *otk* and *otk2* genetically interact.

Given that the off-tracks physically (Linnemannstöns et al., 2014) and genetically interact (this current study), and that Otk is implicated in Sema-1a/PlexA signalling (Winberg et al., 2014), embryos transheterozygous for functional copies of *otk2* and *sema-1a* were employed to investigate whether Otk2 also participates in Sema-1a/PlexA signalling. Indeed a number of branches were absent in *otk2*$^{C26/}$+, *sema1a/*+ embryos; namely, the MN13s (25.4%, Figure 56) and MN12s (34.6%, Figure 58), and the RP3 axon (66.3%, Figure 60). Additionally, the SB (26.9%, Figure 55), MN13s (13.1%, Figure 57), and MN12s (47.4% mild, 36.8% severe, Figure 59) projected anteriorly. All *otk2*$^{C26/}$+, *sema1a/*+ phenotypes are seen in *sema-1a* and/or *otk2* ^{C26} embryos. However, the FB, SB, and ISNb are absent in *sema-1a* embryos. Also, the MN13s simultaneously project anteriorly and posteriorly in both *sema-1a* and *otk2*^{C26} embryos. These data therefore constitute evidence that Otk2 participates in Sema-1a-mediated axon guidance, but also suggest that the extent to which it is required for the organisation of the motor axons varies across branches.

It is possible that Otk2 influences embryonic motor axon guidance through involvement in multiple signalling pathways. Since Otk2 physically associates with Fz2 (Linnemannstöns et al., 2014) and embryos lacking *otk2* or *fz2* activity display similar phenotypes in the motor axons (Inaki et al., 2007; this current study), *otk2*^{C26}/+; *fz2*/+ embryos were analysed to assess the idea that Otk2 and Fz2 influence axonal growth through their involvement in a shared signalling pathway. Indeed, the SB (47.1%, Figure 61), MN13s (23.6%, Figure 62), and RP3 axon (51.3%, Figure 64) were absent in these embryos. Additionally, MN12s grew anteriorly (41.3% mild, 21.7% severe, Figure 63). Interestingly, the SB was not absent significantly more often in *otk2*^{C26} or *fz2* embryos than in wild types. However, there is little difference in the frequency of this phenotype between (1) *otk2*^{C26}/+; *fz2*/+, (2) *otk2*^{C26} and (3) *fz2* embryos (47.1%, 40.6%, and 45.2%, respectively). Similarly, the MN13s are not absent significantly more often in *fz2* embryos than in wild types, though, again, there is little difference in the frequency of this phenotype between (1) *otk2*^{C26}/+; *fz2*/+, (2) *otk2*^{C26} and (3) *fz2*

embryos (23.6%, 30.8%, and 20%, respectively). On the other hand, the MN12s grow anteriorly and the RP3 axon is absent in both *otk2*^{C26} and *fz2* embryos. These results suggest, therefore, that Otk2 and Fz2 might influence embryonic motor axon guidance through their involvement in a shared signalling pathway.

Finally, since Otk also physically associates with Fz2 (Linnemannstöns et al., 2014) and embryos lacking *otk* or *fz2* activity display similar phenotypes in the motor axons (Inaki et al., 2007; this current study), *otk1*^{A1}*/+; fz2/+* embryos were analysed to assess the idea that Otk and Fz2 influence axonal growth through their involvement in a shared signalling pathway. This notion was somewhat supported; the MN13s (20.4%, Figure 65) and MN12s (38.2% mild, 30.9% severe, Figure 66) grew anteriorly in *otk1*^{A1}*/+; fz2/+* embryos. MN12s also grew anteriorly in *otk1*^{A1} and *fz2* embryos. However, while the MN13s grew anteriorly significantly more often *otk1*^{A1} embryos compared to wild types, this was not the case for *fz2* embryos. Nevertheless, MN13s grew anteriorly ~3.2 times more often in *fz2* embryos compared to wild types (not shown), which was marginally significant (p = .056). Various phenotypes were observed in *otk*^{A1} embryos that were not present in *otk*^{A1}*/+; fz2/+* embryos: the ISNb, MN13s, SB, and RP3 axon were absent, and, when present, the SB grew anteriorly, and the MN13s simultaneously grew anteriorly and posteriorly. Therefore, on one hand, the anterior growth of MN13s and MN12s in *otk*^{A1}*/+; fz2/+* embryos implies that *otk* and *fz2* affect the navigation of these axons via a common pathway. On the other hand, since many more phenotypes are seen in *otk*^{A1} embryos, these data suggest that Fz2 only contributes to a limited number of Otk-mediated guidance decisions.

A number of general conclusions can be drawn at this point. The current study has provided evidence that *otk2* is implicated in embryonic motor axon guidance, and it has been argued that it might have roles in both attracting and repelling axons. Genetic interaction experiments suggest that *otk2* might influence axonal trajectories through participation in Sema-1a/PlexA and Wnt4/Fz2 signalling pathways. The enhancement of phenotypes in a line lacking *otk* and *otk2* activity (*BSC199*) provides further support for their participation in a shared pathway. Evidence has also been presented that suggests the embryonic motor axon guidance phenotypes reported by Winberg and colleagues (2001) for the *otk*^{3} allele are also present in the *otk*^{A1} allele. However, the presence of anterior projections in *otk*^{A1} embryos suggests that a model in which Otk's only function is to promote defasciculation is insufficient. It has been proposed here and previously (Cafferty et al., 2004) that Otk might be required for target recognition. Peradziryi and colleagues (2011) implicate Otk in Wnt signalling and suggest that is

required for patterning of embryonic epidermis. Here, an analysis of embryos that are transheterozygous for functional copies of *otk* and *fz2* suggest that Otk's participation in Wnt signalling might also influence motor axon guidance. Finally, the nature of the *fz2* phenotypes reported here do not support Inaki and colleagues' (2007) model, which suggests that *fz2*-expressing axons are repelled by Wnt4. It has been proposed here and previously that Fz2 might also be required for target identification (Sato et al., 2006) and that it may affect synapse development from within muscles (Mosca & Schwarz, 2010).

In short, the current data implicate *otk2* in embryonic motor axon guidance, draw attention to limitations of current models of Otk and Fz2, and suggest overlap between the molecules involved in Sema-1a/PlexA and Wnt4/Fz2 pathways. However, various limitations should be addressed. Firstly, it cannot be claimed with absolute certainty that the genes that were the focus of the present study were responsible for the observed phenotypes. Given the lack of prior evidence, this is particularly true for *otk2*; it is possible that genetic aberrations other than the loss of *otk2* exist within the $otk2^{C26}$ population. To address this, the chromosome harbouring the $otk2^{C26}$ allele should be paired with an alternative chromosome that also lacks *otk2*. If embryos with these two chromosomes exhibit the phenotypes reported here, it could be claimed with a high level of confidence that they are the result of the loss of *otk2* activity. While this test would be prudent, the similarity between the $otk2^{C26}$ and *otk2* gain-of-function phenotypes bolsters the assertion that the loss of *otk2* activity in the $otk2^{C26}$ embryos is the cause of their defects. Additionally, one might check whether the $otk2^{C26}$ phenotypes can be rescued by driving expression of an *otk2*-containing transgenic construct under the control of, for example, *OK371-GAL4*. Besides providing further evidence of the link between *otk2* and the phenotypes, this experiment might provide insights into the cell types within which *otk2* exerts its influence upon embryonic motor neurons.

A second limitation pertains to the claims made regarding genetic interactions, which were put forward on the basis of abnormal phenotypes in embryos transheterozygous for combinations of functional alleles. For example, it has been argued that *otk2* and *sema-1a* encode proteins that participate in a shared signalling pathway because there are axonal aberrations in $otk2^{C26}$/+, *sema-1a*/+ embryos. While axon guidance defects are not normally observed in flies that are heterozygous for a functional copy of an axon guidance gene, it would be advisable to assess whether this is the case for the alleles used in the current study. For instance, the presence of abnormalities in $otk2^{C26}$/+ embryos would call into question the significance of the results of the *otk2* genetic

interaction experiments. It should also be investigated whether there are axon guidance phenotypes in *EY03841/+* embryos. The *EY03841* chromosome was used for *otk2* gain-of-function experiments because it contains a transposon encompassing a UAS upstream of *otk2*. However, it was demonstrated in Chapter 3 that there are severe axonal aberrations in embryos that are homozygous for the *EY03841*17* chromosome, from which the transposon had been precisely excised. Thus, greater confidence in the genetic interaction and *otk2* gain-of-function experiments could be achieved by analysing the axons of the following heterozygotes: (1) $otk2^{C26}$/+, (2) otk^{A1}/+, (3) *sema-1a/+*, (4) *fz2/+*, and (5) *EY03841/+*.

In addition to reinforcing the putative genetic interactions, future work should aim to elucidate the signalling pathways that the off-tracks do and do not participate in within the context of embryonic motor axon guidance. It has been argued here that Otk and Otk2 contribute to Sema-1a/PlexA signalling and Wnt4/Fz2 signalling on the basis of axonal aberrations in embryos transheterozygous for functional copies of either of the off-tracks and *sema-1a* or *fz2*. While prior research suggests that PlexA is a receptor for Sema-1a (Winberg et al., 1998) and that Fz2 is a receptor for Wnt4 (Inaki et al., 2007; Sato et al., 2006), it might be that the off-tracks are involved in Sema-1a and Fz2 pathways that are respectively independent of PlexA and Wnt4. For example, Fz2 can also act as a receptor for Wingless (Wg) within a pathway that affects postsynaptic development in the embryonic somatic musculature (Mosca & Schwarz, 2010). Moreover, in addition to Fz2, Linnemannstöns and colleagues' (2014) Co-IP results indicate that the off-tracks can form complexes with Fz and Wnt2. Fz has been linked to axon guidance in the adult brain (Gombos et al., 2015; Srahna et al., 2006), while Wnt2 has been put forward as a negative regulator of branch formation within the region of muscles 6 and 7 (Liebl, McKeown, & Hing, 2010). Additionally, Wnt2 is implicated in the development of the trachea (Llimargas et al., 2001), with which the growth cones of the ISN make contact (Desai et al., 1997; Hall & Bieber, 1997; Younossi-Hartenstein & Hartenstein, 1993). Thus, further experiments are required to determine which pathways the off-tracks do and do not contribute to and to assess whether phenotypes associated with the off-tracks can be explained by abnormalities in other structures, such as the tracheae. Regarding the former, this could initially be approached by examining the motor axons of embryos that are transheterozygous for functional copies of either of the off-tracks and *plexA*, *wnt2*, *wg*, or *fz*. Regarding the latter, co-staining embryos with 1D4 and 2A12 to visualise the motor neurons and tracheae, respectively, would allow for an assessment of whether abnormal tracheae contribute to guidance phenotypes in experiments involving the off-tracks.

While the current data suggest that *otk2* is implicated in embryonic motor axon guidance, it might also influence growing axons in other parts of the nervous system. *otk2* is strongly expressed in the embryonic central nervous system (Alsbury et al., in preparation; Linnemannstöns et al., 2014; this current study). An interesting feature of its distribution is that it appears to be much more strongly expressed in the region of the anterior commissure compared to the region of the posterior commissure, suggesting that it might play a role in commissure selection for axons crossing the midline. *drl* is expressed in axons that cross the midline via anterior commissures. It encodes a receptor for Wnt5, which acts as a repellent within the region of the posterior commissures (Yoshikawa et al., 2003). *otk2* may have a similar role to that of *drl*. This might be investigated by driving expression of *otk2* in posterior commissures with *Eagle-GAL4* (Dittrich et al., 1997) and staining with BP102 to visualise axons crossing the midline. Linnemannstöns and colleagues (2014) report that both off-tracks are expressed in larval photoreceptors, the axons of which are abnormal in *otk* mutants (Cafferty et al., 2004). Given these observations and the current study's evidence of a genetic interaction between the off-tracks, it would be interesting to assess whether larval photoreceptor axons are aberrant in *otk2* mutants.

In conclusion, the current study has provided evidence that *otk2* is required for embryonic motor axon guidance and that it genetically interacts with *otk, sema-1a,* and *fz2*. It has been suggested, however, that further experiments should be completed to reinforce these claims, such as pairing the $otk2^{C26}$ second chromosome with an alternative chromosome that lacks *otk2* activity, and assessing whether various heterozygotes exhibit guidance defects. Additionally, it has been suggested that further transheterozygous lines be examined to delineate the signalling pathways in which the off-tracks participate, and that the tracheae are examined for their potential contribution to axonal abnormalities. Finally, it has been put forward that the axons of embryonic CNS and larval photoreceptors be assessed in *otk2*-based experiments. These next steps will enhance our understanding of the role of the off-tracks in *Drosophila* axon guidance.

Chapter 5: *CG7565*

5.1. Introduction

CG7565 is predicted to encode a transmembrane protein, orthologous to two mouse and two human proteins, with an extracellular region comprised of two EGF domains, five polycystic kidney disease (PKD) domains, and an Ig domain (Alsbury et al., in preparation; Figure 77). While consisting of seven exons, there are no published data regarding splice variants. *In situ* indicates that CG7565 is expressed in the ventral nerve cord (VNC) between embryonic stages 14 and 16 (Alsbury et al., in preparation; Figure 78), consistent with it having a role in neural development.

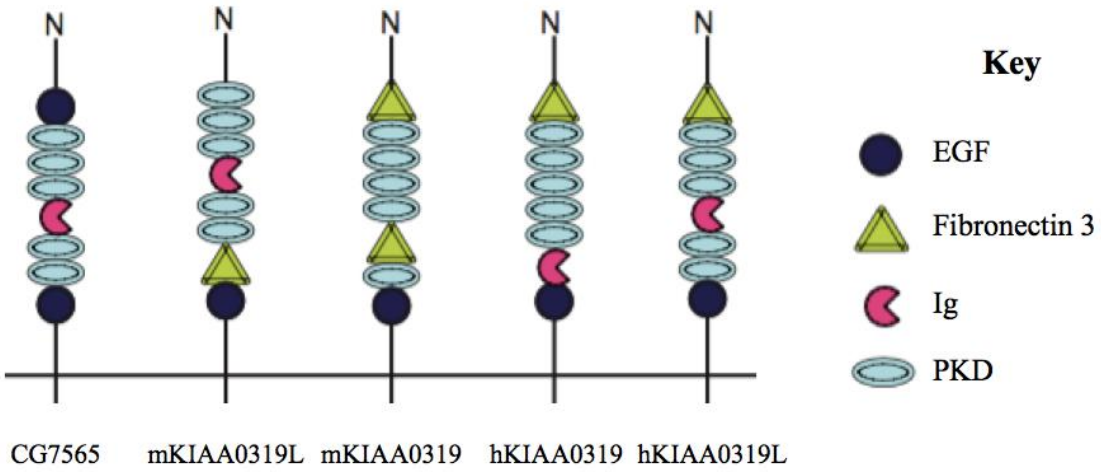

Figure 77. **Extracellular domains of CG7565 and its orthologues** (modified from Alsbury et al., in preparation). CG7565 and its mouse (mKIAA0319L & mKIAA0319) and human (hKIAA0319 & hKIAA0319L) orthologues are constituted of three or four domain types: epidermal growth factor (EGF), fibronectin 3, immunoglobulin (Ig), and polycystic kidney disease (PKD).

Figure 78. **Expression of *CG7565* revealed by *in situ* hybridisation** (modified from Alsbury et al., in preparation). **A.** A lateral view of a stage 14 embryo (up is anterior, left is ventral) with expression evident in the VNC (red arrow). **B.** A lateral view of a stage 16 embryo (up is anterior, left is ventral) with expression evident in the VNC (red arrow).

There are no published data pertaining to its molecular function or involvement in biological processes in *Drosophila*. The mouse orthologues of *CG7565* are KIAA0319 (also known as D130043K22Rik and 4930451E12Rik) and KIAA0319-like (KIAA0319L, also known as AU040320 and A730047D20Rik). No data are published pertaining to the molecular functions or biological processes associated with KIAA0319L (referred to henceforth as mKIAA0319L, where "m" stands for mouse). However, KIAA0319 (referred to henceforth as mKIAA0319) expression is reported to be enriched in dorsal spinal cord relative to control tissue in embryonic day 10.5 mice (Masuda et al., 2009). During this developmental period, the axons of dorsal root ganglion cells extend towards a region of the dorsal spinal cord, the dorsal root entry zone (Ozaki & Snider, 1997), suggesting that KIAA0319 might be implicated in axon guidance, if not in other neurodevelopmental processes.

The human orthologues of *CG7565* are also known as KIAA0319 and KIAA0319L and will henceforth be referred to, respectively, as hKIAA0319 and hKIAA0319L. Association studies indicate that polymorphisms within hKIAA0319L are linked to the autoimmune disorders, systemic sclerosis and systemic lupus erythematosus (Martin et al., 2013), and developmental dyslexia (DD; Couto et al., 2008). DD, which affects 4–10% of the population, is a language-based learning disability (Siegel, 2006), which is not attributable to cognitive, sensory, or learning environment deficits. In post mortem

examinations, Galaburda and Kemper (1979) observed neuronal migration abnormalities in the brains of individuals with DD. Others have determined that reading ability correlates with white mater volume in brain areas associated with language, such as the left temporo-parietal region (Darki et al., 2012), which might reflect aberrant axonal navigation. Perhaps unsurprisingly, polymorphisms within ROBO1, which has been linked to both neuronal migration (Gonda et al., 2013) and axon guidance (Long et al., 2004) in vertebrates, are associated with DD (Hannula-Jouppi et al., 2005). Interestingly, hKIAA0319L binds to Nogo Receptor 1 (NgR1; Poon et al., 2011), which, like ROBO1, is implicated in axonal repulsion (Hasegawa et al., 2004). Moreover, of all the *Drosophila* proteins, NgR1 is most closely related to the Robo1 ligand, Slit (Klinger, 2003). These findings hint at a potential role for *CG7565* within signalling pathways that underlie axons' responses to repellent signals.

Polymorphisms within the other human orthologue of *CG7565*, hKIAA0319, have also been linked to DD (Mascheretti et al., 2014). There is evidence that the rat orthologue of hKIAA0319 is required for neuronal migration and correct dendritic morphology (Peschansky et al., 2010), and SNPs within hKIAA0319 are related to white matter volume in language-associated brain areas (Darki et al., 2012). Regarding Peschansky and colleagues' (2010) report, the orientation of migrating neurons relative to glial fibres is altered in embryonic stage 14 rats injected with KIAA0319 small hairpin RNA (shRNA) into the ventricles of their forebrain, such that neuronal processes are orientated orthogonally to glial fibres instead of parallel to them, suggesting that the protein might be required for appropriate adhesion between the two cell types (Paracchini et al., 2006), a notion supported by evidence of PKD domains promoting adhesion (Ibraghimov-Beskrovnaya et al., 2000). In accordance with these reports, hKIAA0319 is expressed in adult brain (Valeyos-Baeza et al., 2007) and in the developing neocortex of human fetuses (Paracchini et al., 2006). Through alternative splicing and cleavage events, the hKIAA0319 protein can exist in a multitude of forms. Valeyos-Baeza and colleagues (2007) suggest that there are three primary splice variants: variant "A" is a transmembrane protein; variants "B" and "C" lack the transmembrane domain and are proposed to be secreted. Variant A is subjected to at least five cleavage events within its extracellular domain and an intramembrane cleavage. Respectively, these events result in fragments within the extracellular medium that might act as signals for other cells and a cytoplasmic domain that accumulates in nucleoli. Valeyos-Baeza and colleagues (2010) speculate that the accumulation of the cytoplasmic domain in nucleoli might relate to its having a role regulating in gene

expression, though highlight that, given the lack of DNA-interacting motifs, this role would be indirect.

There is, therefore, substantial evidence that the orthologues of *CG7565* influence neuronal migration in rodents (Paracchini et al., 2006; Peschansky et al., 2010). Some evidence indicates that they might have a role in axon guidance, namely: the expression of mKIAA0319 in mouse dorsal spinal cord at a time (embryonic day 10.5) when dorsal root ganglion cells extend axons to the region (Masuda et al., 2009; Ozaki & Snider, 1997); the binding of hKIAA0319 to the axon guidance receptor, NgR1 (Poon et al., 2011); and polymorphisms within hKIAA0319 being linked to DD (Mascheretti et al., 2014), which is associated with decreased white matter volume that might be a consequence of axon guidance defects (Darki et al., 2012). These reports, however, only provide indications of a possible role for *CG7565* and its orthologues in axon guidance, rather than direct evidence. Thus, the current study investigated whether manipulating *CG7565* in fruit flies would cause alterations to the formation of embryonic motor neurons.

5.2. Results

To investigate *CG7565's* role in embryonic motor axon guidance, a range of fly lines were examined, including (1) w^{1118}; $PBac\{5HPw^{+}\}CG7565^{B318}$ (referred to as *B318*), which harbours an insertion within an exonic region of *CG7565*, (2) w^{1118}; $Df(3L)ED4408, P\{w^{+mW.Scer\backslash FRT.hs3}=3'.RS5+3.3'\}ED4408/TM6b^{AbdA\text{-}lacZ}$ (referred to as *ED4408*), which harbours a deletion spanning the full length of *CG7565*, and (3) y^{1} w^{67c23}; P{EPgy2}$Ect4^{EY12902}$ (referred to a *EY12902*), which harbours a UAS-containing insertion upstream of the 5' UTR of *CG7565. EY12902* was crossed with *Mef2-GAL4* and *OK371-GAL4* lines to drive expression of *CG7565* in somatic muscle and motor neurons, respectively, towards the end of embryonic development (Mahr & Aberle, 2006; Rangagnayakulu, Schulz & Olson, 1996).

5.2.1. PCR and gel electrophoresis

Prior to phenotypic analyses, to provide support for the putative position of the transposon in the *B318* line, primers (referred to as 'B318') were designed to bind DNA either side of the transposon, producing a 331 bp product. It was assumed that the transposon would prevent amplification of DNA, especially given the short (30 s) elongation phases used during PCR. This was supported by the presence and absence of bands from DNA of wild type and *B318* flies, respectively (Figure 79).

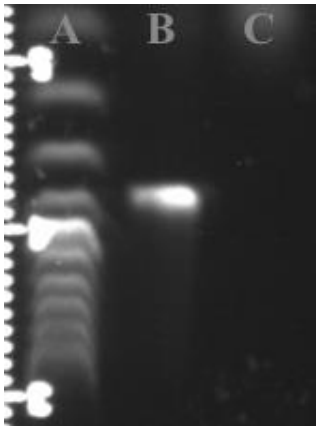

Figure 79. **Gel image of wild type and *B318* DNA amplified with B318 primers**. Lane A shows a 100 bp ladder, with the top band corresponding to 100 bp. Lane B shows a band produced from wild type DNA, which is slightly above the 4th band of the ladder (corresponding to 400 bp). This position is congruent with the expected product size of 331 bp. There is no band in lane C, into which a PCR product consisting of *B318* DNA was loaded. This is consistent with the notion that the transposon in *B318* DNA would inhibit the PCR reaction.

5.2.2. Phenotypic analysis: *B318*

An inspection of the motor neurons of *B318* embryos suggested that various branches were frequently absent or abnormal. Often, the first branch (FB) of the ISN was absent (Figure 81), the second branch (SB) of the ISN was absent (Figure 82) or projected anteriorly (Figure 83), the MN13s were absent (Figure 84) or projected anteriorly (Figure 85), the MN12s projected anteriorly (Figure 86), and the RP3 axon was absent (Figure 87). The full length of a wild type hemisegment, with the branches that are abnormal in *CG7565* experiments indicated, is shown in Figure 80 for reference. Figure 100 (p. 150) shows the penetrance of phenotypes in *B318* embryos, as well as their frequency in all other genotypes analysed in this chapter.

As per Chapter 4, MN12 anterior projections are described as being mild or severe. In wild types, the MN12s typically extend dorsally from the muscle 13 innervation point, and then attach to muscle 12 via posterior projections or posterior and anterior projections of equal length. In mild cases, MN12s extend dorsally, and then attach to muscle 12 via anterior projections or posterior and anterior projections, the latter being greater in length. In severe cases, MN12s extend anteriorly from the muscle 13 innervation point. In such cases, projections were deemed to have grown anteriorly if they extended at an angle equal or greater to 30° from the region of the ISNb between the muscle 6/7 cleft and muscle 13 innervation point.

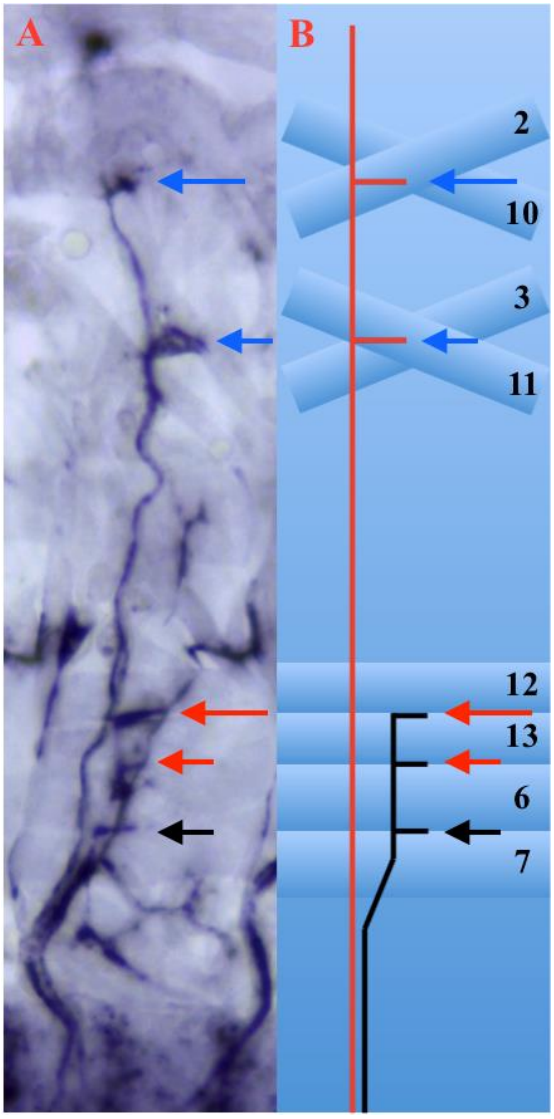

Figure 80. **A wild type hemisegment with the ISNb (comprised of MN12s, MN13s, and the RP3 axon), and the first (FB) and second (SB) branches of the ISN indicated. A.** Wild type hemisegment showing the motor neurons (right is posterior, up is dorsal). The branches that are altered in experiments involving *CG7565* are indicated: SB (long blue arrow), FB (short blue arrow), MN12s (long red arrow), MN13s (short red arrow), and the RP3 axon (short black arrow). **B.** Schematic of a wild type hemisegment showing the ISNb (black) and the ISN (red) (right is posterior, up is dorsal). The branches that are altered in experiments involving *CG7565* are indicated: SB (long blue arrow), FB (short blue arrow), MN12s (long red arrow), MN13s (short red arrow), and the RP3 axon (short black arrow). The muscles in the regions of the ISNb, FB, and SB are indicated by numbers (other branches and muscles are not shown).

FB absent

The FB was absent more often in *B318* hemisegments (20.7%) than in wild types (7.6%) (Figure 81).

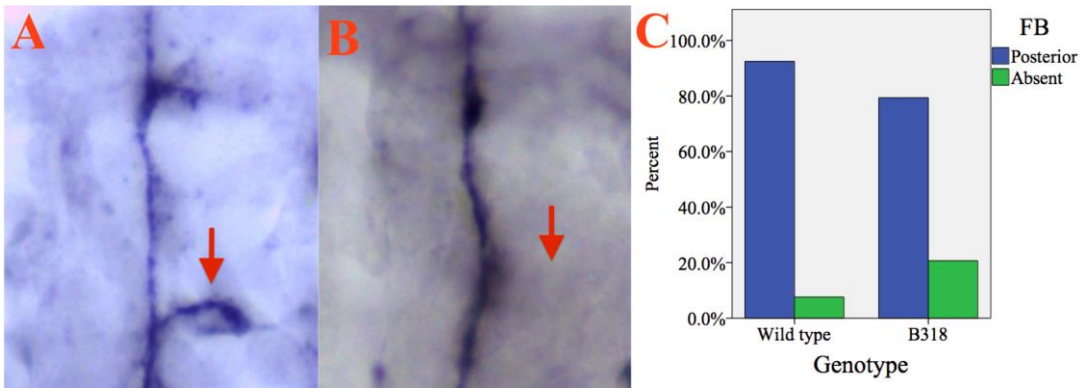

D	FB posterior	FB absent
Wild type	92.4% (195)	7.6% (16)
B318	79.3% (73)	20.7% (19)

Figure 81. Image A (right is posterior, up is dorsal) shows a dorsal section of a wild type hemisegment with the FB indicated (red arrow). Image B (right is posterior, up is dorsal) shows a dorsal section of a *B318* hemisegment without the FB (red arrow). The graph (C) shows the percentage of hemisegments in which the FB projects posteriorly or is absent in 30 wild type and 17 *B318* embryos. The table (D) shows the percentage and number (in parentheses) of hemisegments in which the FB projects posteriorly or is absent in the same embryos.

A chi-square test for independence revealed that the FB was absent significantly more often in *B318* hemisegments than in wild types, χ^2 (1, n = 303) = 10.71, p < .01.

SB absent

The SB was absent more often in *B318* hemisegments (57.1%) than in wild types (30.7%) (Figure 82).

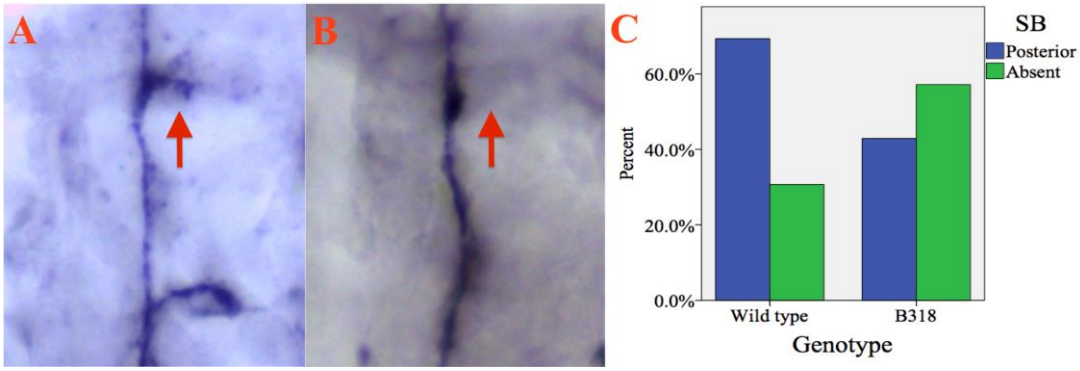

D	SB posterior	SB absent
Wild type	69.3% (70)	30.7% (31)
B318	42.9% (18)	57.1% (24)

Figure 82. Image A (right is posterior, up is dorsal) shows a dorsal section of a wild type hemisegment with the SB indicated (red arrow). Image B (right is posterior, up is dorsal) shows a dorsal section of a *B318* hemisegment without the SB (red arrow). The graph (C) shows the percentage of hemisegments in which the SB projects posteriorly or is absent in 30 wild type and 17 *B318* embryos. The table (D) shows the percentage and number (in parentheses) of hemisegments in which the SB projects posteriorly or is absent in the same embryos.

A chi-square test for independence revealed that the SB was absent significantly more often in *B318* hemisegments than in wild types, χ^2 (1, n = 143) = 8.77, p < .01.

SB anterior

The SB projected anteriorly more often in *B318* hemisegments (50%) than in wild types (9.1%) (Figure 83).

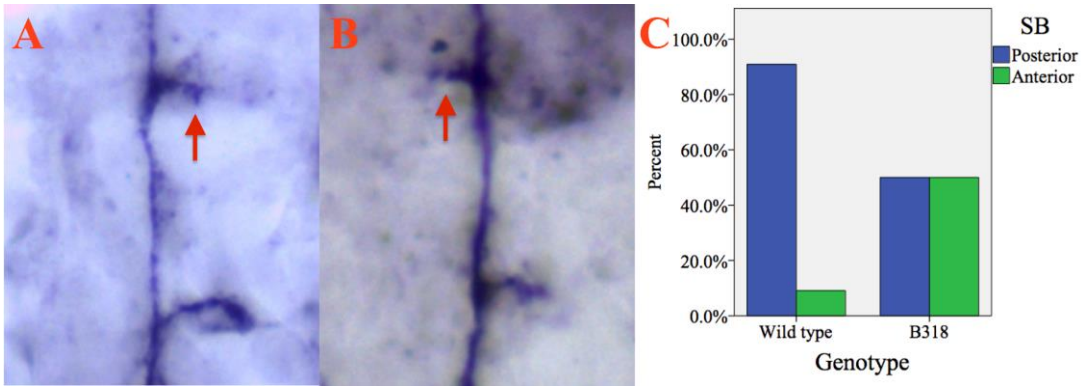

D	SB posterior	SB anterior
Wild type	90.9% (70)	9.1% (7)
B318	50% (18)	50% (18)

Figure 83. Image A (right is posterior, up is dorsal) shows a dorsal section of a wild type hemisegment with the SB projecting posteriorly (red arrow). Image B (right is posterior, up is dorsal) shows a dorsal section of a *B318* hemisegment with the SB projecting anteriorly (red arrow). The graph (C) shows the percentage of hemisegments in which the SB projects posteriorly or anteriorly in 30 wild type and 17 *B318* embryos. The table (D) shows the percentage and number (in parentheses) of hemisegments in which the SB projects posteriorly or anteriorly in the same embryos.

A chi-squared test for independence revealed that the SB projected anteriorly significantly more often in *B318* hemisegments than in wild types, χ^2 (1, n = 113) = 23.83, $p < .001$.

MN13s absent

The MN13s were absent more often in *B318* hemisegments (40%) than in wild types (11.9%) (Figure 84).

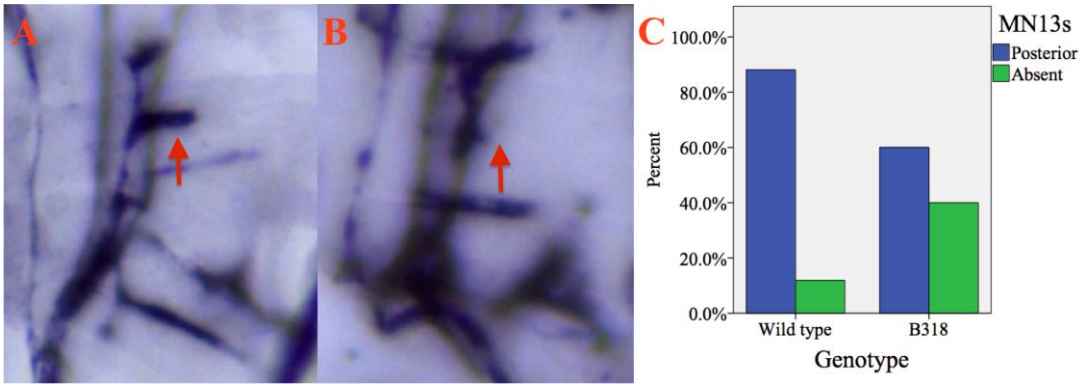

D	MN13s posterior	MN13s absent
Wild type	88.1% (133)	11.9% (18)
B318	60% (27)	40% (18)

Figure 84. Image A (right is posterior, up is dorsal) shows a ventral section of a wild type hemisegment with the MN13s indicated (red arrow). Image B (right is posterior, up is dorsal) shows a ventral section of a *B318* hemisegment without the MN13s (red arrow). The graph (C) shows the percentage of hemisegments in which the MN13s project posteriorly or are absent in 30 wild type and 15 *B318* embryos. The table (D) shows the percentage and number (in parentheses) of hemisegments in which the MN13s project posteriorly or are absent in the same embryos.

A chi-square test for independence revealed that the MN13s were absent significantly more often in *B318* hemisegments than in wild types, χ^2 (1, n = 196) = 18.23, p < .001.

MN13s project anteriorly

The MN13s projected anteriorly more often in *B318* hemisegments (18.2%) than in wild types (2.9%) (Figure 85).

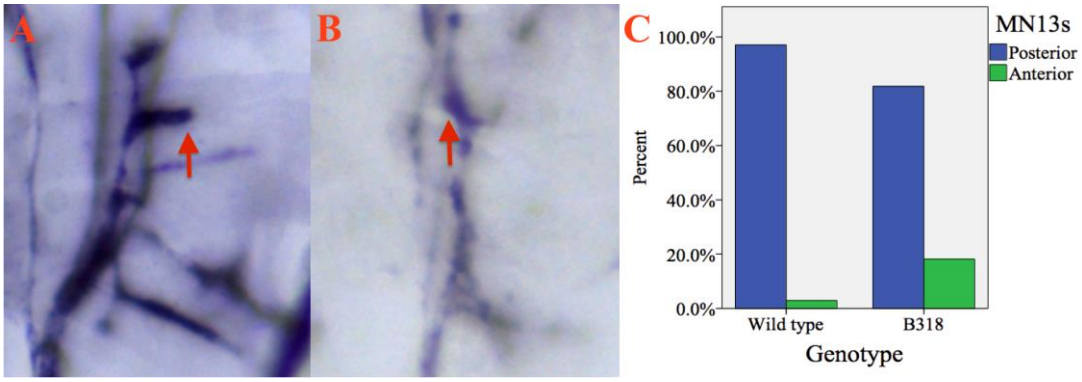

D	MN13s posterior	MN13s anterior
Wild type	97.1% (133)	2.9% (4)
B318	81.8% (27)	18.2% (6)

Figure 85. Image A (right is posterior, up is dorsal) shows a ventral section of a wild type hemisegment in which the MN13s project posteriorly (red arrow). Image B (right is posterior, up is dorsal) shows a ventral section of a *B318* hemisegment in which the MN13s project anteriorly (red arrow). The graph (C) shows the percentage of hemisegments in which the MN13s project posteriorly or anteriorly in 27 wild type and 15 *B318* embryos. The table (D) shows the percentage and number (in parentheses) of hemisegments in which the MN13s project posteriorly or anteriorly in the same embryos.

Fisher's exact test revealed that the MN13s projected anteriorly significantly more often in *B318* hemisegments than in wild types, $p < .01$.

MN12s project anteriorly

The MN12s of *B318* embryos projected anteriorly. 48.3% of *B318* hemisegments exhibited the mild phenotype (Figure 86B), compared to 20% of wild type hemisegments. 6.9% of *B318* hemisegments exhibited the severe phenotype (Figure 86C), compared to 8.8% of wild type hemisegments.

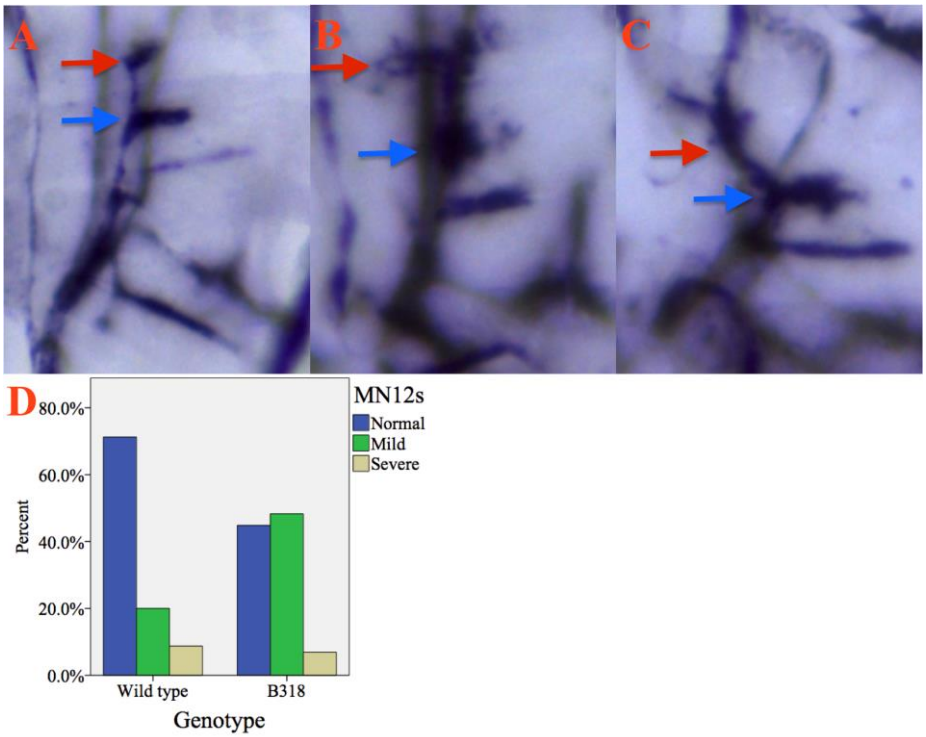

E	MN12s normal	MN12s mild	MN12s severe
Wild type	71.2% (57)	20% (16)	8.8% (7)
B318	44.8% (13)	48.3% (14)	6.9% (2)

Figure 86. Image A (right is posterior, up is dorsal) shows a ventral section of a wild type hemisegment in which the MN12s project dorsally at the muscle 13 innervation point (blue arrow) before projecting posteriorly (red arrow). Image B (right is posterior, up is dorsal) shows a ventral section of a *B318* hemisegment in which the MN12s project dorsally at the muscle 13 innervation point (blue arrow) before projecting anteriorly (red arrow). Image C (right is posterior, up is dorsal) shows a ventral section of a *B318* hemisegment in which the MN12s (red arrow) project anteriorly at the muscle 13 innervation point (blue arrow). The graph (D) shows the percentage of hemisegments that exhibit the normal, mild, and severe phenotypes in 27 wild type and 15 *B318* embryos. The table (E) shows the percentage and number (in parentheses) of hemisegments exhibiting normal, mild, and severe phenotypes in the same embryos.

Fisher's exact test revealed a significant effect of genotype with regard to the trajectory of the MN12s, $p < .05$.

RP3 axon absent

The RP3 axon was absent more often in *B318* hemisegments (55.6%) than in wild types (20.1%) (Figure 87).

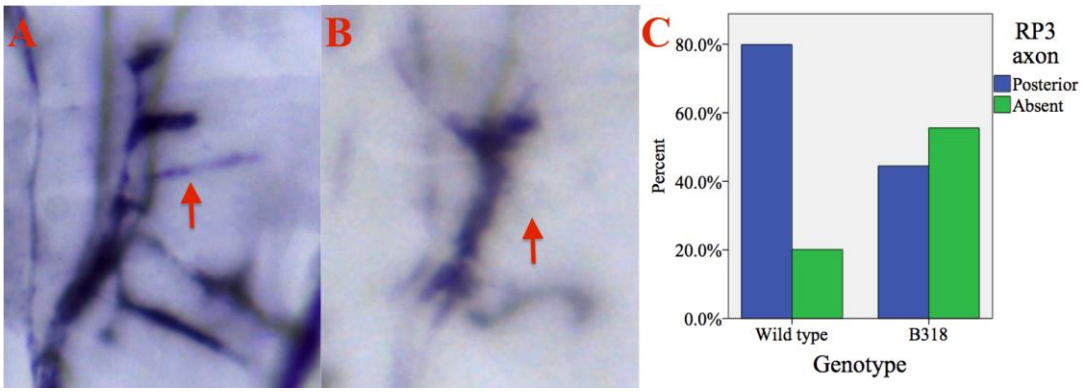

D	RP3 axon posterior	RP3 axon absent
Wild type	79.9% (147)	20.1% (37)
B318	44.4% (24)	55.6% (30)

Figure 87. Image A (right is posterior, up is dorsal) shows a ventral section of a wild type hemisegment with the RP3 axon indicated (red arrow). Image B (right is posterior, up is dorsal) shows a ventral section of a *B318* hemisegment without the RP3 axon (red arrow). The graph (C) shows the percentage of hemisegments in which the RP3 axon projects posteriorly or is absent in 27 wild type and 15 *B318* embryos. The table (D) shows the percentage and number (in parentheses) of hemisegments in which the RP3 axon projects posteriorly or is absent in the same embryos.

A chi-square test for independence revealed that the RP3 axon was absent significantly more often in *B318* hemisegments than in wild types, χ^2 (1, n = 238) = 25.93, p < .001.

5.2.3. Phenotypic analysis: *ED4408*

To provide further support for the notion that lack of *CG7565* activity was the cause of the phenotypes in *B318* embryos, a line with a deficiency spanning the gene, *ED4408*, was also examined. With the exception of the second branch of the ISN (SB) anterior phenotype, *ED4408* embryos exhibited the same phenotypes as those reported for *B318* embryos. That is, the first branch of the ISN (FB) (Figure 88), SB (Figure 89), MN13s (Figure 90), and RP3 axon (Figure 93) were absent. When the MN13s were present, they projected anteriorly (Figure 91), as did the MN12s (Figure 92).

FB absent

The FB was absent more often in *ED4408* hemisegments (38.1%) than in wild types (7.6%) (Figure 88).

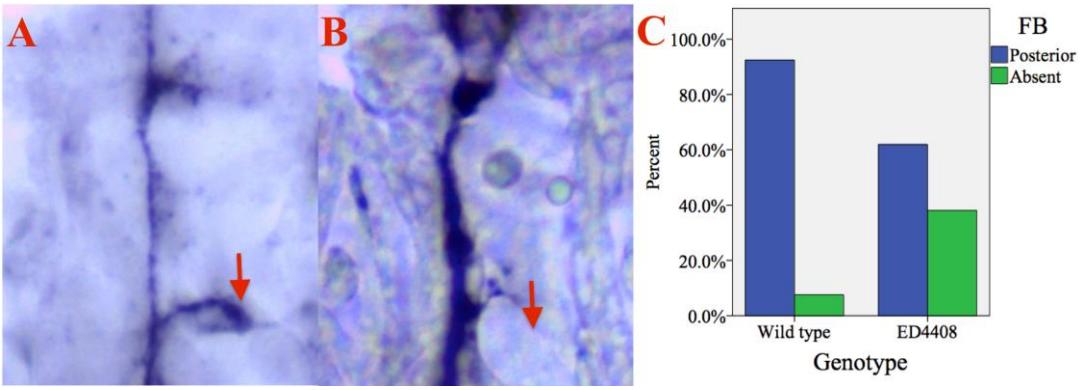

D	FB posterior	FB absent
Wild type	92.4% (195)	7.6% (16)
ED4408	61.9% (26)	38.1% (16)

Figure 88. Image A (right is posterior, up is dorsal) shows a dorsal section of a wild type hemisegment with the FB indicated (red arrow). Image B (right is posterior, up is dorsal) shows a dorsal section of an *ED4408* hemisegment without the FB (red arrow). The graph (C) shows the percentage of hemisegments in which the FB projects posteriorly or is absent in 30 wild type and 6 *ED4408* embryos. The table (D) shows the percentage and number (in parentheses) of hemisegments in which the FB projects posteriorly or is absent in the same embryos.

A chi-square test for independence revealed that the FB was absent significantly more often in *ED4408 hemisegments* than in wild types, χ^2 (1, n = 253) = 29.52, p < .001.

SB absent

The SB was absent more often in *ED4408* hemisegments (66.7%) than in wild types (30.7%) (Figure 89).

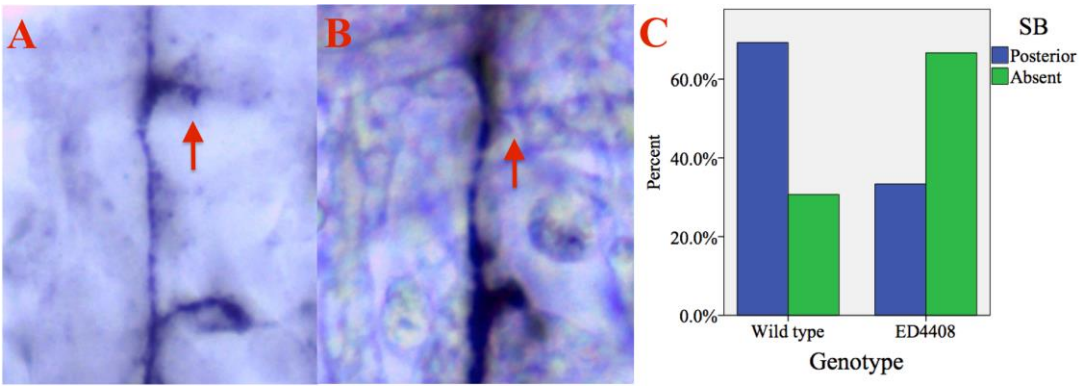

D	SB posterior	SB absent
Wild type	69.3% (70)	30.7% (31)
ED4408	33.3% (7)	66.7% (14)

Figure 89. Image A (right is posterior, up is dorsal) shows a dorsal section of a wild type hemisegment with the SB indicated (red arrow). Image B (right is posterior, up is dorsal) shows a dorsal section of an *ED4408* hemisegment without the SB (red arrow). The graph (C) shows the percentage of hemisegments in which the SB projects posteriorly or is absent in 30 wild type and 6 *ED4408* embryos. The table (D) shows the percentage and number (in parentheses) of hemisegments in which the SB projects posteriorly or is absent in the same embryos.

A chi-square test for independence revealed that the SB was absent significantly more often in *ED4408* hemisegments than in wild types, χ^2 (1, n = 122) = 9.66, p < .01.

MN13s absent

The MN13s were absent more often in *ED4408* hemisegments (46.2%) than in wild types (11.9%) (Figure 90).

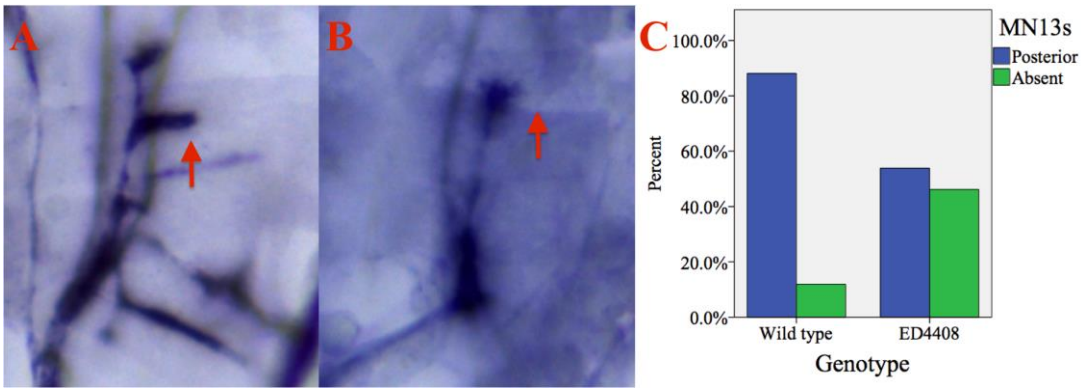

D	MN13s posterior	MN13s absent
Wild type	88.1% (133)	11.9% (18)
ED4408	53.8% (14)	46.2% (12)

Figure 90. Image A (right is posterior, up is dorsal) shows a ventral section of a wild type hemisegment with the MN13s indicated (red arrow). Image B (right is posterior, up is dorsal) shows a ventral section of an *ED4408* hemisegment without the MN13s (red arrow). The graph (C) shows the percentage of hemisegments in which the MN13s project posteriorly or are absent in 27 wild type and 6 *ED4408* embryos. The table (D) shows the percentage and number (in parentheses) of hemisegments in which the MN13s project posteriorly or are absent in the same embryos.

Fisher's exact test revealed that the MN13s were absent significantly more often in *ED4408* hemisegments than in wild types, $p < .001$.

MN13s project anteriorly

The MN13s projected anteriorly more often in *ED4408* hemisegments (17.6%) than in wild types (2.9%) (Figure 91).

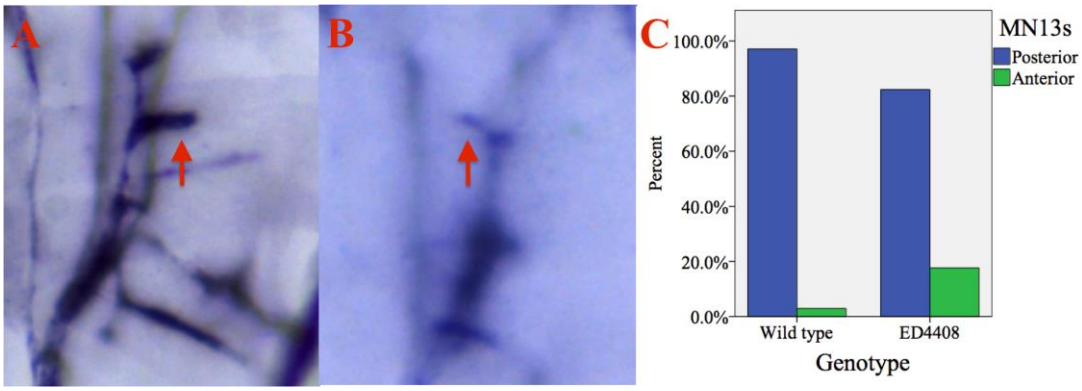

D	MN13s posterior	MN13s anterior
Wild type	97.1% (133)	2.9% (4)
ED4408	82.4% (14)	17.6% (3)

Figure 91. Image A (right is posterior, up is dorsal) shows a ventral section of a wild type hemisegment in which the MN13s project posteriorly (red arrow). Image B (right is posterior, up is dorsal) shows a ventral section of an *ED4408* hemisegment in which the MN13s project anteriorly (red arrow). The graph (C) shows the percentage of hemisegments in which the MN13s project posteriorly or anteriorly in 27 wild type and 6 *ED4408* embryos. The table (D) shows the percentage and number (in parentheses) of hemisegments in which the MN13s project posteriorly or anteriorly in the same embryos.

Fisher's test revealed that the MN13s projected anteriorly significantly more often in *ED4408* hemisegments than in wild types, $p < .05$.

MN12s project anteriorly

The MN12s of *ED4408* embryos projected anteriorly. 18.2% of *B318* hemisegments exhibited the mild phenotype (Figure 92B), compared to 20% of wild type hemisegments. 45.5% of *ED4408* hemisegments exhibited the severe phenotype (Figure 92C), compared to 8.8% of wild type hemisegments.

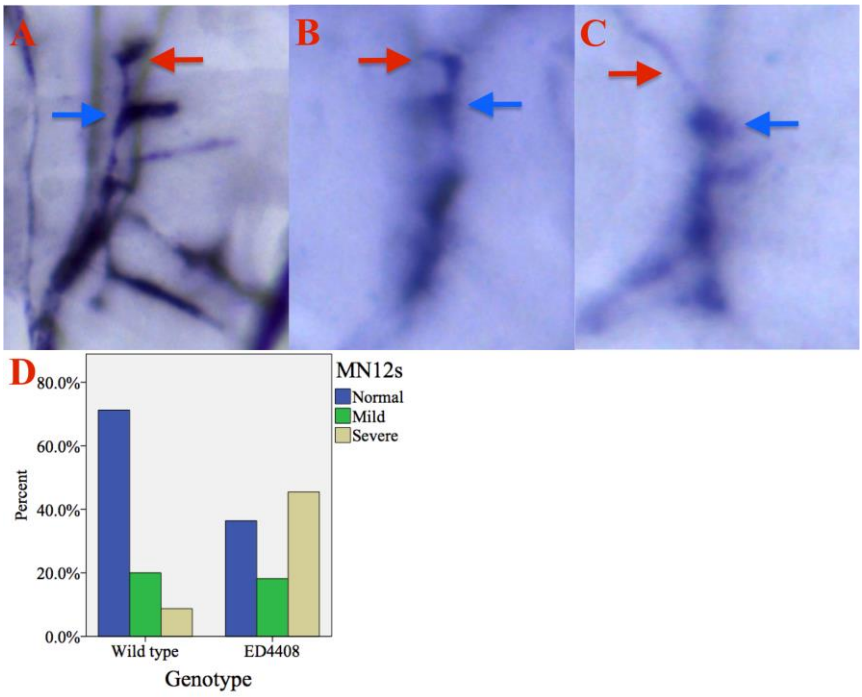

E	MN12s normal	MN12s mild	MN12s severe
Wild type	71.2% (57)	20% (16)	8.8% (7)
ED4408	36.4% (4)	18.2% (2)	45.5% (5)

Figure 92. Image A (right is posterior, up is dorsal) shows a ventral section of a wild type hemisegment in which the MN12s project dorsally at the muscle 13 innervation point (blue arrow) before projecting posteriorly (red arrow). Image B (right is posterior, up is dorsal) shows a ventral section of an *ED44088* hemisegment in which the MN12s project dorsally at the muscle 13 innervation point (blue arrow) before projecting anteriorly (red arrow). Image C (right is posterior, up is dorsal) shows a ventral section of an *ED4408* hemisegment in which the MN12s (red arrow) project anteriorly at the muscle 13 innervation point (blue arrow). The graph (D) shows the percentage of hemisegments that exhibit the normal, mild, and severe phenotypes in 27 wild type and 6 *ED4408* embryos. The table (E) shows the percentage and number (in parentheses) of hemisegments exhibiting normal, mild, and severe phenotypes in the same embryos.

Fisher's exact test revealed a significant effect of genotype with regard to the trajectory of the MN12s, $p < .01$.

RP3 axon absent

The RP3 axon was absent more often in *ED4408* hemisegments (64.5%) than in wild types (20.1%) (Figure 93).

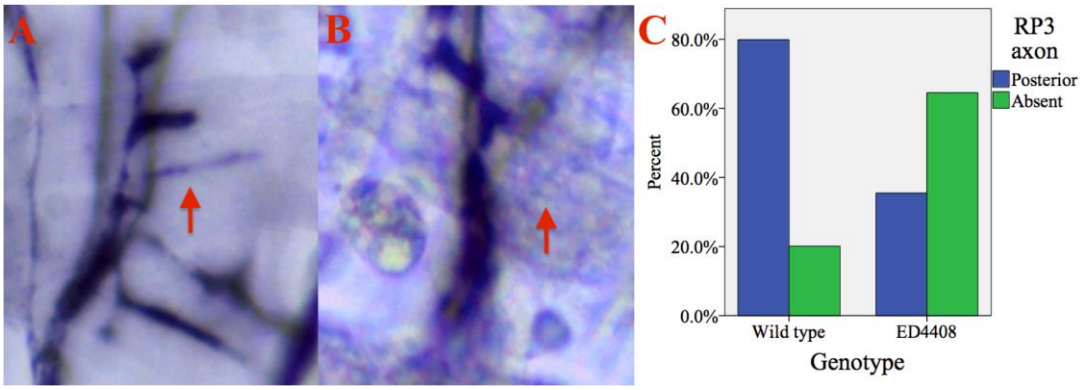

D	RP3 axon posterior	RP3 axon absent
Wild type	79.9% (147)	20.1% (37)
ED4408	35.5% (11)	64.5% (20)

Figure 93. Image A (right is posterior, up is dorsal) shows a ventral section of a wild type hemisegment with the RP3 axon indicated (red arrow). Image B (right is posterior, up is dorsal) shows a ventral section of an *ED4408* hemisegment without the RP3 axon (red arrow). The graph (C) shows the percentage of hemisegments in which the RP3 axon projects posteriorly or is absent in 27 wild type and 6 *ED4408* embryos. The table (D) shows the percentage and number (in parentheses) of hemisegments in which the RP3 axon projects posteriorly or is absent in the same embryos.

A chi-square test for independence revealed that the RP3 axon was absent significantly more often in *ED4408* hemisegments than in wild types, χ^2 (1, n = 215) = 26.85, p < .001.

5.2.4. Phenotypic analysis: *Mef2 X EY12902*

Having established the presence of phenotypes in *CG7565* loss-of-function lines, gain-of-function experiments were completed to attain insights into the precise role of CG7565. The first of these involved crossing the *Mef-GAL4* driver with the *EY12902* line, which harbours a UAS sequence upstream of the 5' UTR of *CG7565*, with the intention of driving CG7565 expression in somatic muscle towards the end of embryonic development (Rangagnayakulu, Schulz & Olson, 1996). As per the *B318* and *ED4408* embryos, those with CG7565 expression driven throughout the somatic musculature exhibited the RP3 axon absent phenotype (Figure 94). However, the

MN12s were not aberrant, and the second branch (SB) of the ISN formed at wild type frequency. The first branch (FB) of the ISN was present more often than in wild types (Figure 95), and the MN13s had a tendency to be elongated towards the posterior (Figure 96). MN13s were deemed to be elongated if their length was greater than the distance between the dorsal edge of their anterior end and the cleft between muscles 6 and 7.

RP3 axon absent

The RP3 axon was absent more often in *Mef2 X EY12902* hemisegments (42.7%) than in wild types (20.1%) (Figure 94).

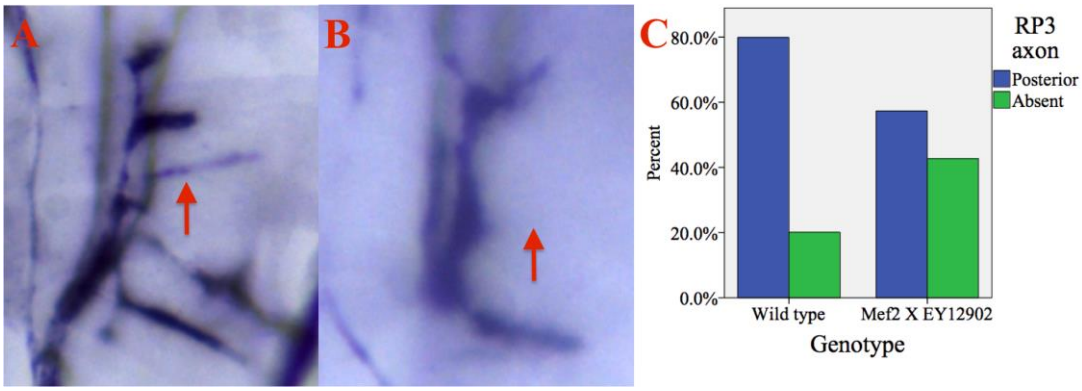

D	RP3 axon posterior	RP3 axon absent
Wild type	79.9% (147)	20.1% (37)
Mef2 X EY12902	57.3% (51)	42.7% (38)

Figure 94. Image A (right is posterior, up is dorsal) shows a ventral section of a wild type hemisegment with the RP3 axon indicated (red arrow). Image B (right is posterior, up is dorsal) shows a ventral section of a *Mef2 X EY12902* hemisegment without the RP3 axon (red arrow). The graph (C) shows the percentage of hemisegments in which the RP3 axon projects posteriorly or is absent in 27 wild type and 10 *Mef2 X EY12902* embryos. The table (D) shows the percentage and number (in parentheses) of hemisegments in which the RP3 axon projects posteriorly or is absent in the same embryos.

A chi-square test for independence revealed that the RP3 axon was absent significantly more often in *Mef2 X EY12902* hemisegments than in wild types, χ^2 (1, n = 273) = 15.36, p < .001.

Reduced FB absence

The FB was present more often in *Mef2 X EY12902* hemisegments (98%) than in wild types (92.4%) (Figure 95).

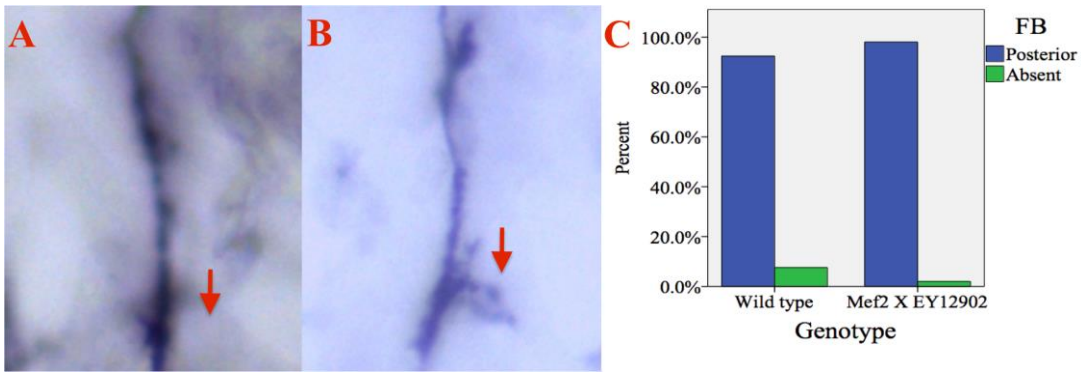

D	FB posterior	FB absent
Wild type	92.4% (195)	7.6% (16)
Mef2 X EY12902	98% (149)	2% (3)

Figure 95. Image A (right is posterior, up is dorsal) shows a dorsal section of a wild type hemisegment without the FB (red arrow). Image B (right is posterior, up is dorsal) shows a dorsal section of a *Mef2 X EY12902* hemisegment with the FB indicated (red arrow). The graph (C) shows the percentage of hemisegments in which the FB projects posteriorly or is absent in 30 wild type and 14 *Mef2 X EY12902* embryos. The table (D) shows the percentage and number (in parentheses) of hemisegments in which the FB projects posteriorly or is absent in the same embryos.

A chi-square test for independence revealed that the FB was present significantly more often in *Mef2 X EY12902* hemisegments than in wild types, χ^2 (1, n = 363) = 5.6, p < .05.

MN13s elongated posteriorly

The MN13s were elongated posteriorly more often in *Mef2 X EY12902* hemisegments (12.2%) than in wild types (2.2%) (Figure 96).

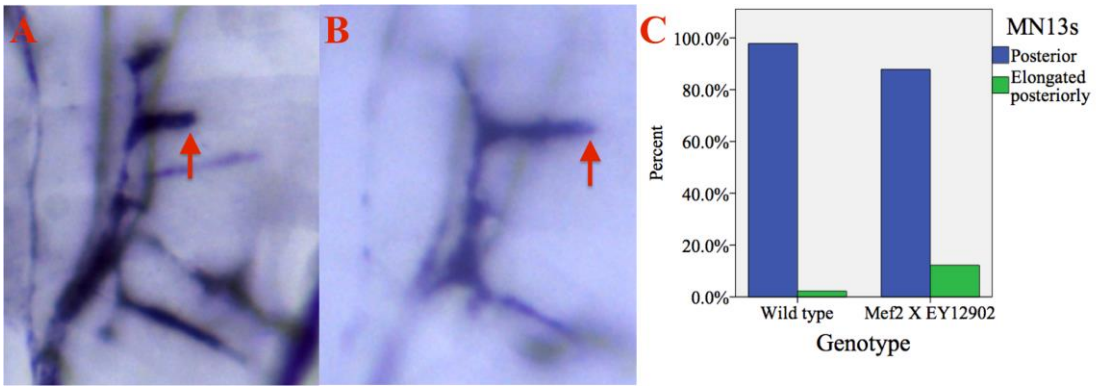

D	MN13s posterior	MN13s elongated posteriorly
Wild type	97.8% (133)	2.2% (3)
Mef2 X EY12902	87.8% (72)	12.2% (10)

Figure 96. Image A (right is posterior, up is dorsal) shows a ventral section of a wild type hemisegment with the MN13s indicated (red arrow). Image B (right is posterior, up is dorsal) shows a ventral section of a *Mef2 X EY12902* hemisegment with the MN13s elongated posteriorly (red arrow). The graph (C) shows the percentage of hemisegments in which the MN13s are of normal length or are elongated in 27 wild type and 10 *Mef2 X EY12902* embryos. The table (D) shows the percentage and number (in parentheses) of hemisegments in which the MN13s are of normal length or are elongated in the same embryos.

Fisher's exact test revealed that the MN13s were elongated posteriorly significantly more often in *Mef2 X EY12902* hemisegments than in wild types, $p < .01$.

5.2.5. Phenotypic analysis: *OK371 X EY12902*

To gain further insights into the precise function of CG7565, a second gain-of-function experiment was completed. *OK371-GAL4* flies were crossed with those of the *CG7565* UAS line, *EY12902*, with the intention of driving expression of CG7565 in motor neurons towards the end of embryonic development (Mahr & Aberle, 2006). As per the *B318* and *ED4408* embryos, those with expression of *CG7565* driven in motor neurons exhibited the MN13s anterior (Figure 97), MN12s anterior (Figure 98), and RP3 axon absent (Figure 99) phenotypes. No abnormalities were observed in the first (FB) or second branch (SB) of the ISN.

MN13s project anteriorly

The MN13s projected anteriorly more often in *OK371 X EY12902* hemisegments (14.9%) than in wild types (2.9%) (Figure 97).

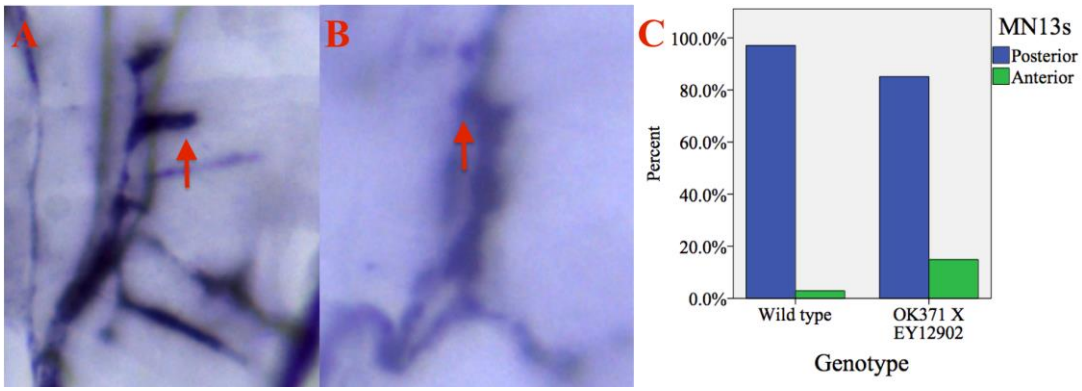

D	MN13s posterior	MN13s anterior
Wild type	97.1% (133)	2.9% (4)
OK371 X EY12902	85.1% (40)	14.9% (7)

Figure 97. Image A (right is posterior, up is dorsal) shows a ventral section of a wild type hemisegment in which the MN13s project posteriorly (red arrow). Image B (right is posterior, up is dorsal) shows a ventral section of an *OK371 X EY12902* hemisegment in which the MN13s project anteriorly (red arrow). The graph (C) shows the percentage of hemisegments in which the MN13s project posteriorly or anteriorly in 27 wild type and 9 *OK371 X EY12902* embryos. The table (D) shows the percentage and number (in parentheses) of hemisegments in which the MN13s project posteriorly or anteriorly in the same embryos.

A chi-square test for independence revealed that the MN13s projected anteriorly significantly more often in *OK371 X EY12902* hemisegments than in wild types, χ^2 (1, n = 184) = 8.93, $p < .01$.

MN12s project anteriorly

The MN12s of *OK371 X EY12902* embryos projected anteriorly. 46.7% of *OK371 X EY12902* hemisegments exhibited the mild phenotype (Figure 98B), compared to 20% of wild type hemisegments. 11.1% of *OK371 X EY12902* hemisegments exhibited the severe phenotype (Figure 98C), compared to 8.8% of wild type hemisegments.

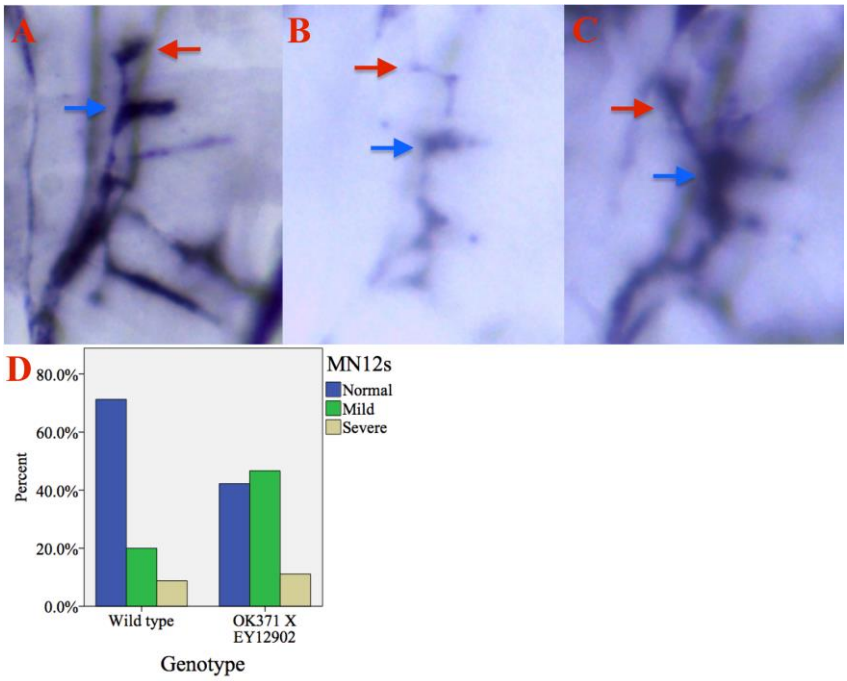

E	MN12s normal	MN12s mild	MN12s severe
Wild type	71.2% (57)	20% (16)	8.8% (7)
OK371 X EY12902	42.4% (19)	46.7% (21)	11.1% (5)

Figure 98. Image A (right is posterior, up is dorsal) shows a ventral section of a wild type hemisegment in which the MN12s project dorsally at the muscle 13 innervation point (blue arrow) before projecting posteriorly (red arrow). Image B (right is posterior, up is dorsal) shows a ventral section of an *OK371 X EY12902* hemisegment in which the MN12s project dorsally at the muscle 13 innervation point (blue arrow) before projecting anteriorly (red arrow). Image C (right is posterior, up is dorsal) shows a ventral section of an *OK371 X EY12902* hemisegment in which the MN12s (red arrow) project anteriorly at the muscle 13 innervation point (blue arrow). The graph (D) shows the percentage of hemisegments that exhibit the normal, mild, and severe phenotypes in 27 wild type and 9 *OK371 X EY12902* embryos. The table (E) shows the percentage and number (in parentheses) of hemisegments exhibiting normal, mild, and severe phenotypes in the same embryos.

Fisher's exact test revealed a significant effect of genotype with regard to the trajectory of the MN12s, $p < .01$.

RP3 axon absent

The RP3 axon was absent significantly more often in *OK371 X EY12902* hemisegments (47.6%) than in wild types (20.1%) (Figure 99).

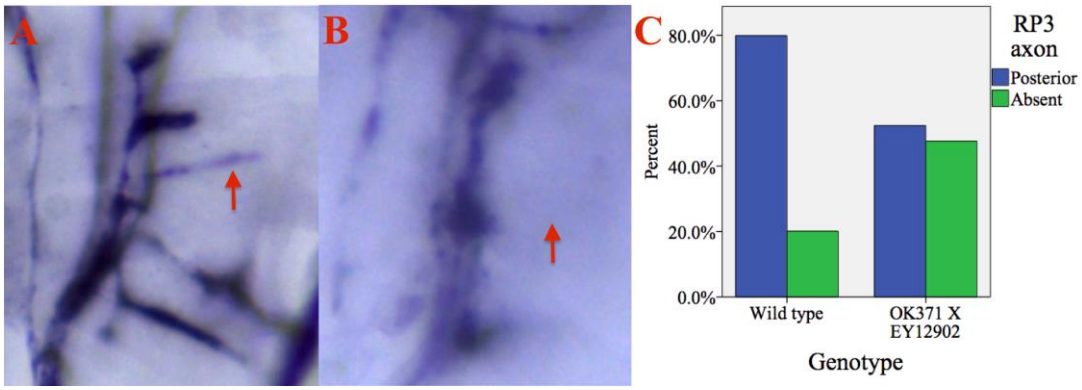

D	RP3 axon posterior	RP3 axon absent
Wild type	79.9% (147)	20.1% (37)
OK371 X EY12902	52.4% (33)	47.6% (30)

Figure 99. Image A (right is posterior, up is dorsal) shows a ventral section of a wild type hemisegment with the RP3 axon indicated (red arrow). Image B (right is posterior, up is dorsal) shows a ventral section of an *OK371 X EY12902* hemisegment without the RP3 axon (red arrow). The graph (C) shows the percentage of hemisegments in which the RP3 axon projects posteriorly or is absent in 27 wild type and 9 *OK371 X EY12902* embryos. The table (D) shows the percentage and number (in parentheses) of hemisegments in which the RP3 axon projects posteriorly or is absent in the same embryos.

A chi-square test for independence revealed that the RP3 axon was absent significantly more often in *OK371 X EY12902* hemisegments than in wild types, χ^2 (1, n = 247) = 17.97, p < .001.

Figure 100. Penetrance of phenotypes in all genotypes analysed in Chapter 5.

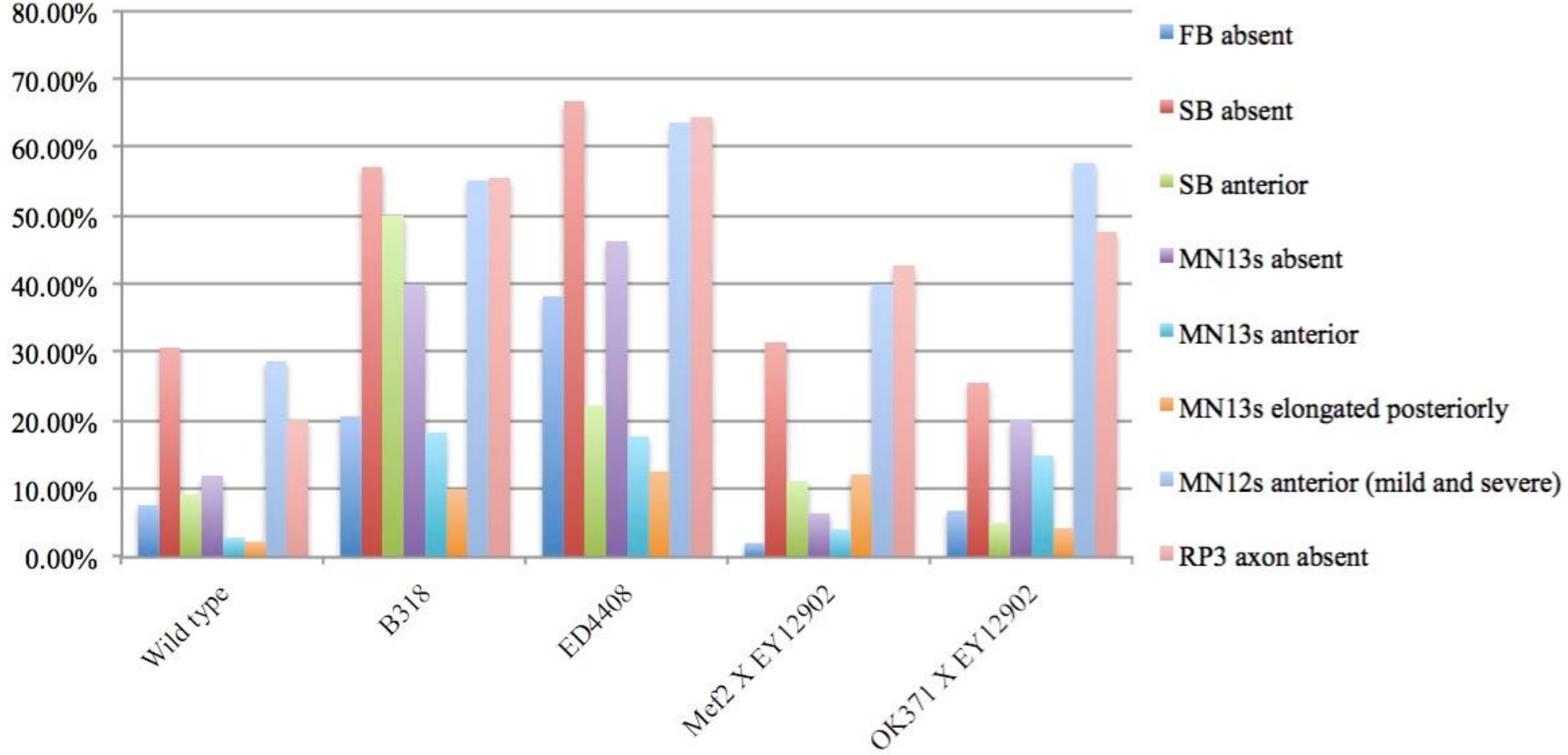

5.3. Discussion

Embryos with the *CG7565* loss-of-function alleles, *B318* and *ED4408*, displayed a range of phenotypes within the embryonic motor neurons. In both lines, the first (FB; Figures 81 & 88) and second (SB; Figures 82 & 89) branches of the ISN, and RP3 axon (Figures 87 & 93) were often absent (respectively, these projections were missing in 20.7%, 57.1%, and 55.6% of *B318* hemisegments, and 38.1%, 66.7%, and 64.5% of *ED4408* hemisegments, compared to 7.6%, 30.7%, and 20.1% of wild type hemisegments). Likewise, the MN13s were frequently missing (Figures 84 & 90) (40% of *B318* hemisegments, 46.2% of *ED4408* hemisegments, compared to 11.9% of wild type hemisegments), or projected to the anterior (Figures 85 & 91) (18.2 of *B318* hemisegments, 17.6% of *ED4408* hemisegments, compared to 2.9% of wild type hemisegments). Similarly, the MN12s had an increased tendency to project anteriorly (Figures 86 & 92) (48.3% and 6.9% of *B318* hemisegments exhibited the mild and severe phenotypes, respectively; 18.2% and 45.5% of *ED4408* hemisegments exhibited the mild and severe phenotypes, respectively, compared to 20% [mild] and 8.8% [severe] in wild types). The SB in *B318* embryos, though not *ED4408* embryos, often projected anteriorly (Figure 83) (50% of hemisegments, compared to 9.1% of wild type hemisegments).

There was some overlap between the loss-of-function phenotypes and the *OK371 X EY12902* gain-of-function phenotypes in that the MN12s and MN13s projected anteriorly (Figures 98 & 97) (46.7% and 11.1% of *OK371 X EY12902* hemisegments exhibited the MN12 mild and severe phenotypes, respectively, compared to 20% [mild] and 8.8% [severe] in wild types; the MN13s projected anteriorly in 14.9% of *OK371 X EY12902* hemisegments, compared to 2.9% of wild type hemisegments). However, with the exception of the RP3 axon (Figure 99) (47.6% of hemisegments, compared to 20.1% of wild type hemisegments), no other axons were absent. The RP3 axon was also absent in *Mef2 X EY12902* embryos (Figure 94) (42.7% of hemisegments, compared to 20.1% of wild type hemisegments), though no other axons were missing or anteriorly orientated. Conversely, the FB was absent less often than in wild types (Figure 95) (2% of hemisegments, compared to 7.6% of wild type hemisegments), and the MN13s were elongated towards the posterior (Figure 96) (12.2% of hemisegments, compared to 2.2% of wild type hemisegments).

Given the nature of the phenotypes, it is possible to speculate upon what role CG7565 might play within axon guidance. This can be approached by considering the consequences of decreasing or increasing attractive or repellent activity within axons or

within exterior tissue (e.g., muscle). Regarding the loss-of-function experiments, since axons were often absent, it seems unlikely that attractive activity within neurons or repellent activity within exterior tissue was lost, both of which would more likely result in premature branching. Thus, it is more probable that repellent activity within neurons or attractive activity within exterior tissue was lost. For example, failures to defasciculate within the ISNb are observed in *sema-1a* mutants, which are thought to reflect the loss of the protein's repellent activity within neurons (Yu et al., 1998). However, two of the phenotypes present when expression was driven in muscle provide support for CG7565 acting within an attractive pathway within muscle; namely, the increased presence of the FB and the posterior elongation of MN13s.

It is possible that the so-called absence of axons is actually a mild form of their tendency to project anteriorly. For example, in the absence of the putative attractive activity of CG7565, axons might be drawn towards the anterior or repelled from the posterior by a range of other factors; strong responses would result in anterior projections, while weaker responses would see axons immobilised amidst a symmetrical distribution of attractive and repellent activity on anterior and posterior sides. The MN12s and MN13s are anteriorly orientated in the loss-of-function embryos, though not when CG7565 expression is driven in muscle, which is consistent with CG7565 being implicated in attractive activity within muscle.

There are, however, potential limitations with the suggestion that CG7565 contributes to axons' attraction to muscles. Firstly, the MN12s and MN13s also project anteriorly when CG7565 expression is driven in motor neurons. Since CG7565's signalling partners would presumably also need to be present in motor neurons for effects to occur, the *OK371 X EY12902* anterior phenotypes suggest that CG7565 might operate within motor neurons in wild types. Therefore, it is a possibility that CG7565 influences axon guidance from within motor neurons as well as from muscles. Upregulating expression of CG7565 in motor neurons might disrupt the ratio of the proteins in the signalling pathway, resulting in loss-of-function, hence the anterior projections in these and the loss-of-function embryos. A second limitation of the model is that the muscles innervated by the ISNb (muscles 6, 7, 12, and 13) extend perpendicularly to the branch and on either side of it. Therefore, if it is assumed that the spatial distribution of cues on the surface of muscles is approximately even, it is not clear how their absence or overexpression would alter axons' preferences for anterior or posterior growth. However, guidance cues expressed within muscles have been observed to localise to specific regions (Davis et al., 1997), thus it is possible that CG7565 and its signalling

partners are distributed unevenly within the VLMs, which might result in axons being presented with contrasting levels of attractive or repellent activity on their anterior and posterior sides. Finally, the absence of the RP3 axon in *Mef2 X EY12902* embryos does not appear to be consistent with the suggestion that CG7565 contributes to attractive activity within muscle. However, utilising an exogenous promoter to drive expression of a protein results, of course, in a disruption of the specific spatiotemporal pattern of the protein's wild type distribution, the nuances of which are likely crucial to correct wiring. For instance, driving expression of Wnt4, a repellent normally expressed in muscle, with a GAL4 line (*5053A*) that drives expression in muscle, has the effect of increasing the size of synapses on muscle 13 due to a reversal of the relative levels of Wnt4 in muscles 12 and 13 (Inaki et al., 2007). Thus, it is conceivable that driving expression of an attractant within muscle might actually reduce neuromuscular innervation because of alterations to the relative levels of the cue in different muscles. Given the elongation of axons innervating muscle 13 and the absence of the RP3 axon in *Mef2 X EY12902* embryos, one possibility was that the RP3 axon was recruited to muscle 13. However, a chi-square test indicated that there was no relationship between the RP3 axon's presence/absence and the formation of the MN13s in these embryos (data not shown).

While the phenotypes might reflect a role for *CG7565* in embryonic motor axon guidance, it is also possible that they are an indirect consequence of other neurodevelopmental events. Given that CG7565 is expressed clearly in the VNC, and not in the periphery, it could be argued that the latter interpretation is likely more valid. However, without closely examining the VNC, the nature of these putative upstream events can only be speculated upon. The current study utilised an anti-FasII antibody (1D4) to visualise the motor neurons, though FasII is also expressed in the longitudinal fascicles of the VNC. Despite this, the time required for the colour reaction to render the motor neurons sufficiently bold exceeds the time required for the longitudinal fascicles to be seen clearly, thus they and their surrounding tissue become too dark and difficult to interpret. Therefore, reducing the length of the colour reaction would be necessary to effectively visualise the longitudinal fascicles, which could then be assessed for axonal aberrations that might account for the motor neuron phenotypes. Utilisation of antibodies for other VNC axon types, such as BP102, which stains commissural axons, might also help in this respect. Likewise, antibodies that mark VNC neuron cell bodies, such as anti-vestigial, might be used to provide insights into whether their migration is affected in experiments involving *CG7565*. In light of research into the gene's mouse, rat, and human orthologues, axon guidance (Masuda et al., 2009) and/or neuronal

migration (Galaburda & Kemper, 1979; Peschansky et al., 2010) abnormalities in the VNC might have occurred in the *CG7565* loss- and/or gain-of-function embryos. A single *B318* embryo and a single *ED4408* embryo exhibited clear aberrations in the VNC (Appendix C; the severity of these was such that they were evident despite the prolonged colour reaction). While these embryos were included in the above analysis of the motor neurons, excluding them did not render the frequencies of any of the motor neuron phenotypes non-significant (data not shown). Moreover, although more subtle VNC phenotypes might be revealed via the means discussed in this paragraph, it should be noted that obvious defects were not observed in the remaining 16 *B318* embryos, in the remaining five *EDD4408* embryos, nor in any of the 14 *Mef2 X EY12902* or 14 *OK371 X EY12902* embryos.

The absence of subsets of axons (i.e., the MN12s, MN13s, FB, SB, and RP3 axon) within the peripheral nerves may, nonetheless, reflect their failing to enter the periphery due to neurodevelopmental abnormalities within the CNS. However, it is less clear how upstream anomalies would contribute to an increased tendency for axons to grow anteriorly. Moreover, the presence of phenotypes within the gain-of-function embryos, in which expression was only driven in peripheral tissues, suggests that signalling partners of CG7565, and thus CG7565 itself, are normally present within the periphery (it is acknowledged, however, that CG7565's signalling partners might interact with other proteins in the periphery, thus their apparent presence in the periphery is not necessarily an indication of CG7565's presence their too). If CG7565 is expressed within the periphery, it might be at low levels and hence was not detected by *in situ* hybridization. Indeed, it is conceivable that CG7565 is expressed in the cell bodies of the motor neurons at high (detectable) levels and, through trafficking into the periphery, is present at low (undetectable) levels in axons. The anterior projections in loss-of-function embryos and the presence of phenotypes of any kind within gain-of-function embryos, therefore, lend support to the idea that CG7565 is directly implicated in embryonic motor axon guidance. However, studies based on hKIAA0319 suggest that the protein exists in multiple forms (Valeyos-Baeza et al., 2007; Valeyos-Baeza et al., 2010); if this is true for CG7565, it is likely that it is implicated in multiple functions, and so the phenotypes observed in the current study might reflect alterations to a range of processes.

For future work, given that CG7565 is strongly expressed in the CNS (Figure 78) and in light of the phenotypes reported for its orthologues (Galaburda & Kemper, 1979; Masuda et al., 2009; Peschansky et al., 2001), it would be interesting to analyse the

VNC for axon guidance- and neuronal migration-based abnormalities by adjusting the colour reaction time and utilising additional antibodies (e.g., BP102, anti-vestigial). Since Slit is the *Drosophila* protein that most closely resembles NgR1 (Klinger et al., 2003), to which hKIAA0319L binds (Poon et al., 2011), it is conceivable that *CG7565* mutants would exhibit *slit*-like phenotypes (see, e.g., Kidd et al., 1999). Indeed, the longitudinal fascicles of the VNC collapse onto the midline in one of the *ED4408* embryos (Appendix C). Although obvious defects were observed in the VNC in only one of the six *ED4408* embryos that were examined, if such abnormalities were found to be a relatively frequent occurrence in embryos with altered *CG7565* activity, it would be worth looking at whether similar phenotypes are present in embryos that are transheterozygous for *CG7565* and *slit* to assess whether they interact genetically. If so, Co-IP experiments, for example, might provide insights into whether CG7565 physically interacts with Slit or other members of the Robo signalling pathway. Since *CG7565*'s human orthologues, *hkiaa0319* and *hkiaa0319l*, and *ROBO1* have been linked to reading disability (Couto et al., 2008; Darki et al., 2012; Hannula-Jouppi et al., 2005; Mascheretti et al., 2014), understanding more about the pathways in which CG7565 participates might provide insights into the molecular and cellular events that underlie DD. Developing a complete picture of CG7565's function will be facilitated by determining the number and nature of the protein's splice variants and cleaved forms through, for instance, reverse transcription PCR (RT-PCR) and western blots, as described by Valeyos-Baeza and colleagues (2007, 2010) for hKIAA0319.

Chapter 6: *CG31814*

6.1. Introduction

Vogel and colleagues (2003) suggest that CG31814 is a transmembrane protein that is characterised by an extracellular region comprised of immunoglobulin (Ig) domains and a cytoplasmic region that lacks kinase or phosphatase activity. Their analyses indicate that it is related to a number of other uncharacterised members of the Ig superfamily (IgSF), namely CG14014, CG14521, CG11320, CG31708, CG4814, CG31646, and CG13020 (also known as and henceforth referred to as CG32791), all of which, excluding CG14014, are members of the DIP family of proteins that also includes CG40378 (also know as CG45781), CG14010, CG42343, CG34391, and CG31814 (Ozkan et al., 2013; discussed further below). With the exception of one report that suggests that CG31708 and CG32791 are implicated in synapse formation (Kurusu et al., 2008; discussed further below), there is no experimental evidence pertaining to the molecular functions of the proteins in this specific cluster, nor regarding the biological processes in which they participate. Many members of the wider IgSF have, however, been linked to axon guidance, including Down syndrome cell adhesion molecule 1 (Dscam1) (Hummel et al., 2003; Sawaya et al., 2008; Schmucker et al., 2000; Shi et al., 2007; Wang et al., 2002; Wojtowicz et al., 2004), Sidestep (Side) (Meyer et al., 2006; Siebert et al., 2009; Sink et al., 2001), Fasciclin 3 (Fas III) (Suzuki et al., 2000), Neuromusculin (Nrm) (Kurusu et al., 2008), Off-track (Otk) (Cafferty et al., 2004; Winberg et al., 2001), Protein tyrosine phosphatase 69D (Ptp69D) (Desai et al., 1996; Jeon et al., 2008; Sun et al., 2001), Beaten path Ia (Beat-Ia) (Fambrough & Goodman, 1996; Zarin et al., 2014), and Beat-IIIc (Inaki et al., 2007). Alsbury and colleagues (in preparation) suggest that CG31814 belongs to a four-member family of Ig proteins that includes CG31708, CG4814, and CG32791 (Figure 101). Their *in situ* data indicate that *CG31814* is expressed in the CNS from embryonic stage 14–16, thus towards the end of embryonic axonal development (Figure 102).

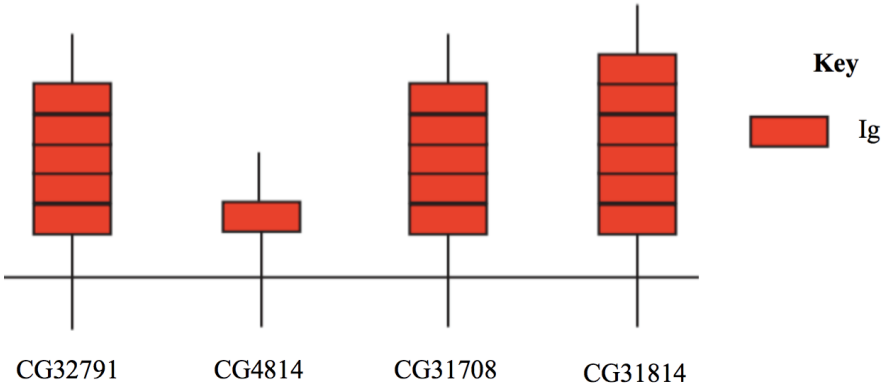

Figure 101. **The extracellular domains of CG31814 and its paralogues** (modified from Alsbury et al., in preparation). The extracellular domains of CG31814 and its paralogues are constituted entirely of Ig domains.

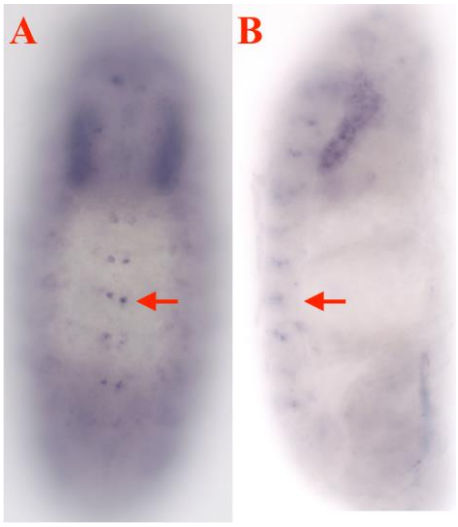

Figure 102. **Expression of *CG31814* revealed by *in situ* hybridisation** (modified from Alsbury et al., in preparation). **A.** A ventral view of a stage 15 embryo (up is anterior) with expression evident in the VNC (red arrow). **B.** A lateral view of a stage 16 embryo (up is anterior, left is ventral) with expression evident in the VNC (red arrow).

Kurusu and colleagues (2008) identified 410 *Drosophila* genes (including *CG31814*), predicted to encode cell-surface and secreted (CSS) proteins. They obtained fly lines with EP-like transposable elements located at the 5' end of each of these genes. EP-like elements contain UAS sequences and, therefore, can be used in gain-of-function studies using the GAL4-UAS system (Brand & Perrimon, 1993). Each line was crossed to a pan-muscle driver, *24B-GAL4*, which drives expression from stage 11 to the end of embryonic development (Luo et al., 1994). First instar larvae were examined for axonal mistargeting or abnormal neuromuscular junction (NMJ) arbors within the ISNb. Abnormalities were observed for 16 of the 410 genes. Two of these, *CG31708* and *CG32791*, were previously identified by Alsbury and colleagues (in preparation) as constituting half of the aforementioned four-member family of uncharacterised Ig

proteins that includes CG31814. Kurusu and colleagues observed abnormal motor neuron synapse formation in larvae ectopically expressing CG31708 and CG32791. Whilst *CG31814* was not one of the 16 identified by Kurusu and colleagues, it is quite possible that, by focusing exclusively on the ISNb, abnormalities in other branches were overlooked.

Ozkan and colleagues (2013) developed an Extracellular Interactome Assay (ECIA), which they applied to the majority of IgSF, fibronectin (FN) III, and leucine rich repeat (LRR) families of the *Drosophila* extracellular proteome (including CG31814). IgSF and LRR families have been shown to be important for neurodevelopmental processes, including axon guidance (Hong et al., 2009; Kurusu et al., 2008; Yamagata, Sanes, & Weiner, 2003) The ECIA involved expressing 'bait' proteins in *Drosophila* cell cultures and assessing whether these would bind alkaline phosphatase conjugated 'prey' proteins. They identified a group of proteins (including paralogues of CG31814: CG32791 and CG31708 [Alsbury et al., in preparation; Vogel et al., 2003]) that selectively associated with those belonging to the IgSF subfamily of Defective in Proboscis Extension Response (Dpr) proteins, which they named the DIPs (Dpr Interacting Proteins). The Dpr family is comprised of 20 members (Nakamura et al., 2002), though little is known about most; phenotypes have only been reported for *dpr1* (behavioural responses to salt; Kong et al., 2010), *dpr3* (store-operated calcium entry; Vig et al., 2006), *dpr9* (behavioural responses to ethanol; Nakamura et al., 2002), and *dpr12* (synaptic target recognition; Kurusu et al., 2008). The majority of Dprs consist of two Ig domains and single transmembrane domains, while the 11-member DIP family is constituted of proteins with three Ig domains and single transmembrane domains (Leahy, 2013). Both Dprs and DIPs are localised to the CNS or the root of the ISN (Ozkan et al., 2013). Although Ozkan and colleagues do not provide evidence of CG31814 interacting with Dprs, they put it forward as a putative DIP based on its sequence similarity to other DIPs. Also, they report that several Dprs were expressed at low levels, which might have compromised whether their signalling partners (potentially including CG31814) could be detected. Indeed, in one of a number of control experiments, which together revealed a false-negative rate of ~50%, they did not detect interactions between Robo and Slit, which constitute two components of a long-established axon guidance complex (Kidd, Bland, & Goodman, 1999). It is therefore conceivable that CG31814 is a DIP protein, some members of which appear to be involved in synaptic development within the musculature of *Drosophila* embryos (Kurusu et al., 2008).

Besides the CG31814 protein likely being of development significance, an intron of *CG31814* is thought to contain an insulator element that is bound by the transcriptional regulator, Suppressor of Hairy-Wing (Su [Hw]; Adryan et al., 2007). Mutations to Su(Hw) binding sites entail widespread alterations to gene expression. Whilst the transposon of the *KG04227* line, which is in the 5' UTR, should not directly affect the insulator element, if it influences the conformational structure of the DNA in the region of *CG31814*, it is conceivable that this might affect the expression of genes other than *CG31814*. An uncharacterised gene, *CG7311*, occupies an intron of *CG31814* and is, therefore, particularly susceptible to disruption in experiments involving *CG31814*.

Various factors therefore suggest that *CG31814* may be involved in nervous system development. These include its being localised to the cellular membrane (Alsbury et al., in preparation; Vogel et al., 2003), its expression within the nervous system (Figure 102), and its relationship to proteins involved in synapse formation in peripheral motor neurons (Alsbury et al., in preparation; Kurusu et al., 2008). Given these observations, *KG04227* embryos, which harbour a *P*-element in the 5' UTR of *CG31814*, were inspected for abnormalities in the formation of peripheral motor neurons. Moreover, a precise excision line, *KG04227*2*, was analysed to assess whether the removal of the transposon would restore wild type phenotypes.

6.2. Results

6.2.1. *KG04227*

To investigate *CG31814*'s role in embryonic motor axon guidance, *CG31814*, $y^{1}w^{67c23}$*; P{SUPor-P)CG31814*^{KG04227}*/CyOwg* (referred to as *KG04227*) embryos were firstly examined. It was assumed that the presence of the *P*-element in *CG31814*'s 5'UTR would disrupt expression (it was not known, however, whether its presence would result in an up- or down-regulation of expression).

6.2.1.1. PCR and gel electrophoresis

To provide support for the putative position of the transposon in the *KG04227* line, primers (referred to as "KG04227," Appendix B) were designed to bind DNA either side of the transposon, producing a 170 bp product. Both primers bind within the 5' UTR. *KG* line flies harbour suppressor-*P* element (P{SUPor-P}) transposons, which are reported to span 11,467 bp (Roseman et al., 1995). Consequently, it was assumed that the transposon would prevent amplification of DNA when using the KG04227 primers, especially given the short (30 s) elongation phases used during PCR. This was

supported by the presence and absence of bands from DNA of wild type and homozygous *KG04227* flies, respectively (Figure 103).

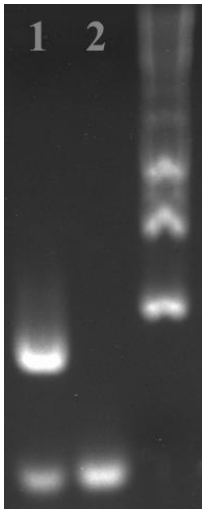

Figure 103. **Gel image of *KG04227* and wild type DNA amplified with KG04227 primers.** Lane 1 shows a band derived from wild type DNA. It is located below the bottom band of the 1 kb ladder (right), which corresponds to DNA of 250 bp, which is consistent with the expected product size of 170 bp. There is, however, no band in lane 2 (*KG04227* DNA), which is thought to reflect the transposon inhibiting the PCR reaction. The absence of a band, therefore, provides support for the reported position of the transposon within the 5' UTR of *CG31814*.

6.2.1.2. Phenotypic analysis: *KG04227*

An inspection of the motor neurons of *KG04227* embryos revealed that they often lacked the first branch of the ISN (FB; Figure 105) or the second branch of the ISN (SB; Figure 106), and that, when present, the SB projected anteriorly (Figure 107). The full length of a wild type segment, with the branches that are abnormal in *KG04227* embryos indicated, is shown in Figure 104 for reference. Table 1 (p.172) shows the penetrance of phenotypes in *KG04227* embryos, as well as their frequency in all other genotypes analysed in this chapter.

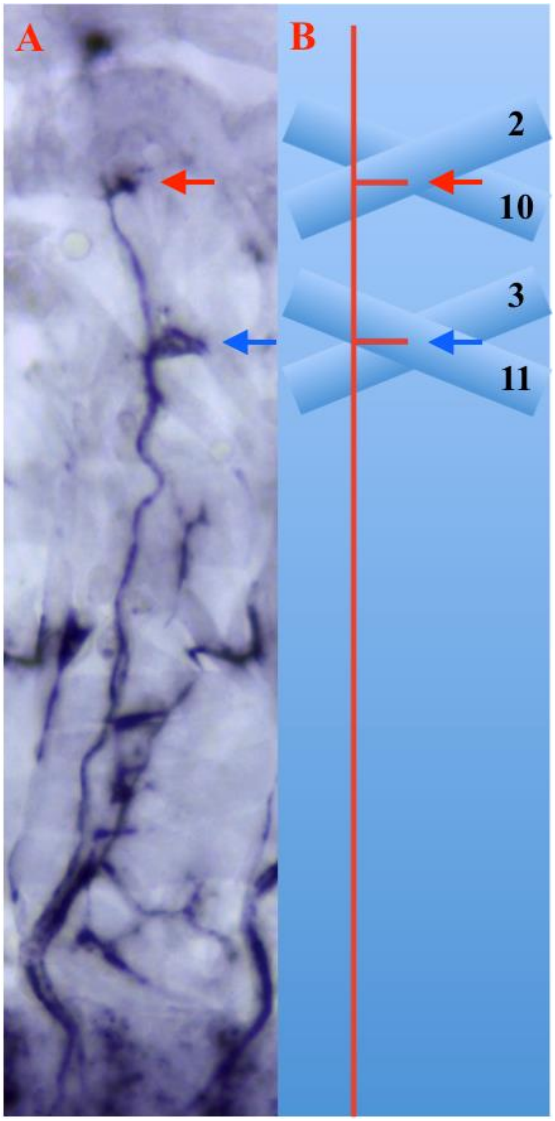

Figure 104. **A wild type ISN with the first (FB) and second (SB) branches of the ISN indicated. A.** Wild type hemisegment showing the motor neurons (right is posterior, up is dorsal). The branches that are altered in experiments involving *KG04227* are indicated: SB (red arrow), FB (blue arrow). **B.** Schematic of a wild type hemisegment showing the ISN. The branches that are altered in experiments involving *KG04227* are indicated: SB (red arrow), FB (blue arrow). The muscles in the regions of the FB and SB are indicated by numbers (other branches and muscles are not shown).

FB absent

The FB was absent more often in *KG04227* hemisegments (29%) than in wild types (7.6%) (Figure 105).

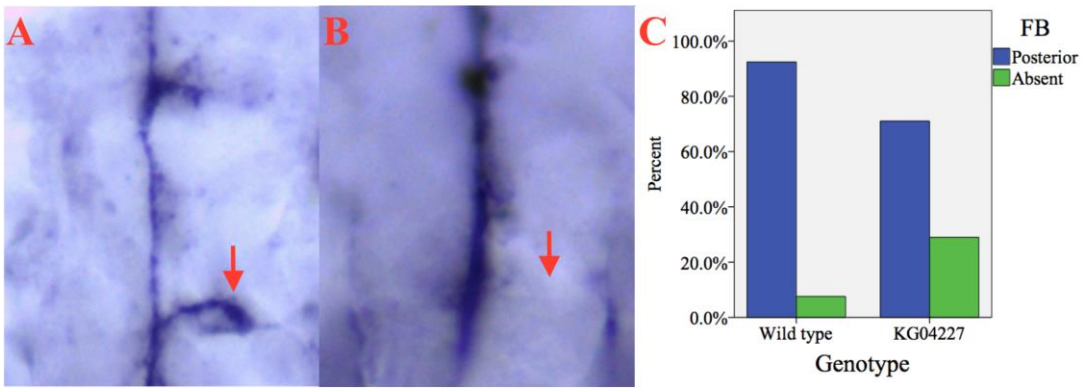

D	FB posterior	FB absent
Wild type	92.4% (195)	7.6% (16)
KG04227	71% (49)	29% (20)

Figure 105. Image A (right is posterior, up is dorsal) shows a dorsal section of a wild type hemisegment with the FB indicated (red arrow). Image B (right is posterior, up is dorsal) shows a dorsal section of a *KG04227* hemisegment without the FB (red arrow). The graph (C) shows the percentage of hemisegments in which the FB projects posteriorly or is absent in 30 wild type and 10 *KG04227* embryos. The table (D) shows the number of hemisegments in which the FB projects posteriorly or is absent in the same embryos.

A chi-square test for independence revealed that the FB was absent significantly more often in *KG04227* hemisegments than in wild types, χ^2 (1, n = 280) = 21.26, p < .001.

SB absent

The SB was also absent more often in *KG04227* hemisegments (66.7%) than in wild types (30.7%) (Figure 106).

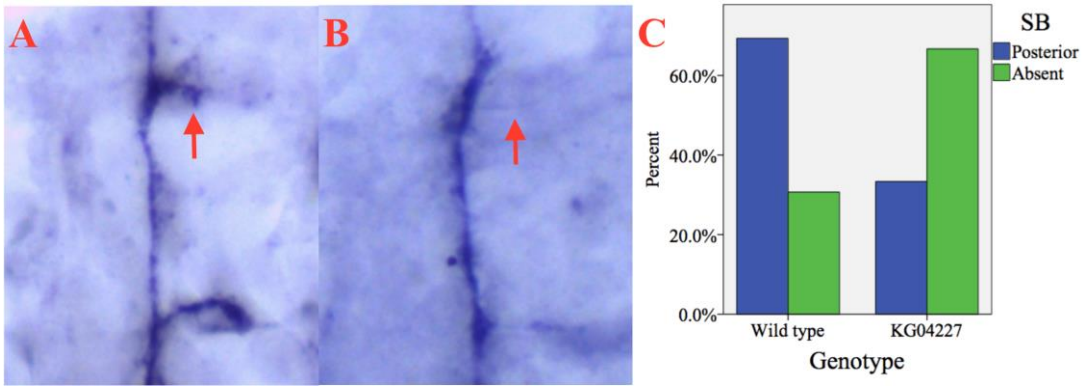

D	SB posterior	SB absent
Wild type	69.3% (70)	30.7% (31)
KG04227	33.3% (13)	66.7% (26)

Figure 106. Image A (right is posterior, up is dorsal) shows a dorsal section of a wild type hemisegment with the SB indicated (red arrow). Image B (right is posterior, up is dorsal) shows a dorsal section of a *KG04227* hemisegment without the SB (red arrow). The graph (C) shows the percentage of hemisegments in which the SB projects posteriorly or is absent in 30 wild type and 10 *KG04227* embryos. The table (D) shows the number of hemisegments in which the SB projects posteriorly or is absent in the same embryos.

A chi-square test for independence revealed that the SB was absent significantly more often in *KG04227* hemisegments than in wild types, χ^2 (1, n = 140) = 15.08, p < .001.

SB anterior

When present, the SB projected anteriorly more often in *KG04227* hemisegments (62.9%) than in wild types (9.1%) (Figure 107).

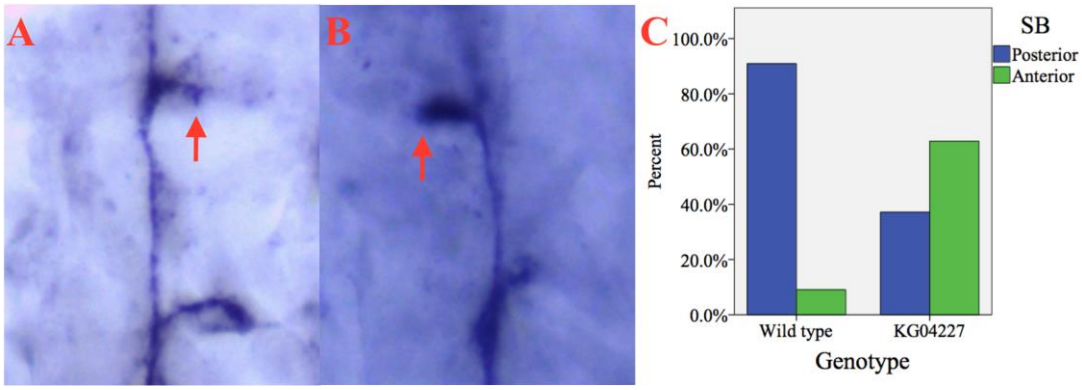

D	SB posterior	SB anterior
Wild type	90.9% (70)	9.1% (7)
KG04227	37.1% (13)	62.9% (22)

Figure 107. Image A (right is posterior, up is dorsal) shows a dorsal section of a wild type hemisegment with the SB projecting posteriorly (red arrow). Image B (right is posterior, up is dorsal) shows a dorsal section of a *KG04227* hemisegment with the SB projecting anteriorly (red arrow). The graph (C) shows the percentage of hemisegments in which the SB projects posteriorly or anteriorly in 30 wild type and 10 *KG04227* embryos. The table (D) shows the number of hemisegments in which the SB projects posteriorly or anteriorly in the same embryos.

A chi-squared for independence revealed that the SB projected anteriorly significantly more often in *KG04227* hemisegments than in wild types, χ^2 (1, n = 112) = 36.25, p < .001.

6.2.2. KG04227*2

6.2.2.1. PCR and sequencing

To provide support for the supposition that the transposon in the 5' UTR of *CG31814* in the *KG04227* embryos was responsible for the phenotypes reported immediately above, embryos of a line, referred to as *KG04427*2*, in which in the transposon had been precisely excised, were examined. The transposon was excised via the following crossing scheme:

♂♂ y^1w^{67c23}; P{SUPorP}CG31814^{KG04227}/CyO; +/+ X ♀♀ w; Sp/CyO; Sb, Δ 2-3/TM6b, Δ 2-3

↓

♂ y^1w^1; P{SUPorP}CG31814^{KG04227}/CyO; Sb, Δ 2-3/+ X ♀♀ w; Sco/CyOwg; +/+

↓

♂ y^1w^1; P{SUPorP}CG31814^{KG04227}/CyOwg; +/+ X ♀♀ w; Sco/CyOwg; +/+

↓

♂♂ y^1w^1; P{SUPorP}CG31814^{KG04227}/Cyowg; +/+ X ♀♀ y^1w^1;P{SUPorP}CG31814^{KG04227}/Cyowg; +/+

The KG04227 primers, which bind either side of the position of the excised element, were applied to *KG04227*2* DNA. It was assumed that the removal of the element would enable the PCR to work. This was supported by the presence of a band derived from the application of the KG04227 primers to *KG04227*2* DNA (not shown). PCRs derived from the application of the KG04227 primers to *KG04227*2* DNA were sent for sequencing to assess whether the excision of the element in *KG04227*2* flies had been precise (i.e., resulting in a restoration of the wild type sequence). The electropherogram (not shown) was inspected for sample quality; only a region of 139 bp, in which each nucleotide had a Eurofins quality score of >=30 (indicating at least 99.9% accuracy of base call), was used for comparisons. The derived sequence was entered into the National Centre for Biotechnology Information's (NCBI) Basic Local Alignment Search Tool (BLAST), which aligned the *KG04227*2* DNA to the wild type 5' UTR of *CG31814*. A comparison of the sequences indicated that, while two non-adjacent nucleotides differed, there were no alterations or deletions adjacent to where the insertion had been, nor were there remnants of the insertion, suggesting that the excision was precise (Figure 108).

```
KG04227*2  TCCTGGCCGCTGTCGTTGGTCCTGCCGCTGTCATTTGCCGGATTTTGGCAGACCTCGCCA
           ||||*|||||||||||||||||||||||||||||||||||||||||||||||||||||||
Wild type  TCCTTGCCGCTGTCGTTGGTCCTGCCGCTGTCATTTGCCGGATTTTGGCAGACCTCGCCA
                                  ↑
KG04227*2  AAGTTGTGAGCGAGTGAAAGTTTTTTGTGCATTTGTCCTGCGGTGCGACTTCGGTTTACC
           ||||||||||||||||||||||||||||||||||||||*|||||||||||||||||||||
Wild type  AAGTTGTGAGCGAGTGAAAGTTTTTTGTGCATTTGTCGTGCGGTGCGACTTCGGTTTACC

KG04227*2  ATTACTCTTGCATTCGCAA
           ||||||||||||||||||
Wild type  ATTACTCTTGCATTCGCAA
```

Figure 108. **Blast result for *KG04227*2* and wild type DNA**. *KG04227*2* DNA, amplified with KG04227 primers, aligns to the wild type 5' UTR of *CG31814*. While two non-adjacent nucleotides (asterisks) differed between the *KG04227*2* and wild type sequences (most likely representing natural variation), there were no alterations or deletions adjacent to where the insertion had been (arrow), suggesting that the excision was precise.

6.2.2.2. Phenotypic analysis: *KG02227*2* vs. *KG04227*

Embryos of the precise excision line, *KG04227*2*, were compared to *KG04227* embryos. The first (FB) and second (SB) branches of the ISN were absent less frequently in *KG04227*2* embryos relative to *KG04227* embryos (Figures 109 and 110). However, there was little difference in the frequency of SB anterior projections between *KG04227*2* and *KG04227* embryos (Figure 111).

FB absent

The FB was absent less often in *KG04227*2* hemisegments (12.5%) than in *KG04227* hemisegments (29%) (Figure 109).

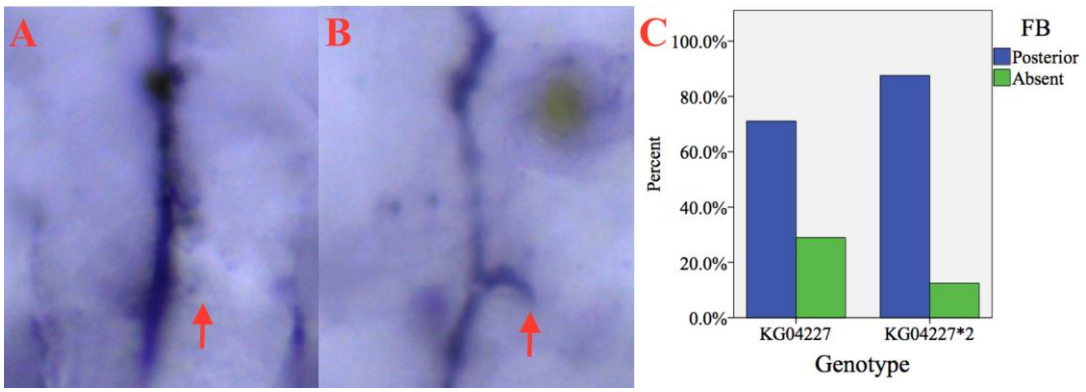

D	FB posterior	FB absent
KG04227	71% (49)	29% (20)
*KG04227*2*	87.5% (63)	12.5% (9)

Figure 109. Image A (right is posterior, up is dorsal) shows a dorsal section of a *KG04227* hemisegment without the FB (red arrow). Image B (right is posterior, up is dorsal) shows a dorsal section of a *KG04227*2* hemisegment with the FB (red arrow). The graph (C) shows the percentage of hemisegments in which the FB projects posteriorly or is absent in 6 *KG04227*2* and 10 *KG04227* embryos. The table (D) shows the number of hemisegments in which the FB projects posteriorly or is absent in the same embryos.

A chi-square test for independence revealed that the FB was absent significantly less often in *KG04227*2* hemisegments than in *KG04227* hemisegments, χ^2 (1, n = 141) = 5.86, $p < .05$.

SB absent

The SB was also absent less often in *KG04227*2* hemisegments (41.9%) than in *KG04227* hemisegments (66.7%) (Figure 110).

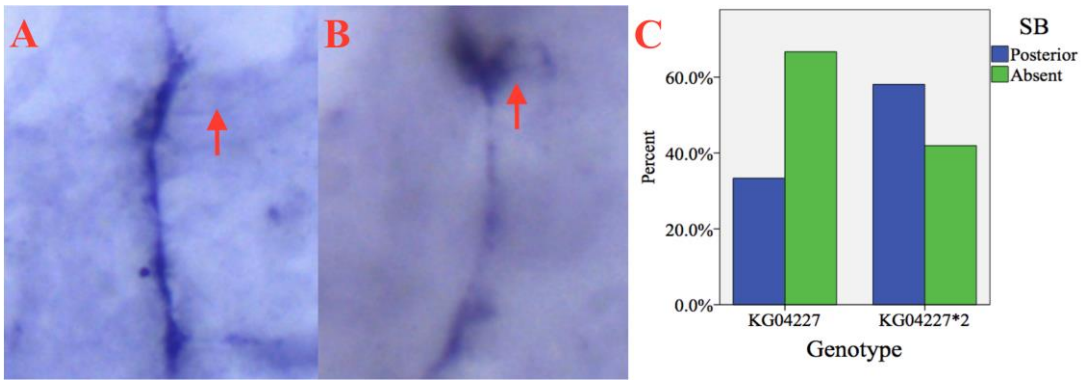

D	SB posterior	SB absent
KG04227	33.3% (13)	66.7% (26)
*KG04227*2*	58.1% (18)	41.9% (13)

Figure 110. Image A (right is posterior, up is dorsal) shows a dorsal section of a *KG04227* hemisegment without the SB (red arrow). Image B (right is posterior, up is dorsal) shows a dorsal section of a *KG04227*2* hemisegment with the SB (red arrow). The graph (C) shows the percentage of hemisegments in which the SB projects posteriorly or is absent in 6 *KG04227*2* and 10 *KG04227* embryos. The table (D) shows the number of hemisegments in which the SB projects posteriorly or is absent in the same embryos.

A chi-square test for independence revealed that the SB was absent significantly less often in *KG04227*2* hemisegments than in *KG04227* hemisegments, χ^2 (1, n = 70) = 4.28, $p < .05$.

SB anterior

There was little difference in the frequency of the SB anterior phenotype between *KG04227*2* (65.4%) and *KG04227* (62.9%) hemisegments (Figure 111).

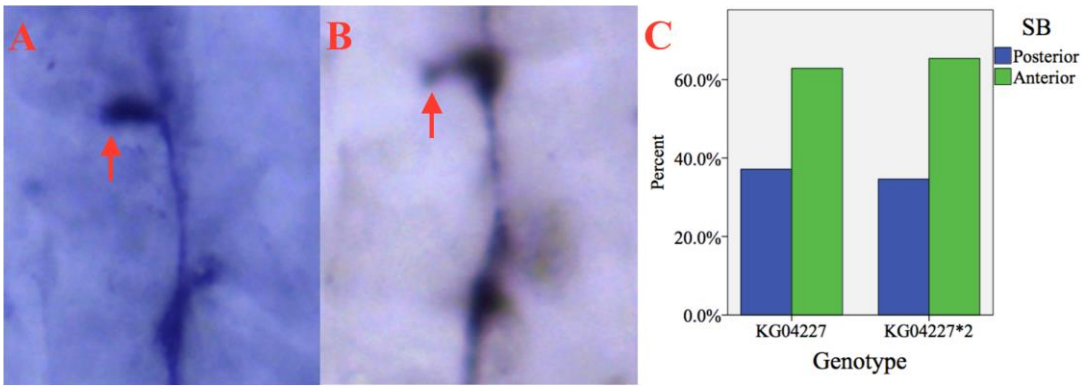

D	SB posterior	SB anterior
KG04227	37.1% (13)	62.9% (22)
*KG04227*2*	34.6% (18)	65.4% (34)

Figure 111. Image A (right is posterior, up is dorsal) shows a dorsal section of a *KG04227* hemisegment with the SB projecting anteriorly (red arrow). Image B (right is posterior, up is dorsal) shows a dorsal section of a *KG04227*2* hemisegment with the SB projecting anteriorly (red arrow). The graph (C) shows the percentage of hemisegments in which the SB projects posteriorly or anteriorly in 6 *KG04227*2* and 10 *KG04227* embryos. The table (D) shows the number of hemisegments in which the SB projects posteriorly or anteriorly in the same embryos.

A chi-square test for independence did not reveal a significant effect of genotype with regard to the frequency of the SB anterior phenotype in *KG04227*2* and *KG04227* hemisegments, χ^2 (1, n = 87) = 0.06, p > .05.

6.2.2.3. Phenotypic analysis: *KG02227*2* vs. wild type

Having established that the first (FB) and second (SB) branches of the ISN were absent less frequently in *KG044227*2* embryos than in *KG04227* embryos (Figures 109 and 110, respectively), but that there was little difference between the genotypes with regard to the SB anterior phenotype (Figure 111), comparisons were made between *KG04227*2* and wild type embryos. The FB and SB were present in *KG04227*2* embryos at frequencies resembling wild types (Figures 112 and 113, respectively). However, the SB projected anteriorly more often in *KG04227*2* embryos compared to wild types (Figure 114).

FB absent

There was little difference in the frequency of the FB absent phenotype between *KG04227*2* (12.5%) and wild type (7.6%) hemisegments (Figure 112).

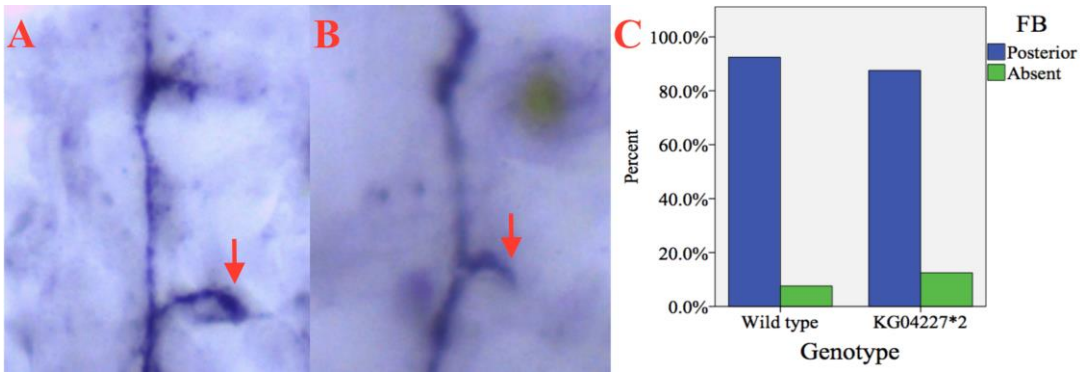

D	FB posterior	FB absent
Wild type	92.4% (195)	7.6% (16)
*KG04227*2*	87.5% (63)	12.5% (9)

Figure 112. Image A (right is posterior, up is dorsal) shows a dorsal section of a wild type hemisegment with the FB indicated (red arrow). Image B (right is posterior, up is dorsal) shows a dorsal section of a *KG04227*2* hemisegment with the FB indicated (red arrow). The graph (C) shows the percentage of hemisegments in which the FB projects posteriorly or is absent in 30 wild type and 6 *KG04227*2* embryos. The table (D) shows the number of hemisegments in which the FB projects posteriorly or is absent in the same embryos.

A chi-square test for independence did not reveal a significant effect of genotype with regard to the frequency of the FB absent phenotype in *KG04227*2* and wild type hemisegments, χ^2 (1, n = 283) = 1.61, p > .05.

SB absent

Likewise, there was little difference in the frequency of the SB absent phenotype between *KG04227*2* (41.9%) and wild type (30.7%) hemisegments (Figure 113).

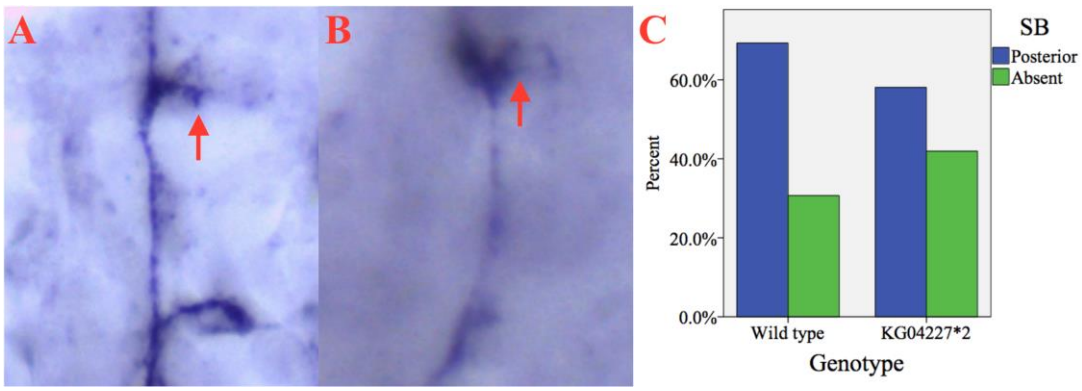

D	SB posterior	SB absent
Wild type	69.3% (70)	30.7% (31)
*KG04227*2*	58.1% (18)	41.9% (13)

Figure 113. Image A (right is posterior, up is dorsal) shows a dorsal section of a wild type hemisegment with the SB indicated (red arrow). Image B (right is posterior, up is dorsal) shows a dorsal section of a *KG04227*2* hemisegment with the SB indicated (red arrow). The graph (C) shows the percentage of hemisegments in which the SB projects posteriorly or is absent in 30 wild type and 6 *KG04227*2* embryos. The table (D) shows the number of hemisegments in which the SB projects posteriorly or is absent in the same embryos.

A chi-square test for independence did not reveal a significant effect of genotype with regard to the frequency of the SB absent phenotype in *KG04227*2* and wild type hemisegments, χ^2 (1, n = 132) = 1.35, $p > .05$.

SB anterior

The SB projected anteriorly more often in *KG04227*2* hemisegments (65.4%) than in wild types (9.1%) (Figure 114).

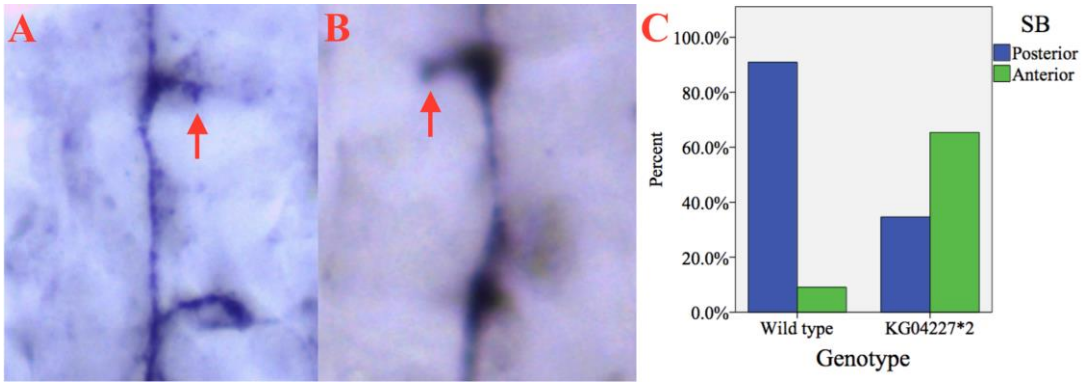

D	SB posterior	SB anterior
Wild type	90.9% (70)	9.1% (7)
*KG04227*2*	34.6% (18)	65.4% (34)

Figure 114. Image A (right is posterior, up is dorsal) shows a dorsal section of a wild type hemisegment with the SB projecting posteriorly (red arrow). Image B (right is posterior, up is dorsal) shows a dorsal section of a *KG04227*2* hemisegment with the SB projecting anteriorly (red arrow). The graph (C) shows the percentage of hemisegments in which the SB projects posteriorly or anteriorly in 30 wild type and 6 *KG04227*2* embryos. The table (D) shows the number of hemisegments in which the SB projects posteriorly or anteriorly in the same embryos.

A chi-squared for independence revealed that the SB projected anteriorly significantly more often in *KG04227*2* hemisegments than in wild types, χ^2 (1, n = 129) = 45.37, p < .001.

Table 1. Summary of the phenotypic analysis of Chapter 6.

	FB absent	SB absent	SB anterior
Wild type	7.6%	30.7%	9.1%
KG04227	**29%***	**66.7%***	**62.9%***
*KG04227*2*	12.5%	41.9%	**65.4%***

*p<.05 (also in bold).

6.3. Discussion

CG31814 is an uncharacterised transmembrane protein of the IgSF (Vogel et al., 2003), many members of which have been linked to axon guidance (Cafferty et al., 2004; Desai et al., 1996; Fambrough & Goodman, 1996; Hummel et al., 2003; Inaki et al., 2007; Jeon et al., 2008; Kurusu et al., 2008; Meyer et al., 2006; Sawaya et al., 2008; Schmucker et al., 2000; Shi et al., 2007; Siebert et al., 2009; Sink et al., 2001; Sun et al., 2001; Suzuki et al., 2000; Wang et al., 2002; Winberg et al., 2001; Wojtowicz et al., 2004; Zarin et al., 2014; Zhan et al., 2004). In light of this, and given that CG31814 is expressed in the embryonic nervous system (Figure 102) and that closely related proteins, namely CG31708 and CG32791 (Alsbury et al., in prepartion; Vogel et al., 2003), have been associated with embryonic motor axon guidance (Kurusu et al., 2008), the current study investigated whether a population with a transposon in the 5'UTR of CG31814 (*KG04427*) would exhibit abnormal embryonic motor axon guidance phenotypes.

The analyses indicated that the first (FB) and second (SB) branches of the ISN were absent in a significant number of *KG04227* hemisegments relative to wild types (Figures 105 and 106; respectively, they were absent in 29% and 66.7% of *KG04227* embryos, compared to 7.6% and 30.7% of wild type hemisegments), and that the SB aberrantly projected to the anterior (rather than the posterior) in a significant number of hemisegments (Figure 107; 62.9% of *KG04227* hemisegments, compared to 9.1% of wild type hemisegments). In line with Kurusu and colleagues (2008), who drove expression of *CG31814* with a pan-muscle driver, aberrations were not detected in the ISNb. In the precise excision population, *KG04227*2*, penetrance of the FB and SB absent phenotypes did not differ significantly from penetrance in wild types (Figures 112 and 113). Respectively, the FB and SB were absent in 12.5% and 41.9% of *KG04227*2* hemisegments, compared to 7.6% and 30.7% of wild type hemisegments. However, the excision failed to rescue the anterior projection of the SB (Figure 114; 65.4% of *KG04227*2* hemisegments, compared to 9.1% of wild type hemisegments). These data suggest that disrupting *CG31814* results in the FB and SB failing to form, but they do not constitute clear evidence of the gene's influence on SB anterior growth.

Determining how CG31814 might exert its effect on the FB and SB is challenging because it was not known whether the 5' UTR insertion in the *KG04227* line would up- or down-regulate the expression of the gene. For example, the insertion could have disrupted a silencer, which might result in increased expression. Conversely, it could have disrupted a promoter, which might result in decreased expression. If it is assumed

that the protein is either implicated in attracting or repelling axons, and that it is either expressed in axons or muscles, eight models are possible based on these three variables (up- or down-regulation, attraction or repulsion, expression in axons or muscles). There are clear reasons why half of these models seem to be incompatible with what was observed. For instance, if CG31814 is implicated in attraction, is expressed in axons, and is down-regulated in the *KG04227* line, it might be expected that the axons of the ISN would defasciculate prematurely rather than not at all, which is inconsistent with the observed absence of the FB and SB. Conversely, if CG31814 is implicated in attraction, is expressed in muscles, and is down-regulated in the *KG04227* line, it might be expected that axons of the ISN would fail to defasciculate because they would not be attracted to the muscle field, which is consistent with the observed FB and SB absent phenotypes. Similar logic, however, can be applied to make the case for the following three models: (1) down-regulation of an axonally expressed repellent; (2) up-regulation of a repellent expressed in muscle; or (3) up-regulation of an axonally expressed attractant. Thus, even when using a simplistic framework, there are multiple conceivable ways in which CG31814 might affect axon guidance.

Moreover, these models are based on various questionable assumptions. Firstly, they assume that hemisegments are self-contained, though axons might be influenced by signals in neighbouring hemisegments. Secondly, they assume that proteins are either implicated in attraction or repulsion, though this is known to depend upon which receptors axons express. For example, *C. elegans* UNC-40 and UNC-5 receptors respectively underlie attractive and repulsive responses to Netrin (Ackerman et al., 1997; Keino-Masu et al., 1996). Thirdly, they assume that proteins are either expressed in axons or muscles, though they might be expressed in both or in other cell types. For example, the growth cones of the ISN make contact with persistent Twist (PT) cells, which are precursors of adult muscles (Bate et al., 1991), and tracheae (Desai et al., 1997; Hall & Bieber, 1997; Younossi-Hartenstein & Hartenstein, 1993). Fourthly, they assume that proteins are expressed in all axons and muscles, though they might only be expressed in subsets; distinct muscles are innervated by the FB and SB (3 and 2, respectively) (Desai et al., 1997). Also, the models do not take into account other proteins that participate in the formation of the FB and/or SB, such as Sema-1a (Yu et al., 1998), Leukocyte-antigen-related-like (Dlar) and Protein tyrosine phosphatase 69D (Ptp69D; Desai et al., 1997), NetA and NetB (Mitchell et al., 1996), Frazzled (Fra; Kolodziej et al., 1996), Sidestep (Side; Sink et al., 2001), Tolloid-related (Tlr; Serpe & O'Connor, 2006), Ptp10D, Ptp4E, and Ptp52F (Jeon et al., 2008), Unc-5 (Labrador et al., 2005) and Neuroglian (Nrg; Hall & Bieber, 1997). Lastly, the models assume that

the abnormal *KG04227* phenotypes reflect local mechanisms. However, since there is only clear evidence of CG31814 expression in the CNS, and not in the PNS (Figure 102), it is possible that the aberrations are an indirect consequence of upstream effects (e.g., axon guidance or neuronal migration defects in the VNC). Nonetheless, considering how CG31814 functions in terms of just three variables allows for the generation of models that can be tested in light of future research that should be based on fly lines that unequivocally represent gain- or loss-of-function.

Given the clear expression of *CG31814* in the CNS and the peripheral axonal phenotypes observed here, future investigations should determine whether axons grow aberrantly in the VNC. The anti-FasII antibody utilised in the current study produces a stronger signal in the VNC than in the periphery, thus embryos with sufficiently bold staining in the periphery present with excessively bold staining of the longitudinal fascicles. It was therefore not ideal to look at the PNS and VNC simultaneously, and reducing the duration of the colour reaction would be required to effectively visualise the VNC. Utilisation of additional antibodies, such as BP102, which allows for visualisation of commissural axons, would allow for a more comprehensive analysis of the VNC.

As suggested above, it is currently very difficult to determine the molecular mechanisms that underlie CG31814's apparent influence over axonal growth. One reason for this is that little is known about the proteins that CG31814 is related to and which it might interact with, namely the Dprs and DIPs (Alsbury et al., in preparation; Kurusu et al., 2008; Ozkan et al., 2013). Experimental evidence of biological processes or molecular function is currently available for only 20% of the Dprs and the DIPs are entirely uncharacterised. It will likely be necessary to determine which members of these families influence motor axon guidance in order to understand more about the role of CG31814. As discussed in the introduction to the chapter, Ozkan et al.'s (2013) ECIA, which was deployed to investigate interactions between the Dpr and DIP proteins, was associated with a high false-negative rate. Utilisation of, for example, Co-Immunoprecipitation (Co-IP) might prove to be of value for identifying further interactions between proteins of these families.

Kurusu and colleagues' study (2008), which included a number of Dprs and DIPs, only used gain-of-function experiments based on the muscle driver, *24B-GAL4*, and was limited to the ISNb. It is conceivable that, among the 410 secreted and cell surface proteins they assessed, axon guidance defects could be attributed to more than the 16 proteins they identified if they had analysed other facets of the motor neurons or had

looked at sensory neurons (visualised with, e.g., 22C10) or at the VNC (visualised with, e.g., 1D4 or BP102). Further phenotypes might also have been identified if loss-of-function lines and alternative GAL4 drivers were employed. For example, they might have driven expression in motor neurons or pan-neuronally with *OK371-GAL4* (Mahr & Aberle, 2006) or *elav-GAL4* (Luo et al., 1994) drivers. Moreover, a greater understanding of the 16 proteins themselves would likely be garnered; by using a range of alternative drivers and loss-of-function lines, more could be inferred about the mechanisms underlying phenotypes. If these experiments were to reveal phenotypes resembling those reported here, it could be investigated, using transheterozygous lines, whether the implicated genes interact with *CG31814*, thereby facilitating a gradual unravelling of the genetic networks in which they participate. On one hand, these experiments would enhance our understanding of the Dprs and DIPs, including CG31814, within the context of *Drosophila* axon guidance. However, it is also noteworthy that Dpr1 and Dpr9 have respectively been linked to behavioural responses to salt and ethanol, and that a human orthologue of the DIPs, Neuronal growth regulator 1 (NEGR1), has been associated with obesity (Kong et al., 2010; Mägi et al., 2013; Nakamura et al., 2002). Therefore, further investigations into the Dprs and DIPs might ultimately have implications for our understanding of substance use disorders. While this suggestion is somewhat undermined by the apparent absence of human orthologues of the Dprs, it is conceivable that there are functional human equivalents, our understanding of which might be enhanced through investigating these *Drosophila* families.

Chapter 7: Discussion and Conclusion

7.1. Discussion

Bioinformatic analyses of the fly proteome suggest that a number of uncharacterised proteins might be implicated in aspects of nervous system development, including axon guidance (Alsbury et al., in preparation; Dolan et al., 2007; Vogel et al., 2003). The current study focused on three axon guidance candidates – *otk2*, *CG7575*, and *CG31814* – and used loss- and gain-of-function experiments to assess whether these genes are involved in embryonic motor axon guidance.

7.1.1. *Otk2* summary

Initially, disrupting *otk2* activity was approached by attempting to imprecisely excise a transposon from the 5' region of *otk2*. PCR, using primers that bind to the 5' end of *otk2*, suggested that an imprecise excision had been achieved in one population, referred to as *EY03841*17*. However, this was not supported by sequencing data. While these did not indicate that genetic material had been lost by the excision, they did suggest that two nucleotides in the 5' UTR differed from those seen in wild types, which might have disrupted *otk2* expression. Nonetheless, utilisation of an Otk2 antibody revealed that *otk2* was expressed in *EY03841*17* embryos. Despite this, they exhibited highly penetrant and severe motor axon guidance defects; namely, the absence of the ISNb, ISNd, SNc, dorsal or lateral branches of the SNa, FB, and SB.

Whether *otk2* is required for axon guidance was subsequently approached by analysing $otk2^{C26}$ embryos (Linnemannstöns et al., 2014), which were shown to harbour defects within the ISN and ISNb. These observations are the first to implicate *otk2* in axon guidance. Analysis of the $otk2^{C26}$ null allele was supplemented with experiments that involved driving *otk2* expression in motor neurons or somatic muscles. It was argued that, taken together, the results of these experiments suggest that *otk2* might have roles in attraction and repulsion and that it might participate in bi-directional signalling.

Among other proteins (discussed below), Linnemannstöns and colleagues (2014) demonstrated that Otk2 could physically interact with Otk and Fz2, suggesting that it might participate in shared signalling pathways with these proteins. Moreover, the fact that Otk2 co-immunoprecipitates with Otk raises the possibility that Otk2 contributes to Sema-1a/PlexA repulsive signalling. *otk*, *fz2*, and *sema-1a* have all previously been linked to embryonic motor axon guidance (Ayoob et al., 2004; Ayoob et al., 2006; Chak & Kolodkin, 2014; Cho et al., 2012; Inaki et al., 2007; Terman et al., 2002; Winberg et

al., 1998; Winberg et al., 2001; Yang & Terman, 2012; Yu et al., 1998; Yu, Huang, & Kolodkin, 2000.). In the current study, embryos transheterozygous for functional copies of *otk2* and *fz2*, *otk*, or *sema-1a* all exhibited defects resembling those observed in $otk2^{C26}$ embryos, suggesting that *otk2* participates in signalling pathways associated with these genes. Additionally, *BSC199* embryos, which lack *otk* and *otk2* activity, exhibited more severe phenotypes throughout the motor axons, supporting the idea that the off-tracks are implicated in a shared pathway.

Embryos without *otk*, *fz2*, or *sema-1a* activity were also analysed, which all exhibited motor axon phenotypes. The otk^{A1} and *sema-1a* phenotypes resembled those reported in previous studies (Ayoob et al., 2004; Ayoob et al., 2006; Chak & Kolodkin, 2014; Cho et al., 2012; Terman et al., 2002; Winberg et al., 1998; Winberg et al., 2001; Yang & Terman, 2012; Yu et al., 1998; Yu, Huang, & Kolodkin, 2000), though the presence of additional phenotypes, such as the MN12s and MN13s projecting anteriorly, draw attention to the limitations of models pertaining to these genes that restrict them to a role in defasciculation. Inaki and colleagues (2007) measured the surface areas of MN12 and MN13 synapses in experiments involving *fz2* and concluded that it is required for MN12s to grow away from muscle 13. Such measurements were not taken in the current study, though the *fz2* phenotypes seemed qualitatively incongruent with Inaki and colleagues' descriptions (e.g., the MN12s grew anteriorly). In light of these observations and a prior report that suggests that *fz2* affects synapse development post-synaptically (Mosca & Schwarz, 2010), it has been suggested that a more elaborate model of *fz2*'s influence on embryonic motor axons is required. Since phenotypes were observed in embryos transheterozygous for functional copies of *otk* or *otk2* and *fz2*, future models of *fz2* should account for the influence of the off-tracks.

7.1.2. *CG7565* summary

Determining whether *CG7565* is implicated in embryonic motor axon guidance was approached by analysing two loss-of-function lines, *B318* (CDS insertion) and *EDD4408* (deficiency), and by completing two gain-of-function experiments, whereby *CG7565* expression was driven in the motor neurons or somatic muscles. Each of these four experiments revealed aberrations in the ISN and ISNb, which are the first phenotypes of any kind to be linked to *CG7565*. A role for *CG7565* in axon guidance is, however, congruent with reports of nervous system anomalies in experiments involving its vertebrate orthologues, KIAA0319 and KIAA0319L (Darki et al., 2012; Galaburda & Kemper, 1979; Paracchini et al., 2006; Peschansky et al., 2010). Based on the nature of the *CG7565* phenotypes, such as elongation of MN13s in *Mef2 X EY12902* embryos

and the presence of phenotypes in *OK371 X EY12902* embryos, it was argued that CG7565 might be implicated in attracting axons to the muscles and that it might be capable of bi-directional signalling.

7.1.3. *CG31814* summary

As with *CG7565*, prior to the current study, no phenotypes had been linked to *CG31814*. Investigating whether *CG31814* is implicated in axon guidance was approached by examining the motor neurons of embryos with a transposon in the gene's 5' UTR. The FB and SB were absent in these embryos or the SB projected anteriorly. Precisely excising the transposon rescued the FB and SB absent phenotypes, but not the SB anterior phenotype. These observations constitute the first evidence of *CG31814*'s role in axon guidance and are congruent with the suggestion that it encodes a protein of the DIP family, members of which have been linked to larval synaptic development in the periphery (Kurusu et al., 2008; Ozkan et al., 2013).

7.1.4. Limitations and future directions

While the *EY03841*17* embryos exhibited severe phenotypes in the motor axons, the gene (or genes) responsible was not identified. However, it was argued that the phenotypes are likely attributable to an aberration on the 2nd chromosome, which was balanced in the *EY03841*17* population; since the aberration appears to entail semi-lethality, it is probable that it would have been lost through recombination if it were associated with one of the other (unbalanced) chromosomes. Thus, it was proposed that a screen be completed, whereby the *EY03841*17* chromosome is paired with deficiency chromosomes that collectively span the 2nd chromosome. This might reveal that a characterised gene associated with similar phenotypes, such as *eve* (Labrador et al., 2005; Landgraf et al., 1999b) or *beat* (Fambrough & Goodman, 1996; Landgraf et al., 1999a; Siebert et al., 2009), is responsible for the *EY03841*17* phenotypes, though it is certainly conceivable that an aberration within an uncharacterised gene is the cause.

One limitation was not pairing the loss-of-function alleles used in the current study (*otk^{A1}*, *otk2^{C26}*, *BSC199*, *sema-1a*, *fz2*, *B318*, *ED4408*) with alternative loss-of-function alleles (e.g., deficiencies spanning the gene of interest). Without having done this, it remains possible that abnormal phenotypes are attributable to genetic aberrations other than those related to the genes of interest. However, similarities between the phenotypes associated with different alleles used to study a particular gene suggest that the genes of interest were responsible for the observed motor axon phenotypes. For instance, *otk2^{C26}* phenotypes were comparable to those observed in the two *otk2* gain-of-function

experiments; it seems highly unlikely that the chromosomes used in these three experiments would harbour unaccounted for aberrations that happen to affect certain embryonic motor axons in a particular way. Moreover, in *BSC199* embryos, which lacked *otk* and *otk2* activity, there were seemingly enhanced *otk* an *otk2* phenotypes. The same argument can be made based on the similarity between the *CG7565* loss-of-function alleles, *B318* and *ED4408*. While the same cannot be said for the *sema-1a* and *fz2* experiments, which were each based on single alleles, axon guidance phenotypes have previously been reported for these genes on the basis of experiments with various alleles (Ayoob et al., 2004; Ayoob et al., 2006; Chak & Kolodkin, 2014; Cho et al., 2012; Terman et al., 2002; Winberg et al., 1998; Winberg et al., 2001; Yang & Terman, 2012; Yu et al., 1998; Yu, Huang, & Kolodkin, 2000). Therefore, while pairing alternative loss-of-function alleles with each other might increase confidence in the results, looking at the current phenotypes collectively suggests that the genes of interest do affect embryonic motor axon guidance. This claim might also be supported by completing rescue experiments, which could either express transgenes under the control of endogenous promoters or specific GAL4 drivers (e.g., *OK371*, *Mef2*). The latter would have the added benefit of allowing for an examination of the tissues from which the genes affect axonal growth.

A second limitation pertains to the gain-of-function and genetic interaction experiments. For example, the *otk2* gain-of-function experiment used the *EY03841* chromosome for its UAS in the 5' region of the gene. However, it was argued in Chapter 3 that the *EY03841* chromosome contains an unidentified aberration that causes severe motor axon phenotypes. Therefore, it is possible that the embryos used in the gain-of-function experiments exhibited mild motor axon phenotypes because they possessed one copy of the *EY03841* chromosome. Thus, it would be prudent to assess whether there are phenotypes in these embryos in the absence of GAL4 activity. This also applies to the *EY12902* chromosome used in *CG7565* experiments. Nonetheless, certain observations suggest that increases in *otk2* or *CG7565* activity in specific tissues (i.e., motor neurons or somatic muscles) were the cause of the reported phenotypes. Firstly, as put forward immediately above, there were clear similarities between loss- and gain-of-function phenotypes. However, secondly, there were also differences between embryos misexpressing *otk2* or *CG7565* in certain tissues. For instance, MN13s were enlarged posteriorly when *CG7565* activity was driven in somatic muscle, though this was not observed when it was driven in motor neurons. Likewise, misexpression of *otk2* in somatic muscle was associated with absence of the FB, which, conversely, was present more often than in wild types when *otk2* was misexpressed in motor neurons. The

phenotypes reported for transheterozygous embryos in Chapter 4 might also be attributable to reducing the dosage of one or the other genes, rather than reflecting a genetic interaction between them. Again, it would be shrewd to look at embryos heterozygous for single genes to investigate this. Nonetheless, it is likely that the phenotypes seen in transheterozygous embryos are due to genetic interactions. The first reason for claiming this is that the nature, breadth and penetrance of phenotypes in transheterozygous embryos generally resembled those seen in embryos homozygous for their respective alleles (otk^{A1}, $otk2^{C26}$, *fz2*, *sema-1a*); one would expect penetrance to decrease upon reducing dosage if phenotypes were attributable solely to one or the other genes rather than an interaction between them. Secondly, the genetic interaction data reported here are congruent with Linnemannstöns and colleagues' (2014) report of interactions between the Otk, Otk2, and Fz2 proteins. Although it has not been investigated whether Otk2 physically interacts with Sema-1a, its interaction with Otk, which physically interacts with PlexA (Winberg et al., 2001), provides an indirect link between Sema-1a and Otk2.

Given the clear expression of *otk2*, *CG7565*, and *CG31814* in the embryonic VNC, future investigations should assess whether axons in the VNC develop normally when the activity of these genes is abolished or increased. It was suggested in Chapter 4 that the expression pattern of *otk2* is particularly interesting since its signal is much clearer in the region of anterior commissures relative to posterior commissures. This is also the case for *otk*. It might be that *otk* and *otk2* are involved in commissure selection, which could be investigated by using *Eagle-GAL4* to drive expression in the posterior commissures. In light of *otk2*'s expression in larval retinal cells (Linnemannstöns et al., 2014) and *otk*'s involvement in their guidance (Cafferty et al., 2004), it would also be interesting to investigate whether *otk2* is involved in retinotopic mapping. A small number of embryos with *CG7565* loss-of-function alleles (*B318* and *ED4408*) exhibited axonal defects in the VNC (Appendix C), supporting the idea that *CG7565* might be required for axon guidance in the CNS. The collapse of longitudinal fascicles onto the midline in an *ED4408* embryo resembles what it seen in *slit* mutants (Kidd et al., 1998; Seeger et al., 1993). Of course, a greater number of *CG7565* loss-of-function embryos would need to be seen to exhibit the phenotype to increase confidence in the supposition that loss of *CG7565* activity was the cause. While the suggestion of a link between *CG7565* and *slit* based on phenotypic similarity is rather speculative, the idea is somewhat bolstered by the observation that the CG7565 orthologue, hKIAA0319L, binds to NgR1 (Poon et al., 2011), which is the vertebrate protein that most closely resembles *Drosophila* Slit (Klinger et al., 2003). Should axon guidance defects be

observed consistently in the VNC upon inspecting a greater number of *CG7565* loss-of-function embryos, it would be interesting and straightforward to analyse embryos transheterozygous for functional copies of *CG7565* and *slit* in order to investigate whether they genetically interact.

slit has also been linked to aberrations in the embryonic motor axons (Kidd, Bland, & Goodman, 1999), thus genetic interactions between *slit* and *CG7565* could also be assessed by examining the periphery. Such experiments would represent a starting point for revealing the genetic network in which *CG7565* is embedded. Similar experiments are required to do the same for *CG31814*. As a DIP (Ozkan et al., 2013), the most suitable candidates for assessing genetic interactions with *CG31814* are other DIPs and Dprs. However, since these families are largely uncharacterised, it will be necessary to assess whether their members are also implicated in motor axon guidance. Thus, unravelling the networks in which *CG31814* operates represents an opportunity to begin characterising a number of other genes that, given their expression patterns (Ozkan et al., 2013), likely have important roles in nervous system development. The current study has already begun to link *otk2* to established axon guidance signalling pathways (i.e., Sema-1a/PlexA, Wnt4/Fz2). However, Linnemannstöns and colleagues (2014) suggest that Otk2 also interacts with Fz and Wnt2, both of which have been associated with nervous system development (Gombos et al., 2015; Liebl, McKeown, & Hing, 2010; Srahna et al., 2006). It will, therefore, be valuable to assess whether there are genetic interactions between *otk2*, *fz*, and *wnt2* by analysing the motor neurons of transheterozygous embryos.

7.2. Conclusion

The current study has provided evidence that three largely or completely uncharacterised genes – *otk2*, *CG7565*, and *CG31814* – are involved in guiding embryonic motor axons in *Drosophila*. It has also revealed novel phenotypes in established axon guidance genes (*otk*, *sema-1a*, and *fz2*), thus drawing attention to limitations of current models. The need for more sophisticated theories of how these genes influence axons has also been highlighted by revealing previously unreported genetic interactions. Although genetic interactions were only investigated within the context of *otk2*, suggestions have been made regarding how to unravel the networks in which *CG7565* and *CG31814* participate. All three genes have vertebrate orthologues, thus, in addition to enhancing our understanding of *Drosophila* neurobiology, the observations presented here might ultimately contribute to insights into the signalling pathways and mechanisms that underlie human nervous system development.

Bibliography

Abrell, S., & Jäckle, H. (2001). Axon guidance of Drosophila SNb motoneurons depends on the cooperative action of muscular Krüppel and neuronal capricious activities. *Mechanisms of Development*, *109*, 3–12.

Akhmanova, A., Hoogenraad, C. C., Drabek, K., Stepanova, T., Dortland, B., Verkerk, T., … Galjart, N. (2001). Clasps are CLIP-115 and -170 associating proteins involved in the regional regulation of microtubule dynamics in motile fibroblasts. *Cell*, *104*(6), 923–35. doi:10.1016/S0092-8674(01)00288-4

Ackerman, S. L., Kozak, L. P., Przybrski, S. A., Rund, L. A., Boyer, B. B., & Knowles, B. B. (1997). The mouse rostral cerebellar malformation gene encodes an UNC-5-like protein. *Nature*, *386*(6627), 838–842.

Adryan, B., Woerfel, G., Birch-Machin, I., Gao, S., Quick, M., Meadows, L., … White, R. (2007). Genomic mapping of Suppressor of Hairy-wing binding sites in Drosophila. *Genome Biology*, *8*(8), R167. doi:10.1186/gb-2007-8-8-r167

Al-Anzi, B., & Wyman, R. J. (2009). The Drosophila immunoglobulin gene turtle encodes guidance molecules involved in axon pathfinding. *Neural Development*, *4*, 31. doi:10.1186/1749-8104-4-31

Alavi, M., Andrews, G., Gillis, T., & Kidd, T. (2015). *Dscam Switches Slit Repulsion to Attraction via the Robo Receptor*. 56th Annual Drosophila Research Conference, Chicago.

Anitha, A, Nakamura, K., Yamada, K., Suda, S., Thanseem, I., Tsujii, M., … Mori, N. (2008). Genetic analyses of roundabout (ROBO) axon guidance receptors in autism. *American Journal of Medical Genetics. Part B, Neuropsychiatric Genetics : The Official Publication of the International Society of Psychiatric Genetics*, *147B*(7), 1019–27. doi:10.1002/ajmg.b.30697

Ayoob, J. C., Terman, J. R., & Kolodkin, A. L. (2006). Drosophila Plexin B is a Sema-2a receptor required for axon guidance. *Development (Cambridge, England)*, *133*(11), 2125–35. doi:10.1242/dev.02380

Ayoob, J. C., Yu, H., Terman, J. R., & Kolodkin, A. L. (2004). The Drosophila Receptor Guanylyl Cyclase Gyc76C Is Required for Semaphorin-1a–Plexin A-Mediated Axonal Repulsion. *The Journal of Neuroscience : The Official Journal of the Society for Neuroscience*, *24*(30), 6639–6649. doi:10.1523/JNEUROSCI.1104-04.2004

Bagnard, D., Vaillant, C., Khuth, S. T., Dufay, N., Lohrum, M., Puschel, a W., … Thomasset, N. (2001). Semaphorin 3A-vascular endothelial growth factor-165 balance mediates migration and apoptosis of neural progenitor cells by the recruitment of shared receptor. *The Journal of Neuroscience : The Official Journal of the Society for Neuroscience*, *21*(10), 3332–41. Retrieved from http://www.ncbi.nlm.nih.gov/pubmed/11331362

Bao, H., Berlanga, M. L., Xue, M., Hapip, S. M., Daniels, R. W., Mendenhall, J. M., … Zhang, B. (2007). The atypical cadherin flamingo regulates synaptogenesis and helps prevent axonal and synaptic degeneration in Drosophila. *Molecular and Cellular Neurosciences*, *34*(4), 662–78. doi:10.1016/j.mcn.2007.01.007

Bashaw, G. J., Kidd, T., Murray, D., Pawson, T., & Goodman, C. S. (2000). Repulsive axon guidance: Abelson and Enabled play opposing roles downstream of the roundabout receptor. *Cell*, *101*(7), 703–15. Retrieved from http://www.ncbi.nlm.nih.gov/pubmed/10892742

Bate, M., Rushton, E., & Currie, D. A. (1991). Cells with persistent twist expression are the embryonic precursors of adult muscles in Drosophila. *Development (Cambridge, England)*, *113*(1), 79–89.

Bateman, J., Shu, H., & Van Vactor, D. (2000). The guanine nucleotide exchange factor trio mediates axonal development in the Drosophila embryo. *Neuron*, *26*(1), 93–106. doi:10.1016/S0896-6273(00)81141-1

Bazigou, E., Apitz, H., Johansson, J., Lorén, C. E., Hirst, E. M. a, Chen, P. L., … Salecker, I. (2007). Anterograde Jelly belly and Alk Receptor Tyrosine Kinase Signaling Mediates Retinal Axon Targeting in *Drosophila*. *Cell*, *128*(5), 961–975. doi:10.1016/j.cell.2007.02.024

Berger, J., Senti, K.-A., Senti, G., Newsome, T. P., Asling, B., Dickson, B. J., & Suzuki, T. (2008). Systematic identification of genes that regulate neuronal wiring in the Drosophila visual system. *PLoS Genetics*, *4*(5), e1000085. doi:10.1371/journal.pgen.1000085

Bossing, T., & Brand, A. H. (2002). Dephrin, a transmembrane ephrin with a unique structure, prevents interneuronal axons from exiting the Drosophila embryonic CNS. *Development (Cambridge, England)*, *129*(18), 4205–18. Retrieved from http://www.ncbi.nlm.nih.gov/pubmed/12183373

Brand, A. H., & Perrimon, N. (1993). Targeted gene expression as a means of altering cell fates and generating dominant phenotypes. *Development (Cambridge, England)*, *118*(2), 401–15. Retrieved from http://www.ncbi.nlm.nih.gov/pubmed/8223268

Brankatschk, M., & Dickson, B. J. (2006). Netrins guide Drosophila commissural axons at short range. *Nature Neuroscience*, *9*(2), 188–194. doi:10.1038/nn1625

Brose, K., Bland, K. S., Wang, K. H., Arnott, D., Henzel, W., Goodman, C. S., … Kidd, T. (1999). Slit proteins bind Robo receptors and have an evolutionarily conserved role in repulsive axon guidance. *Cell*, *96*(6), 795–806. Retrieved from http://www.ncbi.nlm.nih.gov/pubmed/10102268

Bruckner, K. (1997). Tyrosine Phosphorylation of Transmembrane Ligands for Eph Receptors. *Science*, *275*(5306), 1640–1643. doi:10.1126/science.275.5306.1640

Cafferty, P., Yu, L., & Rao, Y. (2004). The receptor tyrosine kinase Off-track is required for layer-specific neuronal connectivity in Drosophila. *Development (Cambridge, England)*, *131*(21), 5287–95. doi:10.1242/dev.01406

Cao, J., Li, Y., Xia, W., Reddig, K., Hu, W., Xie, W., … Han, J. (2011). A Drosophila metallophosphoesterase mediates deglycosylation of rhodopsin. *The EMBO Journal*, *30*(18), 3701–13. doi:10.1038/emboj.2011.254

Cautinat, A., Sa, J. A., Garratt, A. N., Talmage, D. A., Role, L. W., Charnay, P., & Marı, O. (2006). Tangential Neuronal Migration Controls Axon Guidance: A Role for Neuregulin-1 in Thalamocortical Axon Navigation. *Cell*, *125*(1), 127–142. doi:10.1016/j.cell.2006.01.042

Chak, K., & Kolodkin, A. L. (2014). Function of the Drosophila receptor guanylyl cyclase Gyc76C in PlexA-mediated motor axon guidance. *Development (Cambridge, England)*, *141*(1), 136–47. doi:10.1242/dev.095968

Chen, R., Khatri, P., Mazur, P. K., Polin, M., Zheng, Y., Vaka, D., … Sweet-Cordero, E. A. (2014). A meta-analysis of lung cancer gene expression identifies PTK7 as a survival gene in lung adenocarcinoma. *Cancer Research*, *74*(10), 2892–2902. doi:10.1158/0008-5472.CAN-13-2775

Chen, C. M., & Struhl, G. (1999). Wingless transduction by the Frizzled and Frizzled2 proteins of Drosophila. *Development (Cambridge, England)*, *126*(23), 5441–5452.

Chilton, J. K. (2006). Molecular mechanisms of axon guidance. *Developmental Biology*, *292*(1), 13–24. doi:10.1016/j.ydbio.2005.12.048

Cho, J. Y., Chak, K., Andreone, B. J., Wooley, J. R., & Kolodkin, A. L. (2012). The extracellular matrix proteoglycan perlecan facilitates transmembrane semaphorin-mediated repulsive guidance. *Genes & Development*, *26*(19), 2222–35. doi:10.1101/gad.193136.112

Connell-Crowley, L., Vo, D., Luke, L., & Giniger, E. (2007). Drosophila lacking the Cdk5 activator, p35, display defective axon guidance, age-dependent behavioral deficits and reduced lifespan. *Mechanisms of Development*, *124*(5), 341–9. doi:10.1016/j.mod.2007.02.002

Couch, J. A., Chen, J., Rieff, H. I., Uri, E. M., & Condron, B. G. (2004). Robo2 and Robo3 Interact With Eagle To Regulate Serotonergic Neuron Differentiation. *Development (Cambridge, England)*, *131*(5), 997–1006. doi:10.1242/dev.00962

Couto, J. M., Gomez, L., Wigg, K., Cate-Carter, T., Archibald, J., Anderson, B., … Barr, C. L. (2008). The KIAA0319-Like *(KIAA0319L)* Gene on Chromosome 1p34 as a Candidate for Reading Disabilities. *Journal of Neurogenetics*, *22*(4), 295–313. doi:10.1080/01677060802354328

Crowner, D., Le Gall, M., Gates, M. A., & Giniger, E. (2003). Notch Steers Drosophila ISNb Motor Axons by Regulating the Abl Signaling Pathway. *Current Biology*, *13*(15), 967–972. doi:10.1016/S

Darki, F., Peyrard-Janvid, M., Matsson, H., Kere, J., & Klingberg, T. (2012). Three dyslexia susceptibility genes, DYX1C1, DCDC2, and KIAA0319, affect temporo-parietal white matter structure. *Biological Psychiatry*, *72*(8), 671–676. doi:10.1016/j.biopsych.2012.05.008

Davie, C. A. (2008). A review of Parkinson's disease. *British Medical Bulletin*, *86*(1), 109–127. doi:10.1093/bmb/ldn013

Davis, G. W., Schuster, C. M., & Goodman, C. S. (1997). Genetic analysis of the mechanisms controlling target selection: target-derived Fasciclin II regulates the pattern of synapse formation. *Neuron*, *19*(3), 561–573. doi:10.1016/S0896-6273(00)80372-4

Dent, E. W., Gupton, S. L., & Gertler, F. B. (2011). The growth cone cytoskeleton in Axon outgrowth and guidance. *Cold Spring Harbor Perspectives in Biology*, *3*(3), 1–39. doi:10.1101/cshperspect.a001800

Desai, C. J., Gindhart, J. G., Goldstein, L. S. B., & Zinn, K. (1996). Receptor tyrosine phosphatases are required for motor axon guidance in the Drosophila embryo. *Cell*, *84*(4), 599–609. doi:10.1016/S0092-8674(00)81035-1

Desai, C. J., Krueger, N. X., Saito, H., & Zinn, K. (1997). Competition and cooperation among receptor tyrosine phosphatases control motoneuron growth cone guidance in Drosophila. *Development (Cambridge, England)*, *124*(10), 1941–52. Retrieved from http://www.ncbi.nlm.nih.gov/pubmed/9169841

Dittrich, R., Bossing, T., Gould, A. P., Technau, G. M., & Urban, J. (1997). The differentiation of the serotonergic neurons in the Drosophila ventral nerve cord depends on the combined function of the zinc finger proteins Eagle and Huckebein. *Development (Cambridge, England)*, *124*(13), 2515–2525.

Drescher, U., Kremoser, C., Handwerker, C., Löschinger, J., Noda, M., & Bonhoeffer, F. (1995). In vitro guidance of retinal ganglion cell axons by RAGS, a 25 kDa tectal protein related to ligands for Eph receptor tyrosine kinases. *Cell*, *82*(3), 359–70. Retrieved from http://www.ncbi.nlm.nih.gov/pubmed/7634326

Eastwood, S. L., & Harrison, P. J. (2008). Decreased mRNA expression of netrin-G1 and netrin-G2 in the temporal lobe in schizophrenia and bipolar disorder. *Neuropsychopharmacology*, *33*(4), 933–45. doi:10.1038/sj.npp.1301457

Eisenhaber, B., Bork, P., & Eisenhaber, F. (1999). Prediction of potential GPI-modification sites in proprotein sequences. *Journal of Molecular Biology*, *292*(3), 741–58. doi:10.1006/jmbi.1999.3069

Fambrough, D., & Goodman, C. S. (1996). The Drosophila beaten path gene encodes a novel secreted protein that regulates defasciculation at motor axon choice points. *Cell*, *87*(6), 1049–58. Retrieved from http://www.ncbi.nlm.nih.gov/pubmed/8978609

Firat-karalar, E. N., & Welch, M. D. (2011). NIH Public Access. *Current Opinion in Cell Biology*, *23*(1), 4–13. doi:10.1016/j.ceb.2010.10.007.New

Firtel, R.A. & Chung, C.Y., 2000. The molecular genetics of chemotaxis: sensing and responding to chemoattractant gradients. *Bioessays*, *22*(7), 603-615.

Fisher, A. M. (1922). On the interpretation of X^2 from contingency tables, and the calculation of P. *Journal of the Royal Statistical Society*, *85*(1), 87–94.

Fox, A. N., & Zinn, K. (2005). The heparan sulfate proteoglycan syndecan is an in vivo ligand for the Drosophila LAR receptor tyrosine phosphatase. *Current Biology : CB*, *15*(19), 1701–11. doi:10.1016/j.cub.2005.08.035

Fujita, S. C., Zipursky, S. L., Benzer, S., Ferrús, a, & Shotwell, S. L. (1982). Monoclonal antibodies against the Drosophila nervous system. *Proceedings of the National Academy of Sciences of the United States of America*, *79*(24), 7929–33. Retrieved from http://www.pubmedcentral.nih.gov/articlerender.fcgi?artid=347463&tool=pmcentrez&rendertype=abstract

Galaburda, A. M., & Kemper, T. L. (1979). Cytoarchitectonic abnormalities in developmental dyslexia: a case study. *Annals of Neurology*, *6*(2), 94–100.

Garcia-Lopez, P., Garcia-Marin, V., & Freire, M. (2010). The histological slides and drawings of Cajal. *Frontiers in Neuroanatomy*, *4*(March), 1–16. doi:10.3389/neuro.05.009.2010

Gombos, R., Migh, E., Antal, O., Mukherjee, A., Jenny, A., & Mihály, J. (2015). The Formin DAAM Functions as Molecular Effector of the Planar Cell Polarity Pathway during Axonal Development in Drosophila. *Journal of Neuroscience*, *35*(28), 10154–10167.

Gonda, Y., Andrews, W. D., Tabata, H., Namba, T., Parnavelas, J. G., Nakajima, K., … Uchino, S. (2013). Robo1 Regulates the Migration and Laminar Distribution of Upper-Layer Pyramidal Neurons of the Cerebral Cortex. *Cerebral Cortex*, *23*(6), 1495–1508. doi:10.1093/cercor/bhs141

Gorczyca, M. G., Phillis, R. W., & Budnik, V. (1994). The role of tinman, a mesodermal cell fate gene, in axon pathfinding during the development of the transverse nerve in Drosophila. *Development (Cambridge, England)*, *120*(8), 2143–52. Retrieved from http://www.ncbi.nlm.nih.gov/pubmed/7925017

Grady, C. L., & Keight, L. (2002). Studies of Altered Social Cognition in Neuropsychiatric Disorders Using Functional Neuroimaging. *Canadian Journal of Psychiatry*, *47*(4), 327–336.

Grenningloh, G., Rehm, E. J., & Goodman, C. S. (1991). Genetic analysis of growth conse guidance in Drosophila: fasciclin II functions as a neuronal recognition molecule. *Cell*, *67*(1), 45–57.

Grueber, W. B., Ye, B., Yang, C.-H., Younger, S., Borden, K., Jan, L. Y., & Jan, Y.-N. (2007). Projections of Drosophila multidendritic neurons in the central nervous system: links with peripheral dendrite morphology. *Development*, *134*(1), 55–64. doi:10.1242/dev.02666

Hall, S. G., & Bieber, A. J. (1997). Mutations in the Drosophila Neuroglian cell adhesion molecule affect motor neuron pathfinding and peripheral nervous system patterning. *Journal of Neurobiology*, *32*(3), 325–340. doi:10.1002/(SICI)1097-4695(199703)32:3<325::AID-NEU6>3.0.CO;2-9

Hannula-Jouppi, K., Kaminen-Ahola, N., Taipale, M., Eklund, R., Nopola-Hemmi, J., Kääriäinen, H., & Kere, J. (2005). The Axon Guidance Receptor Gene ROBO1 Is a Candidate Gene for Developmental Dyslexia. *PLoS Genetics*, *1*(4), e50. doi:10.1371/journal.pgen.0010050

Harrison, R. G. (1910). The outgrowth of the nerve fibre as a mode of protoplasmic movement. *Journal of experimental zoology*, *9*(4), 787–846.

Harris, R., Sabatelli, L. M., & Seeger, M. A. (1996). Guidance cues at the Drosophila CNS midline: identification and characterization of two Drosophila Netrin/UNC-6 homologs. *Neuron*, *17*(2), 217–28. Retrieved from http://www.ncbi.nlm.nih.gov/pubmed/8780646

Hartmann, C., Landgraf, M., Bate, M., & Jäckle, H. (1997). Kruppel target gene knockout participates in the proper innervation of a specific set of Drosophila larval muscles. *EMBO Journal*, *16*(17), 5299–5309. doi:10.1093/emboj/16.17.5299

Hasegawa, Y. (2004). Promotion of Axon Regeneration by Myelin-Associated Glycoprotein and Nogo through Divergent Signals Downstream of Gi/G. *Journal of Neuroscience*, *24*(30), 6826–6832. doi:10.1523/JNEUROSCI.1856-04.2004

Hattori, D., Millard, S. S., Wojtowicz, W. M., & Zipursky, S. L. (2008). Dscam-mediated cell recognition regulates neural circuit formation. *Annual Review of Cell and Developmental Biology*, *24*, 597–620. doi:10.1146/annurev.cellbio.24.110707.175250

He, H., & Noll, M. (2013). Differential and redundant functions of gooseberry and gooseberry neuro in the central nervous system and segmentation of the Drosophila embryo. *Developmental Biology*, *382*(1), 209–23. doi:10.1016/j.ydbio.2013.05.017

Heron, J., Hyde, S., Grozeva, D., Hamshere, M., & Williams, N. (2005). Operation of the Schizophrenia Susceptibility Gene, Neuregulin 1, Across Traditional Diagnostic Boundaries to Increase Risk for Bipolar Disorder. *Archives of General Psychiatry*, *62*(June), 642–648.

Hill, G. W., Purcell, E. K., Liu, L., Velkey, J. M., Altschuler, R. a, & Duncan, R. K. (2012). Netrin-1-mediated axon guidance in mouse embryonic stem cells overexpressing neurogenin-1. *Stem Cells and Development*, *21*(15), 2827–37. doi:10.1089/scd.2011.0437

Hinck, L. (2004). The versatile roles of "axon guidance" cues in tissue morphogenesis. *Developmental Cell*, *7*(6), 783–93. doi:10.1016/j.devcel.2004.11.002

Hindges, R., Mclaughlin, T., Genoud, N., Henkemeyer, M., Leary, D. D. M. O., & Jolla, L. (2002). EphB Forward Signaling Controls Directional Branch Extension and Arborization Required for Dorsal-Ventral Retinotopic Mapping, *35*(3), 475–487.

Hong, K., Hinck, L., Nishiyama, M., Poo, M., Tessier-Lavigne, M., & Stein, E. (1999). A Ligand-Gated Association between Cytoplasmic Domains of UNC5 and DCC Family Receptors Converts Netrin-Induced Growth Cone Attraction to Repulsion. *Cell*, *97*(7), 927–941. doi:10.1016/S0092-8674(00)80804-1

Hong, W., Zhu, H., Potter, C. J., Barsh, G., Zinn, K., & Luo, L. (2010). NIH Public Access, *12*(12), 1542–1550. doi:10.1038/nn.2442.Leucine-Rich

Hoskins, R., & Evans-holm, M. (2011). Inverse PCR and Sequencing of P -element, piggyBac and Minos Insertion Sites in the Drosophila Gene Disruption Project I. Fly Genomic DNA Prep, 1–12.

Hoang, B., & Chiba, a. (1998). Genetic analysis on the role of integrin during axon guidance in Drosophila. *The Journal of Neuroscience : The Official Journal of the Society for Neuroscience*, *18*(19), 7847–55. Retrieved from http://www.ncbi.nlm.nih.gov/pubmed/9742153

Hu, H., Marton, T. F., & Goodman, C. S. (2001). Plexin B mediates axon guidance in Drosophila by simultaneously inhibiting active Rac and enhancing RhoA signaling. *Neuron*, *32*(1), 39–51. Retrieved from http://www.ncbi.nlm.nih.gov/pubmed/11604137

Huang, J., Wang, Y., Raghavan, S., Feng, S., Kiesewetter, K., & Wang, J. (2011). Human down syndrome cell adhesion molecules (dscams) are functionally conserved with drosophila dscam[tm1] isoforms in controlling neurodevelopment. *Insect Biochemistry and Molecular Biology*, *41*(10), 778–787. doi:10.1016/j.ibmb.2011.05.008

Huang, Z., Yazdani, U., Thompson-Peer, K. L., Kolodkin, A. L., & Terman, J. R. (2007). Crk-associated substrate (Cas) signaling protein functions with integrins to specify axon guidance during development. *Development (Cambridge, England)*, *134*(12), 2337–2347. doi:10.1242/dev.004242

Hummel, T., Krukkert, K., Roos, J., Davis, G., & Klämbt, C. (2000). Drosophila Futsch/22C10 is a MAP1B-like protein required for dendritic and axonal development. *Neuron*, *26*(2), 357–70. Retrieved from http://www.ncbi.nlm.nih.gov/pubmed/10839355

Hummel, T., Vasconcelos, M. L., Clemens, J. C., Fishilevich, Y., Vosshall, L. B., & Zipursky, S. L. (2003). Axonal targeting of olfactory receptor neurons in Drosophila is controlled by Dscam. *Neuron*, *37*(2), 221–31. doi:10.1016/S0896-6273(02)01183-2

Hung, R.-J., Spaeth, C. S., Yesilyurt, H. G., & Terman, J. R. (2012). SelR/MsrB Reverses Mical-mediated Oxidation of Actin to Regulate F-actin Dynamics. *Nature Cell Biology*, *29*(6), 997–1003. doi:10.1016/j.biotechadv.2011.08.021.Secreted

Hung, R.-J., Yazdani, U., Yoon, J., Wu, H., Yang, T., Gupta, N., … Terman, J. R. (2010). Mical links semaphorins to F-actin disassembly. *Nature*, *462*(7282), 823–827. doi:10.1016/j.micinf.2011.07.011.Innate

Ibraghimov-Beskrovnaya, O., Bukanov, N. O., Donohue, L. C., Dackowski, W. R., Klinger, K. W., & Landes, G. M. (2000). Strong homophilic interactions of the Ig-like domains of polycystin-1, the protein product of an autosomal dominant polycystic kidney disease gene, PKD1. *Human Molecular Genetics*, *9*(11), 1641–9. Retrieved from http://www.ncbi.nlm.nih.gov/pubmed/10861291

Inaki, M., Yoshikawa, S., Thomas, J. B., Aburatani, H., & Nose, A. (2007). Wnt4 is a local repulsive cue that determines synaptic target specificity. *Current Biology : CB*, *17*(18), 1574–9. doi:10.1016/j.cub.2007.08.013

Ishii, N., Wadsworth, W. G., Stern, B. D., Culotti, J. G., Hedgecock, E. M. (1992). UNC-6, a laminin-related protein, guide cell and pioneer axon migration in C. elegans. *Neuron*, *9*(5), 873–881.

Jeon, M., Nguyen, H., Bahri, S., & Zinn, K. (2008). Redundancy and compensation in axon guidance: genetic analysis of the Drosophila Ptp10D/Ptp4E receptor tyrosine phosphatase subfamily. *Neural Development*, *3*(January), 3. doi:10.1186/1749-8104-3-3

Jeong, S., Juhaszova, K., & Kolodkin, A. (2013). The Control of Semaphorin-1a-mediated Reverse Signalling by Opposing Pebble and RhoGAPp190 Functions in Drosophila, *76*(4), 721–734. doi:10.1016/j.neuron.2012.09.018.

Jin, J., Ryu, H. S., Lee, K. B., & Jang, J.-J. (2014). High Expression of Protein Tyrosine Kinase 7 Significantly Associates with Invasiveness and Poor Prognosis in Intrahepatic Cholangiocarcinoma. *PLoS ONE*, *9*(2), e90247. doi:10.1371/journal.pone.0090247

Kawano, H., Horie, M., Honma, S., Kawamura, K., Takeuchi, K., & Kimura, S. (2003). Aberrant trajectory of ascending dopaminergic pathway in mice lacking Nkx2.1. *Experimental Neurology*, *182*(1), 103–112. doi:10.1016/S0014-4886(03)00030-X

Keino-Masu, K., Masu, M., Hinck, L., Leonardo, E. D., Chan, S. S., Culotti, J. G., & Tessier-Lavigne, M. (1996). Deleted in Colorectal Cancer (DCC) encodes a netrin receptor. *Cell*, *87*(2), 175–85. Retrieved from http://www.ncbi.nlm.nih.gov/pubmed/8861902

Keleman, K., & Dickson, B. J. (2001). Short- and long-range repulsion by the Drosophila Unc5 netrin receptor. *Neuron*, *32*(4), 605–17. Retrieved from http://www.ncbi.nlm.nih.gov/pubmed/11719202

Kenji, A., Yamada, K., Iwayama, Y., & Yamakawa, K. (2008). Association study between the Down syndrome cell adhesion molecule (DSCAM) and bipolar disorder. *Psychiatric Genetics*, *18*(1), 1–10.

Kidd, T., Bland, K. S., & Goodman, C. S. (1999). Slit is the midline repellent for the robo receptor in Drosophila. *Cell*, *96*(6), 785–94. Retrieved from http://www.ncbi.nlm.nih.gov/pubmed/10102267

Kidd, T., Brose, K., Mitchell, K. J., Fetter, R. D., Tessier-lavigne, M., Goodman, C. S., & Tear, G. (1998a). Roundabout Controls Axon Crossing of the CNS Midline and Defines a Novel Subfamily of Evolutionarily Conserved Guidance Receptors. *Cell*, *92*, 205–215.

Kidd, T., Russell, C., Goodman, C. S., & Tear, G. (1998b). Dosage-sensitive and complementary functions of roundabout and commissureless control axon crossing of the CNS midline. *Neuron*, *20*(1), 25–33. Retrieved from http://www.ncbi.nlm.nih.gov/pubmed/9459439

Klinger, M. (2003). Identification of Nogo-66 Receptor (NgR) and Homologous Genes in Fish. *Molecular Biology and Evolution*, *21*(1), 76–85. doi:10.1093/molbev/msg241

Koch, N., Kobler, O., Thomas, U., Qualmann, B., & Kessels, M. M. (2014). Terminal Axonal Arborization and Synaptic Bouton Formation Critically Rely on Abp1 and the Arp2/3 Complex. *PLoS ONE*, *9*(5), e97692. doi:10.1371/journal.pone.0097692

Kohsaka, H., & Nose, A. (2009). Target recognition at the tips of postsynaptic filopodia: accumulation and function of Capricious. *Development (Cambridge, England)*, *136*(7), 1127–1135. doi:10.1242/dev.027920

Kolodkin, A. L., & Tessier-Lavigne, M. (2011). Mechanisms and molecules of neuronal wiring: a primer. *Cold Spring Harbor Perspectives in Biology*, *3*(6). doi:10.1101/cshperspect.a001727

Kolodziej, P. A., Timpe, L. C., Mitchell, K. J., Fried, S. R., Goodman, C. S., Jan, L. Y., & Jan, Y. N. (1996). frazzled Encodes a Drosophila Member of the DCC Immunoglobulin Subfamily and Is Required for CNS and Motor Axon Guidance. *Cell*, *87*(2), 197–204. doi:10.1016/S0092-8674(00)81338-0

Kong, E. C., Allouche, L., Chapot, P. A., Vranizan, K., Moore, M. S., Heberlein, U., & Wolf, F. W. (2010). Ethanol-regulated genes that contribute to ethanol sensitivity and rapid tolerance in Drosophila. *Alcoholism, Clinical and Experimental Research*, *34*(2), 302–16. doi:10.1111/j.1530-0277.2009.01093.x

Krogh, A., Larsson, B., von Heijne, G., & Sonnhammer, E. L. (2001). Predicting transmembrane protein topology with a hidden Markov model: application to complete genomes. *Journal of Molecular Biology*, *305*(3), 567–80. doi:10.1006/jmbi.2000.4315

Kurusu, M., Cording, A., Taniguchi, M., Menon, K., Suzuki, E., & Zinn, K. (2008). A screen of cell-surface molecules identifies leucine-rich repeat proteins as key mediators of synaptic target selection. *Neuron*, *59*(6), 972–85. doi:10.1016/j.neuron.2008.07.037

Labrador, J. P., O'keefe, D., Yoshikawa, S., McKinnon, R. D., Thomas, J. B., & Bashaw, G. J. (2005). The homeobox transcription factor even-skipped regulates netrin-receptor expression to control dorsal motor-axon projections in Drosophila. *Current Biology : CB*, *15*(15), 1413–9. doi:10.1016/j.cub.2005.06.058

Landgraf, M., Baylies, M., & Bate, M. (1999a). Muscle founder cells regulate defasciculation and targeting of motor axons in the Drosophila embryo. *Current Biology*, *9*(11), 589–592. doi:10.1016/S0960-9822(99)80262-0

Landgraf, M., Roy, S., Prokop, A, VijayRaghavan, K., & Bate, M. (1999b). even-skipped determines the dorsal growth of motor axons in Drosophila. *Neuron*, *22*(1), 43–52. Retrieved from http://www.ncbi.nlm.nih.gov/pubmed/10027288

Law, A. J., Lipska, B. K., Weickert, C. S., Hyde, T. M., Straub, R. E., Hashimoto, R., … Weinberger, D. R. (2006). Neuregulin 1 transcripts are differentially expressed in schizophrenia and regulated by 5 SNPs associated with the disease. *Proceedings of the National Academy of Sciences of the United States of America*, *103*(17), 6747–6752.

Leahy, D. J. (2013). Piecing together the extracellular puzzle. *Cell*, *154*(1), 23–5. doi:10.1016/j.cell.2013.06.014

Lee, H., Engel, U., Rusch, J., Scherrer, S., Sheard, K., & Van Vactor, D. (2004). The microtubule plus end tracking protein orbit/MAST/CLASP acts downstream of the tyrosine kinase Abl in mediating axon guidance. *Neuron*, *42*(6), 913–926. doi:10.1016/j.neuron.2004.05.020

Lesnick, T. G., Papapetropoulos, S., Mash, D. C., Ffrench-Mullen, J., Shehadeh, L., de Andrade, M., … Maraganore, D. M. (2007). A genomic pathway approach to a complex disease: axon guidance and Parkinson disease. *PLoS Genetics*, *3*(6), e98. doi:10.1371/journal.pgen.0030098

Liebl, F. L. W., McKeown, C., Yao, Y., & Hing, H. K. (2010). Mutations in Wnt2 alter presynaptic motor neuron morphology and presynaptic protein localization at the drosophila neuromuscular junction. *PLoS ONE*, *5*(9), 1–11. doi:10.1371/journal.pone.0012778

Linnemannstöns, K., Ripp, C., Honemann-Capito, M., Brechtel-Curth, K., Hedderich, M., & Wodarz, A. (2014). The PTK7-related transmembrane proteins off-track and off-track 2 are co-receptors for Drosophila Wnt2 required for male fertility. *PLoS Genetics*, *10*(7), e1004443. doi:10.1371/journal.pgen.1004443

Liu, W., Sato, A., Khadka, D., Bharti, R., Diaz, H., Runnels, L. W., & Habas, R. (2008). Mechanism of activation of the Formin protein Daam1. *Proceedings of the National Academy of Sciences of the United States of America*, *105*(1), 210–215. doi:10.1073/pnas.0707277105

Llimargas, M., & Lawrence, P. A. (2001). Seven Wnt homologues in Drosophila: a case study of the developing tracheae. *Proceedings of the National Academy of Sciences of the United States of America*, *98*(25), 14487–14492. doi:10.1073/pnas.251304398

Long, H., Sabatier, C., Ma, L., Plump, A., Yuan, W., Ornitz, D. M., … Tessier-Lavigne, M. (2004). Conserved roles for Slit and Robo proteins in midline commissural axon guidance. *Neuron*, *42*(2), 213–223. doi:10.1016/S0896-6273(04)00179-5

Lowery, L. A., Lee, H., Lu, C., Murphy, R., Obar, R. A., Zhai, B., & Zhan, Y. (2010). Parallel genetic and proteomic screens identify msps as a clasp-abl pathway interactor in Drosophila. *Genetics*, *185*(4), 1311–1325. doi:10.1534/genetics.110.115626

Lowery, L. A., & Van Vactor, D. (2009). The trip of the tip: understanding the growth cone machinery. *Nature Reviews. Molecular Cell Biology*, *10*(5), 332–343. doi:10.1038/nrm2679

Lu, X., Borchers, A. G. M., Jolicoeur, C., Rayburn, H., Baker, J. C., & Tessier-lavigne, M. (2004). PTK7 / CCK-4 is a novel regulator of planar cell polarity in vertebrates. *Nature*, *430*(July), 93–98. doi:10.1038/nature02555.1.

Luo, L., Liao, Y. J., Jan, L. Y., & Jan, Y. N. (1994). Distinct morphogenetic functions of similar small GTPases: Drosophila Drac1 is involved in axonal outgrowth and myoblast fusion. *Genes & Development*, *8*(15), 1787–1802. doi:10.1101/gad.8.15.1787

Mägi, R., Manning, S., Yousseif, A., Pucci, A., Santini, F., Karra, E., … Batterham, R. L. (2013). Contribution of 32 GWAS-Identified Common Variants to Severe Obesity in European Adults Referred for Bariatric Surgery. *PLoS ONE*, *8*(8), e70735. doi:10.1371/journal.pone.0070735

Mahr, A., & Aberle, H. (2006). The expression pattern of the Drosophila vesicular glutamate transporter: A marker protein for motoneurons and glutamatergic centers in the brain. *Gene Expression Patterns*, *6*(3), 299–309. doi:10.1016/j.modgep.2005.07.006

Marin, O., Yaron, A., Bagri, A., Tessier-Lavigne, M., & Rubenstein, J. L. (2001). Sorting of striatal and cortical interneurons regulated by semaphorin-neuropilin interactions. *Science*, *293*(5531), 872–875. doi:10.1126/science.1061891

Markow, T. a, Beall, S., & Matzkin, L. M. (2009). Egg size, embryonic development time and ovoviviparity in Drosophila species. *Journal of Evolutionary Biology*, *22*(2), 430–4. doi:10.1111/j.1420-9101.2008.01649.x

Martin, J. E., Assassi, S., Diaz-Gallo, L. M., Broen, J. C., Simeon, C. P., Castellvi, I., … Martin, J. (2013). A systemic sclerosis and systemic lupus erythematosus pan-meta-GWAS reveals new shared susceptibility loci. *Human Molecular Genetics*, *22*(19), 4021–4029. doi:10.1093/hmg/ddt248

Mascheretti, S., Riva, V., Giorda, R., Beri, S., Lanzoni, L. F. E., Cellino, M. R., & Marino, C. (2014). KIAA0319 and ROBO1: evidence on association with reading and pleiotropic effects on language and mathematics abilities in developmental dyslexia. *Journal of Human Genetics*, *59*(4), 189–97. doi:10.1038/jhg.2013.141

Masuda, T., Kai, N., Sakuma, C., Kobayashi, K., Koga, H., & Yaginuma, H. (2009). Laser capture microdissection and cDNA array analysis for identification of mouse KIAA/FLJ genes differentially expressed in the embryonic dorsal spinal cord. *Brain Research*, *1249*, 61–67. doi:10.1016/j.brainres.2008.10.028

Matthes, D. J., Sink, H., Kolodkin, A. L., & Goodman, C. S. (1995). Semaphorin II Can Function as a Selective Inhibitor of Specific Synaptic Arborizations. *Cell*, *61*, 631–639.

McIntosh, A. M., Job, D. E., Moorhead, T. W. J., Harrison, L. K., Lawrie, S. M., & Johnstone, E. C. (2005). White matter density in patients with schizophrenia, bipolar disorder and their unaffected relatives. *Biological Psychiatry*, *58*(3), 254–7. doi:10.1016/j.biopsych.2005.03.044

McIntosh, A. M., Moorhead, T. W. J., Job, D., Lymer, G. K. S., Muñoz Maniega, S., McKirdy, J., … Hall, J. (2008). The effects of a neuregulin 1 variant on white matter density and integrity. *Molecular Psychiatry*, *13*(11), 1054–9. doi:10.1038/sj.mp.4002103

Meyer, R. L. (1998). Roger Sperry and his chemoaffinity hypothesis. *Neuropsychologia*, *36*(10), 957–80. Retrieved from http://www.ncbi.nlm.nih.gov/pubmed/9845045

Meyer, F., & Aberle, H. (2006). At the next stop sign turn right: the metalloprotease Tolloid-related 1 controls defasciculation of motor axons in Drosophila. *Development (Cambridge, England)*, *133*(20), 4035–4044. doi:10.1242/dev.02580

Meyer, F., & Moussian, B. (2009). Drosophila multiplexin (Dmp) modulates motor axon pathfinding accuracy. *Development Growth and Differentiation*, *51*(5), 483–498. doi:10.1111/j.1440-169X.2009.01111.x

Merino, C., Penney, J., González, M., Tsurudome, K., Moujahidine, M., O'Connor, M. B., … Haghighi, P. (2009). Nemo kinase interacts with Mad to coordinate synaptic growth at the Drosophila neuromuscular junction. *The Journal of Cell Biology*, *185*(4), 713–25. doi:10.1083/jcb.200809127

Ming, G. L., Song, H. J., Berninger, B., Holt, C. E., Tessier-Lavigne, M., & Poo, M. M. (1997). cAMP-dependent growth cone guidance by netrin-1. *Neuron*, *19*(6), 1225–1235. doi:10.1016/S0896-6273(00)80414-6

Mitchell, K. J., Doyle, J. L., Serafini, T., Kennedy, T. E., Tessier-Lavigne, M., Goodman, C. S., & Dickson, B. J. (1996). Genetic analysis of Netrin genes in Drosophila: Netrins guide CNS commissural axons and peripheral motor axons. *Neuron*, *17*(2), 203–15. Retrieved from http://www.ncbi.nlm.nih.gov/pubmed/8780645

Moon, R. T., Kohn, A. D., Ferrari, G. V. De, & Kaykas, A. (2004). WNT and β-catenin signalling: diseases and therapies. *Nature Reviews Genetics*, *5*(9), 691–701. doi:10.1038/nrg1427

Monschau, B., Kremoser, C., Ohta, K., Tanaka, H., Kaneko, T., Yamada, T., … Drescher, U. (1997). Shared and distinct functions of RAGS and ELF-1 in guiding retinal axons. *The EMBO Journal*, *16*(6), 1258–67. doi:10.1093/emboj/16.6.1258

Mosca, T. J., & Schwarz, T. L. (2010). The nuclear import of Frizzled2-C by Importins-β11 and α2 promotes postsynaptic development. *Nature Neuroscience*, *13*(8), 935–943. doi:10.1016/j.micinf.2011.07.011.Innate

Nakamoto, M., Cheng, H. J., Friedman, G. C., McLaughlin, T., Hansen, M. J., Yoon, C. H., … Flanagan, J. G. (1996). Topographically specific effects of ELF-1 on retinal axon guidance in vitro and retinal axon mapping in vivo. *Cell*, *86*(5), 755–66. Retrieved from http://www.ncbi.nlm.nih.gov/pubmed/8797822

Nakamura, M., Baldwin, D., Hannaford, S., Palka, J., & Montell, C. (2002). Defective proboscis extension response (DPR), a member of the Ig superfamily required for the gustatory response to salt. *The Journal of Neuroscience : The Official Journal of the Society for Neuroscience*, *22*(9), 3463–72. doi:20026336

Neukomm, L. J., Burdett, T. C., Gonzalez, M. a, Züchner, S., & Freeman, M. R. (2014). Rapid in vivo forward genetic approach for identifying axon death genes in Drosophila. *Proceedings of the National Academy of Sciences of the United States of America*, *111*(27), 9965–9970. doi:10.1073/pnas.1406230111

Neumüller, R. A., Richter, C., Fischer, A., Novatchkova, M., Neumüller, K. G., & Knoblich, J. A. (2011). Genome-wide analysis of self-renewal in Drosophila neural stem cells by transgenic RNAi. *Cell Stem Cell*, *8*(5), 580–93. doi:10.1016/j.stem.2011.02.022

Neves, G., Zucker, J., Daly, M., & Chess, A. (2004). Stochastic yet biased expression of multiple Dscam splice variants by individual cells. *Nature Genetics*, *36*(3), 240–246. doi:10.1038/ng1299

Nielsen, H., Brunak, S., & von Heijne, G. (1999). Machine learning approaches for the prediction of signal peptides and other protein sorting signals. *Protein Engineering*, *12*(1), 3–9. Retrieved from http://www.ncbi.nlm.nih.gov/pubmed/10065704

Nose, A. (2012). Generation of neuromuscular specificity in Drosophila: novel mechanisms revealed by new technologies. *Frontiers in Molecular Neuroscience*, *5*(May), 62. doi:10.3389/fnmol.2012.00062

O'Donnell, M. P., & Bashaw, G. J. (2013). Src inhibits midline axon crossing independent of Frazzled/Deleted in Colorectal Carcinoma (DCC) receptor tyrosine phosphorylation. *The Journal of Neuroscience : The Official Journal of the Society for Neuroscience*, *33*(1), 305–14. doi:10.1523/JNEUROSCI.2756-12.2013

O'Keefe, D. D., Edgar, B. a, & Saucedo, L. J. (2010). EndoGI modulates Notch signaling and axon guidance in Drosophila. *Mechanisms of Development*, *128*(1-2), 59–70. doi:10.1016/j.mod.2010.10.001

Oyallon, J., Apitz, H., Miguel-Aliaga, I., Timofeev, K., Ferreira, L., & Salecker, I. (2012). Regulation of locomotion and motoneuron trajectory selection and targeting by the Drosophila homolog of Olig family transcription factors. *Developmental Biology*, *369*(2), 261–76. doi:10.1016/j.ydbio.2012.06.027

Olofsson, B., & Page, D. T. (2005). Condensation of the central nervous system in embryonic Drosophila is inhibited by blocking hemocyte migration or neural activity. *Developmental Biology*, *279*(1), 233–43. doi:10.1016/j.ydbio.2004.12.020

Osteloh, J. M., Yang, J., Rooney, T. M., Fox, A. N., Adalbert, R., Powell, E. H., … Freeman, M. R. (2012). dSarm/Sarm1 is required for activation of an injury-induced axon death pathway. *Science*, *337*(6093), 481–484.

Ozaki, S., & Snider, W. D. (1997). Initial trajectories of sensory axons toward laminar targets in the developing mouse spinal cord. *Journal of Comparative Neurology*, *380*(2), 215–229.

Ozkan, E., Carrillo, R. A., Eastman, C. L., Weiszmann, R., Waghray, D., & Johnson, K. G. (2013). Resource An Extracellular Interactome of Immunoglobulin and LRR Proteins Reveals Receptor-Ligand Networks. *Cell*, *154*(1), 228–239.

Paracchini, S., Thomas, A., Castro, S., Lai, C., Paramasivam, M., Wang, Y., … Monaco, A. P. (2006). The chromosome 6p22 haplotype associated with dyslexia reduces the expression of KIAA0319, a novel gene involved in neuronal migration. *Human Molecular Genetics*, *15*(10), 1659–1666. doi:10.1093/hmg/ddl089

Parks, A. L., Cook, K. R., Belvin, M., Dompe, N. a, Fawcett, R., Huppert, K., … Francis-Lang, H. L. (2004). Systematic generation of high-resolution deletion coverage of the Drosophila melanogaster genome. *Nature Genetics*, *36*(3), 288–92. doi:10.1038/ng1312

Parrish, J. Z., Kim, M. D., Lily, Y. J., & Yuh, N. J. (2006). Genome-wide analyses identify transcription factors required for proper morphogenesis of Drosophila sensory neuron dendrites. *Genes and Development*, *20*(7), 820–835. doi:10.1101/gad.1391006

Pepple, K. L., Anderson, A. E., Frankfort, B. J., & Mardon, G. (2006). A Genetic Screen in Drosophila for Genes Interacting With senseless During Neuronal Development Identifies the Importin moleskin. *Genetics*, *175*(1), 125–141. doi:10.1534/genetics.106.065680

Peradziryi, H., Kaplan, N. A., Podleschny, M., Liu, X., Wehner, P., Borchers, A., & Tolwinski, N. S. (2011). PTK7/Otk interacts with Wnts and inhibits canonical Wnt signalling. *The EMBO Journal*, *30*(18), 3729–40. doi:10.1038/emboj.2011.236

Peradziryi, H., Tolwinski, N. S., & Borchers, A. (2012). The many roles of PTK7: A versatile regulator of cell-cell communication. *Archives of Biochemistry and Biophysics*, *524*, 71–76. doi:10.1016/j.abb.2011.12.019

Peschansky, V. J., Burbridge, T. J., Volz, A. J., Fiondella, C., Wissner-Gross, Z., Galaburda, A. M., … Rosen, G. D. (2010). The effect of variation in expression of the candidate dyslexia susceptibility gene homolog Kiaa0319 on neuronal migration and dendritic morphology in the rat. *Cerebral Cortex*, *20*(4), 884–897. doi:10.1093/cercor/bhp154

Pipes, G. C. T., Lin, Q., Riley, S. E., & Goodman, C. S. (2001). The Beat generation: a multigene family encoding IgSF proteins related to the Beat axon guidance molecule in Drosophila. *Development*, *4552*, 4545–4552.

Polleux, F., Morrow, T., & Ghosh, A. (2000). Semaphorin 3A is a chemoattractant for cortical apical dendrites. *Nature*, *404*(6778), 567–73. doi:10.1038/35007001

Poon, M.-W., Tsang, W.-H., Sun-On, C., Li, H.-M., Ng, H.-K., & Waye, M M.-Y. (2011). Dyslexia-Associated Kiaa0319-Like Protein Interacts with Axon Guidance Receptor Nogo Receptor 1. *Cellular and Molecular Neurobiology*, *31*, 27–35.

Pulido, D., Campuzano, S., Koda, T., Modolell, J., & Barbacid, M. (1992). Dtrk, a Drosophila gene related to the trk family of neurotrophin receptors, encodes a novel class of neural cell adhesion molecule. *The EMBO Journal*, *11*(2), 391–404. Retrieved from http://www.pubmedcentral.nih.gov/articlerender.fcgi?artid=556467&tool=pmcentrez&rendertype=abstract

Raghavan, S., & White, R. A. (1997). Connectin mediates adhesion in Drosophila. *Neuron*, *18*(6), 873–80. Retrieved from http://www.ncbi.nlm.nih.gov/pubmed/9208855

Ranganayakulu, G., Schulz, R. A., & Olson, E. N. (1996). Wingless signaling induces nautilus expression in the ventral mesoderm of the Drosophila embryo. *Developmental Biology*, *176*(1), 143–8. doi:10.1006/dbio.1996.9987

Rickmyre, J. L., DasGupta, S., Ooi, D. L.-Y., Keel, J., Lee, E., Kirschner, M. W., … Lee, L. A. (2007). The Drosophila homolog of MCPH1, a human microcephaly gene, is required for genomic stability in the early embryo. *Journal of Cell Science*, *120*(20), 3565–3577. doi:10.1242/jcs.016626

Rønn, L. C., Hartz, B. P., & Bock, E. (1998). The neural cell adhesion molecule (NCAM) in development and plasticity of the nervous system. *Experimental Gerontology*, *33*(7-8), 853–64. Retrieved from http://www.ncbi.nlm.nih.gov/pubmed/9951628

Rose, D., Zhu, X., Kose, H., Hoang, B., Cho, J., & Chiba, A. (1997). Toll, a muscle cell surface molecule, locally inhibits synaptic initiation of the RP3 motoneuron growth cone in Drosophila. *Development (Cambridge, England)*, *124*(8), 1561–71. Retrieved from http://www.ncbi.nlm.nih.gov/pubmed/9108372

Roseman, R. R., Johnson, E. A., Rodesch, C. K., Bjerke, M., Nagoshi, R. N., & Geyer, P. K. (1995). A P Element Containing suppressor of Hairy-wing Binding Regions Has Novel Properties for Mutagenesis in Drosophila Melanogaster. *Genetics*, *141*, 1061–1074.

Rosoff, W. J., Urbach, J. S., Esrick, M. a, McAllister, R. G., Richards, L. J., & Goodhill, G. J. (2004). A new chemotaxis assay shows the extreme sensitivity of axons to molecular gradients. *Nature Neuroscience*, *7*(6), 678–682. doi:10.1038/nn1259

Rothenberg, M. E., Rogers, S. L., Vale, R. D., Jan, L. Y., & Jan, Y. N. (2003). Drosophila pod-1 crosslinks both actin and microtubules and controls the targeting of axons. *Neuron*, *39*(5), 779–791. doi:10.1016/S0896-6273(03)00508-7

Sánchez-Soriano, N., & Prokop, A. (2005). The influence of pioneer neurons on a growing motor nerve in Drosophila requires the neural cell adhesion molecule homolog FasciclinII. *The Journal of Neuroscience : The Official Journal of the Society for Neuroscience*, *25*(1), 78–87. doi:10.1523/JNEUROSCI.2377-04.2005

Sato, M., Umetsu, D., Murakami, S., Yasugi, T., & Tabata, T. (2006). DWnt4 regulates the dorsoventral specificity of retinal projections in the Drosophila melanogaster visual system. *Nature Neuroscience*, *9*(1), 67–75. doi:10.1038/nn1604

Sawaya, M. R., Wojtowicz, W. M., Andre, I., Qian, B., Wu, W., Baker, D., & Zipursky, S. L. (2008). A Double S Shape Provides the Structural Basis for the Extraordinary Binding Specificity of Dscam Isoforms. *Cell*, *134*(6), 1007–1018. doi:10.1016/j.cell.2008.07.042

Schindelholz, B., Knirr, M., Warrior, R., & Zinn, K. (2001). Regulation of CNS and motor axon guidance in Drosophila by the receptor tyrosine phosphatase DPTP52F. *Development (Cambridge, England)*, *128*(21), 4371–82. Retrieved from http://www.ncbi.nlm.nih.gov/pubmed/11684671

Seeger, M., Tear, G., Ferres-Marco, D., & Goodman, C. S. (1993). Mutations affecting growth cone guidance in Drosophila: genes necessary for guidance toward or away from the midline. *Neuron*, *10*(3), 409–26. Retrieved from http://www.ncbi.nlm.nih.gov/pubmed/8461134

Serpe, M., & O'Connor, M. B. (2006). The metalloprotease tolloid-related and its TGF-beta-like substrate Dawdle regulate Drosophila motoneuron axon guidance. *Development (Cambridge, England)*, *133*(24), 4969–4979. doi:10.1242/dev.02711

Schindelholz, B., Knirr, M., Warrior, R., & Zinn, K. (2001). Regulation of CNS and motor axon guidance in Drosophila by the receptor tyrosine phosphatase DPTP52F. *Development (Cambridge, England)*, *128*(21), 4371–82. Retrieved from http://www.ncbi.nlm.nih.gov/pubmed/11684671

Schmucker, D., Clemens, J. C., Shu, H., Worby, C. A., Xiao, J., Muda, M., … Zipursky, S. L. (2000). Drosophila Dscam is an axon guidance receptor exhibiting extraordinary molecular diversity. *Cell*, *101*(6), 671–84. doi:10.1016/S0092-8674(00)80878-8

Serafini, T., Kennedy, T. E., Galko, M. J., Mirzayan, C., Jessell, T. M., & Tessier-Lavigne, M. (1994). The netrins define a family of axon outgrowth-promoting proteins homologous to C. elegans UNC-6. *Cell*, *78*(3), 409–24. Retrieved from http://www.ncbi.nlm.nih.gov/pubmed/8062384

Shi, L., Yu, H.-H., Yang, J. S., & Lee, T. (2007). Specific *Drosophila* Dscam juxtamembrane variants control dendritic elaboration and axonal arborization. *The Journal of Neuroscience*, *27*(25), 6723–6728. doi:10.1523/JNEUROSCI.1517-07.2007

Shirvan, A., Ziv, I., Fleminger, G., Shina, R., He, Z., Brudo, I., … Barzilai, A. (1999). Semaphorins as mediators of neuronal apoptosis. *Journal of Neurochemistry*, *73*(3), 961–71. Retrieved from http://www.ncbi.nlm.nih.gov/pubmed/10461885

Shishido, E., Ono, N., Kojima, T., & Saigo, K. (1997). Requirements of DFR1/Heartless, a mesoderm-specific Drosophila FGF-receptor, for the formation of heart, visceral and somatic muscles, and ensheathing of longitudinal axon tracts in CNS. *Development (Cambridge, England)*, *124*(11), 2119–2128.

Siebert, M., Banovic, D., Goellner, B., & Aberle, H. (2009). Drosophila motor axons recognize and follow a Sidestep-labeled substrate pathway to reach their target fields. *Genes & Development*, *23*(9), 1052–62. doi:10.1101/gad.520509

Siegel, L. S. (2006). Perspectives on dyslexia. *Paediatrics & Child Health*, *11*(9), 581–7. Retrieved from http://www.pubmedcentral.nih.gov/articlerender.fcgi?artid=2528651&tool=pmcentrez&rendertype=abstract

Sink, H., Rehm, E. J., Richstone, L., Bulls, Y. M., & Goodman, C. S. (2001). sidestep encodes a target-derived attractant essential for motor axon guidance in Drosophila. *Cell*, *105*(1), 57–67. Retrieved from http://www.ncbi.nlm.nih.gov/pubmed/11301002

Sink, H., & Whitington, P. M. (1991). Pathfinding in the central nervous system and periphery by identified embryonic Drosophila motor axons. *Development (Cambridge, England)*, *112*(1), 307–316.

Song, J. K., Kannan, R., Merdes, G., Singh, J., Mlodzik, M., & Giniger, E. (2010). Disabled is a bona fide component of the Abl signaling network. *Development (Cambridge, England)*, *137*(21), 3719–3727. doi:10.1242/jcs.082412

Sperry, R. W. (1963). Chemoaffinity in the Orderly Growth of Nerve Fiber Patterns and Connections. *Proceedings of the National Academy of Sciences of the United States of America*, *50*, 703–10. Retrieved from http://www.pubmedcentral.nih.gov/articlerender.fcgi?artid=221249&tool=pmcentrez&rendertype=abstract

Srahna, M., Leyssen, M., Ching, M. C., Fradkin, L. G., Noordermeer, J. N., & Hassan, B. A. (2006). A signaling network for patterning of neuronal connectivity in the Drosophila brain. *PLoS Biology*, *4*(11), 2076–2090. doi:10.1371/journal.pbio.0040348

Strutt, D., Madder, D., Chaudhary, V., & Artymiuk, P. J. (2012). Structure-function dissection of the frizzled receptor in Drosophila melanogaster suggests different mechanisms of action in planar polarity and canonical Wnt signaling. *Genetics*, *192*(4), 1295–313. doi:10.1534/genetics.112.144592

Sun, Q., Schindelholz, B., Knirr, M., Schmid, A., & Zinn, K. (2001). Complex genetic interactions among four receptor tyrosine phosphatases regulate axon guidance in Drosophila. *Molecular and Cellular Neurosciences*, *17*(2), 274–91. doi:10.1006/mcne.2000.0939

Suzuki, E., Rose, D., & Chiba, A. (2000). The ultrastructural interactions of identified pre- and postsynaptic cells during synaptic target recognition in Drosophila embryos. *Journal of Neurobiology*, *42*(4), 448–459.

Terman, J. R., & Kolodkin, A. L. (2004). Nervy links protein kinase A to plexin-mediated semaphorin repulsion. *Science*, *203*, 1204–1207.

Terman, J. R., Mao, T., Pasterkamp, R. J., Yu, H.-H., & Kolodkin, A. L. (2002). MICALs, a family of conserved flavoprotein oxidoreductases, function in plexin-mediated axonal repulsion. *Cell*, *109*(7), 887–900. Retrieved from http://www.ncbi.nlm.nih.gov/pubmed/12110185

Tessier-Lavigne, M., & Goodman, C. S. (1996). The Molecular Biology of Axon Guidance. *Science*, *274*(5290), 1123–1133. doi:10.1126/science.274.5290.1123

Tessier-Lavigne, M., Placzek, M., Lumsden, A. G. S., Dodd, J., & Jessell, T. M. (1988). Chemotropic guidance of developing axons in the mammalian central nervous system. *Nature*, *336*, 775–778.

Thor, S., & Thomas, J. B. (1997). The Drosophila islet gene governs axon pathfinding and neurotransmitter identity. *Neuron*, *18*(3), 397–409. Retrieved from http://www.ncbi.nlm.nih.gov/pubmed/9115734

Toyofuku, T., Zhang, H., Kumanogoh, A., Takegahara, N., Suto, F., Kamei, J., … Kikutani, H. (2004). Dual roles of Sema6D in cardiac morphogenesis through region-specific association of its receptor , Plexin-A1, with off-tack and vascular endothelial growth factor receptor type 2. *Genes & Development*, 1–13. doi:10.1101/gad.1167304.Kolodkin

Umemiya, T., Takasu, E., Takeichi, M., Aigaki, T., & Nose, A. (2002). Forked end: a novel transmembrane protein involved in neuromuscular specificity in drosophila identified by gain-of-function screening. *Journal of Neurobiology*, *51*(3), 205–14. doi:10.1002/neu.10063

Vactor, D. V, Sink, H., Fambrough, D., Tsoo, R., & Goodman, C. S. (1993). Genes that control neuromuscular specificity in Drosophila. *Cell*, *73*(6), 1137–53. Retrieved from http://www.ncbi.nlm.nih.gov/pubmed/8513498

Velayos-Baeza, A., Levecque, C., Kobayashi, K., Holloway, Z. G., & Monaco, A. P. (2010). The dyslexia-associated KIAA0319 protein undergoes proteolytic processing with γ-secretase-independent intramembrane cleavage. *Journal of Biological Chemistry*, *285*(51), 40148–40162. doi:10.1074/jbc.M110.145961

Velayos-Baeza, A., Toma, C., da Roza, S., Paracchini, S., & Monaco, A. P. (2007). Alternative splicing in the dyslexia-associated gene KIAA0319. *Mammalian Genome*, *18*(9), 627–634.

Vig, M., Peinelt, C., Beck, A., Koomoa, D. L., Rabah, D., Koblan-Huberson, M., Kraft, S., Turner, H., Fleig, A., Penner, R., & Kinet, J. P. (2006). CRACM1 is a plasma membrane protein essential for store-operated Ca2+ entry. *Science*, *312*(5777), 1220–1223.

Vogel, C., Teichmann, S. A., & Chothia, C. (2003). The immunoglobulin superfamily in Drosophila melanogaster and Caenorhabditis elegans and the evolution of complexity. *Development (Cambridge, England)*, *130*(25), 6317–28. doi:10.1242/dev.00848

Vrailas, A. D., Marenda, D. R., Cook, S. E., Powers, M. A., Lorenzen, J. A., Perkins, L. A., & Moses, K. (2006). smoothened and thickveins regulate Moleskin/Importin 7-mediated MAP kinase signaling in the developing Drosophila eye, *133*(8), 1485–1494.

Walter, J., Henke-Fahle, S., & Bonhoeffer, F. (1987). Avoidance of posterior tectal membranes by temporal retinal axons. *Development (Cambridge, England)*, *101*(4), 909–13. Retrieved from http://www.ncbi.nlm.nih.gov/pubmed/3503703

Wang, J., Zugates, C. T., Liang, I. H., Lee, C. H. J., & Lee, T. (2002). Drosophila Dscam is required for divergent segregation of sister branches and suppresses ectopic bifurcation of axons. *Neuron*, *33*(4), 559–571. doi:10.1016/S0896-6273(02)00570-6

Weigmann, K., Klapper, R., Strasser, T., Rickert, C., Technau, G., Jäckle, H., … Klämbt, C. (2003). FlyMove – a new way to look at development of Drosophila. *Trends in Genetics*, *19*(6), 310–311. doi:S0168952503001148 [pii]

Weng, Y.-L., Liu, N., DiAntonio, A., & Broihier, H. T. (2011). The cytoplasmic adaptor protein Caskin mediates Lar signal transduction during Drosophila motor axon guidance. *The Journal of Neuroscience: The Official Journal of the Society for Neuroscience*, *31*(12), 4421–33. doi:10.1523/JNEUROSCI.5230-10.2011

Wharton, K. A., Franks, R. G., Kasai, Y., & Crews, S. T. (1994). Control of CNS midline transcription by asymmetric E-box-like elements: similarity to xenobiotic responsive regulation. *Development (Cambridge, England)*, *120*(12), 3563–3569.

Williams, N. M., Preece, A., Spurlock, G., Norton, N., Williams, H. J., Zammit, S., … Owen, M. J. (2003). Support for genetic variation in neuregulin 1 and susceptibility to schizophrenia. *Molecular Psychiatry*, *8*(5), 485–7. doi:10.1038/sj.mp.4001348

Wilson, C., Goberdhan, D. C., & Steller, H. (1993). Dror, a potential neurotrophic receptor gene, encodes a Drosophila homolog of the vertebrate Ror family of Trk-related receptor tyrosine kinases. *Proceedings of the National Academy of Sciences of the United States of America*, *90*(15), 7109–7113. doi:10.1073/pnas.90.15.7109

Winberg, M. L., Mitchell, K. J., & Goodman, C. S. (1998). Genetic Analysis of the Mechanisms Controlling Target Selection: Complementary and Combinatorial Functions of Netrins, Semaphorins, and IgCAMs. *Cell*, *93*(4), 581–591.

Winberg, M. L., Noordermeer, J. N., Tamagnone, L., Comoglio, P. M., Spriggs, M. K., Tessier-Lavigne, M., & Goodman, C. S. (1998). Plexin A is a neuronal semaphorin receptor that controls axon guidance. *Cell*, *95*(7), 903–16. Retrieved from http://www.ncbi.nlm.nih.gov/pubmed/9875845

Winberg, M. L., Tamagnone, L., Bai, J., Comoglio, P. M., Montell, D., & Goodman, C. S. (2001). The transmembrane protein Off-track associates with Plexins and functions downstream of Semaphorin signaling during axon guidance. *Neuron*, *32*(1), 53–62. Retrieved from http://www.ncbi.nlm.nih.gov/pubmed/11604138

Wojtowicz, W. M., Flanagan, J. J., Millard, S. S., Zipursky, S. L., & Clemens, J. C. (2004). Alternative splicing of Drosophila Dscam generates axon guidance receptors that exhibit isoform-specific homophilic binding. *Cell*, *118*(5), 619–33. doi:10.1016/j.cell.2004.08.021

Wu, C., & Nusse, R. (2002). Ligand receptor interactions in the Wnt signaling pathway in Drosophila. *The Journal of Biological Chemistry*, *277*(44), 41762–9. doi:10.1074/jbc.M207850200

Wu, Z., Sweeney, L. B., Ayoob, J. C., Chak, K., Andreone, B. J., Ohyama, T., … Kolodkin, A. L. (2011). A combinatorial semaphorin code instructs the initial steps of sensory circuit assembly in the Drosophila CNS. *Neuron*, *70*(2), 281–98. doi:10.1016/j.neuron.2011.02.050

Yamada, S., Uchimura, E., Ueda, T., Nomura, T., Fujita, S., Matsumoto, K., … Miyake, J. (2007). Identification of twinfilin-2 as a factor involved in neurite outgrowth by RNAi-based screen. *Biochemical and Biophysical Research Communications*, *363*(4), 926–30. doi:10.1016/j.bbrc.2007.09.069

Yamagata, M., Sanes, J. R., & Weiner, J. A. (2003). Synaptic adhesion molecules. *Current Opinion in Cell Biology*, *15*(5), 621–632. doi:10.1016/S0955-0674(03)00107-8

Yamakawa, K., Huo, Y. K., Haendel, M. A., Hubert, R., Chen, X. N., Lyons, G. E., & Korenberg, J. R. (1998). DSCAM: A novel member of the immunoglobulin superfamily maps in a Down syndrome region and is involved in the development of the nervous system. *Human Molecular Genetics*, *7*(2), 227–237. doi:10.1093/hmg/7.2.227

Yang, T., & Terman, J. R. (2012). 14-3-3 Couples Protein Kinase A to Semaphorin Signaling and Silences Plexin RasGAP-Mediated Axonal Repulsion. *Neuron*, *74*(1), 108–121. doi:10.1016/j.neuron.2011.12.034

Yao, K. M., & White, K. (1994). Neural specificity of elav expression: defining a Drosophila promoter for directing expression in the nervous system. *Journal of Neurochemistry*, *63*(1), 41–51.

Yoshikawa, S., McKinnon, R. D., Kokel, M., & Thomas, J. B. (2003). Wnt-mediated axon guidance via the Drosophila Derailed receptor. *Nature*, *422*(6932), 583–8. doi:10.1038/nature01522

Younossi-Hartenstein, A., & Hartenstein, V. (1993). The Role of the Tracheae and Musculature during Pathfinding of Drosophila Embryonic Sensory Axons. *Developmental Biology*, *158*, 430–447.

Yu, H., Araj, H. H., Ralls, S. A., & Kolodkin, A. L. (1998). The Transmembrane Semaphorin Sema I Is Required in Drosophila for Embryonic Motor and CNS Axon Guidance. *Neuron*, *20*, 207–220.

Yu, H. H., Huang, A. S., & Kolodkin, A L. (2000). Semaphorin-1a acts in concert with the cell adhesion molecules fasciclin II and connectin to regulate axon fasciculation in Drosophila. *Genetics*, *156*(2), 723–31. Retrieved from http://www.pubmedcentral.nih.gov/articlerender.fcgi?artid=1461270&tool=pmcentrez&rendertype=abstract

Zallen, J. A., Cohen, Y., Hudson, A. M., Cooley, L., Wieschaus, E., & Schejter, E. D. (2002). SCAR is a primary regulator of Arp2/3-dependent morphological events in Drosophila. *Journal of Cell Biology*, *156*(4), 689–701. doi:10.1083/jcb.200109057

Zarin, A. A., Asadzadeh, J., Hokamp, K., McCartney, D., Yang, L., Bashaw, G. J., & Labrador, J. P. (2014). A transcription factor network coordinates attraction, repulsion, and adhesion combinatorially to control motor axon pathway selection. *Neuron*, *81*(6), 1297–1311. doi:10.1016/j.neuron.2014.01.038

Zhu, B., Pennack, J. a., McQuilton, P., Forero, M. G., Mizuguchi, K., Sutcliffe, B., … Hidalgo, A. (2008). Drosophila neurotrophins reveal a common mechanism for nervous system formation. *PLoS Biology*, *6*(11), 2476–2495. doi:10.1371/journal.pbio.0060284

Appendices

Appendix A – Genes linked to motor axon guidance phenotypes

Structures referred to in the third column are branches that are missing or morphologically abnormal in loss- and gain-of-function experiments involving the genes in the first column. The MN12s, MN13s, and RP3 axon are facets of the ISNb, thus where "ISNb" is mentioned, this indicates that the whole branch failed to enter the region of the VLMs. Therefore, "MN12s," "MN13s," and "RP3 axon" indicate that the ISNb entered the region of the VLMs, though these individual projections were absent or abnormal.

Gene (FlyBase symbol)	Chromosome	Branches with phenotypes	References
14-3-3ε	3rd	MN12s, RP3, MN13s	Yang & Terman, 2012.
abl tyrosine kinase (abl)	3rd	ISNb, SNa, MN12s, MN13s	Lee et al., 2004; Lowery et al., 2010; Song et al., 2010.
αPS1 (mew)	X	ISNb, ISNd, SNc, MN13s	Hoang & Chiba, 1998; Huang et al., 2007.
αPS2 (if)	X	ISNb, SNd, SNc, MN13s	Hoang & Chiba, 1998; Huang et al., 2007.
baboon (babo)	2nd	MN12s, MN13s	Serpe & O'Connor, 2006.
beaten path (beat)	2nd	ISNb, ISNd, SNa, SNc, MN12s, MN13s	Fambrough & Goodman, 1996; Landgraf et al., 1999; Siebert et al., 2009.
beaten path Ic (beat-Ic)	2nd	RP3	Pipes et al., 2001.
capricious (caps)	3rd	ISNb, MN12s, RP3, MN13s	Abrell & Jäckle, 2001; Kohsaka & Nose, 2009.
caskin (ckn)	2nd	ISNb, ISNd	Weng et al., 2011.
cdk5 activator-like protein (cdk5α)	2nd	SNa	Connell-Crowley et al., 2007.

chickadee (chic)	2nd	MN12s	Vactor et al., 1993.
chromosome bows (chb)	3rd	ISNb	Lee at al., 2004.
clueless (clu)	2nd	MN12s, MN13s	Vactor et al., 1993.
commissureless (comm)	3rd	RP3	Kidd, Bland, & Goodman, 1999.
connectin (con)	3rd	ISNb, SNa, SNc, MN12s, RP3, MN13s	Fambrough & Goodman, 1996; Raghavan & White, 1997; Yu, Huang, & Kolodkin, 2000.
crk-associated substrate (p130CAS)	3rd	ISNb, ISNd, SNa, MN12s, RP3, MN13s	Huang et al., 2007.
dawdle (daw)	2nd	MN12s, MN13s	Serpe & O'Connor, 2006.
derailed-2 (drl-2)	2nd	MN12s	Inaki et al., 2007.
disabled (dab)	3rd	SNa, MN12s, MN13s	Song et al. (2010).
dreadlocks (dock)	2nd	ISNd	Weng et al., 2011.
endonuclease G inhibitor (endoGI)	2nd	ISNb, SNc	O'Keefe et al., 2010.
even skipped (eve)	2nd	ISNb, ISNd, SNc	Labrador et al., 2005; Landgraf et al. (1999).
extra-extra (exex)	3rd	MN12s, MN13s	Oyallon et al., 2012.
fasciclin II (fas2)	X	ISNb, SNa, MN12s, MN13s	Abrell & Jäckle, 2001; Fambrough & Goodman, 1996; Sink et al., 2001; Yu, Huang, & Kolodkin, 2000.
frazzled (fra)	2nd	ISN (FB/SB), SNc, RP3	Kolodziej et al., 1996; Labrador et al., 2005; O'Donnell and Bashaw, 2013; Winberg et al., 1998.

frizzled 2 (fz2)	2nd	MN12s	Inaki et al., 2007.
forked end (fend)	X	MN12s, MN13s	Umemiya et al., 2002.
gooseberry (gsb)	2nd	SNa, SNc	He & Noll, 2013.
gooseberry-neuro (gsb-n)	2nd	SNa, SNc	He & Noll, 2013.
guanylyl cyclase at 76C (gyc76C)	3rd	SNa, MN12s, RP3, MN13s	Ayoob et al., 2004; Chak & Kolodkin, 2014.
kermit	2nd	MN12s, RP3, MN13s	Chak & Kolodkin, 2014.
knockout (ko)	3rd	RP3, MN13s	Hartmann et al., 1997.
krüppel (kr)	2nd	ISNb, MN12s, MN13s	Abrell & Jäckle, 2001; Hartmann et al., 1997.
leukocyte-antigen-related-like (lar)	2nd	ISN (FB/SB), ISNb, SNa	Desai et al., 1997; Fox & Zinn, 2005; Schindelholz et al., 2001; Sun et al., 2001.
molecule interacting with casL (mical)	3rd	ISNb, SNa, MN12s, RP3, MN13s	Ayoob, Terman, & Kolodkin, 2006; Hung et al., 2012; Terman et al., 2002.
multiplexin (mp)	3rd	ISNb	Meyer & Moussian, 2009.
nervy (nvy)	2nd	SNa, ISNb, MN12s, RP3, MN13s	Terman & Kolodkin, 2004.
netrin-A (netA)	X	ISN (FB/SB), SNa, RP3	Labrador et al., 2005; Mitchell et al., 1996.
netrin-B (netB)	X	ISN (FB/SB), SNa, SNc, RP3	Labrador et al., 2005; Mitchell et al., 1996; Winberg, Mitchell, & Goodman, 1998.
neuroglian (nrg)	X	ISN (FB/SB)	Hall & Bieber, 1997.
neurotrophin 1 (nt1)	3rd	SNa, MN12s, MN13s	Zhu et al., 2008.

notch (n)	X	ISNb	Crowner et al., 2003.
off-track (otk)	2nd	ISNb, MN12s, RP3, MN13s	Winberg et al., 2001.
olig family (oli)	2nd	ISNb, MN12s, RP3, MN13s	Oyallon et al., 2012.
pebble (pbl)	3rd	MN13s	Jeong et al., 2013.
plexin-A (plex-A)	4th	ISNb, SNa, MN12s, RP3, MN13s	Ayoob, Terman, & Kolodkin, 2006; Ayoob et al., 2004; Chak & Kolodkin, 2014; Cho et al., 2012; Terman et al., 2002; Winberg et al., 1998; Winberg et al., 2001; Yang & Terman, 2012.
plexin-B (plex-B)	4th	ISNb, MN12s, RP3	Ayoob, Terman, & Kolodkin, 2006; Cho et al., 2012; Hu et al., 2001.
pod1	X	ISNb	Rothenburg et al., 2003.
protein kinase, cAMP-dependent, catalytic subunit 1 (pka-C1)	2nd	MN12s, MN13s	Yang & Terman, 2012.
protein tyrosine phosphatase 10D (ptp10D)	X	ISN (FB/SB), ISNb, SNa	Jeon et al., 2008; Sun et al., 2001.
protein tyrosine phosphatase 4E (ptp4E)	X	ISN (FB/SB)	Jeon et al., 2008.
protein tyrosine phosphatase 52F (ptp52F)	2nd	ISN (FB/SB)	Jeon et al., 2008.
protein tyrosine phosphatase 69D (ptp69D)	3rd	ISN (FB/SB), ISNb SNa, MN12s, RP3, MN13s	Desai et al., 1996; Jeon et al., 2008, Sun et al., 2001.
protein tyrosine	3rd	ISNb, SNa, MN12s,	Desai et al., 1996; Sun

phosphatase 99A (ptp99A)		MN13s	et al., 2001.
punt (put)	3rd	MN12s	Serpe & O'Connor, 2006.
rac1 (rac1)	3rd	ISNb	Hu et al., 2001.
rho GTPase activating protein p190 (rhoGAPp190)	X	MN12s, MN13s	Jeong et al., 2013.
semaphorin-1a (sema-1a)	2nd	ISN (FB/SB), ISNb, SNa, MN12s, RP3, MN13s	Ayoob et al., 2004; Ayoob et al., 2006; Chak & Kolodkin, 2014; Cho et al., 2012; Terman et al., 2002; Winberg et al., 1998; Winberg et al., 2001; Yang & Terman, 2012; Yu et al., 1998; Yu, Huang, & Kolodkin, 2000.
semaphorin-1b (sema-1b)	2nd	RP3	Winberg et al., 1998.
semaphorin-2a (sema-2a)	2nd	SNa, SNc, RP3, MN13s	Matthes et al., 1995; Winberg, Mitchell, & Goodman, 1998.
semaphorin-2b (sema-2b)	2nd	MN12s	Wu et al., 2011.
sidestep (side)	3rd	ISN (FB/SB), ISNb, ISNd, SNc, SNa, MN12s, RP3, MN13s	Meyer & Aberle, 2006; Siebert et al., 2009; Sink et al., 2001.
slit (sli)	2nd	RP3	Kidd, Bland, & Goodman, 1999.
smad on X (smox)	X	MN12s, MN13s	Serpe & O'Connor, 2006.
spatzle (spz)	3rd	SNa, MN12s, MN13s	Zhu et al., 2008.
spatzle 5 (spz5)	3rd	SNa, MN12s, MN13s	Zhu et al., 2008.
syndecan (sdc)	2nd	ISNb, SNa	Fox & Zinn, 2005.

starry night (stan)	2nd	MN12s, MN13s	Bao et al., 2007.
stranded at second (sas)	3rd	MN13s	Vactor et al., 1993.
tartan (trn)	3rd	MN12s	Kohsaka & Nose, 2009.
terribly reduced optic lobes (trol)	X	MN12s, RP3	Cho et al., 2012.
tolkin (tok)	3rd	ISN (FB/SB), ISNb, SNc, MN12s, RP3, MN13s	Meyer & Aberle, 2006; Serpe & O'Connor, 2006.
toll (tl)	3rd	RP3	Rose et al., 1997.
trio (trio)	3rd	SNa, MN12s, MN13s	Bateman et al., 2000; Song et al., 2010.
turtle (tutl)	2nd	MN12s, RP3	Al-Anzi & Wyman, 2009.
unc-5 (unc-5)	2nd	ISNb, SNa	Labrador et al., 2005.
walkabout (wako)	2nd	MN12s, MN13s	Vactor et al., 1993.
wnt oncogene analog 4 (wnt4)	2nd	MN12s, MN13s	Inaki et al., 2007.

Appendix B – Primers

Primer name	Forward primer sequence	Reverse primer sequence
8964 excision	ACAATCGTCGTCTTCCGTTC	GCGTTACCATCAGTGGGTCT
8964 insertion	GTCACGCTTTATTATCCTGCCA	TTTCACCGAAAGCAACCGTA
EY.3.F	(8964 insertion forward primer)	CCTTTCACTCGCACTTATTG
MPPE	CGGTTGCTTTCGGTGAAATA	CCCAAGATTCTCAAGATTGC
B318	CGTGACCAATTCAACCACTG	GGGAGGCTTCACAAACACAT
KG04227	CTATCTGACGTGCGAGTTGC	TGCGAATGCAAGAGTAATGG

Appendix C – The VNC in *CG7565* loss-of-function embryos

In late stage 16 wild type embryos (A), the VNC has straight, uniform longitudinal fascicles running along the anteroposterior axis (left is posterior, right is anterior). In a late stage 16 *B318* embryo (B), the longitudinal fascicles have collapsed onto the midline. In a late stage 16 *ED4408* embryo (C), the longitudinal fascicles are relatively normal in the two most anterior (left) segments, though are unravelled across the rest of the embryo.

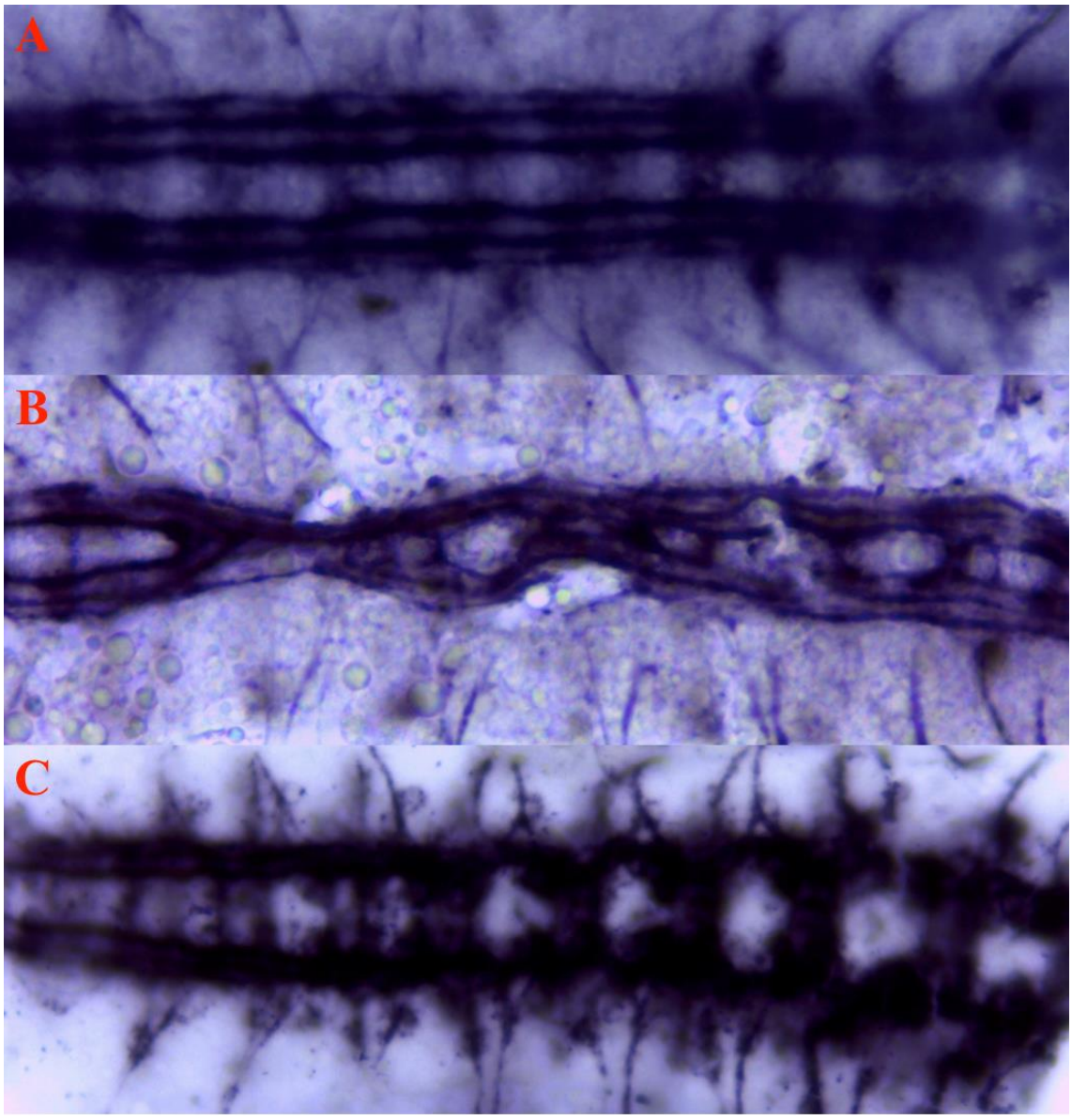

Appendix D – Flies

With the exception of *otk*^{A1} and *otk2*^{C26}, which were gifts from Linnemannstöns and colleagues (2014), all flies were acquired from the Bloomington Stock Center.

Name in thesis	**Genotype**	**Description**
B318	*w*^{1118}; *PBac{5HPw*$^{+}$*}CG7565*^{B318}	Insertion at 3L:8,090,013 (within a *CG7565* exon)
BSC199	*w*^{118}; *Df(2R)BSC199/CyO*	Deletion from 2R:7779605 to 2R:8059989 (removes *otk* and *otk2*)
ED4408	*w*^{1118}; *Df(3L)ED4408, P{w*$^{+mW.Scer\FRT.hs3}$*=3'.RS5+3.3'}ED4408/TM6b*$^{AbdA\text{-}lacZ}$	Deletion from 3L:7,979,107 to 3L:8,299,574 (removes *CG7565*)
EY03841	*y*^{1} *w*^{67c23}; *P{EPgy2}EY03841/CyO*	UAS-containing insertion upstream of *otk2* (2R:12,025, 300)
EY12902	*y*^{1} *w*^{67c23}*; P{EPgy2}Ect4*^{EY12902}	UAS-containing insertion upstream of *CG7565* (3L:8,091,921)
fz2	*y*^{1} *w*^{67c23}*; P{Epgy2}fz2*^{EY02025}	Insertion at 3L:19,170,637 (within a *fz2* exon)
KG04227	*y*^{1}*w*^{67c23}*; P{SUPor-P)CG31814*^{KG04227}*/CyO*	Insertion at 2L:13,717,159 (within 5' UTR of *CG31814*)
Mef2	*Mef2-Gal4*	Somatic muscle driver
OK371	*OK371-Gal4*	Motor neuron driver
otk^{A1}	*otk*^{A1}	*otk* null allele
otk2^{C26}	*otk2*^{C26}	*otk2* null allele (also partially deletes *MPPE*)
sema-1a	*y*^{1}*w*^{67c23}*; P{lacW}Sema-1a*^{k13702}*/CyOwg*	Insertion at 2L:8,544,219 (within a *sema-1a* intron)
w; *Sp/CyO*; *Sb, Δ 2-3/TM6b, Δ 2-3*	*w*; *Sp/CyO*; *Sb, Δ 2-3/TM6b, Δ 2-3*	Source of transposase activity